TOWARD A MOLECULAR UNDERSTANDING OF IRON HOMEOSTASIS IN THE OPPORTUNISTIC PATHOGEN *PSEUDOMONAS AERUGINOSA*. THE ROLE OF BACTERIOFERRITIN B.

By

SAROJA KUMARI WEERATUNGA

B.Sc. (Honors), University of Peradeniya, 2003
Peradeniya, Sri Lanka.

Submitted to the Department of Chemistry and the
Faculty of the Graduate School of the University of Kansas
In Partial fulfillment of the requirements for the degree of
Doctor of Philosophy

Committee members:

_____
Mario Rivera, Ph. D. (Chair)

_____
George Wilson, Ph.D.

_____
Robert C. Dunn, Ph. D.

_____
Susan Lunte, Ph. D.

_____
Michael Johnson, Ph.D

_____
Jennifer Laurence, Ph.D

Date Defended: February 21st, 2011

The Dissertation Committee for **Saroja Kumari Weeratunga** certifies that this is the approved version of the following dissertation:

TOWARD A MOLECULAR UNDERSTANDING OF IRON HOMEOSTASIS IN THE OPPORTUNISTIC PATHOGEN *PSEUDOMONAS AERUGINOSA*.

THE ROLE OF BACTERIOFERRITIN B.

Committee members:

_____
Mario Rivera, Ph. D. (Chair)

_____
George Wilson, Ph.D.

_____
Robert C. Dunn, Ph. D.

_____
Susan Lunte, Ph. D.

_____
Michael Johnson, Ph.D

_____
Jennifer Laurence, Ph.D

Date Approved: _____

ABSTRACT

Bacterioferritin B is an important protein for *P. aeruginosa* as it is capable of storing about 4000 Fe^{3+} ions in the form of ferric hydroxy phosphate in its core and release when it is required by the cell. Our research was aimed at understanding the mechanisms and pathways of iron uptake and mobilization from Pa BfrB which are considered as two vital processes of this protein molecule. The recombinant Pa-BfrB was overexpressed and purified to homogeneity. The structural studies of Pa BfrB were carried out by solving four crystal structures: (1) crystals grown from Pa BfrB without a mineral core (as-isolated), (2) mineralized with ~600 iron atoms (mineralized), (3) crystals soaked in a Fe^{2+} solution and (Fe soak) and (4) Fe soaked crystals soaked in a crystallization solution (double soak). Crystal structures revealed that it is composed of 24 subunits arranged as a sphere and can bind 12 heme molecules per protein. Further, crystallographic studies elegantly showed that iron ions to be stored inside the cavity are taken into the inner cavity of the protein via the ferroxidase pores on the surface. Both crystallographic and solution experiments provide evidence to show that these Fe^{2+} ions are oxidized at the ferroxidase center and subsequently internalized via a gated mechanism operated by the amino acid residue His130 at the ferroxidase center.

An interaction between BfrB and apo Bfd (Bcaterioferritin associated ferredoxin) was found to be necessary for efficient mobilization of iron from the mineral core of BfrB. In addition, the thus far mysterious role of heme in bacterioferritins was revealed for the first time and was experimentally demonstrated that ferric ion mineral core of BfrB is reduced by the heme mediated efficient transfer of electrons from the reductase to the core. Additional experiments show that Bfd binds to BfrB with a ratio of 12:1 to support the efficient mobilization of iron from

BfrB and it was found that Bfd is not functioning as a typical ferredoxin in the iron mobilization process of BfrB as it is the apo Bfd not the holo Bfd which is involved in the iron mobilization from the inner cavity of BfrB. Crystallographic data suggest that four-fold pores may be the dominant route of iron release from the inner cavity of BfrB. Results of the studies carried out with site directed mutagenesis and Elastic Network Model calculations provided experimental evidence suggesting that the main path way of iron release is through the four fold pores of BfrB.

ACKNOWLEDGMENTS

I would like to thank Prof. Mario Rivera for giving me this wonderful opportunity to work with him in his laboratory which made this journey an enriching life experience. I greatly appreciate his guidance, encouragement and the invaluable support given to me all the time. You were an excellent teacher and a great mentor to me.

I would like to extend my sincere gratitude for my committee members Dr. Robert Dunn, Dr. Susan Lunte, Dr. Michael Johnson, Dr. George Wilson and Dr.Jennifer Laurence for their kind support and advice.

I am extremely thankful to my loving husband Kalanka Goonawarna for his endless love, patience, understanding and support given to me all the time. This achievement would not have been possible without you in my life. I also thankful to my precious little daughter Githmi Goonawarna for her sweet love which made me happy in all my difficult times.

I would like to express my deepest gratitude to all our collaborators; especially, Dr. Scott Lovell who solved the crystal structures of my proteins and also helped me a lot to understand the crystallographic concepts. Thank you very much for your valuable time and effort. I am also thankful to Dr. Feimeng Zhou at California State Univesity for helping us with SPR experiments. In addition, I would like to thank Dr.Jennifer Laurence and her group members for letting me use their AKTA purifier system, Dr. Chris Fischer and his group for giving me the opportunity to use their stopped flow spectrophotometer and also to Dr. Phillip Gao and his group members for allowing me to use their instruments.

I greatly appreciate the support and friendship of the past and present members of the Rivera group; Dr. Yuhong Zeng, Dr. An Wang, Dr. Aileen Alontaga, Baily Morgan, Casey Gee, Dr. Juan Carlos Rodriguez, Dr. Huili Yao, Grace Jepkorir, Yan Wang, Pavithra Vani Nama, and Ritesh Kumar. I was happy to work with all of you and thanks for making the time in the lab enjoyable and memorable.

I take this opportunity to thank all my teachers in my elementary schools, (Vidyaloka Vidyalaya, Kadawata, and Jayakodi Maha Vidyalaya, Ganemulla, Sri Lanka), my High school (Sirimavo Bandaranayaka Vidyalaya, Colombo, Sri Lanka) and in my university (University of Peradeniya, Peradeniys, Sri Lanka) for guiding me to the correct path of the life.

All these achievements were possible because of the wonderful blessings and constant love of my loving parents, two brothers (Viranga and Chami) and my ever loving sister (Shammi). Dear Mom and Dad, I really appreciate your hard work, positive thoughts, all the hopes you had on me, and everything you have done so far to raise me as a good person and bring me to this successful position in my life. This wonderful achievement is the result of your sweat and tears. My ever loving Grandma, my one and only aunt (Asoka) and uncle (Sarath) are greatly acknowledged for their support in many ways at many important milestones in my life and their kind, loving words all the time.

Finally I would like to thank everyone who helped me in many ways to make my journey successful.

DEDICATION

To

My Great Parents

(Mr.D.C Weeratunga and Mrs. Somalatha Nawagamuwage)

TABLE OF CONTENTS

LIST OF TABLES

LIST OF FIGURES

CHAPTER 1

CHAPTER 2

CHAPTER 3

APPENDIX II

LIST OF SCHEMES

CHAPTER 1

LIST OF APPENDICES

ABBREVIATIONS

ABC	ATP-binding cassette
ALA	δ-Aminolevulinic acid
Bfr	Bacterioferritin
Bfd	Bacterioferritin associated ferredoxin
DMSO	Dimethyl sulfoxide
Dps	DNA binding protein from starved cells
DTT	Dithiothreitol
FAD	Flavin adenine dinucleotide
$FADH_2$	Fully reduced flavin adenine dinucleotide
Ftn	Ferritin
FPR	Ferredoxin NADP reductase
Hb	Hemoglobin
HO	Heme oxygenase
IPTG	Isopropyl-β-D-thiogalactopyranoside
MES	2-(N-morpholino)ethanesulfonic acid
NADPH	Nicotinamide adenine dinucleotide (phosphate)
OD	Optical density
Pa	*Pseudomonas aeruginosa*
PCR	Polymerase chain reaction
PDB	Protein data bank
PMSF	Phenylmethylsulfonyl flouride
SDS PAGE	Sodium dodecyl sulfate polyacrylamide gel electrophoresis
SPR	Surface plasmon resonance
TCEP	Tris (2-carboxyethyl)-phosphine hydrochloride
Tris	Tris(hydroxymethyl)aminomethane
UV-Vis	Ultraviolet-visible
WT	Wildtype

CHAPTER I
Introduction

Pseudomonas aeruginosa is a Gram-negative opportunistic pathogen that can cause severe nosocomial infections in immunocompromised patients. For instance, *P. aeruginosa* causes chronic lung infections in ~90% of cystic fibrosis patients and is also responsible for secondary infections in burn victims and cancer patients [1]. Furthermore, it has been recently found that approximately half of the known strains of *P. aeruginosa* have developed antibiotic resistance genes [2]. Recent findings, however, suggest that iron, particularly heme-iron, is essential for successful colonization (infection) of mammalian hosts [3]. The above finding implies that molecules capable of inhibiting iron/heme-iron acquisition pathways or interfering with iron trafficking mechanisms in *P. aeruginosa* may constitute a new class of antibiotics. Therefore, a molecular level understanding of iron acquisition paths, regulation mechanisms and metabolism is required, in order to rationally develop drugs to combat *Pseudomonas* infections.

Iron is the second most abundant metal and the fourth most abundant element in the earth's crust [4]. Because of its abundance and versatility, iron is considered as an essential element for virtually all forms of life. It is found in many enzymes as an important cofactor in many electron transfer proteins [4]. Furthermore, since iron ions exist in several oxidation states they can act as catalysts in many cellular reactions such as DNA synthesis, nitrogen fixation and respiration [6]. Under physiological conditions iron possesses two readily interchangeable oxidation states, Fe (II) and Fe (III), and these are involved in many redox reactions [7]. The redox potential of Fe^{2+}/Fe^{3+} fluctuates from -490 mV to +330 mV (Vs SHE) and mainly depends on the ligands that are coordinated to iron. Thus, as a very useful redox mediator in biology, iron can be found in proteins in many different

forms such as iron-sulfur clusters, heme groups, iron nickel clusters, and mono- or binuclear species [7]. In the early years of life, Fe^{2+} was considered as a biologically "friendly" metal. However, with the advent of oxygen-rich environment the soluble Fe^{2+} (0.1 M at pH 7.0) became extremely insoluble Fe^{3+} (10^{-18} M at pH 7.0) and as a result this key nutrient became scarce and growth limiting for many organisms [6, 8]. In addition, cellular Fe^{2+} can react with metabolically produced H_2O_2 and generate reactive hydroxyl radicals:

$$Fe^{2+} + H_2O_2 \rightarrow Fe^{3+} + OH^- + OH^{\cdot} \qquad \text{(Reaction 1; Fenton reaction)}$$

In addition, one-electron reduction of O_2 by ferrous ions produces superoxide radicals which in turn reduce ferric ions to ferrous ions (Reaction 2).

$$O_2^{\cdot -} + Fe^{3+} \rightarrow O_2 + Fe^{2+} \qquad \text{(Reaction 2)}$$

The sum of the above two reactions is called the Haber-Weiss reaction which generates hydroxyl anions, oxygen and reactive hydroxyl radicals as products. It is noteworthy, however, that the Haber –Weiss reaction can take place only in the presence of catalytic amounts of a redox active metal such as iron.

$$H_2O_2 + O_2^{\cdot -} \rightarrow OH^- + OH^{\cdot} + O_2 \qquad \text{(Reaction 3; Haber-Weiss reaction)}$$

Hydroxyl radicals are very reactive and can damage cells by inducing lipid peroxidation, degradation of biomolecules and breakage of DNA strands [9]. As a consequence of the insolubility of ferric ions and toxicity of ferrous ions, all living organisms were compelled to develop efficient ways of acquiring, storing and utilizing iron.

Iron acquisition by Bacteria.

Bacteria have adopted several mechanisms to acquire iron from the surroundings. Basically they use three methods to acquire iron [4]. (1) Lower the external pH by releasing hydroxyl acids such as citrate and malate to make insoluble ferric ions more soluble [10]. (2) Organisms such as *Listeria monocytogenes* secrete chemical species capable of reducing insoluble Fe^{3+} ions to soluble Fe^{2+} ions [11]. (3) Secrete ferric ion chelating compounds such as siderophores which are low molecular weight compounds (< 1000 Da) with a very high affinity ($K_{aff} > 10^{30}$) and specificity for ferric ions. These molecules are synthesized and secreted by bacteria during iron starvation conditions. Reduction and chelation are the two mostly employed methods to acquire iron [10]. Some *E. coli* strains can produce a type of siderophore called aerobactin at a very high concentration (200 mg L^{-1}) [12, 13]. Once soluble siderophores are secreted to the outside environment, they form hexadentate octahedral complexes with ferric ions. These iron bound siderophores are then taken into the cytoplasm via the cytosolic membrane (CM). Gram-negative and Gram-positive bacteria employ two different mechanisms to internalize the iron bound siderophores (Scheme 1) [4]. Gram-negative bacteria have two cell membranes called outer (OM) and cytosolic membrane (CM) whereas Gram-positive bacteria have only one membrane (CM) surrounding the cytoplasm. In Gram-negative bacteria, iron-siderophore complexes are first received by specific OM receptor proteins such as FepA, FecA and FhuA prior to internalization. Since these iron-siderophore complexes are too large to diffuse through OM channels, transport of these complexes across the OM requires energy. As a result, these iron complexes are actively transported across the OM into the periplasm, using the energy-transducing TonB-ExbB-ExbD system [4]. Once the iron-siderophore complexes are in the periplasm, they are bound by the ATP-binding cassette (ABC) transporters found in the CM

and delivered to the cytoplasm (Scheme 1A). On the other hand, in Gram-positive bacteria, ferri-siderophore complexes are transported through the CM by binding-protein-dependent ATP binding cassette permease proteins. These ABC permeases are similar to ABC transporters of Gram negative bacteria except that these binding proteins are lipoproteins attached to the external surface of the CM (Scheme 1B). Once these ferric ion complexes are delivered to the cytoplasm, they are either reduced to dissociate as ferrous ions from the complex or in some organisms, siderophores are broken down to release iron ions [4, 8, 14].

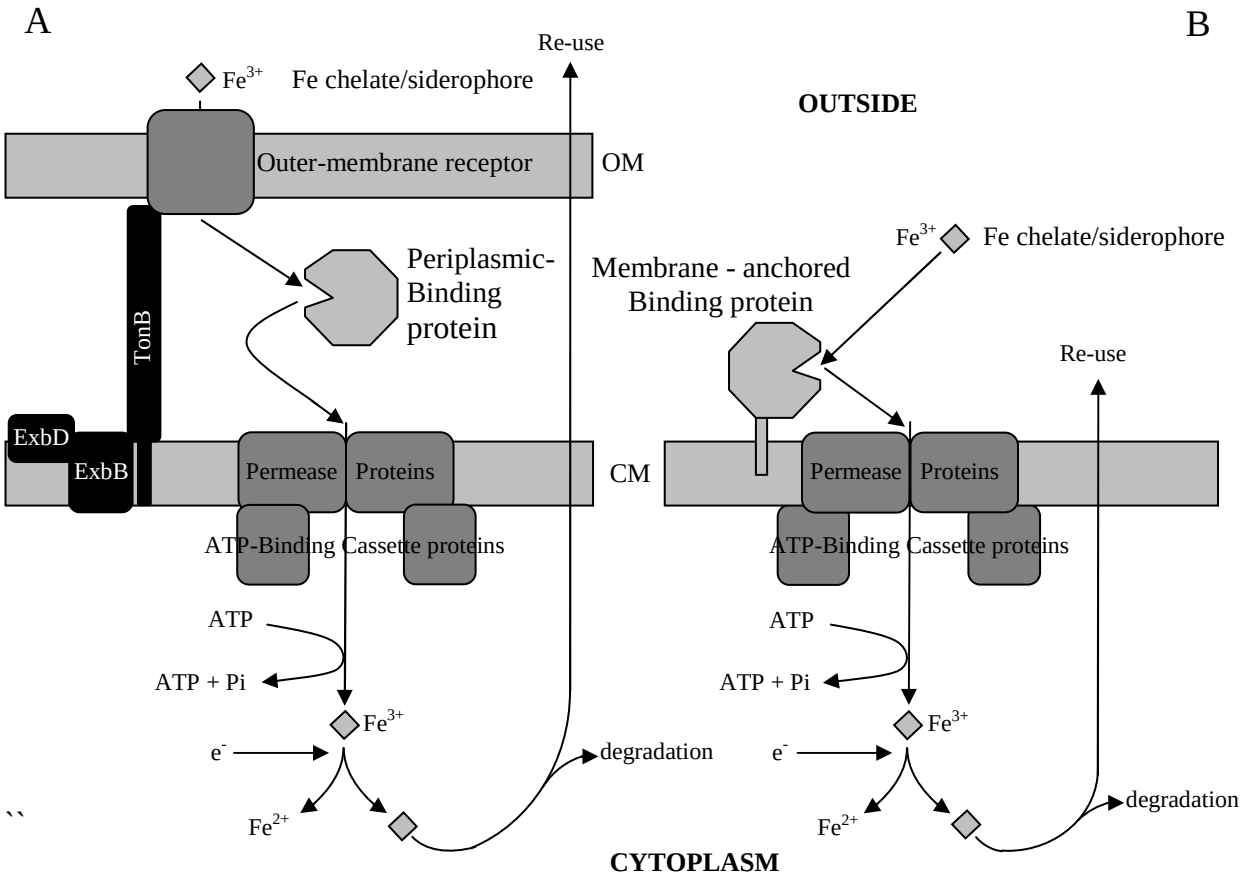

Scheme1: Schemetic representation of siderophore-mediated iron uptake by (A) Gram-negative and (B) Gram-positive bacteria (4).

In addition to siderophore mediated iron acquisition some bacteria have developed other efficient ways of acquiring iron from hosts. As an example, *Neisseria* sp. have been identified to possess transferrin and lactoferrin receptors in their OM and which are induced under iron depleted conditions. Transferrin and lactoferrin are mammalian iron binding proteins which maintain the free extracellular iron concentration at about 10^{-18} M. Bacterial tansferrin and lactoferrin receptors are capable of identifying apo- and holo- transferrin/lactoferrin. Once the holo lactoferrin/transferin is identified and bound by these receptors, iron is detached from the protein at the cell surface and is internalized. Subsequently, apo-lactoferrin/transferrin is released extracellularly [15, 16]

Heme is the most abundant form of iron in the body and unambiguously many pathogenic bacteria use heme as their main source of iron [4]. Extracellular pathogenic bacteria can access host heme, when heme and hemoglobin are liberated from the red blood cells by the catalytic action of enzymes such as hemolysins and proteases. Once heme is released from hemoglobin, host proteins such as hemopexin and albumin can bind these heme groups or on the other hand, pathogenic bacteria may directly transport those hemes into their cells. These bacteria have the ability to use heme, hemoglobin or hemopexin-heme complexes as their main sources of iron [4]. The OM receptors of Gram-negative bacteria can bind heme or heme omplexes and then the detached heme groups are internalized across the OM in a TonB-ExbB-ExbD dependent manner. In addition, some bacteria have the ability to secrete “hemophores” which can bind extracellular hemopexin and hemoglobin and transport these heme complexes to OM receptors. Later, these heme groups are delivered to the cytoplasm across the CM via ABC permeases. In the cytoplasm, heme is degraded by the enzyme heme oxygenase to release iron [17, 18].

Eventhough iron is an essential element for bacteria, a relatively high concentration of ferrous ions in the cytosol can cause severe damage to other biological macromolecules. Therefore, to overcome the potentially toxic effects and the poor availability of free iron, bacteria have evolved efficient ways of storing and maintaining cellular iron in a safe form. The most effective method utilized by many organisms including bacteria, is to store iron as an inorganic mineral inside a cavity of a special type of iron storage protein called ferritin or ferritin-like protein [19, 20].

Iron storage proteins

Bacteria and other organisms have evolved iron storage proteins to efficiently regulate their intracellular iron concentrations. These iron storage proteins have the ability to oxidize soluble and potentially toxic Fe^{2+} ions to Fe^{3+} ions and store the latter as a stable ferric iron mineral. When the extracellular iron becomes limited, the iron deposits contained inside iron storage protein can be mobilized to sustain metabolism. Three types of iron storage proteins have been identified and categorized into three sub-families, under the family of ferritins: the classic ferritins (Ftn), found in both prokaryotes and eukaryotes, the heme containing bacterioferritins (Bfr), present only in eubacteria (bacteria characterized by a rigid cell wall and, in motile types, flagella; the true bacteria) and the dodecameric ferritins (Dps, DNA binding proteins from starved cells) found only in prokaryotes [21]. Some organisms, however, have been shown to contain all three types of iron storage proteins and in some cases multiple ferritin and bacterioferritin genes exist. Although these three types of iron storage proteins are evolutionary distantly related, they tend to have similar structural and functional features [4, 22].

(1) Classic Ferritins (Ftn)

Ferritins, which are ubiquitous iron storage proteins found in both prokaryotes and eukaryotes, have evolved to sequester thousands of iron atoms in a mineralized, non toxic and bioavailable form. These supramolecular nanostructures are cytosolic proteins capable of oxidizing excess ferrous ions to ferric ions and storing them as an iron mineral. When exogenous iron becomes limited, the stored iron is used for various cellular biochemical reactions such as respiration, photosynthesis, DNA synthesis and nitrogen fixation, [6]. Another favorable consequence of storing iron as a mineral is that the cells are protected from the detrimental reactive hydroxyl radicals generated by ferrous ions [23, 24]. Abdul-Tehrani and co workers found two phenotypes upon deactivating the iron storage protein Ferritin A gene (*ftnA*) of *Escherichia coli*: (a) reduced growth rate under iron depleted conditions and (b) low cellular iron content (50%) in the stationary phase under iron replete conditions. These growth phenotypes were observed only when the medium was precultured with sufficient iron allowing ferritins to store iron during the post exponential growth. Thus, stored iron could be used as an intracellular iron source during subsequent growth under iron starvation conditions. Moreover, Ferritins from *Campylobacter jejuni and Helicobactor pylori* have also been found to play a role in promoting iron limited growth. These observations are in agreement with the important iron storage function played by ferritins in the cell. [4, 25-27]. As mentioned before, classic ferritins are found in both eukaryotes and prokaryotes. In the following, the well characterized eukaryotic ferrtin will be discussed first, followed by a description of the lesser understood bacterial ferritins and bacterioferritins.

Ferritins are polymeric proteins, composed of 24 subunits arranged as a dodecahedron with 4,3,2 octahedral symmetry (Figure 1-1A) that forms a hollow spherical assembly with a central cavity capable of holding approximately 4500 iron atoms. The diameter of the ferritin central cavity is ~8 nm and the external diameter is ~12 nm. The thickness of the protein shell, surrounding the cavity is ~2 nm. Each ferritin subunit is composed of five alpha helices (A-E) arranged in a four helix bundle (A-D) and a short C-terminal helix (E), which is perpendicular to the central axis of the four helix bundle (Figure 1-1B) [28-30].

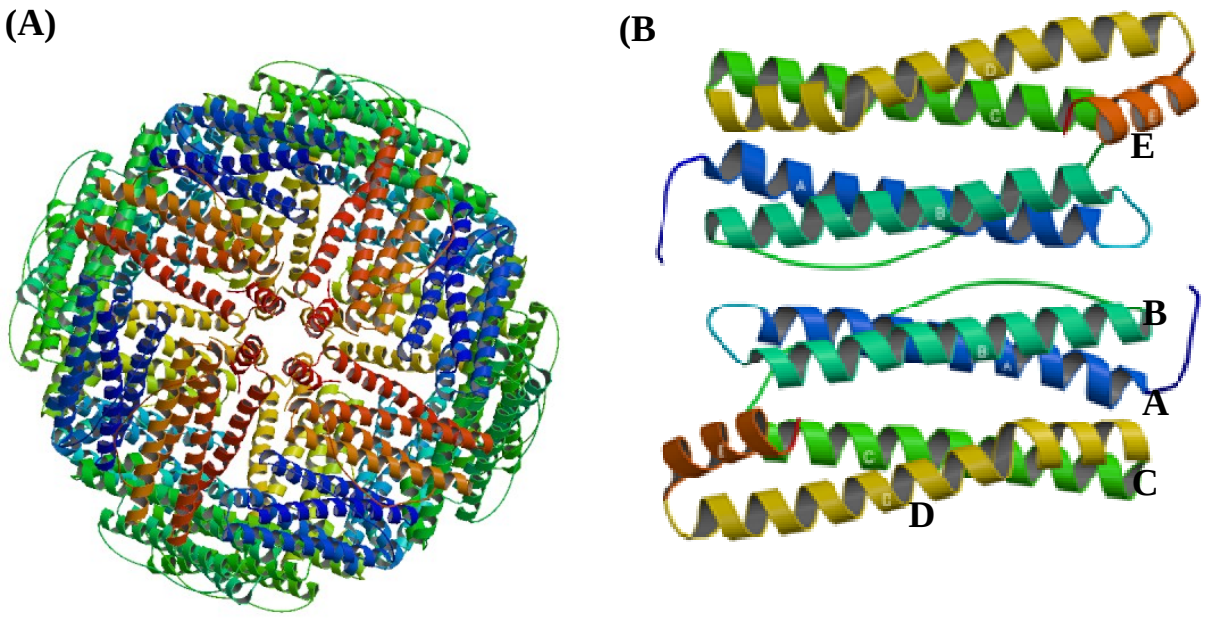

Figure 1-1: Crystal structures of a (A) 24-meric ferritin molecule from *E.coli* [28] (B) subunit dimer of a horse spleen ferritin [29].

Mammalian ferritins are heteropolymers composed of two types of subunits called H (heavy) chain and L (light) chain subunits. These two types of subunits are structurally homologous and have 55% of amino acid sequence identity. The ratio of H chain / L chain of

ferritins varies depending on the tissue from which the ferritin is originated. For example, the ferritins isolated from heart tissues have a high ratio of H chains / L chains whereas ferritins from liver tissues have a high ratio of L chains/H chains [31-34]. Eventhough these two types of subunits have a 55% amino acid sequence similarity, their functions are different. The H chain subunits have a dinuclear iron center in the middle of each four helix bundle, called ferroxidase center where oxidation of Fe^{2+} to Fe^{3+} occurs in the presence of oxygen. L chains do not have a ferroxidase center and therefore L-chain rich mammalian ferritins oxidize Fe^{2+} ions much slower than H-chain rich mammalian ferritins. Consequently, it is thought that these L-chain rich ferrtins are involved in forming crystalline iron particles of different sizes (nucleation) to initiate the formation of iron mineral inside the inner core [24]. Mamalian ferritins have six 4-fold and eight 3-fold pores located along the 4-fold and 3-fold symmetry axes of the molecule, respectively. These 3-fold pores have three highly conserved aspartate and glutamate residues located at the base of the pore, which make these pores hydrophilic in nature [9]. In addition, various metal ions have been observed bound to these 3-fold pores and therefore, it is believed that these 3-fold pores may act as main routes of iron entry and exit into the eukayotic ferritin cavity [35, 36]. In agreement with this notion, it has been observed that when the conserved Asp and Glu in 3-fold pores of mammalian ferritins are mutated, the ferroxidase activity and iron incorporation have been decreased [35]. Interactions of four subunits of the ferritin molecule form six 4-fold pores and these pores are lined with hydrophobic residues such as Leu. The function of these 4-fold pores in eukaryotic ferritins is not clear. However, since these pores are hydrophobic in nature, it is believed that these may be involved in diffusion of oxygen and hydrogen peroxide molecules in and out of the ferritin molecule [24, 34, 35, 36].

The bacterial counterparts of ferritin are called bacterial ferritins. Their structure is strikingly similar to human H-chain ferritin, despite modest amino acid sequence identity, ~ 22% [38]. The most understood bacterial ferritin is the FtnA from *E.coli.* Even though, there is another ferritin called FtnB in *E.coli*, it has not been well studied. Similar to eukaryotic ferritins, the bacterial ferritins are also made of 24 subunits arranged in a nearly spherical molecule. Each subunit has a ferroxidase center in the middle of each four helix bundle. Further, there are six 4-fold channels (diameter ~0.4 nm) aligned with the four fold axes of the molecule and are lined with hydrophobic residues in the central part and hydrophilic residues at both ends of the channels. The eight 3-fold channels (diameter ~0.4 nm), lined with both hydrophobic and hydrophilic residues, are formed at the three fold symmetry axes of the protein molecule. Bacterial ferritins have another type of channel, the so called B pores which are absent in eukaryotic ferritins. It is thought that the function of these B-pores may be similar to that of 3-fold channels of eukaryotic ferritns [28, 39]. Ferritins from other bacteria such as *Campylobactor jejuni* and *Helicobactor pylori* have been isolated and the crystal structures of those two bacterial ferritins have been observed to have many structural similarities to FtnA from *E.coli* [40, 41].

Recently two ferritins from the hyperthermophillic archea *Archaeoglobus fulgidis* and *Pyrococcus furiosis* have been structurally characterized. The 4,3,2 symmetry and other structural features of *P. furiosis* are similar to bacterial ferritins. However, the 24 subunits of *A. fulgidis* ferritins are arranged in 3, 2 tetrahedral symmetry instead of typical 4,3,2 octahedral symmetry found in other bacterial ferritins. There are four channels in these proteins, called super-pores which connect the mineral core with the outside environment. B-channels have also

been identified in these archaeal ferritins. However, as in other bacterial ferritins, the exact functions of these channels are not yet clearly known [42, 43].

(2). DNA binding proteins from starved cells (Dps)

Dps is another ferritin-like iron storage protein found in bacteria and archaea. Similar to classic ferritins, these are also polymeric proteins. Although Dps are distantly related to ferritin in terms of amino acid sequence, they share a few structural similarities with ferritins. Dps are composed of 12 subunits arranged in 4,3,2 octahedral symmetry (Figure 1-2A). Unlike the ferritin inner core, the Dps inner core can store only about 500 iron atoms and their ferroxidase centers are located between two adjacent subunits, where each of the two iron atoms of the ferroxidase center are coordinated by amino acid residues from two adjacent symmetry related subunits [19, 22].

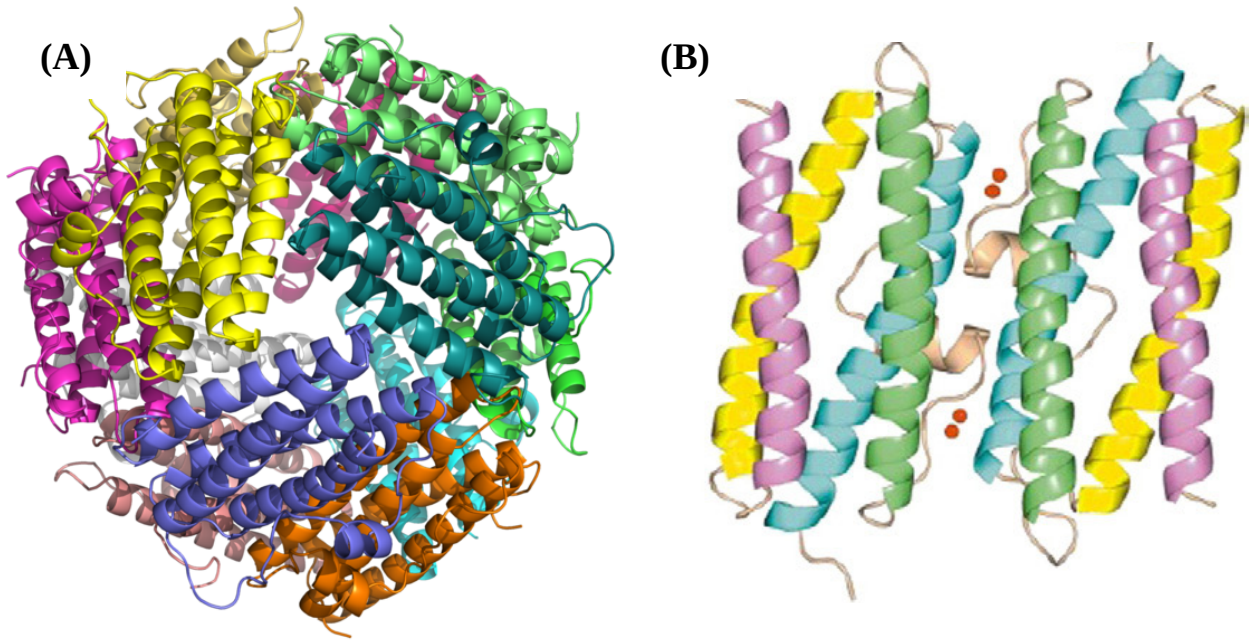

Figure 1-2: Crystal structures of (A) 12-meric Dps from *Listeria innocua* [44] and (B) a subunit dimer of Dps from *Bacillus brevis* [29].

The first Dps protein identified was from *E. coli*, a dodecameric sphere with a 4,3,2, symmetry. As is typical of Dps protein structure, the ferroxidase center of *E.coli* Dps is also located at inter subunit sites. However, Dps from *Listeria innocua* has only one Fe^{3+}ion at its ferroxidase center and the other Fe^{3+} ion site is occupied by a water molecule [4, 19]. The Dps protein isolated from *Streptococcus suis* uptakes iron through four hydrophilic pores found in that protein. Similar to H chain ferritins, the incorporated Fe^{2+} ions are oxidized by molecular oxygen at the ferroxidase center [45]. The composition of the Dps mineral core has not been well studied yet. However, X-ray absorption near edge structure (XANES) studies show that the mineral core of Dps from *Trichodesmium erythraeum* is comprised of octahedrally coordinated Fe^{3+} [46]. Dps is not considered as a major iron storing protein in the cell. Its main function is to protect cellular DNA from different nucleases and oxidative agents [23]. Under nutrient-limited conditions, such as during the stationary growth phase, cells do not have sufficient energy to synthesize new proteins or enzymes. Therefore it is difficult for bacteria to survive oxidative stress conditions during the stationary phase. Non-specific DNA-binding proteins such as Dps are expressed during the stationary phase and as a result, Dps is the most abundant protein during that growth phase. It has been found that Dps protects the chromosomal DNA from reactive oxygen species (ROS) under oxidative stress conditions during the stationary phase. Dps protein interacts directly with DNA and forms a stable, highly ordered nucleoprotein, called a biocrystal, by which DNA is protected from ROS [47]. On the other hand, Dps can also incorporate cellular free Fe^{2+} into its inner core as Fe^{3+} ions, thus limiting the production of hydroxyl radicals by fenton chemistry. It has been found that all Dps proteins have the ability to bind and sequester Fe^{2+} ions but only a few bacterial Dps proteins such as Dps from *E.coli* and *Mycobacterim smegmatis* can bind both iron and DNA. Eventhough no

relationship has been established between iron binding and DNA binding, all Dps proteins appear to function as DNA protecting proteins under oxidative stress conditions [48, 49].

(3). Bacterioferritins (Bfr)

Bacterioferritins are another group of bacterial iron storage proteins categorized under the broad family of ferritins [27]. As mentioned earlier, these proteins are heme containing iron storage proteins found exclusively in bacteria. Similar to classic ferritins, bacterioferritins play a very important role in iron storage and detoxification in the bacterial cell.

Discovery of Bacterioferritins

Bacterioferritins were earlier known as cytochrome b_1 and were originally discovered in *E. coli* by Keilin in 1934 [50]. The same protein was later purified independently from *E. coli* by Fujita *et a.l* [51] and Deeb *et al*. [52]. The purified cytochrome b_1 was spectrophotometrically characterized by its reduced electronic absorption spectrum which exhibits a Soret, α and β bands at 425, 557.5 and 527.5 nm, respectively. Consequently, this protein was also known as cytochrome $b_{557.5}$. The same protein was later purified from *E.coli* strain K-12 by Yarive *et al.* and this protein was observed to have similar structural features to the recombinant bacterial ferritin (FtnA) isolated from *E.coli.* Therefore, this novel protein was named as bacterioferritin [53]. Subsequently, "cytochrome b_1" isolated by the Deeb and Harber method and "bacterioferritin", obtained via antibody precipitation method of Yarive, were independently expressed, purified and crystallized. The crystallographic data of the two proteins were compared and it was concluded that both cytochrome b_1 and bacterioferritin were in fact the same protein [52].

Structure of Bacterioferritins

Bacterioferritins are polymeric proteins made of 24 subunits are arranged in 4,3,2 octahedral symmetry to form a nearly spherical protein with a hollow cavity (Figure 1-3A). Each subunit is made of five alpha helices (A-E) in which four of the helices (A-D) are arranged parallel to each other and the C terminal short fifth helix (E) is perpendicular to the central axis of the four helix bundle (Figure 1-3B) [28].

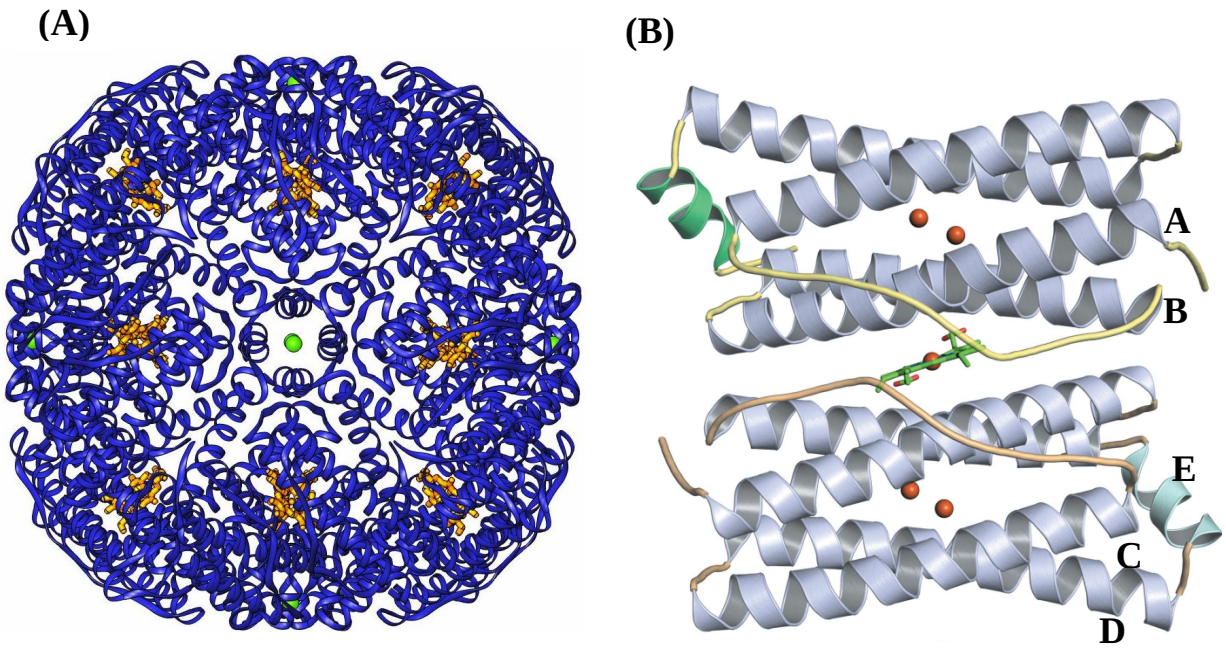

Figure 1-3: Crystal structures of (A) 24-meric BfrB from *P. aeruginosa* and (B) a subunit dimer of Bfr from *E.coli* [71] showing the heme group located between two adjacent subunits and the two ferroxidase iron atoms in the middle of each subunit.

Even though the Bfr subunits are structurally similar to H-chain ferritin subunits, their amino acid sequence identity is only 20%. Bfrs are unique in the family of ferritins as they can bind 12 heme groups per Bfr molecule. These heme groups are located at inter subunit sites, coordinated

by two methionine residues (Met52) from two adjacent subunits related to one another by 2-fold symmetry. The heme macrocylcle is attached to the protein by non-covalent interactions and the coordination of iron by Met 52 via a bis-thioether axial coordination. The heme iron is low spin in both oxidation states, suggesting a possible function of heme in electron transport [39, 54]. Although most Bfrs contain iron-protoporphyrin IX (heme), Bfr from *Desulfovibrio desulfuricans* has iron-coproporphyrin III instead of heme [39]. The ferroxidase center of Bfr is located in the middle of each subunit and similar to bacterial feritins and mammalian H-chain ferritins, it is also a dinuclear ion center made of two iron ions coordinated by six amino acid residues. In contrast to the structure of the ferroxidase centers of mammalian and bacterial ferritins, however, the ferroxidase center of Bfr is symmetric (Figure 1-4). As shown in the figure below, each His and Glu residues act as capping ligands to iron ions while the other two Glu residues act as bridging ligands to the two iron ions.

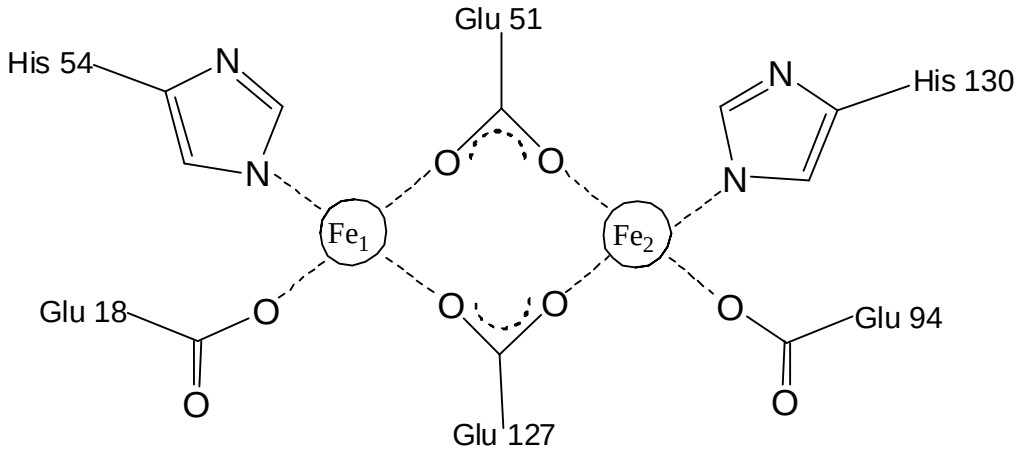

Figure 1-4: Schematic representation of the structure of symmetric ferroxidase center in Bfr.

Similar to mammalian and bacterial ferritins, Bfrs also have eight 3-fold channels and six 4-fold channels along the three fold and six fold symmetry axes of the molecule, respectively.

The 4-fold pores of bacterioferritins are hydrophilic whereas the 4-fold pores of mammalian ferritins are hydrophobic. Similar to mammalian ferritins, 3-fold pores of Bfrs are hydrophilic. But the pore forming residues are not conserved between mammalian ferritins and Bfrs [39]. In addition to 4-fold and 3-fold pores, the B pores are located at the interface of two Bfr subunit dimers and these B pores are thought to have the same function as 3-fold pores of mammalian ferritns. The amino acid residues Glu/Gln135, Glu132, Glu66 and Asn/Glu34, lining these B pores are well conserved among Bfrs (Figure 1-5) [70]

Bfr from Pseudomonas aeruginosa

Bfrs have been isolated and characterized from many different types of bacteria such as *E.coli, A.vinelandii, D.desulfuricans, and R.capsulatus*; all these Bfrs are homopolymers. Bacteria such as *Pseudomonas aeruginosa, Pseudomonas putida* and cynobacterium *Synechocystis,* on the othr hand, were thought to have two types of subunits [39]. For example, early studies of Bfr from *P. aeruginosa* suggested that this protein is made of two subunits, called α and β. The relative proportions of the two subunits, however, varied from preparation to preparation and the α-subunit was consistently the most abundant [38]. More recent studies on Bfr from *P aeruginosa* have established that there are two genes coding for two Bfr proteins (BfrA and BfrB), termed *bfrA* and *bfrB* respectively [56]. When the amino acid sequences of BfrA and BfrB are compared with those corresponding to Bfrs from *E.coli* [57], *Azotobacter vinelandii* [58] and *Mycobacterium smegmatis* [59] (Figure 1-6), it is interesting to observe that the Met52 is absent from the sequence of BfrA. This observation suggests that BfrA may not bind heme, although, the amino acid residues that coordinate the diiron ferroxidase center are conserved in all sequences shown in figure 1-6. Hence, eventhough BfrA does not bind heme, it

may bind ferroxidase iron and exhibit the ferroxidase activity. Consequently, the term bacterioferritin A (BfrA) may not be the correct term for this protein as it likely does not bind heme. Therefore, it may be more appropriate to state that the *bfrA* gene likely codes for a bacterial ferritin but not a heme binding bacterioferritin. Consequently, the only bacterioferritin from *P. aeruginosa* is called BfrB. Our research was aimed at isolating, characterizing and understanding the mechanisms of iron trafficking and the role in cellular iron homeostasis of BfrB from *P.aeruginosa.*

```
                      10        20        30        40        50        60
                       |         |         |         |         |         |
Pa-BfrB               MKGDKKVIQHLNKILGNELIAINQYFLHSRMWNDWGLKRLGAHEYHESIDEMKHADKLIE
A.vinelandii          MKGDKIVIQHLNKILGNELIAINQYFLHARMYEDWGLEKLGKHEYHESIDEMKHADKLIK
E. coli               MKGDTKVINYLNKLLGNELVAINQYFLHARMFKNWGLKRLNDVEYHESIDEMKHADRYIE
M.smegmatis           MQGDPDVLKLLNEQLTSELTAINQYFLHSKMQDNWGFTELAEHTRAESFEEMRHAETITD
R.capsulatus          MKGDAKVIEFLNAALRSELTAISQYWVHFRLQEDWGLAKMAKKSREESIEEMGHADKIIA
Pa-FtnA               MQGHPEVIDYLNTLLTGELAARDQYFIHSRMYEDWGFSKLYERLNHEMEEETQHADALLR

                      70        80        90       100       110       120
                       |         |         |         |         |         |
Pa-BfrB               RILFLEGLPNLQDLGKLLIGENTQEMLQCDLNLELKATKDLREAIVHCEQVHDYVSRDLL
A.vinelandii          RILFLEGLPNLQELGKLLIGEHTKEMLECDLKLEQAGLPDLKAAIAYCESVGDYASRELL
E. coli               RILFLEGLPNLQDLGKLNIGEDVEEMLRSDLALELDGAKNLREAIGYADSVHDYVSRDMM
M.smegmatis           RILLLDGLPNYQRLFSLRVGQTLREQFEADLAIEYEVLERLKPGIVLCREKQDATSARLL
R.capsulatus          RILFLEGHPNLQKLDPLRIGEGPRETLECDLAGEHDALKLYREARDYCAEVGDIVSKNIF
Pa-FtnA               RILLLEGTPRMRPD.DIHPGTTVPEMLEADLKLERHVRAALAKGIALCEQ HKDFVSRDI

                     130       140       150       160
                      |         |         |         |
Pa-BfrB               KDILESEEEHIDYLETQLGLIQKVGLENYLQSHMHEDD---
A.vinelandii          EDILESEEDHIDWLETQLDLIDKIGLENYLQSQMDE-----
E. coli               IEILRDEEGHIDWLETELDLIQKMGLQNYLQAQIREEG---
M.smegmatis           EQILADEETHIDYLETQLQLMDKLGDALYAAQCVSRPPGSA
R.capsulatus          ESLITDEEGHVDFLETQISLYDRLGPQGFALLNAAPMDAAE
Pa-FtnA               LKAQLADTEEDHAYWLEQQLGLIARMGLENYLQSQI
```

Figure 1-5: Bacterioferritin sequences from different organisms aligned against *P. aeruginosa* BfrB and FtnA: Residues involved in the ferroxidase center, as well as Met-52 (highlighted in red), which coordinates the heme axially and the residues lining B pores (highlighted in blue) , are shown. The sequences were aligned with the aid of ClustalW [60].

BfrB from *P aeruginosa* (Pa-BfrB) has not been recombinantly overexpressed or characterized before. It was overexpressed, isolated, purified and characterized for the first time in our laboratory [55], as part of the research description in chapter 2. Our investigations show that Pa-BfrB has a molecular architecture typical of bacterioferritins, with an external diameter of ~118 Å and an internal cavity diameter of ~73 Å. Pa-BfrB has an intra subunit ferroxidase center where two iron atoms (Fe_1 and Fe_2) are coordinated by four glutamate and two histidine residues. The two ferroxidase iron atoms of Pa-BfrB are coordinated to Glu18/His54 (Fe_1) and Glu94/His130 (Fe_2) and Glu51/Glu127 act as the bridging ligands connecting Fe_1 and Fe_2. Since this coordination generates a highly symmetrical ferroxidase center, it is categorized as a class II dinuclear iron center, similar to the dinuclear iron centers found in the hydroxylase subunit of methane monooxygenase and R2 subunit of ribonucleotide reductase [61, 62]. The ferroxidase center ligands of many Bfr proteins are positioned to bind iron. However, His 130 of *P. aeruginosa* has been observed to undergo a conformational change before it binds iron [63]. More details of the structure of ferroxidase center will be presented in chapter 2. As is typical of Bfrs, Pa BfrB binds 12 heme groups. These are located at inter subunit sites, coordinated by two methionine residues (Met52) from adjacent subunits. The function of the heme groups in Bfrs were not known before. The research carried out in our laboratory discovered the function of heme in Bfrs for the first time. It has been found that heme in Pa-BfrB act to mediate electrons from a reductase into the inner cavity of the protein to reduce the ferric iron mineral [55]. More details of those experiments will be in chapter 3. Similar to ferritins, the symmetric arrangement of BfrB subunits has generated several types of channels through the protein shell. Pa-BfrB has eight 3-fold channels and six 4-fold channels. In addition to these channels, there are twelve other channels called B-channels which are found where one subunit dimer meets the other.

However, the function of these specific channels is not yet clearly established [39]. Nevertheless, it has been postulated that in *P. aeruginosa*, anions such as phosphate and cations such as iron are taken into the inner core via 3-fold and 4-fold channels respectively.

General mechanism of iron uptake by Bacterioferritins

Bfr from *E.coli* (Ec-Bfr) is the most studied and well characterized bacterioferritin. Therefore, in the following text, the iron uptake mechanism of Ec-Bfr will be presented, which previous to our investigations was considered to be the mechanism of iron uptake utilized by all bacterioferritins. It is noteworthy, however, that our research uncovered a different mechanism for iron uptake by Pa-BfrB. Details regarding of these findings will be presented in chapter 2.

X.Yan and co workers have established the mechanism of iron uptake by Ec-Bfr. According to their findings, this process is explained in three basic steps [64]:

(1) Binding of Fe^{2+} ions at the ferroxidase center (phase 1),

(2) Oxidation of Fe^{2+} to Fe^{3+} (phase 2)

(3) Mineralization of Fe^{3+} ions in the inner cavity (phase 3).

Phase 1 has been identified as the fastest phase ($t_{1/2}$ ~50 ms) in the iron uptake mechanism.

$$2Fe^{2+} + P^z \leftrightarrow [Fe_2 - P]^z + 4H^+ \qquad \text{Phase 1}$$

P^z and $[Fe_2 - P]^z$ represent the apoprotein with a net charge Z and the diferrous complex at the ferroxidase center respectively, two Fe^{2+} ions are bound to the ferroxidase center forming a diferrous complex and releasing four protons. Two of these protons are thought to be released from the deprotonation of two histidine residues, the source of the other two protons is not clear,

but could be derived from two of the four glutamate residues at the ferroxidase center. Phase 2 of the reaction corresponds to the oxidation of Fe^{2+} to Fe^{3+} at the ferroxidase center and is much slower phase than phase 1. When Fe^{2+} ions are oxidized at the ferroxidase center, a diferric complex $[Fe_2O - P]^z$ or most probably a μ-oxo-bridged diferic complex is thought to be formed.

$$[Fe_2 - P]^z + \frac{1}{2}O_2 \rightarrow [Fe_2O - P]^z \qquad \text{Phase 2}$$

Phase 3 corresponds to the mineralization of Fe^{3+} ions in the inner core and is the slowest phase ($t_{1/2}$ ~300 ms) in the model [64]. Therefore the overall reaction including the oxidation of Fe^{2+} ions (phase 2) and the mineralization (pahse 3) can be written as follows,

$$4Fe^{2+} + O_2 + 6H_2O \rightarrow 4FeO(OH)_{core} + 8H^+$$

The three phases mentioned above in *E. coli* have also been identified in *P aeruginosa*. However, our investigations carried out with Pa-BfrB indicate that the rates of the phases of iron uptake are quite different from those of *E.coli* and also suggest a different mechanism of iron uptake [63]. The results of those investigations will be discussed in detail in chapter 2.

Once Fe^{2+} ions are oxidized to Fe^{3+} at the ferroxidase center, they migrate to the inner core to form the iron mineral which is composed mainly of iron and phosphate. The ratio of iron/phosphate, however, varies depending on the type of ferritin molecule. Animal ferritins have been observed to have a higher ratio of iron/phosphate than that of bacterial ferritins and bacterioferritins [67]. In addition, high resolution electron microscopy and electron diffraction data have shown that phosphate rich cores of bacterioferritins are disordered, whereas the mineral cores of mammalian ferritin are ordered with diffraction properties similar to Ferrihydrite ($5Fe_2O_3.9H_2O$) [67-69].

Research Problem and Rationale

Iron is used as a cofactor in many important proteins such as cytochromes, electron transfer and respiratory proteins, by many bacteria including the opportunistic pathogen *Pseudomonas aeruginosa.* Therefore iron is considered an essential element for successful colonization and infection of *P aeruginosa* in host organisms [65]. The concentration of free iron in the host cell, however, is very low (~10^{-9} M). In addition, the iron concentration in extracellular fluid and on mucosal surfaces of mammalian hosts is very limited as these iron ions are sequestered by mammalian iron binding proteins, such as transferring and lactoferrin [66]. To overcome the poor availability of this essential nutrient, many pathogenic bacteria including *P aeruginosa* have evolved efficient regulatory systems to sequester, uptake, and manage iron [65].

Recent findings suggest that iron, particularly heme-iron, is essential for successful colonization (infection) of mammalian hosts [3]. The above findings imply that molecules capable of inhibiting iron/heme-iron acquisition pathways or interfering with iron trafficking mechanisms in *P. aeruginosa* may constitute a new class of antibiotics. Therefore, a molecular level understanding of iron storage proteins, iron acquisition paths, regulation mechanisms and metabolism is required, in order to rationally develop drugs to combat *Pseudomonas* infections In *P.aeruginosa*, BfrB, one of the iron storage proteins in the cell, is capable of storing thousands of iron atoms in the form of a ferric ion mineral, which can be released in the soluble form (Fe^{2+}) when needed for various cellular reactions. However, as mentioned before, the mechanisms of iron uptake and release by Pa-BfrB, and its physiological partners involved in these processes are not so far known. Consequently, our studies were focused on characterizing Pa-BfrB,

understanding its mechanisms of iron uptake and release, and identifying its physiological partners involved in these iron regulatory mechanisms. This fundamental work is expected to ultimately use for the elucidation of the protein-protein interactions that facilitate iron acquisition and subsequent iron-metabolism inside *P. aeruginosa* and the development of small molecules (antibiotics) that interfere with those protein protein interactions. To this end, a series of ground breaking studies on Pa-BfrB were carried out in our laboratory and we believe that our findings are yielding important foundational understanding which paves the way toward the development of antimicrobials that target iron homeostasis.

BfrB from *P. aeruginosa* was first overexpressed and purified to homogeneity. Then as chapter 2 reveals, the protein was biochemically characterized using UV-vis spectroscopy. To elucidate the pathway of iron uptake by *P. aeruginosa*, apo and holo/mineralized BfrB were crystallized and their structures analyzed in detail by X – ray crystallography. To corroborate some of the findings obtained from iron uptake studies by crystallography, iron incorporation assays were carried out in solution using stopped flow spectroscopy. The results of these studies are presented in chapter 2 with a detailed discussion of the results. Two other proteins from *P.aeruginosa*, namely, Ferredoxin NADP reductase (Fpr) and Bacterioferritin associated ferredoxin (Bfd) are believed to be involved as the physiological partners of BfrB in the release of iron from the mineral core. In order to investigate the above hypothesis protein-protein interaction assays were carried out with BfrB, Fpr and Bfd, and these results are presented in detail in chapter 3. The effect of Bfd on the rate of iron release from BfrB core was investigated by carrying out protein assays with different Bfd concentrations. In addition, the function of the heme group in BfrB was also established for the first time in our laboratory. Details regarding these findings are presented in chapter 3. As chapter 2 reveals, Pa-BfrB has six 4-fold, eight 3-

fold and 12 B-pores connecting the mineral core with the outside environment. The specific functions of these pores and their importance in iron regulation inside the cell are not yet clearly established. However, some of our structural findings led us to hypothesize that the four fold pores may be the routes of iron release from the inner core. In order to investigate this hypothesis and to elucidate the pathway and the residues involved in moving iron out of the protein, site directed mutagenesis studies were carried out on possible iron coordinating amino acid residues in the 4-fold pore. Iron mobilization experiments were carried out with one of the mutants of BfrB, truncated BfrB, and the rates of iron release were compared with those of wild type in order to gain a better understanding on the pathway of iron release from the inner core of BfrB. Elastic Network Model calculations were also used to corroborate our findings on the process of iron release. Chapter 4 is devoted to a discussion of our experimental results in the context of the above findings. However, further investigations are required to gain a molecular level understanding of iron regulatory mechanisms inside the cell which may lead to a discovery of an important approach to prevent or treat pseudomonas infections in the host.

References

[1] van Delden, C (2004) .Virulence Factors in *Pseudomonas aeruginosa*. *Pseudomonas* 2, 3-45.

[2] Lambert, P.A. (2002) Machanisms of Antibiotic Resistance in Pseudomonas aeruginosa. *Journal of Royal Soiety of Medicine* 95, 22-26.

[3] Weele, R., Tasler, R., Zeng, Y., Rivera, M., et.al. (2004) The Heme oxygenase(s) - Phytochrome System of *Pseudomonas aeruginosa. The Journal of Biological Chemistry*, 279, 45791-45802.

[4] Andrews, S.C.; Robinson, A.K.; Rodriguez-Quinones, F. (2003) Bacterial Iron Homeostasis. *FEMS Microbiology Reviews* 27, 215-237.

[5] Harrison, P.M.; Andrews, S.C.; Artymiuk, G.C.; Ford, G.C.; Guest, J.R.; Hirzmann, D.M.; Lawson, D.M.; Livingstone, J.C.; Smith, J.M,A.; Treffry, A.; Yewdall, S.J. (1991) Probing Structure-Function Relations in Ferritin and Bacterioferritin. *Advances in inorganic chemistry* 36, 449-485.

[6] Carrando, M.A. (2003) Ferritins, Iron Uptake and Storage from the Bacterioferritin Veiwpoint. *The EMBO journal* 22, 1959-1968.

[7] Andrews, S.C. (1998) Iron Storage of Bacteria. *Advances in microbial physiology* 40, 281-351.

[8] Arguin, M.; Massé, E. (2005) Ironing out the problem: New Mechanisms of Iron Homeostasis. *TRENDS in biochemical sciences* 30, 462-467.

[9] Harrison, P.M.; Arosio, P. (1996) The Ferritins:Molecular Properties, Iron Storage Function and Cellular Regulation. *Biochimica et Biophysica Acta* 1275, 161-203.

[10] Guerinot, M.L. (1994) Microbial Iron Transport. *Annual Review of Microbiology* 48, 743-772.

[11] Cowart, R.E.; Foster, B.G. (1985) Differential Effects of Iron in the Growth of *L.monocytogenes*: Minimum Requiremnets and Mechanism of Acquisition. *Journal of Infectious Disease* 151, 721-730.

[12] Byers, B.R.; Arceneaux, J.E.L.(1998) Microbial Iron Transport: Iron acquisition by pathogenic microorganisms. In: metal ions in Biological Systems (Sigel, A and Sigel, H., Eds) Vol 35 pp. 37-66.

[13] Braun, V. (1985) The Iron Transport Systems of *Escherichia coli*: The enzymes of Biological Membranes (Martonosi, A.N., Ed) pp.617-652. Plenum press, New York.

[14] Baquero, F.; Delgado-Iribarren, A.; Martinez, J.L. (1990) Mechanisms of Iron Acquisition and Bacterial Virulence. *FEMS Microbiology Reviews* 75, 45-56.

[15] Bullen, J.J.; Rogers, H.J.; Griffiths, E. (1978) Role of Iron in Bacterial Infection. *Current Topics in Microbiology and Immunology* 80, 1-35.

[16] Cornelissen, C.N.; Sparling, P.F. (1994) Iron Piracy: Acquisition of Transferrin Bound Iron by Bacterial Pathogens. *Molecular Microbiology* 14, 843-850.

[17] Wang, A.; Zeng, Y.; Han, H.; Weeratunga, S.; Morgan, B.M.; Moënne-loccoz, P.; Schönbrunn, E,; Rivera, M. (2007) Biochemial and Structural Chracterization of Pseudomonas aeruginosa Bfd and Fpr: Ferredoxin $NADP^+$ Reductase and Not Ferredoxin is the Redox partner of Heme Oxygenase unde Iron Starvation Conditions. *Biochemistry* 46, 12198-12211.

[18] Genco, C.A.; Dixon, D.W. (2001) Emerging Strategies in Microbial Heme Capture. *Molecular Microbiology* 39, 1-11.

[19] Lewin, A.; Moore, G.R.; Le Brun, N.E. (2005) Formaton of Protein Coated Minerals. *The Royal Society of Chemistry*, 3597-3610.

[20] Crow, A.; Lawson, T.L.; Lewin, A.; Moore, G.R.; Le Brun, N.E. (2009) Structural Basis for Iron Mineralization by Bacterioferritin. *Journal of American Chemical Society 131, 6808-6813.*

[21] Andrews, S.C. (2010) The Ferritin –like Superfamily: Evolution of the Biological Iron Storeman froma rubreythin-like Ancestor. *Biochimica Biophysica Acta* 1800, 691-705.

[22] Castruita, M.;Elmegreen, L.A.,Shaked, Y.; Steifel, E.I.; morel, F.M.M. (2007) Comparison of the Kinetics of Iron Release from a Marine (*Trichodesmium erythrium*) Dps Protein and Mamalian Ferritttin in the Presence and Absence of Ligands. *Journal of Inorganic Biochemistry* 101, 1686-1691.

[23] Smith, J.L. (2004) The Physiological Role of Ferritin-Like Compounds in Bacteria. *Critical Reveiws in Microbiology* 30, 173-185.

[24] Abdallah, F.B (2010) The iron Redox and Hydrolysis Chemistry of the ferritins. *Biochimica et Biophisica Acta* 1800, 719-731.

[25] Wai, S.N.; Nakayama, K.; Umen, K.; Moriya, T.; Amako, K. (1996) Construction of Ferritin-defecient mutant of *Campylobacter jejuni*: Contribution of Ferritin to Iron Storage and Protection against Oxidative Stress. *Molecular Microbiology* 20, 1127-1134.

[26] Bereswill, S.; Waidner, U.; Odenbreit, S.; Lichte, F.; Fassbinder, F.; Bode, G.; Kist, M. (1986) Structural, Functional and Mutational Analysis of of the *pfr* Gene Encoding a Ferritin from *Helicobactor pylori*. *Microbiology* 144, 2505-2516.

[27] Abdul-Tehrani, H.; Hudson, J.A.; Chang, y.; Timms, A.R.; Hawkins, C.; Williams, J.M.; Harrison, P.M.; Guest, J.R.; Andrews, S.C. (1999) Ferritin Mutants of *Escherichia coli* Are Iron Deficient and Growth Impaired, and *fur* Mutants are Iron Deficient. *Journal of Bacteriology* 181, 1415 -1428.

[28] Le Brun, N.E.; Crow, A.; Murphy, M.E.P.; Mauk, A.G.; Moore, G.R. (2010) Iron Core Mineralisation in Prokaryotic Ferritins. *Biochimica et Biophysica Acta* 1800, 732-744.

[29] Crichton, R.R.; Declercq, J. (2010) X-ray Structures of Ferritins and Related Proteins. *Biochimica et Biophysica Acta* 1800, 706-718.

[30] Shi, H.; Bencze, K. Z.; Stemmler, T.L.; Philpott, C.C. (2008) A Cystolic Iron Chaperon that Delivers Iron to Ferritin. Science 320, 1207-1210.

[31] Watt, R.K.; Hilton, R.J.; Graff, D.M. (2010) Oxido-Reduction is not the Only Mechanism Allowing Iron to Traverse the Ferritin Protein Shell. *Biochimica etBiophysica Acta* 1800, 745-759.

[32] Chasteen, N.D.; Harrison, P.M. (1999) Mineralization in Ferritin: An Efficient Means of of Iron Storage. *Journal of Structural Biology* 126, 173-185.

[33] Santambrogio, P.; Levi, S.; Cozzi, A,; Corsi, B.; Arosio, P.(1996) Evidence that the Specificity of Iron Incorporation into Homopolymers of Human Ferriin L- and H- C is Conferred by the Nucleation and Ferroxidase Centers. *Journal of Biochemistry* 314, 139-144.

[34] Douglas, T.; Ripoll, D.R. (1998) Calculated Electrostatic Gradients in Recombinant Human H-Chain Ferritin. *Protein Science* 7, 1083-1091.

[35] Levi, S.; Santambrogio, P.; Corsi, B.; Cozzi, A.; Arosio, P. (1996) Evidence that Residues Exposed on the Three-Fold Channels have Active Roles in the Mechanism of Ferritin Iron Incorporation. *Biochem. J*. 317, 467-473

[36] Theil, E.C.; Takagi, H.; Small, G.W.; He, L,;Tipton, A.R.; Danger, D. (2000) The Ferritin Iron Entry and Exit Problem. *Inorganica Chimica Acta* 297, 242-251.

[37] Takahashi, T.; Kuyucak, S. (2003) Functional Properties of Threefold and Fourfold Channels in Ferritin Deduced from Electrostatic Calculations. *Biophys.J*. 84, 2256-2263.

[38] Moore, G.R.; Kadir, H. A.; Al-Masad, K.; Le Brun, N.E.; Thomson, A.J; Greenwood, C.; Keen, J. N.; Findlay, J. B. C. (1994) Structural Heterogeneity of Pseudomonas aeruginosa Bacterioferritin, *Biochemistry* 304, 493-497.

[39] Macedo, S.; Romao, C.V.; Mitchelle, E.; Matias, P.M.; Liu, M.Y.; Xavier, A.V.; Legall, J.; Teixeira, M.; Lindley, P.; Carrondo, M.A.; (2003) The Nature of the di-iron Site in the

Bacterioferritin from *Desulfovibrio desulfuricans*. *Nature Structural Biology* 10, 285-290.

[40] Clerte, S.; Dautant, A,; d'Estaintot, B.L.; Gallios, B.; Mizunoe, Y.; Wai, S. N.; Preciguox, G. (1999) Expression, Purification, Crystallization and Preliminary X-Ray Diffraction Results from *Campylobacter jejuni* Ferritin. *Acta Crystallographica D Biological Crystallography* 55, 299-301.

[41] Cho. K. J.; Shin, H. J.; Lee, J. H.; Kim, K. J.; park, S. S.; Lee, Y.; Lee, C.; Kim, K.H. (2009) The Crystal Structure of Ferritin from Helicobacter pylori Reveals Unusual Conformational Changes for Iron Uptake. *Journal of Moecular Biology* 390, 83-98.

[42] Johnson, E.; Cascio, D.; Sawaya, M.R.; Gingery, M.; Schroder, I.(2005) Crystal Structures of a Tetrahedral Open Pore Ferritin from the Hyperthermophylic Archaeon *Archaeoglobus fulgidis*. *Structure* 13, 637-648.

[43] Tatur, J.; Hagen, W.R.; Matias, P.M. (2007) Crystal Structure of the Ferritin from the Hyperthermophylic Archael anaerobe *Pyrococcus furiosis*. *Journal of Biological Inorganic Chemistry* 12, 615-630.

[44] Ilari, A.; Stefanini, S.; Chiancone, E.; Tsernoglou, D. (2000) The Dodecameric Ferritin from *Listeria innocua* Contains a Novel Intersubunit Iron-Binding Site. *Nature structuralBiology* 7, 38-43

[45] Pulliainen, A.T.; Kauko, A.; Haataja, S.; Papageorgiou, A.C.; Finne, J. (2005) Dps/Dpr Ferritin-Like Protein: Insights into the Mechanism of Iron Incorporation and Evidence for a Central Role in Cellular Iron Homeostasis in *Streptococcus suis. Molecular Microbiology* 57, 1086-1100

[46] Castruita, M.; Saito, M.; Schottel, P.C.; Elmgreen, L.A.; Myneni, S.; Stiefel, E.I.; Morel, F.M.M. (2006) Overexpression and Characterization of an Iron Storage and DNA-Binding Dps Protein from *Trichodesmium erythraeum. Applied Environmental Microbiology* 72, 2918-2924.

[47] Hong, Y.; Wang, G.; Maier, R. (2006) *Helicobacter hepaticus* Dps Proteins Plays an Important Rrole in Protecting DNA from Oxidative Damage. *Free radical Research* 40, 597-605.

[48] Wolf, S.G.; Frenkiel, D.; Arad, T.; Finkel, S.E.; Kolter, R.; Minskey, A. (1999) DNA protection by Stress-Induced biocrystallization. *Nature* 400, 83-85

[49] Gupta, S.; Chatterji, D.(2003) Bimodal Protection of DNA by *Mycobacterim smegmatis* DNA-binding protein fron Stationary phase Cells. *Journal of Biological Chemistry* 278, 5235-5241.

[50] Keilin, D. (1934) Cytochrome and the Direct Spectroscopic Observation of Oxidase. *Nature*, 133, 290-291.

[51] Fujita, T.; Itagaki, E.; Sato, R.; (1963) Purification and Properties of Cytochrome b_1 from *Escherichia coli*. *Journal of Biochemistry* 53, 282-290.

[52] Deeb, S.S.; Hager, L.P.; (1964) Crystalline cytochrome b_1 from *Escherichia coli*. *Journal of Biochemistry* 239, 1024-1031.

[53] Yarive. J.; Kalb, A.; Sperling, R.; Bauminger E.R. (1981) The Composition and the Structure of Bacterioferritin of *Escherichia coli. The Biochemical Journal* 197, 171-175.

[54] Moore, G.R.; Mann, S.; Bannistre, J.V (1986) Isolation and Properties of the complex Nonheme-Iron Containig Cytochrome b557 (Bacterioferritin) from *Pseudomonas aeruginosa. Journal of Inorganic Biochemistry* 28, 329-336.

[55] Weeratunga, S.K.; Gee, C.E.; Lovell, S.; Zeng, Y.;Woodin,Y.; Rivera,M. (2009) Binding of Pseudomonas aeruginosa Apobacterioferritin-Associated Ferredoxin to bacterioferritin B Promotes the Heme Mediation of Electron Delivery and Mobilization of core Mineral Iron. *Biochemistry 48,* 7420-7431.

[56] Ma, J.F.; Ochsner, U.A.; Klotz,M.G,; Nanayakkara, V.K.;Howell, M.L.; Johnson, Z.; Posey, J.E.; Vasil, M.L.; Monaco, J.J.;Hasset, D.J. Bacterioferitin A Modulates Catalase A (KatA) Activity and Resistance to Hydrogen peroxide in *Pseudomonas aeruginosa*. (1999) *Journal of Bacteriology* 181, 3730-3742.

[57] Frolow, F.; Kalb, A.J.; Yarive, J. (1994) Structure of a Unique Twofold Symmetric Haem- Binding Site. *Nature Structural Biology* 1, 453-460.

[58] Liu, H.L.; Zhou, H. N.; Xing, W. M.; Zhao, J. F.; Li, S. X.; Huang, J. F.; Bi. R. C. (2004) 2.6 Å Resolution of Crystal Structure of the Bacterioferritin from *Azatobactor vinelandii*. *FEBS Letters* 573, 93-98.

[59] Janowski, R.; Auerbach-Nevo, T.; Weiss, M. S.; (2007) Bacterioferritin from *Mycobacterium smegmatis* Contains Zinc in its Dinuclear Site. *Protein Science* 17, 1138-1150.

[60] Larkin, M. A., Blackshields, G., Brown, N. P., McGettigan, P. R., McWilliam, H., Valentin, F., Wallace, I. M., Wilm, A., Lopez, R., Thompson, J. D., Gibson, T. J., and Higgins, D. G. (2007) Clustal W and Clustal X Version 2.0, *Bioinformatics 23*, 2947-2948.

[61] Nordlund, B.M.; Sjoberg, B.M.; Eklund, H.; (1990) 3-Dimensional structure of the Free Radical Protein of Ribonucleotide Reductase. *Nature* 345, 593-598.

[62] Rosenzweig, A.C.; Frederick, C.J.; Lippard, S.J.; Nordlund, P. (1993) Crystal Structure of a Bacterial Nonheme Iron Hydroxylase that Catalyzes the Biological Oxidation of Methane. *Nature* 366, 537-543.

[63] Weeratunga, S.K.; Lovell, S.; Yao,H.; Battaile, K.P.; Fischer, C.J.; Gee, C.E.; Rivera, M. (2010) Structural Studies of Bacterioferritin B from Pseudomonas aeruginosa Suggests a Gating Mechanism of Iron Uptake via the Ferreoxidase Center. *Biochemistry 49*, 1160-1175.

[64] Yang, X.; Le Brun, N.E.; Thomson, A.J.; Moore G.R.; Chasteen, N.D. (2000) The iron Oxidation and Hydrolysis Chemistry of Escherichia coli Bacterioferritin. *Biochemistry* 39, 4915-4923.

[65] Brown, S.; Holden, D. (2002) Iron Acquisition by Gram-Positive Bacterial Pathogens. *Microbes and Infection* 4, 1149-1156.

[66] Posey, J.E.; Gheradini, F.C. (2000) Lack of a Role for Iron in the Lyme Disease Pathogen. *Science* 288, 1651-1653.

[67] Moore, G.R.; Mann, S.; Bannister, J.V. (1986) Isolation and Properties of the Complex Nonheme-Iron Containing Cytodhrome b_{557} (bacterioferritin) from *Pseudomonas aeruginosa*. *Journal of Inorganic Biochemistry 28*, 329-336.

[68] Mann, S.; Bannister, J.V.; Williams, R.J.P. (1986) Reconstituted and Native Iron-Cores of Bacterioferritin and Ferritin. *Journal of Molecular Biology 198*, 405-416.

[69] Watt, G.D.; Frankel, R.B.; Papaefthymiou, G.C.; Spartalian, K.;Steifel, E.I.; (1986) Redox Properties and MossbaurSpectroscopy of *Azatobacter vinelandii* Bacterioferitin. *Biochemistry* 25, 4330-4336.

[70] Swartz, L., Kuchinskas, M., Li, H., Poulos, T. L., and Lanzilotta, W. N. (2006) Redox-Dependent Structural Changes in the *Azotobacter vinelandii* Bacterioferritin: New Insights into the Ferroxidase and Iron Transport Mechanism. *Biochemistry 45*, 4421-4428.

[71] Eerde, A.V.; Loo, W.; Oost, J.V.; Dijkstra, B.W. (2006) Fortuitous Structure Determination of ‘as-isolated’*Escherichia coli* Bacterioferritin in a Novel Crystal Form. *Acta Crystallographica F62*, 1061-1066.

CHAPTER II

Biochemical and Structural Characterization of Bacterioferritin B Reveals a Gated Mechanism of Iron Uptake

Introduction

Iron storage proteins such as ferritins and ferrtin-like proteins are capable of solubilizing and storing large amounts of iron (III) in the form of a ferric mineral. Consequently these proteins protect cells from the toxicity generated by free Fe^{2+} while providing a source of iron for cellular processes. These iron storage proteins function by oxidizing Fe^{2+} using oxygen as electron acceptors and storing the resultant Fe^{3+} as an iron mineral inside the inner core. In the studies carried out with eukaryotic ferritins, two mechanisms of iron oxidation have been observed; at higher concentrations of iron, O_2 is reduced to H_2O and at lower iron concentrations (less than 50 Fe^{2+} ions/ferritin), O_2 is reduced to H_2O_2 [1]. In addition, studies with bacterioferritins from *Escherichia coli* and *Azotobactor vinelandii* showed that O_2 is reduced to H_2O when Fe^{2+} is oxidized to Fe^{3+} [2, 3].

In the process of iron uptake, first Fe^{2+} ions are bound to the exterior surface of the protein and then these iron ions are transported to the interior of the protein to form a diferrous center called ferroxidase center, where Fe^{2+} ions are oxidized to $Fe^{3+.}$ Mammalian ferritins are composed of two types of subunits; H-chains and L-chains. However, the ferroxidase centers, which are essential for the iron mineralization process, are located only in the H-chain subunits [4]. In Bfr, the ferroxidase centers are located in the middle of each subunit and have a symmetric architecture withe two bridging Glu ligands (Glu 51 and Glu 127) and two His and

Glu residues as capping ligands (Glu18/His54 and Glu94/His130) [2,5,6,7] (Figure 2-1A). The arrangement of ligands in the Bfr ferroxidase center is similar to that of the diiron centers of diiron type II proteins such as soluble methane monooxygenase and ribonucleotide reductase [8]. These diiron centers are stable and act as cofactors in the protein. In contrast to the structure of the ferroxidase center of Bfr, in mammalian ferritin, only one iron of the ferroxidase center is coordinated by a capping His ligand and the two iron ions are bridged only by Glu62 [2, 7] (Figure 2-1B). Bacterial ferritins, on the other hand have the distinctive di-iron ferroxidase center found in mammalian ferritins. However, in addition to the di-iron center, there is another iron binding site, called C site which is unique to the bacterial ferritins (Figure 2-1C) (10). According to the kinetic and structural studies that have been carried out on the mineralization processes of ferritin-like proteins over the past two decades, two models of iron uptake have been postulated. Each model is thought to consist of three distinct kinetic phases [5, 7, 9]. In the first model, phase 1 starts by binding Fe^{2+} ions to a vacant ferroxidase center followed by phase 2 where Fe^{2+} ions are oxidized to form an unstable diferric species. Phase 3 is the movement of the oxidized Fe^{3+} into the interior of the protein towards the inner core for mineralization. Another new cycle of iron uptake starts upon binding Fe^{2+} to the vacant ferroxidase center. Therefore, in the first model, the ferroxidase center acts as a substrate for the oxidation of iron and also a pore for iron internalization. In the second model, the first two phases are similar to those in the first model. In the third phase, however, a stable diferric center is created at the ferroxidase center that serves strictly as a cofactor. Fe^{2+} ions are believed to enter the Bfr cavity via channels of the protein molecule.

(A)

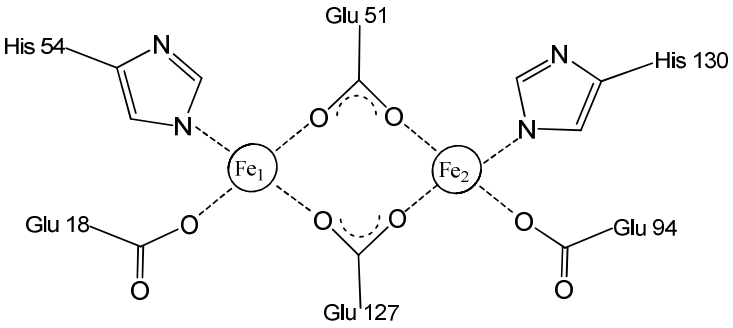

(B)

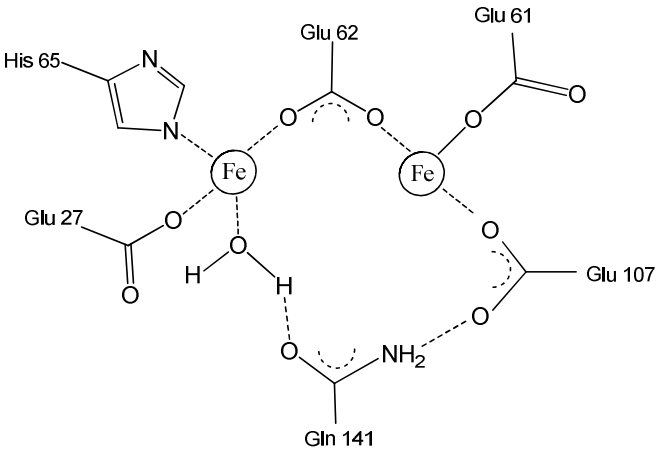

(C)

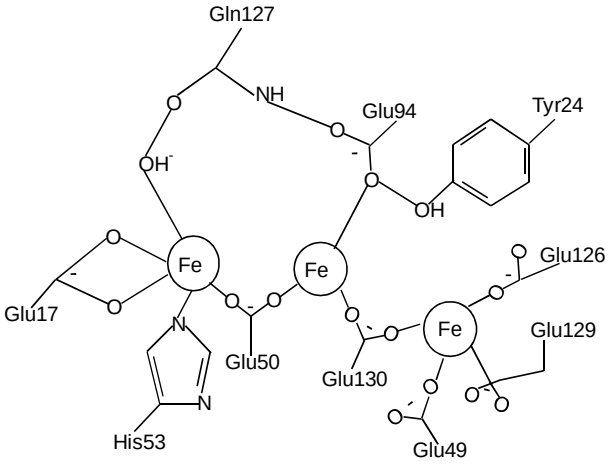

Figure 2-1: Schematic representation of (A) the symmetrical ferroxidase center typical of bacterioferritin (B) the ferroxidase center of human H-chain ferritin and (C) the tri nuclear ferroxidase center of Ferritin A from *E.coli*.

These Fe^{2+} ions are oxidized at the nucleating centers and the electrons released from their oxidation are passed to the ferroxidase center where these electrons are used to reduce O_2 and H_2O_2. Observations from the kinetic studies carried out with eukaryotic ferritins indicate that at low iron loads (<50 Fe^{2+} ions/ferritin molecule), the Fe^{2+} is oxidized by the ferroxidase center with a Fe^{2+}: O_2 stoichiometry of 2:1. However, at higher iron loads the stoichiometry of Fe^{2+}:O_2 changes to 4:1 [1]. Bfr from *E. coli* (Ec-Bfr) is the most studied Bfr so far and the information that have been derived from these studies are very important to elucidate the mechanisms of iron uptake in other bacterioferritins [2, 5, 7, 9]. Kinetic and structural data obtained from the mineralization studies of Ec-Bfr clearly indicate that the second model of iron uptake is operated in *E. coli*. Additional information on kinetic studies of Ec-Bfr strongly suggests that the Ec-Bfr ferroxidase center is stable and not converted to apo form (without iron bound to the ferroxidase center) spontaneously [2, 5]. It has also been observed that the apo form of the Ec-Bfr ferroxidase center is pre formed, so that Fe^{2+} ions can bind to the ferroxidase center with minimal structural reorganization. However, structural studies do not indicate any evidence of translocation of the oxidized iron from the ferroxidase center to the inner cavity. Therefore both kinetic and structural observations made from the studies with Ec-Bfr suggest that the ferroxidsae center of Ec-Bfr acts as a true catalytic center, rather than a pore for internalization of iron [11].

The structures of Bfrs from *Azatobactor vinelandii* (Av) [12], *Mycobacterium smegmatis* (Ms) [13], *Desulfovibrio desulfuricans* (Dd) [14], *Rhodobactor capsulatus* (Rc) [15], also provide valuable information about possible processes of iron uptake operative in bacteria. The ferroxidase center of Dd Bfr contains iron in the “as isolated” Dd Bfr. However, one ferroxidase iron ion is lost if the protein is reduced and allowed to oxidize in air. This observation indicates

that Dd Bfr ferroxidase center may function as a pore for iron internalization [14]. In addition, the ferroxidase center of Ms Bfr has been observed to contain zinc instead of iron and the ferroxidase center of Rc-Bfr has been found to be devoid of iron or any other metal ion in the protein as isolated. In the structure of Av-Bfr the ferroxidase center is occupied by iron. However, the Fe_2 position (nomenclature as in figure 2-1A) tends to have a low occupancy which has been interpreted to suggest that the oxidized iron has been translocated from the ferroxidase center to the inner cavity [12]. It is important to note that in the ferroxidase center of Av-Bfr, the side chain of His130 has moved away from Fe_2 whereas Glu47 has moved closer. This observation may suggest that the concerted motion of these side chains may function as a gate for the translocation of iron form the ferroxidase center to the cavity [12]. According to the observations made with the structures of Ec, Av and Dd Bfr, it is clear that the ferroxidase centers of Bfr proteins do not operate in the same manner. Some Bfrs have stable ferroxidase centers which function strictly as cofactors for the oxidation of Fe^{2+} that entered the cavity via channels (yet to be determined) in the protein, whereas other Bfrs seem to have "unstable" ferroxidase centers which serve as a center for Fe^{2+} oxidation and also a pore for iron internalization. Eventhough the function of the stable ferroxidase centers such as in Ec-Bfr is known [10], the function of the "unstable" ferroxidase centers is yet to be established.

Experimental Procedures

Cloning of Pseudomonas aeruginosa BfrB.

The gene encoding for *P. aeruginosa* BfrB (PA3531) was synthesized, subcloned into a pET 11a vector and sequenced (GeneScript Corp., Pisctaway, NJ). The gene was engineered with silent mutations introducing codons favored by *E. coli* [16] and with *Nde* I and *BamH* I restriction enzyme sites at the 5' and 3' ends respectively for subcloning into the pET 11a vector (Figure 2-2). The pET 11a vector harboring the *bfrB* gene was then transformed into *E.coli* Arctic express RIL competent cells (Stratagene, La Jolla,CA).

Expression and purification of *P. aeruginosa* BfrB.

A single colony of E. coli Arctic express RIL cells harboring the recombinant pET11-a/bfrB construct was cultured overnight at 37 °C in 50 mL of LB medium containing 100 μg/mL ampicilin and 20 μg/mL gentamicin. The cells were subsequently subcultured in 1 L of fresh LB containing no antibiotics and grown for 3 h at 37 °C. Cells were then transferred to a shaker incubator pre-equilibrated at 10 °C and incubated for 30 min before protein expression was induced by addition of isopropyl 1-thiol-D-galactopyranose (IPTG) to a final concentration of 1 mM. Cells were cultured for additional 48 h at 10 °C before they were harvested by centrifugation (4500 rpm for 10 min) and stored at -20 °C. The cell paste was resuspended in 50 mM Tris-HCl, pH 7.6 (2 mL/g cell paste) and PMSF (0.5 mM), DTT (5 mM), protease inhibitor cocktail (Sigma-Aldrich, St. Louis, MO) and DNAse (Sigma-Aldrich, St. Louis, MO) were added before the cells were lysed by constant cell disrupter (Constant Systems Ltd, LowMarch, Northants).

5' *Nde*1

CATATG AAA GGC GAT AAA AAA GTG ATC CAG CAT CTG AAT AAA ATT

M K G D K K V I Q H L N K I

CTG GGT AAT GAA CTG ATT GCG ATT AAT CAG TAT TTT CTG CAT AGC CGC ATG

L G N E L I A I N Q Y F L H S R M

TGG AAT GAT TGG GGC CTG AAA CGT CTG GGC GCG CAT GAA TAT CAT GAA AGC

W N D W G L K R L G A H E Y H E S

ATT GAT GAA ATG AAA CAT GCG GAT AAA CTG ATC GAA CGT ATT CTG TTT CTG

I D E M K H A D K L I E R I L F L

GAA GGT CTG CCG AAT CTG CAG GAT CTG GGC AAA CTG CTG ATT GGT GAA AAC

E G L P N L Q D L G K L L I G E N

ACC CAG GAA ATG CTG CAG TGC GAT CTG AAT CTG GAA CTG AAA GCG ACC AAA

T Q E M L Q C D L N L E L K A T K

GAT CTG CGT GAA GCG ATC GTG CAT TGC GAA CAG GTG CAT GAT TAT GTT AGC

D L R E A I V H C E Q V H D Y V S

CGT GAT CTG CTG AAA GAT ATC CTG GAA AGC GAA GAA GAA CAT ATT GAT TAT

R D L L K D I L E S E E E H I D Y

CTG GAA ACC CAG CTG GGT CTG ATT CAG AAA GTG GGC CTG GAA AAC TAT CTG

L E T Q L G L I Q K V G L E N Y L

CAG AGC CAT ATG CAT GAA GAT GAT TAAGGATCC

Q S H M H E D D ***Bam*H1 3'**

Figure 2-2: DNA and corresponding amino acid sequence of *bfrB* from *P. aeruginosa*. *Nde* I and *Bam*H I restriction endonuclease sites were constructed at the 5' and 3' ends for subcloning.

Cell debris were pelleted by centrifugation at 4 °C and 19,500 rpm and the resultant supernatant was loaded onto a Q-Sepharose Fast Flow column (12 cm x 2.5 cm i.d.) equilibrated with 50 mM Tris-HCl (pH 7.6). The column was washed with three column volumes of 50 mM Tris-HCl (pH 7.6) before the protein was eluted using the same buffer with a linear gradient (0 mM - 600 mM) of NaCl. Fractions containing BfrB were pooled and reconstituted with heme by titrating with a solution of hemin (2 mg/mL in DMSO) until the absorbance of the Soret band (418 nm) no

longer changed. The resultant protein solution was dialyzed against 4 L of 50 mM Tris-HCl (pH 7.6) for 12 h at 4 °C with at least two buffer changes. The resultant solution was then applied to a hydroxyapatite Bio-Gel column (10 cm x 2.5 cm i.d.) and washed with approximately 5 column volumes of 50 mM Tris-HCl (pH 7.6). BfrB was eluted with a linear gradient of potassium phosphate (50 mM-800 mM, pH 7.6). Fractions containing BfrB (red) were pooled and dialyzed overnight against 4 L of 50 mM Tris-HCl (pH 7.6) at 4 °C, with at least two buffer changes; the resultant solution was loaded to a second Q-Sepharose Fast Flow column (12 cm x 2.5 cm i.d.) and eluted as described above for the first ion exchange column. Fractions containing BfrB were loaded onto a second hydroxyapatite Bio-Gel column (10 cm x 2.5 cm i.d.) and the protein eluted using conditions identical to those described above for the first hydoxyapatite column. Fractions with absorbance ratio $A_{280}/A_{418} < 0.7$ were pooled and dialyzed against 100 mM potassium phosphate (pH 7.6) and determined to be pure by 15 % SDS-PAGE.

Analysis of heme in Pa BfrB.

The pure protein, as isolated, binds 12 heme groups per BfrB molecule. The content of heme was determined by adding 100 µL of pyridine to 400 µL of BfrB in 1 mL of 50 mM Tris buffer (pH 7.6). The protein solution was then transferred to an anaerobic chamber (Coy Labs, Grass Lake, MI) and allowed to degas for 3-4 hours. Excess sodium dithionite was added to the protein mixture to reduce the heme in BfrB. The UV-visible spectrum of reduced heme was recorded and the average concentration of heme in BfrB was determined using the extinction coefficients of previously reported pyridine hemochromes at 525 nm and 555 nm (ε_{525} = 17.0 mM^{-1} cm^{-1} and ε_{555} = 33.9 mM^{-1} $cm^{-1)}$ (17).

Analysis of phosphate content in the Pa BfrB core.

BfrB mineral core is mainly composed of iron and phosphate. The phosphate content was determined by measuring the concentration of a complex formed between malachite green and phosphomolybdate. A standard phosphate curve was prepared using 1, 3, 6, 9, 12 µM $NaH_2PO_4.H_2O$ solutions and used to calculate the phosphate concentration of the complex. The reaction mixture contains 2.96 mL of protein sample or the standard phosphate solution, 240 µL of 24% (V/V) H_2SO_4, 400 µL of 0.1M $Na_2MoO_4.H_20$ and 400 µL of malachite green [0.185 mg/ml of 1% poly (vinyl alcohol)]. The reagents are allowed to react for ~ 10 hours and the absorbance of the green complex formed was measured at 623 nm. The concentration of phosphate was determined using the prepared standard curve [18].

Determination of molecular mass of Pa BfrB.

The molecular weight of BfrB was estimated with the aid of a high resolution size exclusion column (Superdex 200 16/60 Prep, GE Healthcare) equilibrated with 100 mM potassium phosphate (pH 7.6) and 1 mM tris (2-carboxyethyl)-phosphine hydrochloride (TCEP). The column was calibrated with a set of molecular weight standards (GE Healthcare) that included ferritin (440,000 Da), aldolase (158,000 Da), conalbumin (75,000 Da) and ovalbumin (43,000 Da) and a calibration curve was prepared using their elution volumes. A sample of pure BfrB was passed through the same column and the molecular weight of the protein was determined by using its elution volume.

Mineralizaton of iron in the Pa BfrB cavity.

Pa-BfrB as isolated contains only a small amount of iron in its core (~ 5 – 10 iron atoms per molecule). Therefore, protein to be used in experiments was incorporated with ~ 600 iron atoms per molecule. A solution of ferrous ammonium sulfate was prepared inside an anaerobic chamber (Coy Labs, Grass Lake, MI), placed in a container capped with a rubber septum and removed from the anaerobic chamber. Concentrated HCl (50 μL/100 mL) was added to the anaerobic ferrous ammonium sulfate solution through the septum with the aid of a Hamilton microsyringe and a needle. The resultant solution was added to a stirred solution of 0.002 mM Pa BfrB and 5.0 mM TCEP in 100 mM potassium phosphate buffer, pH 7.6 in aliquots delivering 50 Fe^{2+}/Pa BfrB, until 600 Fe^{2+}/Pa BfrB had been added. Ten minutes were allowed after the addition of one aliquot before the next was added. The mineralization process was monitored spectrophotometrically following the absorbance near 320 nm with the aid of a USB 2000 spectrophotometer (Ocean Optics, Dunedin, FL).

Analysis of non-heme iron in the Pa BfrB core.

1 mL of concentrated HCl was added to 1 mL of BfrB (0.003 mM) and the mixture incubated for 15 min, followed by addition of 1 mL of ascorbic acid (25 g/L) and 5 mL of saturated aqueous sodium acetate. A purple color developed upon the addition of 1 mL of ferrozine (5 g/L) and after 15 min the concentration of iron was determined from the electronic absorption spectrum using the absorbance at 562 nm (ε_{562} = 27.9 mM^{-1} cm^{-1}) [18].

Crystallization and data collection.

Crystallization studies were carried out in the Protein Structure Laboratory at the Delbert M. Shankel Structural Biology Center (University of Kansas, Lawrence, KS) and the structure of BfrB was solved by Dr. Scott Lovell.

Mineralized or non-mineralized (as-isolated) Pa BfrB was concentrated to 10 mg/mL and 9 mg/mL, respectively in 100 mM potassium phosphate pH 7.6, 5 mM TCEP for crystallization. Crystals were grown under aerobic conditions in Compact Jr. (Emerald biosystems) sitting drop vapor diffusion plates using 1μL of crystallization solution and 1 μL of protein equilibrated against 100 μL of crystallization solution at 20 ^{o}C. Red prisms were obtained within 24 hours from the following conditions: Mineralized BfrB (Wizard 2 #2, Emerald biosystems) 35% (v/v) 2-methyl-2,4-pentanediol, 100 mM MES pH 6.0, 200 mM Li_2SO_4 (Appendix 1), as isolated Pa BfrB (Cryo 1 #11, Emerald biosystems) 35% (v/v) 2-methyl-2,4-pentanediol, 100 mM Tris pH 8.5, 200 mM $(NH_4)_2SO_4$ (Appendix 2). To prepare samples with iron bound ferroxidase center, crystals of mineralized BfrB were soaked aerobically for 15 min in crystallization solution (35% v/v 2-methyl-2,4-pentanediol, 100 mM MES pH 6.0, 200 mM Li_2SO_4) 50 mM $FeSO_4$. Doubly soaked crystals were prepared by aerobically soaking mineralized BfrB crystals in the same crystallization solution containing 50 mM $FeSO_4$, followed by aerobically soaking for 15 min in the same crystallization solution without $FeSO_4$. Single crystals were transferred to a fresh drop of crystallization solution which also served as a cryoprotectant and frozen in liquid nitrogen for data collection. Data were collected at 100 K at the Advanced Photon Source (APS) beamline 17-BM (IMCA-CAT) using an ADSC Quantum 210 CCD detector at λ = 1.0000 Å. Additional data were collected from the same crystals for mineralized and Fe soak crystals at λ = 1.6314 Å in order to measure an anomalous signal from potentially bound Fe ions. Although the X-ray

fluorescence K edge emission peak of Fe has a maximum approximately at 1.73 Å, at 1.6314 Å a prominent anomalous signal can be observed for Fe ions.

Structure solution and refinement.

Intensities were integrated and scaled using the HKL2000 package [19]. Structure solution was carried out by molecular replacement with Molrep [20] using the full 24 subunit assembly of Ec BfrB as the search model (PDB: 1BFR). Rotation and translation searches for the 24-subunit assembly yielded a clear solution with a correlation coefficient of 0.735. The refined model of Pa BfrB was used as the search model for subsequent data sets. For the as isolated Pa BfrB, a single subunit from the final mineralized Pa BfrB structure was used as the search model. Six molecules were positioned with Molrep yielding a correlation coefficient of 0.703. Structure refinement and manual model building were performed with Refmac [21] and Coot [22] respectively. Medium NCS restraints were applied to the double soaked model. Figures were prepared using the Ribbons [23] and CCP4mg [24] software packages. Structure validation was performed with Molprobity [25].

Iron uptake in solution

Pa BfrB to be used in the experiments was prepared by extensively dialyzing the pure, as-isolated protein against 100 mM MES, 100 mM KCl, pH 6.5. Fe^{2+} oxidation by Pa-BfrB was measured with the aid of a conventional diode-array UV-vis spectrophotometer (Ocean Optics, Dunedin, FL), following addition of 50 Fe^{2+}/Pa BfrB molecule to a solution of Pa BfrB (0.8 μM) at 30 °C in 100 mM MES buffer, 100 mM KCl, pH 6.5 in a 1.0 cm path length cuvette equipped with a stirring bar. The process was also studied with the aid of a Applied Photophysics SX.18MV-R Stopped-Flow Spectrophotometer (Applied Photophysics Ltd.,

Leatherhead, UK), which was used to study the iron uptake process by mixing solutions of ferrous ammonium sulfate and Pa BfrB in Fe^{2+}:protein ratios of 30, 50, 100, 200 and 300. These experiments were also carried out at 30 °C in 100 mM MES buffer, 100 mM KCl, pH 6.5; protein concentration was 1.0 μM (after mixing) and the path length was 1.0 cm. Progress curves, monitored at 320 nm, were obtained from averaging 6 replicates for each Fe^{2+} concentration. Rate constants were calculated by fitting the first 5 s of progress curves obtained upon addition of 30, 50 and 100 Fe^{2+} ions, which allowed distinction between the fast and slow phases, to a single exponential function.

Results

Overexpression, Purification and Characterization of Pa BfrB

BfrB expressed in *E.coli* Arctic express RIL cells was soluble and could be purified to homogeneity. The pure BfrB protein produced a single band in the 15% SDS-PAGE gel which corresponds to an approximate MW of 18000 Da (Figure 2-3A). This is in good agreement with the molecular mass of 18553 Da calculated from the amino acid sequence of a BfrB subunit. In addition, the molecular mass of BfrB molecule, was estimated to be 447 ± 1 kDa from its average elution volume (V_e= 58.9 ± 0.05 mL) of a calibrated Superdex 200 column. The estimated MW confirmed the oligomerization of the BfrB molecule as a 24mer and the MW of one subunit was calculated as 18.6 kDa. The MW of a subunit estimated from both experiments is in good agreement with molecular mass of 18553 Da calculated from the amino acid sequence of a BfrB subunit. The electronic absorption spectrum of pure BfrB has a Soret band maximum at 418 nm and α and β bands at 567 nm and 527 nm respectively (black trace of figure 2-3B).

The UV-vis spectrum of pure BfrB displays another characteristic weak band at 740 nm (inset of Figure 2-3B) which is consistent with axial methionine ligation of the heme group [26].

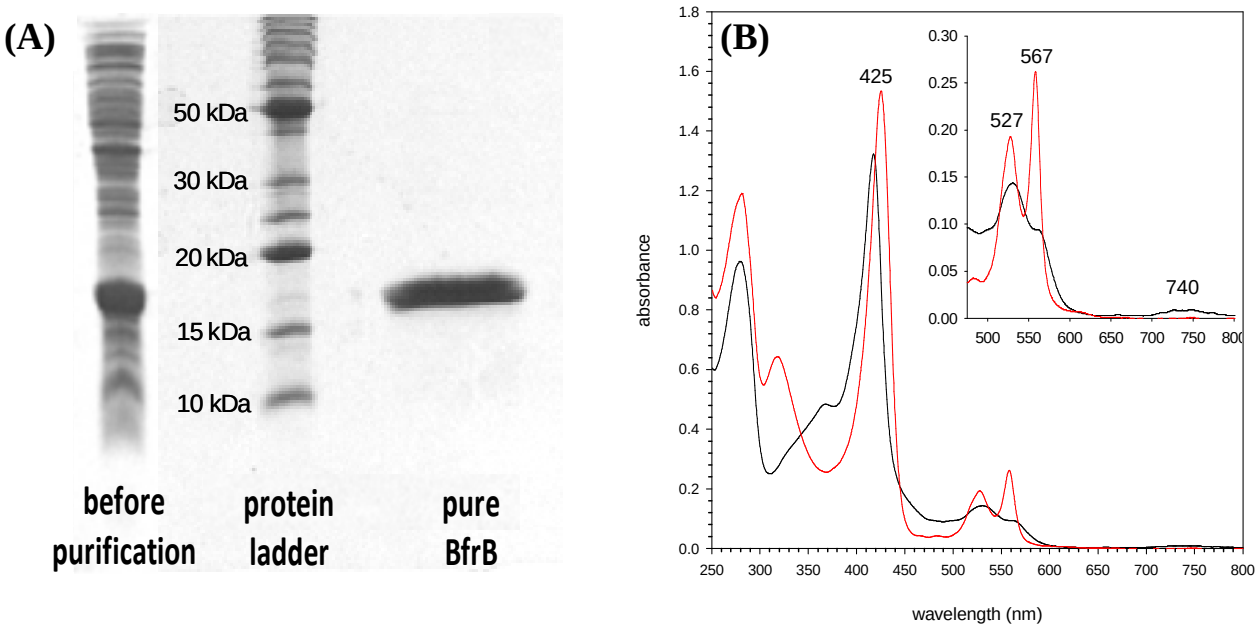

Figure 2-3: (A) SDS-PAGE (15%) analysis of BfrB purified to homogeneity. (B) Electronic absorption spectra of oxidized-BfrB (black trace) and reduced-BfrB (red trace) in 100 mM potassium phosphate, pH 7.6. The inset shows the α and β bands in the visible region.

The reduced spectrum of BfrB was obtained by adding sodium dithionite to pure, as isolated BfrB and has the Soret band, α and β bands at 425 nm, 567 nm and 527 nm respectively. The reduced BfrB spectrum does not show the characteristic band at 740 nm, as expected [ ](black trace of figure 2-3B). It is interesting to observe that the reduced spectrum of BfrB could be obtained only by adding dithionite to the BfrB devoid of a mineral core (~ 5-10 Fe/BfrB). If BfrB contains a mineral core, it is difficult to reduce the heme group even upon addition of a large excess of dithionite under strict anaerobic conditions.

Although pure BfrB was obtained in high concentration as judged by the SDS-PAGE, the pale red color of the protein indicates that BfrB does not have the full complement of heme. This observation suggests that when BfrB is overexpressed in *E. coli*, it may not have incorporated the full amount of heme.

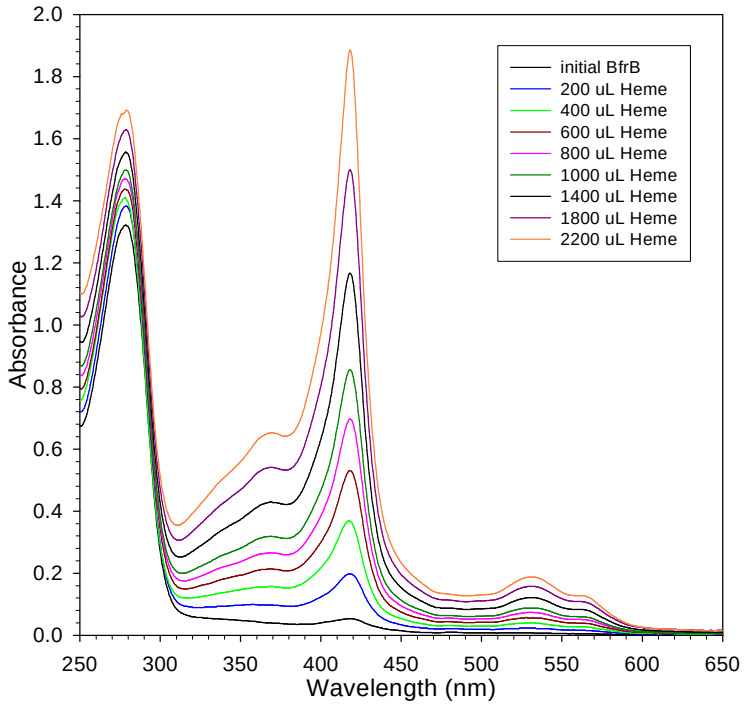

Figure 2-4: Spectral changes observed upon reconstituting recombinant BfrB with exogenous heme.

Therefore, BfrB containing fractions eluting from the first ion exchange column (as explained in the experimental section) were reconstituted with heme (Figure 2-4). The initial spectrum of BfrB, before adding heme (black trace in Figure 2-4) has a A_{280}/A_{418} ratio higher than 10. However, upon reconstitution with heme the intensiy of the Soret band increases and eventually the ratio of A_{280}/A_{418} becomes less than 1(red trace in Figure 2-4). This observation confirms

that the recombinant protein as isolated from *E.coli* has a low content of heme. However, the analysis of the heme content after reconstitution revealed that one BfrB molecule can bind 12 heme groups. Therefore BfrB is thought to be structurally similar to other structurally characterized bacterioferritins which are able to incorporate 12 heme molecules axially coordinated by two Met ligands. Further, analysis of the core iron in as isolated BfrB showed that it contains only 5-15 iron atoms per BfrB molecule. In order to increase the iron and the heme content of the recombinant BfrB, the expression medium was supplemented with $Fe(SO_4)_2$ (4 mg/L) and δ-aminolevulinic acid (ALA) (17 mg/L). Nevertheless, 'as isolated' BfrB had a low content of iron and heme. ALA was used to supplement the medium to increase the amount of heme produced during expression of BfrB, as it has been shown that the expression medium enriched with ALA increases the yield of heme bound proteins [27, 28]. The low content of iron and heme of overexpressed BfrB may be due to the fact that the host *E.coli* cannot supply all the required iron and heme for the overexpressing protein which in turn creates a strain on the iron uptake and iron homeostasis processes of the host *E.coli* strain. On the other hand, an attempt to purify BfrB without heme was not successful as it did not produce properly assembled 24meric BfrB. These results suggest that heme may be necessary for this protein to maintain its proper oligomerization and long term stability. However, after few extra purification steps, it was possible to purify BfrB without heme to homogeneity as judged by the presence of a single band at ~ 18 kDa in a 15% SDS-PAGE gel. To determine the size of the purified BfrB devoid of heme, it was passed through a Superdex 200 column previously calibrated with molecular weight markers. Interestingly, the peak corresponding to the molecular mass of a 24-mer (447 kDa) was absent and three other peaks corresponding to molecular weights of masses of 30, 92 and 254

kDa were present. These results indicate that the protein may have disassembled into several subunits due to the lack of stability provided by the heme.

Preparation of Iron-loaded Pa BfrB

BfrB with iron-loaded inner core was prepared by titrating a solution of apo BfrB (BfrB devoid of iron in the inner core) with an anaerobic solution of ferrous ammonium sulfate [$Fe(NH_4)_2(SO_4)_2$] solution. The experiment was carried out in air to allow the oxidation of Fe^{2+} to Fe^{3+} to take place. The oxidation of Fe^{2+} occurs by two competing reactions: In one reaction, Fe^{2+} is oxidized by apo BfrB using dissolved oxygen as the electron acceptor and the resulting Fe^{3+} is incorporated in the inner cavity of BfrB. In the competitive process, the Fe^{2+} ions are rapidly oxidized by the oxygen dissolved in the protein solution and the resulting Fe^{3+} can be hydrolyzed into insoluble colloidal hydrous oxide. Some of the protein molecules may be electrostatically attached to the iron colloid and precipitate together with the colloid which results in significant loss of protein. To prevent protein precipitation during mineralization, an aliquot of Fe^{2+} which is equivalent to 10% of the total iron to be loaded was added at a time. The next aliquot of Fe^{2+} was added after 15 minutes allowing time for the previously added iron to oxidize and mineralize. After each addition of iron the reaction mixture was centrifuged to separate any colloidal iron oxide formed. The black trace in figure 2-5 shows the spectrum of BfrB containing 10 iron atoms per protein molecule in its core, before the addition of Fe^{2+} with a A_{280}/A_{418} ratio of 0.69. Upon addition of Fe^{2+} into the protein solution a gradual increase in the intensity of the absorption near 280 nm was observed.

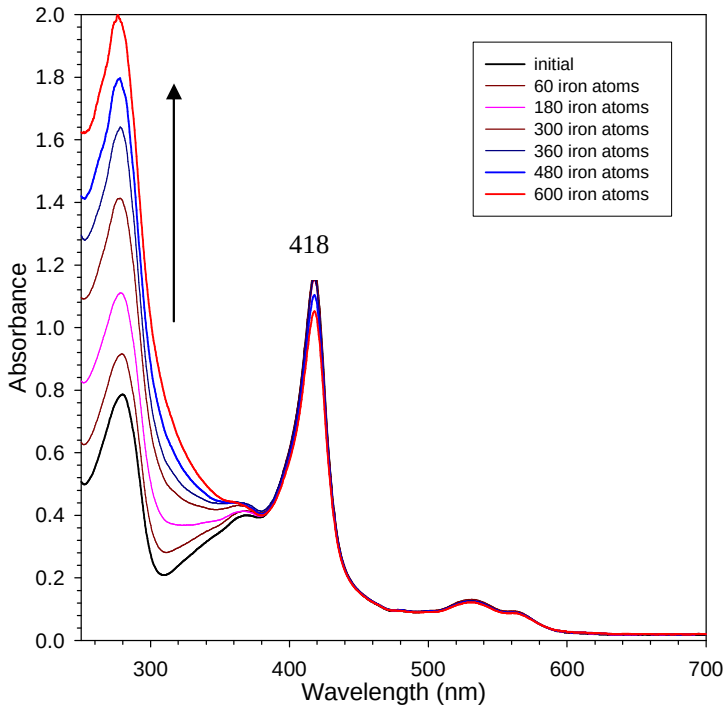

Figure 2-5: Family of electronic absorption spectra illustrating the intensity changes brought about by reconstituting the core of Pa BfrB with iron.

The intensity of absorption at 280 nm is increased because mineralized iron in the inner core shows absorption similar to band-edge bands displayed by polycrystalline semiconductors [28]. The group of spectra in figure 2-5 also indicates that as the intensity of the band near 280 increases the intensity of the Soret band remains almost constant; the small decrease of the intensity of the Soret band is due to minute losses of protein caused by the precipitation with the iron colloid formed after each addition of Fe^{2+}. In addition, the preservation of the baseline of the family of spectra provides good evidence on the fact that the centrifugation step carried out in between each addition of iron efficiently removes any colloidal iron formed. This approach of mineralization yielded high recovery (85%) of protein with an iron content of 600 ± 40 iron per BfrB molecule. The phosphate to iron ratio of the BfrB mineral was determined to be ~ 1-3

which corroborates the fact of typical bacterioferritins isolated from native sources having high phosphate content [30-34].

Crystallization of Pa-BfrB

Initial crystal screening trials of recombinant mineralized Pa-BfrB formed red prisms from various crystallization conditions (Figure 2-6). These crystals were orthorhombic and composed of 24 Pa-BfrB molecules in the asymmetric unit. It diffracted to the highest resolution of 2.1 Å (Table 2-1). 'As isolated' Pa BfrB formed red crystals of the form of Orthorhombic I, with six BfrB molecules in the asymmetric unit.

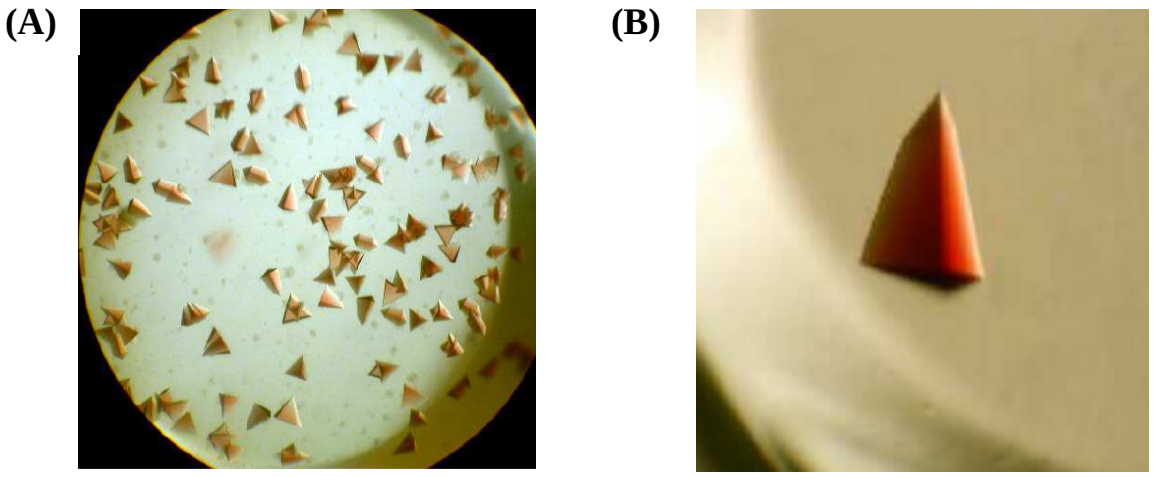

Figure 2-6: (A) Red prismatic single crystals of recombinant Pa BfrB formed in compact Jr. sitting drop vapor diffusion plates. (B) A single crystal of recombinant Pa BfrB.

The crystals from mineralized Pa-BfrB were soaked in the crystallization solution containing 50 mM $FeSO_4$ (Fe soaked Pa-BfrB) for 15 minutes and used to acquire diffraction data. In addition, the diffraction data were also collected from the crystals obtained after soaking the Fe soaked Pa-BfrB crystals for 15 minutes in a crystallization solution which does not contain iron (double-

soaked Pa-BfrB). All the crystal structures solved from above experiments had very similar properties. However, important differences were observed in the processes of binding of iron to the ferroxidase center and the external and internal surfaces of the protein.

Table 2-1. Crystallographic data for Pa BfrB.

	BfrB ("as isolated")	**BfrB (minearalized)**	**BfrB (Fe Soak)**	**BfrB (Double Soak)**
Data Collection				
Unit-cell parameters (Å)	a = 122.76	a = 125.81	a = 125.72	a = 125.71
	b = 126.27	b = 202.76	b = 203.28	b = 203.21
	c = 168.55	c = 207.55	c = 207.73	c = 207.87
Space group	$I222$	$P2_12_12_1$	$P2_12_12_1$	$P2_12_12_1$
Resolution (Å)	50.0-2.07 (2.14-2.07)	50.0-2.10 (2.18-2.10)	50.0-2.25 (2.33-2.25)	50.0-2.80 (2.90-2.80)
Wavelength (Å)	1.6531	1.0000	1.0000	1.6531
Temperature (K)	100	100	100	100
Observed reflections	550,190	2,179,278	1,858,510	955,818
Unique reflections	79,588	309,226	251,658	131,241
$\langle I/\sigma(I)\rangle$[1]	20.3 (2.4)	16.2 (2.0)	13.1 (1.9)	13.0 (2.3)
Completeness (%)[1]	99.5 (97.8)	99.9 (99.4)	99.7 (98.5)	100 (100)
Redundancy[1]	6.9 (5.3)	7.0 (6.3)	7.4 (5.6)	7.3 (6.5)
R_{merge} (%)[1, 2]	9.0 (50.4)	10.9 (66.9)	13.5 (69.2)	17.0 (75.3)
Refinement				
Resolution (Å)	50.0-2.07	50.0-2.10	50.0-2.25	50.0-2.80
Molecules / asu	6	24	24	24
Reflections (working/test)	75,351 / 3,973	291,584 / 15,512	237,971 / 12,585	124,548 / 6,600

R_{factor} / R_{free} (%)[3]	19.7 / 24.5	19.3 / 24.4	17.3 / 22.6	19.5 / 23.7
No. of atoms (protein / heme / Fe^{2+} / K^+ / water)	7703 / 172 / 0 / 2 / 363	30,491 / 516 / 0 / 6 / 1,512	30,932 / 516 / 96 / 6 / 1,648	30,414 / 516 / 24 / 6 / 0
Model Quality				
R.m.s deviations				
Bond lengths (Å)	0.023	0.021	0.022	0.016
Bond angles (^{o})	1.929	1.824	1.856	1.553
Average *B* factor (Å^2)				
All Atoms	38.8	27.3	25.3	39.5
Protein	38.5	26.9	24.8	39.4
Heme	39.6	27.8	28.8	46.6
K^+ / Fe^{2+}	25.3	23.9 / NA	29.5 / 30.4	31.4 / 49.4
Water	44.2	35.8	33.2	
Coordinate error based on R_{free} (Å)	0.171	0.174	0.194	0.337
Ramachandran Plot				
Favored (%)		99.8	99.6	99.3

1) Values in parenthesis are for the highest resolution shell.

2) $R_{merge} = \Sigma_{hkl}\Sigma_i |I_i(hkl) - \langle I(hkl)\rangle| / \Sigma_{hkl}\Sigma_i I_i(hkl)$, where $I_i(hkl)$ is the intensity measured for the *i*th reflection and $\langle I(hkl)\rangle$ is the average intensity of all reflections with indices hkl.

3) $R_{factor} = \Sigma_{hkl} ||F_{obs}(hkl)| - |F_{calc}(hkl)|| / \Sigma_{hkl} |F_{obs}(hkl)|$; Rfree is calculated in an identical manner using 5% of randomly selected reflections that were not included in the refinement.

These four crystal structures were used to structurally characterize BfrB to aid in the elucidation of the mechanism of iron uptake. According to the crystallographic data, Pa-BfrB consists of 24

subunits and is assembled as a nearly spherical molecule with external and internal diameters of~118 Å and ~73 Å respectively. Each Pa-BfrB subunit is made of four α-helices which are arranged nearly parallel to each other and a short C-terminal α-helix almost perpendicular to the four-helix bundle. One Pa-BfrB molecule can bind 12 heme groups and each heme group is located between two subunits and axially coordinated by a methionine (Met52) from each subunit (Figure 2-7).

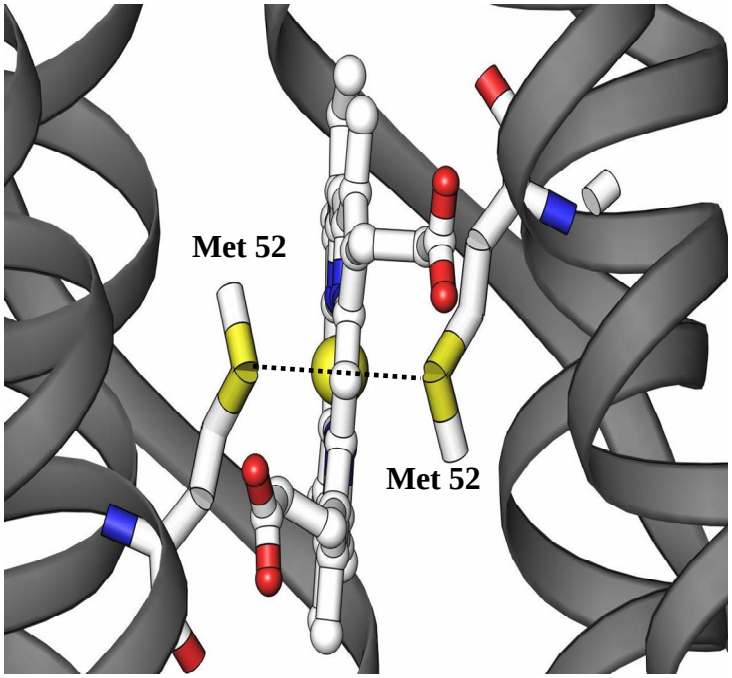

Figure 2-7: Heme group coordinated by two Met52 residues at the inter subunit site of two adjacent subunits of BfrB from *P. aeruginosa*.

In the as-isolated crystal form, two of the heme molecules were located on the 2-fold crystallographic axes bisecting the CHA, Fe, and CHC atoms. Heme molecule is not a symmetrical molecule. Therefore, it should adopt two orientations in a 50:50 ratio and in Pa-

BfrB, it is related by the 2-fold crystallographic axis. In addition three and four fold axes traverse through the 3-fold and 4-fold channels in the molecule and potassium ions were observed in the 4-fold channels of all the solved structures of Pa-BfrB (Figure 2-8).

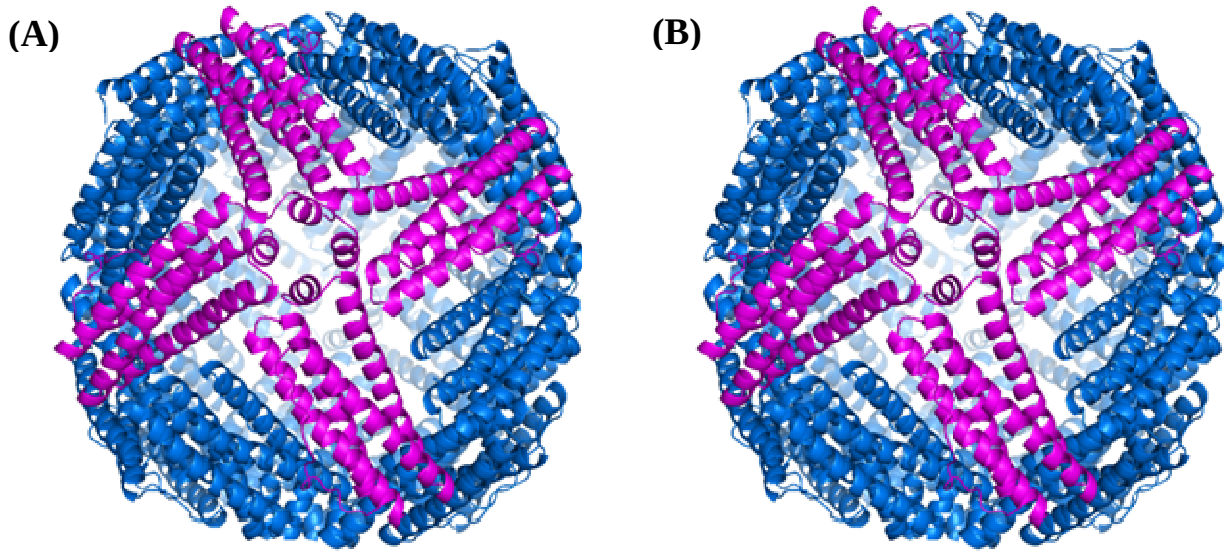

Figure 2-8: Structure of recombinant Pa BfrB viewed along a (A) 4-fold axis and (B) 3-fold axis of the molecule.

The ferroxidase center of Pa BfrB is unstable

Ferroxidase center of Pa-BfrB is made of six amino acid residues which are highly conserved among all bacterioferritins of known structure [30]. In Pa-BfrB, Glu18 and His54 act as terminal ligands to Fe_1 and Glu94 and His130 act as terminal ligands to Fe_2. The two iron atoms are bridged by Glu51 and Glu127 (Figure 2-9A).

(A)

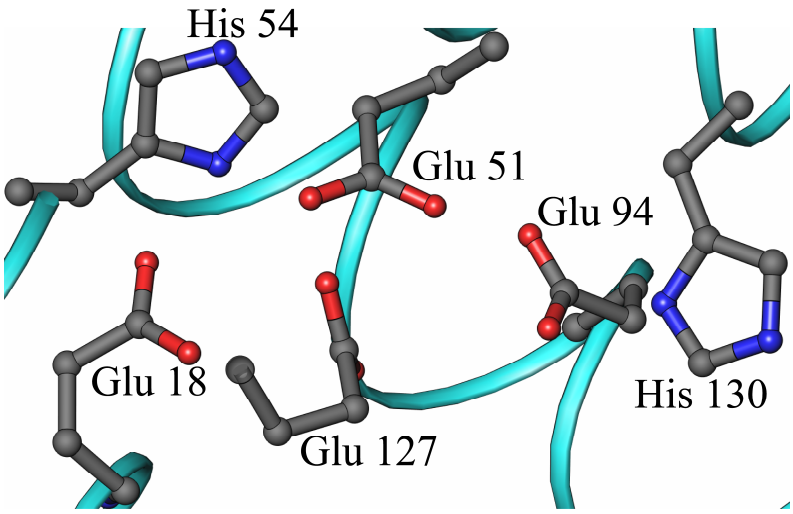

(B)

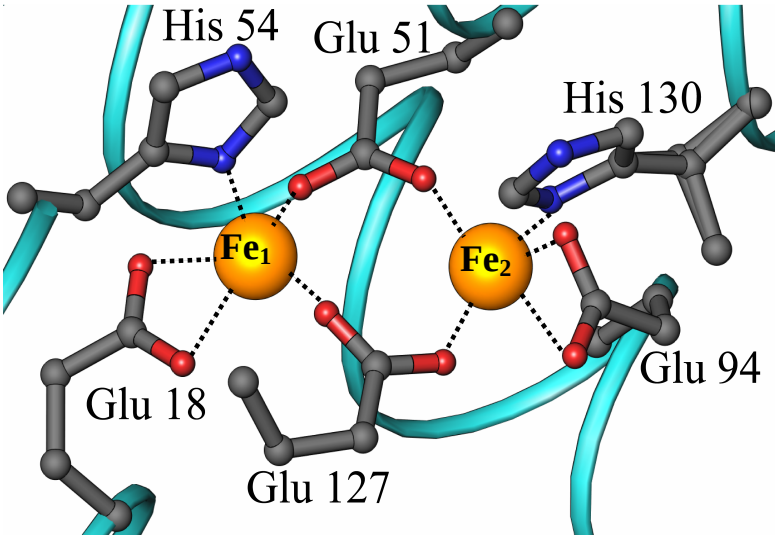

Figure 2-9: Structure of (A) empty ferroxidase center and (B) iron bound ferroxidase center of Pa BfrB showing two different conformations of His130.

Even though the electron density maps for these residues in the structure solved from as-isolated Pa-BfrB were well defined, electron density due to metal ions in this site was not observed. This clearly indicates that the ferroxidase center of as-isolated Pa-BfrB is empty. It is important to note that eventhough most of the ferroxidase center residues are pre-arranged to bind iron, His 130 is rotated away from the ferroxidase center and would require a conformational change to bind Fe_2 ion (Figure 2-9B). As mentioned in the experimental procedures, anomalous Fourier analysis was carried out using data collected at 1.6314 Å. These experiments generated a strong anomalous signal created from the Fe atoms at the heme sites. However, negligible electron density was observed at the ferroxidase center, which confirms that the ferroxidase center of as-isolated Pa-BfrB is empty. A sample of as-isolated Pa-BfrB was reconstituted with ~ 600 iron atoms (mineralized) to prepare a protein sample to obtain a structure with an iron-filled ferroxidase center. As figure 2-5 shows, upon addition of aliquots of iron to the protein, a gradual increase in the absorption near 320 nm was observed, which resulted from the growth of iron mineral in the core of ferritin-like molecules [29]. After adding the last aliquot of iron, the mineralized solution was incubated overnight at 4 ºC and then it passed through a G-25 column to remove any non-mineralized excess iron. The iron content of the mineralized protein was analyzed and a core of ~600 ± 40 was observed, signifying that the protein had been successfully mineralized. The crystal structure of mineralized Pa-BfrB, which was solved to 2.1 Å resolution, is nearly identical to the structure obtained from the as-isolated Pa BfrB, including an empty ferroxidase center. Moreover, the ligands which coordinate the two iron atoms at the ferroxidase center of mineralized Pa BfrB, have the same conformations similar to those found in the as-isolated Pa BfrB together with the His130 side chain rotated away from the diiron center (Figure 2-8A). Eventhough the protein had been mineralized with ~600 iron atoms before the

crystallization; the ferroxidase center does not contain iron. This observation indicates that the diiron center in Pa-BfrB is unstable.

The Crystal form of Pa-BfrB is functional.

In the experiments carried out to incorporate iron to the ferroxidase center, crystals of mineralized Pa-BfrB were soaked in a Fe^{2+} solution for 15 minutes and then the Fe soaked crystals were flash frozen for data collection. The structure of the Fe soaked Pa-BfrB revealed four types of iron bound to the protein.

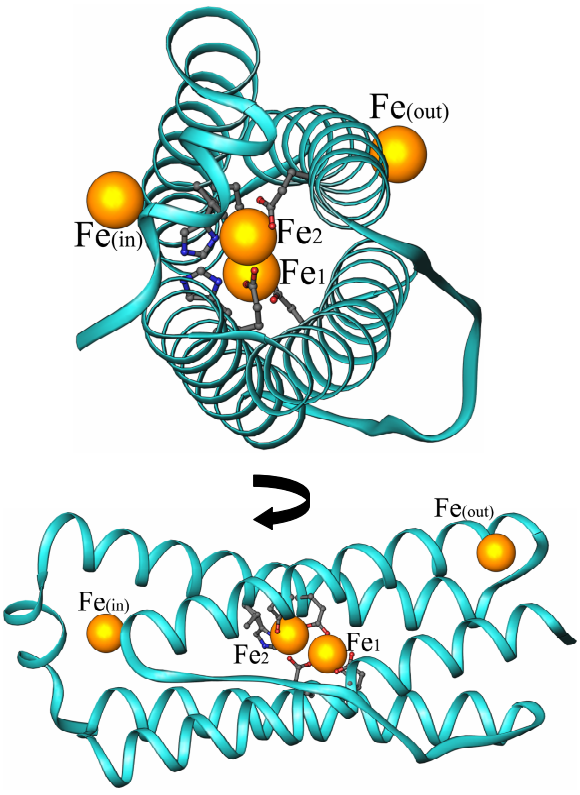

Figure 2-10: Views of a single subunit of Fe soaked Pa BfrB showing the iron atoms (gold spheres) located on the outer surface of the protein Fe_{out}, the inner surface Fe_{in}, and the ferroxidase iron atoms located in the center of the helix bundle.

The structure showed two iron ions bound to the ferroxidase center and iron ions bound to the exterior and the interior surfaces of the protein. This observation suggests that Pa-BfrB is functional even in the crystalline form, where it is capable of internalizing iron from the external solution into the interior of the protein. As a result, the Fe soaked crystal structure of Pa-BfrB can be considered as a representation of a snapshot of the iron uptake process. As figure 2-10 illustrates, the structure of a monomeric subunit of the Fe soaked crystal structure contains three types of iron: two iron ions at the ferroxidase center , located within the helix bundle, Fe bound to the external surface of the protein ($Fe_{(out)}$) and iron bound to the internal surface of the protein ($Fe_{(in)}$). The Fe soaked crystal structure also revealed that the ferroxidase centre of Pa-BfrB is coordinated by Glu18, His54 (terminal ligands to Fe_1), Glu94, His130 (terminal ligands to Fe_2) and Glu51, Glu127 (bridging ligands of Fe_1 and Fe_2) (Figure 2-9).

The presence of these iron was demonstrated by the strong peaks in the electron density map (F_0 - F_c), as well as a strong anomalous signal from data acquired at 1.6314 Å. Each subunit of the Pa BfrB structure showed a nearly complete iron occupancy of their ferroxidase centers, which is reflected in anomalous peak intensities and B factors for Fe_1 and Fe_2 comparable to those of heme iron (Table 2 and Figure 2-11).

The average distance of Fe_1 and Fe_2 was observed to be 4.00 Å with a range of 3.96-4.04 Å, which are similar to the distances observed in the structures of Av Bfr [12, 35] and Dd Bfr [14] in their reduced form, and it is consistent with a di-Fe^{2+} oxidation state [8].

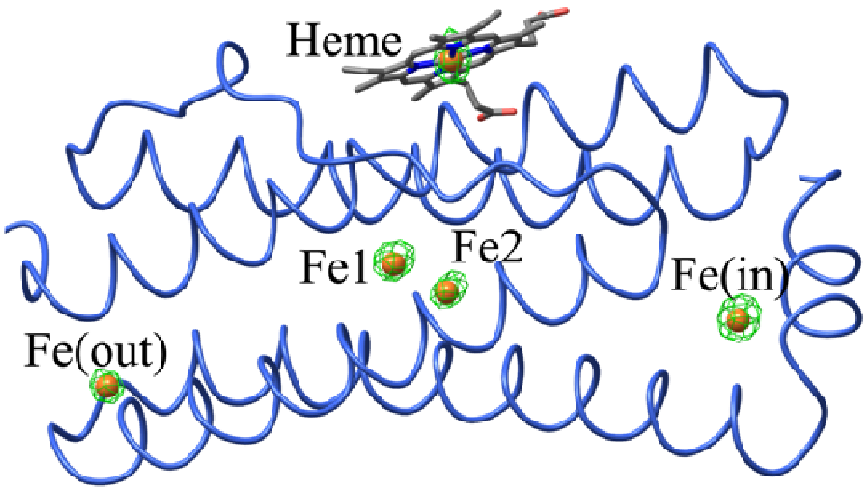

Figure 2-11: Single subunit of BfrB showing the anomalous difference map (green mesh) calculated from data collected at λ = 1.6314 Å contoured at 6σ. Fe atoms are represented as gold spheres and the neighboring heme atoms are drawn as sticks.

Table 2-2. Anomalous peak heights and *B*-factors for Fe atoms in the Fe soaked structure. .

	$Fe_{(out)}$		Fe_1		Fe_2		$Fe_{(in)}$		Heme Fe		
Subunit	***B*** **(Å^2)**	**Peak Height[a]**	***B*** **(Å^2)**	**Peak Height[a]**	***B*** **(Å^2)**	**Peak Height[a]**	***B*** **(Å^2)**	**Peak Height[a]**	**Heme #**	***B*** **(Å^2)**	**Peak Height**
A	26.6	11.7	24.4	11.2	37.8	10.3	25.8	12.9	1	22.4	12.1
B	32.9	8.1	25.9	12.4	35.0	11.1	25.4	12.5	2	22.5	12.7
C	33.4	9.0	23.6	11.8	34.0	11.1	21.0	13.5	3	21.4	12.8
D	37.5	8.0	26.4	12.2	35.4	9.2	24.4	12.9	4	22.2	14.1
E	36.7	8.1	24.7	14.0	35.2	9.7	21.7	12.2	5	22.6	12.1
F	32.1	7.9	27.1	11.9	33.2	9.1	24.5	12.8	6	26.4	12.5
G	37.4	9.4	25.0	12.2	35.5	10.1	22.7	12.9	7	25.8	12.5

H	39.5	8.2	27.4	11.3	36.3	8.7	25.7	11.8	8	23.6	13.0
I	35.4	9.0	27.3	13.1	38.2	8.6	25.3	11.7	9	23.5	13.3
J	43.2	8.6	24.3	11.2	36.8	8.7	21.3	14.6	10	21.2	12.9
K	31.9	10.7	24.0	14.3	31.8	10.7	24.5	14.3	11	26.1	12.8
L	32.6	9.0	26.6	12.6	34.1	10.3	24.5	13.6	12	20.7	12.1
M	42.7	7.5	28.6	11.0	35.1	9.4	24.6	13.2			
N	39.3	7.3	29.7	11.9	40.4	8.7	28.4	11.4			
O	45.2	7.6	31.1	11.3	40.0	8.1	24.2	12.7			
P	40.3	8.0	28.3	10.5	35.4	9.2	29.3	12.2			
Q	23.8	14.0	26.1	10.0	32.1	7.3	24.0	13.6			
R	29.2	9.9	24.1	11.6	33.1	8.2	26.0	13.3			
S	32.4	8.3	25.7	10.8	33.7	9.6	22.5	13.2			
T	33.5	9.3	23.0	12.0	36.5	9.2	22.0	12.8			
U	31.7	9.5	26.2	12.1	35.5	9.1	19.7	13.8			
V	34.3	11.0	23.1	11.7	32.5	8.5	21.2	11.7			
W	35.7	9.3	26.3	12.1	34.4	10.3	25.5	12.3			
X	42.1	7.4	28.3	11.2	39.2	8.6	28.2	12.1			
Avg.[b]	**35.4**	**9.0**	**26.1**	**11.9**	**35.5**	**9.3**	**24.3**	**12.8**	**Avg.**	**23.2**	**12.7**

[a] Peak heights were determined from the anomalous Fourier difference electron density map from data collected at λ =1.6314 Å.

[b] Average *B*-factors and peak heights for each Fe site

Figure 2-12 shows a superimposition of the empty (green) and filled (magenta)ferroxidase centers illustrating the fact thet His130 is rotated away from the diiron center in the empty ferroxidase center and undergoes structural reorganization upon binding with iron.

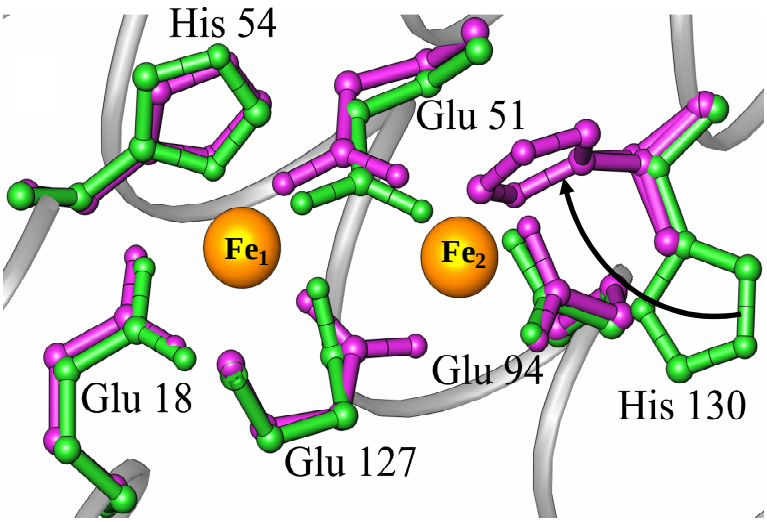

Figure 2-12: Overlay of the mineralized (green) and Fe soaked (magenta) Pa BfrB structures showing their ferroxidase centers.

As figure 2-12 depicts, in the presence of iron, His130 rotates towards the diiron center to coordinate Fe_2. This conformational flexibility shown by His130 is associated with the binding and oxidation of external Fe^{2+} at the ferroxidase center. The oxidized Fe_2 is released into the interior of the protein as the His 130 rotates away from the ferroxidase center to adopt its non coordinating conformation. Therefore, the conformational flexibility of His130 may be important in gating iron from the ferroxidase center into the iron core. In addition, when the mineralized and Fe soaked structures are superimposed, the residual electron density from the Fe soaked structure fits closely to the His 130 of the mineralized structure, indicating that the His 130 in the Fe soaked structure has two conformations. One conformation would be that of His 130 coordinated to Fe_2 (70% occupancy) and the other similar to the conformation seen in the empty ferroxidase center (figure 2-12 green conformation). According to these observations, it

is clear that in the as isolated and mineralized structures, His130 adopts the non coordinating conformation and move to the coordinating conformation only in the presence of iron at the ferroxidase center. Therefore, the Fe soaked structure represents a snapshot of the iron uptake process by the ferroxidase center in which His130 has been caught in the process of returning to its coordinative conformation. To further investigate whether the oxidation of the protein in air would form a ferroxidase center with iron at the Fe_1 position and nearly empty Fe_2, the mineralized Pa BfrB crystals were soaked in an iron solution for 15 minutes, followed by a soak in crystallization solution for 15 minutes. Then the crystals were flash frozen for data collection. The structure obtained (double–soaked) from these crystals showed a ferroxidase center completely devoid of iron. The conformation of the side chains of the ferroxidase center ligands were observed to be identical to those adopted in the structures of as isolated and mineralized crystals, in which the side chain of His130 is in its non coordinative conformation. Weak residual difference density was observed in the ferroxidase center due to the low-occupancy of iron. In addition, relatively larger peaks were observed in the difference electron density maps at the $Fe_{(in)}$ sites. Refinement of Fe ions with full occupancy at these sites resulted in B factors that were 2-3 times higher than those of the average value of the model. The lengthened non bonded contacts between $Fe_{(in)}$ and His153/His155 at these sites and the relatively weak electron density compared to those of the Fe soaked structure most probably reflect the dynamic motions likely resulting in incorporation of $Fe_{(in)}$ in the core mineral. Further, higher B factors relative to those of the overall model were observed due to the presence of potassium ions in the 4-fold pores refined with occupancy of 0.5. All these unique observations and findings indicate the fact that the diiron center of this protein is relatively labile. The observed dynamic behavior of the diiron center could be a property which allows Pa BfrB to uptake iron efficiently via the ferroxidase

center. These ideas were further investigated with the aid of kinetic studies, an dthe corresponding observations and conclusions will be presented later in this chapter.

Ferroxidase pore

The outer surface of the Pa BfrB structure reveals a pore that probably functions as a pathway for the translocation of Fe^{2+} from the outer surface of the protein to the ferroxidase center and oxidized iron (Fe^{3+}) from the ferroxidase center to the inner core.

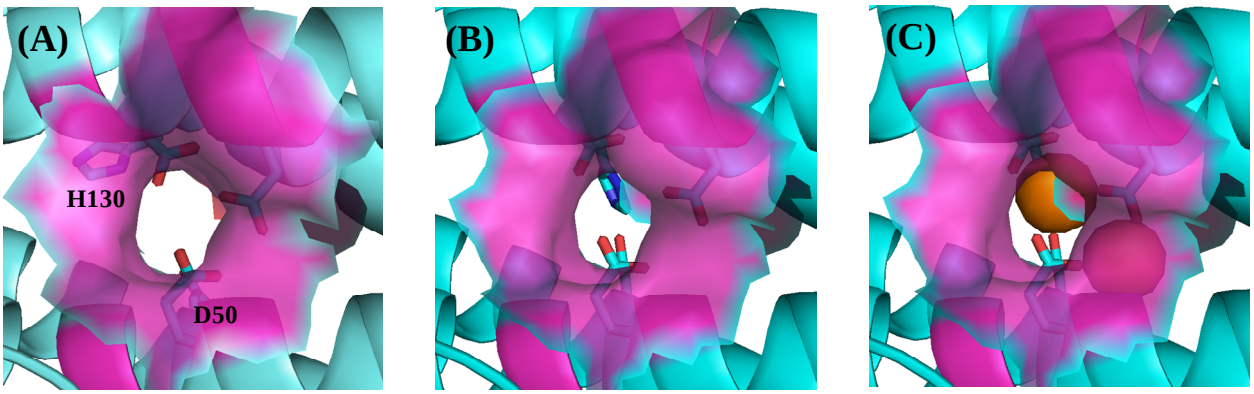

Figure 2-13: Stereo view of the ferroxidase pore viewed from the protein exterior. The semi-transparent surface representation (magenta) is constituted by residues lining the pore wall (Asn17, Ile20, Leu93, Lys93 and Ala97). (A) The "gate-open" conformation of the Asp50 and His130 side chains allows a nearly unobstructed view of the interior cavity through the pore. (B) The "gate-closed" conformation of Asp50 and His130 obstruct the bottom of the pore and poise H130 to coordinate Fe_2. The ferroxidase iron is not shown for clarity. (C) View identical as in (B) but showing the ferroxidase iron ions as orange spheres. The side chain is His130 is below Fe_2, which is located at the bottom of the pore. Fe_1 in the interior can be seen through the semi-transparent surface.

A semitransparent surface representation of the mineralized Pa BfrB structure (apoferroxidase) in Figure 2-13 shows a section of a pore that leads towards the ferroxidase center from the exterior of the protein. The walls of this pore are made of the backbone and the side chain of Asn17, the side chain of Ile20, Leu93, the hydrophobic component of the Lys96 side chain and the back bone of Ala97. The carboxyl oxygens of Glu51 and Glu94 which are the terminal and bridging ligands in the ferroxidase center respectively can be observed at the bottom of the pore. It can be clearly observed (Figure 2-13A) that the conformation of the His130 side chain in the mineralized structure does not obstruct the pore, which we termed the "gate open" conformation. Figure 2-13B represents an identical view of the Fe-soaked structure (holo ferroxidase) where iron atoms are not shown. In this structure the His 130 has adopted its "gate closed" conformation, serving as a cap at the end of the pore and also as a ligand to Fe_2. Figure 2-13C is identical to the figure 2-13B, except that the ferroxidase iron ions have been added, clearly showing Fe_2 at the bottom of the pore. The Fe_2 is coordinated by the ligands Glu94 and His130 and bridged to Fe_1 by Glu51 and Glu127. As illustrated in the above figure 2-13, Fe^{2+} enters the ferroxidase center through the ferroxidase pore, where it is captured by the ferroxidase ligands including His130. Upon binding with Fe^{2+}, His130 moves from its "gate open" conformation to "gate closed" conformation. This conformational change of His130 may be triggered by small conformational changes that occur when the di-Fe^{2+} complex is formed. Subsequently, the di-Fe^{2+} complex is oxidized to di-Fe^{3+} at the ferroxidase center leading to a shorter inter nuclear distance [8], which in turn may trigger the His130 to change its conformation to gate open conformation. In addition, this change of the conformation may have also been triggered by the subtle ligand rearrangement required to accommodate an μ-oxo or μ-hydroxo bridged di-Fe^{3+} moiety. Furthermore, in addition to the conformational change of

His130, another important change in the side chain of D50 was also observed. As shown in figure 2-13A the side chain of D50 does not obstruct the pore. However, it may be contributing to cover the bottom of the pore in the gate closed conformation (figure 2-12C). Therefore, it can be clearly seen that the concerted motions of D50 and His130 are very important in opening and closing the gate for the translocation of Fe^{3+} from the ferroxidase center to the interior cavity

Three and four fold pores in Pa BfrB.

Figure 2-8 shows that the core of bacterioferritn is connected to the exterior of the protein by six 4-fold and eight 3-fold channels. As is shown in the figure 2-14A, the entrance to the 3-fold channel from the outside, is formed by three Glu109 side chains which form salt bridges with three Arg117 side chains, thus restricting pore access. The structure of iron soaked Pa BfrB reveals that the interior of the 3-fold pore the side chains of Lys 121 may be disordered, as there was no electron density observed beyond the β carbons (Figure 2-14B). However, residual electron density was observed in the 3-fold pore which may be due to the presence of either sulfate or phosphate ions, subsequent refinements revealed that the residual electron density was due to a presence of a sulfate ion in the pore.

Sulfate ions are present in the soaking solution which is prepared using 50 mM $FeSO_4$ and also in the crystallization solution which contain 200 mM $LiSO_4$. Since SO_4^{2-} ions were observed only in the Fe soaked crystal structure, it can be hypothesized that 3-fold pores may function as pathways of anion uptake in Pa-BfrB. However, further studies are required to confirm this idea of anion trafficking through 3-fold pores in Pa BfrB.

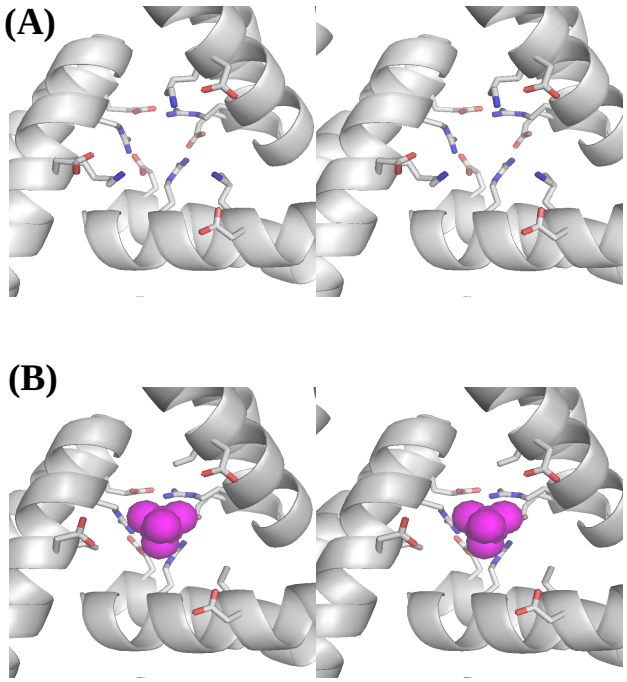

.

Figure 2-14: (A) Stereo view of a three-fold channel in the mineralized Pa BfrB structure, viewed from the interior cavity (O is in red and N in blue) (B) Identical view of a three-fold channel in the Fe-soaked structure. The interior of the pore shows the presence of sulfate (magenta) and disorder in the side chains of Lys21.

There are six 4-fold pores in Pa BfrB, located along the four fold axis of the molecule. Figure 2-15 shows a 4-fold pore in the structure of mineralized Pa BfrB, with a potassium ion coordinated by the side chains of Asn148 and Gln151 residues. Negligible anomalous difference density was observed in the 4-fold pore in a data set collected at 1.6314 Å, thus eliminating the possibility that the metal ion in the 4-fold pore is iron. Further, when Fe ions or water molecules were modeled at these sites, residual negative or positive difference density was observed. In addition, potassium ions were also observed in equivalent positions of the 4-fold pores in Fe soaked crystal structure. The analysis of the data sets collected at 1.6314 Å, from the Fe soaked

Pa BfrB crystals, provides strong evidence to confirm that the Fe ions are absent in the 4-fold pores due to the absence of anomalous difference density in the 4-fold pore which contrasts with the strong anomalous signals observed from the heme iron, ferroxidase iron and $Fe_{(in)}$ and $Fe_{(out)}$ (Table 2-2).

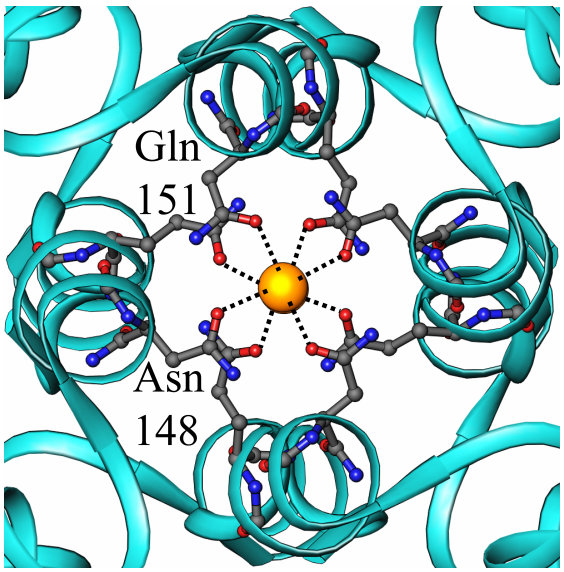

Figure 2-15: View of a 4-fold pore where a potassium ion (yellow sphere) is coordinated by Gln151 and Asn148. The potassium ion in the four fold pore is present in the as isolated, mineralized, Fe-soaked and double-soaked structures.

The potassium ions observed in both Fe soaked and non soaked crystals are from the protein storage buffer which contains 100 mM potassium phosphate. In addition to the structure of Pa BfrB, two independent structures of Av Bfr have also been observed to contain metal ions (Fe and Ba) in the 4-fold pores coordinated by Asn148 and Gln151 [11, 34]. These observations suggest that Fe ions may enter or exit the protein via the 4-fold pores in the molecule.

Iron bound to the Internal [$Fe_{(in)}$] and external [$Fe_{(out)}$] surface

In addition to the iron ions observed at the ferroxidase center, the mineralized Fe soaked crystal structure revealed the presence of two additional iron sites. One site is located on the exterior surface of the protein, is termed $Fe_{(out)}$, and the other site was found on the internal surface, protruding into the internal cavity, termed as $Fe_{(in)}$.

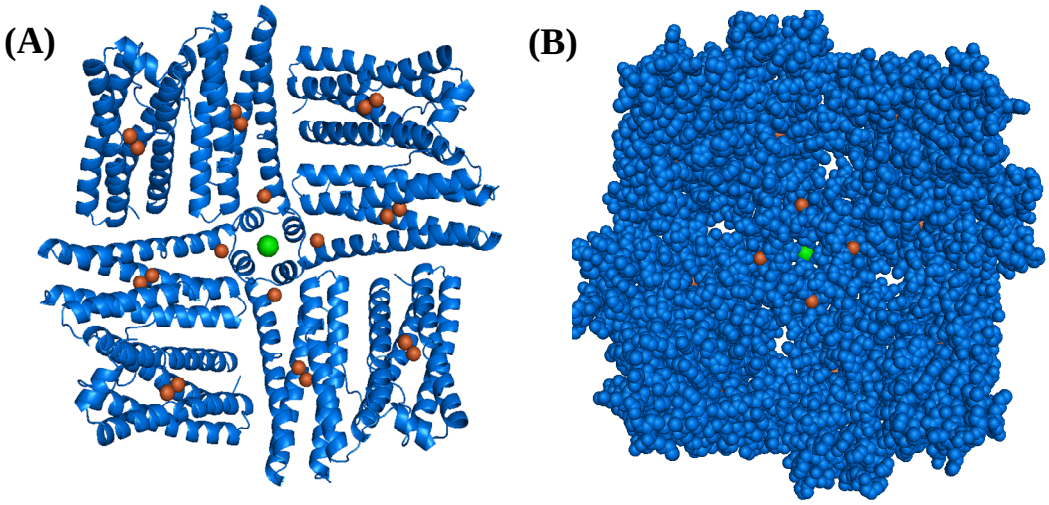

Figure: 2-16 (A) A four fold-pore and neighboring B pores in the Fe-soaked Pa BfrB structure viewed from the interior cavity. The iron and potassium ions are represented by orange and green spheres, respectively. (B) An identical view in CPK rendering, which facilitates visualization of the B pores and of the four $Fe_{(in)}$ ions surrounding the four-fold pore.

Figure 2-16A depicts a part of the BfrB molecule including a 4-fold pore, viewed from the interior of the protein. The 4-fold pore shown here is made of the subunits E, J, Q and V and the subunits I, F, R and U are also arranged with the 4-fold pore forming subunits to form a different type of pores, the so called B-pores [14]. Four of those B pores can clearly be seen in the CPK rendering in figure 2-16B. In figure 2-16A, a potassium ion (green sphere) was observed in the

4-fold pore coordinated by Asn148 and Glu151. In addition, four iron atoms were found surrounding each 4-fold pore and each iron atom is coordinated by His 155 and His153 from different subunits. As figure 2-17shows the octahedral coordination of each iron atom is completed by the water molecules.

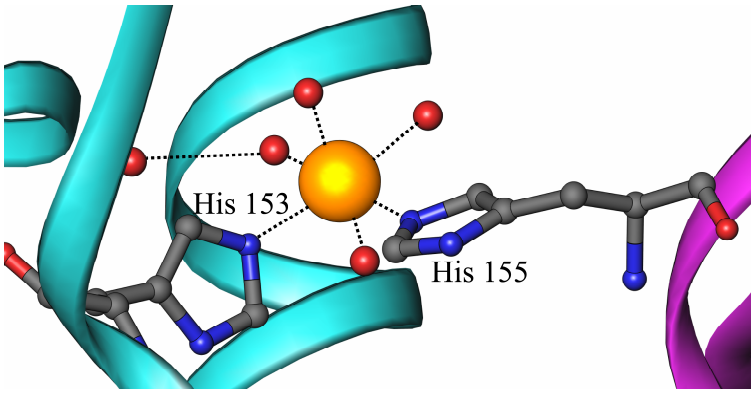

Figure 2-17: Non-bonded contacts between Fe ions and histidine residues. Fe ions and water molecules are represented as gold and red spheres, respectively. Fe_{in} is coordinated by His 153 from subunit J and His 155 from subunit E.

According to the crystal structures analyzed, and as illustrated in figure 2-18, three pathways of iron entry into the Pa BfrB inner core can be postulated: (1) via the ferroxidase pore, (2) via the 4-fold pores, and (3) via the B pores. When iron enters via the ferroxidase pore a change of the conformation of His 130 from its gate open to its gate closed conformation allows Fe^{3+} ions to move into the interior of the protein. At this position, Fe^{3+} ion is thought to be interacting with Glu47, His46, His43 and/or Tyr133, through which the Fe^{3+} ion moves to its position in the interior of the protein.

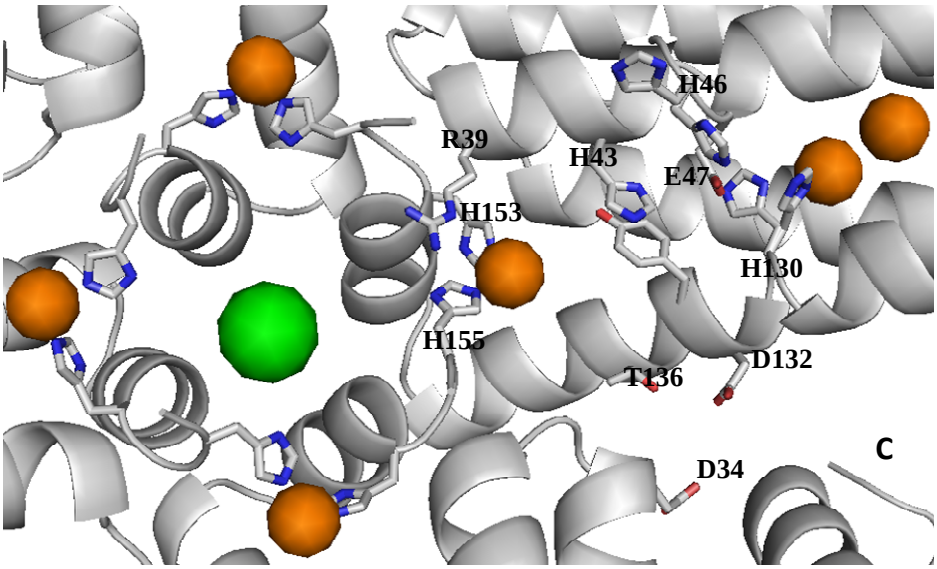

Figure 2-18: Different possible routes for moving iron ions from the ferroxidase pore, four-fold pore or B pores to their $Fe_{(in)}$ position.

In addition to the conformational change observed in His 130, His 46 was also observed to have two conformations which may be associated with the translocation of iron from the ferroxidase center to the $Fe_{(in)}$ position. Iron ions (likely Fe^{2+}) entering through 4-fold pores may be moved to the $Fe_{(in)}$ position in the interior of the protein through the interactions of Arg39 and His155 from different subunits. Iron entering through the B pores are assumed to interact with the side chains of Asp34, Thr136, Asp132 which may form a coordinating path towards the position of $Fe_{(in)}$. A study carried out with Ec Bfr has shown that the crystal form of Ec Bfr is also functional and can mineralize iron [11]. These iron ions have been observed in the interior of the protein, but at a different position from which was observed in Pa BfrB. In Ec Bfr, $Fe_{(in)}$ has been observed directly below the ferroxidase center, coordinated by Asp50 and His46. Another iron site on the surface of the Pa BfrB ($Fe_{(out)}$) was observed in the mineralized Fe

soaked crystal structure where it is coordinated by His10, His 107 and three water molecules (Figure 2-19B).

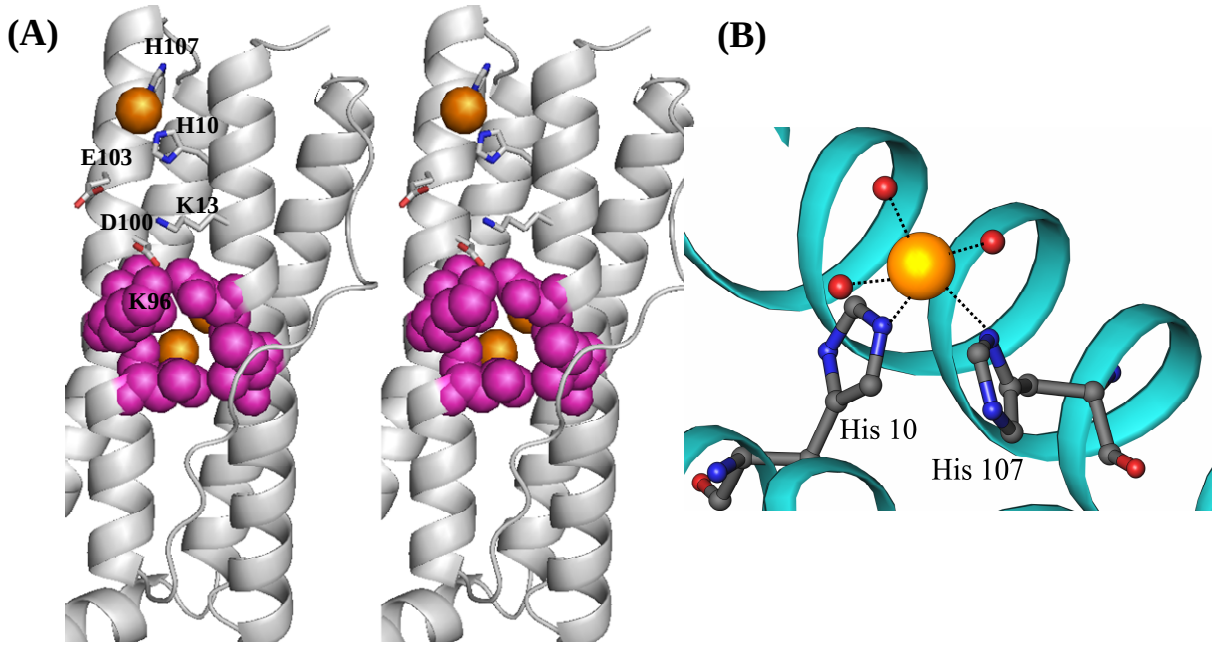

Figure 2-19: (A) Stereoveiw of the location of $Fe_{(out)}$ on the external surface of the Fe-soaked structure, where it is coordinated by His10, His107 and three water molecules. Iron ions are in orange, nitrogen atoms are in blue, oxygen atoms in red and residues lining the external outermost layer of the pore are in magenta and in CPK rendering. (B) Non-bonded contacts between Fe_{out} and surface residues His 10 and His 107.

The position of $Fe_{(out)}$ is closer to the ferroxidase pore, which may allow relativey easy translocation of iron from the outer surface to the ferroxidase pore. These $Fe_{(out)}$ sites show a near full occupancy in the crystal structure (Table 2-2) indicating a moderate to high affinity of

the Pa BfrB outer surface for iron and may be very important in capturing, coordinating and guiding iron ions towards the internalization pathway. As figure 2-19A clearly illustrates $Fe_{(out)}$ may be moved towards the ferroxidase pore through the interactions of the hydrophilic side chains of His10, His 107, E103, D100 and K13. Figure 2-19A shows the residues lining the ferroxidase pore in CPK rendering and the hydrophilic side chains which connect the $Fe_{(out)}$ with the pore in stick rendering. The side chain of Lys96 makes a salt bridge with Asp100 and when an Fe ion reaches the ferroxidase pore from its $Fe_{(out)}$ position, it may induce a conformational change of Asp100 that breaks the salt bridge with Lys96. Consequently, the conformation of Lys96 may also change, providing a pathway for the Fe^{2+} to enter the ferroxidase pore.

Iron uptake in solution by Pa BfrB confirms the notion of a gated mechanism of iron uptake via the ferroxidase center.

The preliminary experiments on the iron uptake by as-isolated Pa BfrB were carried out using conventional diode array spectrophotometer. Aliquots of Fe^{2+} solution containing 50 Fe^{2+} ions per protein molecule were added while monitoring the change of absorbance at 320 nm. These experiments were carried out at pH 6.5 at 30 ºC, in order to compare the observations with those made with Ec Bfr [2, 5]. The results obtained with Pa BfrB were completely different from those obtained with Ec Bfr.

As figure 2-20 shows, upon addition of 50 Fe^{2+} ions to Pa BfrB, a rapid increase of the absorbance near 300 nm (plotted at 320 nm) is observed and then it reaches a plateau and remains constant thereafter. The magnitude of the increase of absorbance at 320 nm at every addition of an aliquot of iron was observed to be nearly constant, suggesting that the ferroxidase

center of Pa BfrB is labile and once all the Fe^{2+} ions are oxidized at the ferroxidase center, it becomes empty.

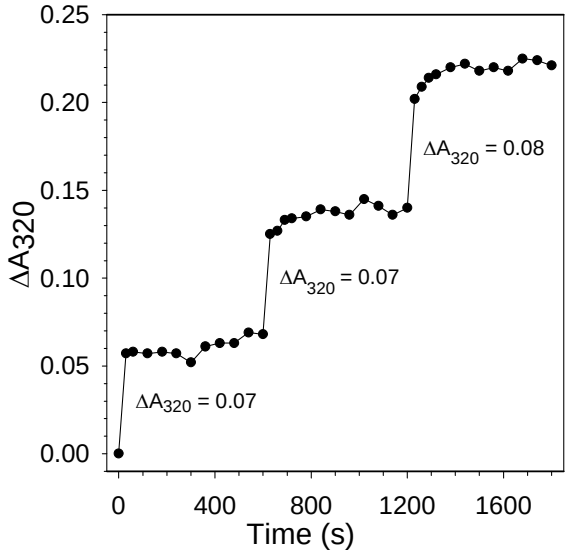

Figure 2-20: Change in ΔA_{320} upon subsequent additions of Fe^{2+} aliquots (50 Fe^{2+} ions per BfrB molecule) to a solution of as isolated Pa BfrB (0.8 μM) in 100 mM MES buffer, 100 mM KCl, pH 6.5. These observations are in good agreement with the fact that the ferroxidase centers of as-isolated, mineralized and double soaked structures are vacant. Since the initial steps of the iron uptake process occurs very rapidly, a stopped flow spectrophotometer was used to investigate the iron uptake by Pa BfrB in detail. To this end, a solution of Pa BfrB was mixed with solutions containing Fe^{2+} in different proportions (30, 50, 100, 200 and 300 Fe^{2+} ions/BfrB). The change of the absorbance at 320 nm was monitored to follow the mineralization process of Pa BfrB.

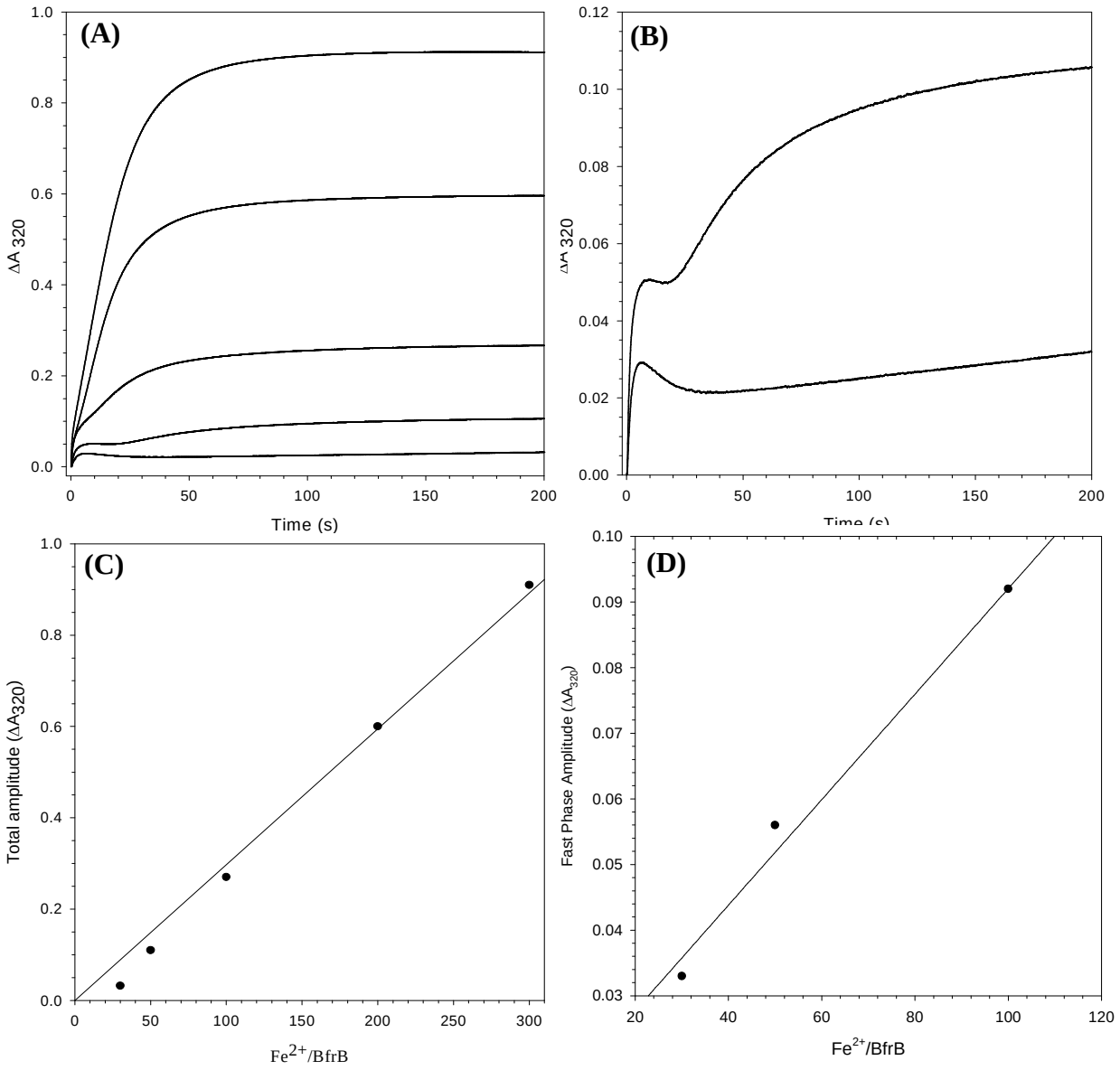

Figure 2-21: (A) Progress curves obtained after the addition of 30, 50, 100, 200 and 300 Fe^{2+} ions per Pa BfrB molecule in 100 mM MES buffer, 100 mM KCl, pH 6.5 and 30 °C. (B) Progress curves corresponding to the addition of 50 and 100 Fe^{2+} ions in (A) are shown to more clearly illustrate the decrease in absorbance that follows the fast phase. (C) A plot of the amplitude obtained at the end of 200 s for the progress curves in (A). (D) A plot of the amplitude of the fast phase as a function of Fe^{2+} load; the amplitudes were obtained from fitting

the first 5 s of the progress curves in (A), obtained after the addition of 30, 50 and 100 Fe^{2+} ions, to a mono exponential expression.

As illustrated in figure 2-21A, when the iron load is ≤ 100 Fe^{2+} ions/BfrB, two distinct phases can be observed. The fast phase lasts for < 10 s and the slower phase becomes faster gradually, as the iron load increases. Upon addition of 200 and 300 Fe^{2+}/BfrB the two phases can no longer be clearly distinguished. It is noteworthy that in the plots obtained by adding 30 and 50 Fe^{2+} ions / BfrB, the rapid increase at 320 nm corresponding to the fast phase is followed by a decrease in absorbance before initiating the slower phase (Figure 2-21B). This observation could be explained if the initial rapid increase in ΔA_{320} (fast phase) corresponds to the oxidation of the di-Fe^{2+} center to form di-Fe^{3+} center which is most probably μ-oxo (or μ-hydroxo)-bridged. The decrease of the absorbance at 320 nm observed after the fast phase is likely due to the migration of Fe^{3+} ions to the inner core where mineralization (slow phase) takes place. However, upon addition of higher iron loads (200, 300 Fe^{2+}/BfrB), the decrease of the absorbance at 320 nm cannot be observed as it is masked by the earlier onset of the slower phase with a large amplitude. Therefore, the results obtained from the structural studies showing that the ferroxidase center of Pa BfrB is vacated when Fe^{3+} ions are moved to the interior core, were further confirmed with the observations made in the stopped flow experiments where a decrease in the absorbance at 320 nm after the first fast phase was observed upon addition of low iron loads (< 100) to the protein. The iron uptake process of Pa BfrB with higher iron loads (> 200 Fe^{2+}/BfrB) takes ~100 s to complete, whereas that of Ec Bfr takes ~ 800 s at the same pH and temperature [5]. Further, unlike in Ec Bfr, a slow phase is observed in Pa BfrB with low iron loads which may correspond to the mineralization in the inner core. When the progress curves obtained at similar low iron loads in Pa BfrB and Ec Bfr are compared, in Ec Bfr, only the fast

phase is observed since the iron at the ferroxidase center is not translocated into the inner cavity [5]. The mineralization phase in Pa BfrB with low iron loads (<50 Fe^{2+}/Bfr) appears to take place very slowly and it does not seem to reach the completion even at 200 s. Figure 2-21C is plotted with the amplitudes of the slow phase of each iron load at 200 s against the number of iron atoms added per Pa BfrB molecule. It can be clearly seen that the amplitude of the plot obtained with 30 Fe^{2+}/BfrB has relatively low amplitude than what was expected according to the trend of the amplitudes obtained at higher iron loads. This slower mineralization phase at a load of 30 Fe^{2+}/BfrB could be due to the slow nucleation process resulted by the relatively small number of available Fe^{3+} ions. The rate of mineralization increases with the addition of higher iron loads such that the distinction between the two phases cannot be observed. The amplitude and the rate of the fast phase were calculated by fitting a monoexponential function to the first 5 s of the progress curves of 30, 50, and 100 Fe^{2+}/BfrB. The plot obtained by plotting the amplitude of the fast phase as a function of the iron load clearly shows that the fast phase does not saturate at an iron load of 50 Fe^{2+}/BfrB (Figure 2-21D).

In comparison, a similar plot obtained in Ec Bfr studies shows a saturation of the amplitude at the iron load of 50 Fe^{2+}/Bfr, which has been interpreted to explain the notion that the Ec Bfr ferroxidase center is stable and does not regenerate (Figure 2-22) [5, 11]. When the values of the rate constants of the fast phase of Pa and Ec Bfr are compared, a higher rate can be observed in Pa BfrB (pH 6.5, 30 ºC), and protein concentration is 1 µM) than that of Ec Bfr [38]. However, the above rates cannot be directly compared due to the fact that the Ec Bfr studies have been carried out with a lower protein concentration of (0.5 µM).

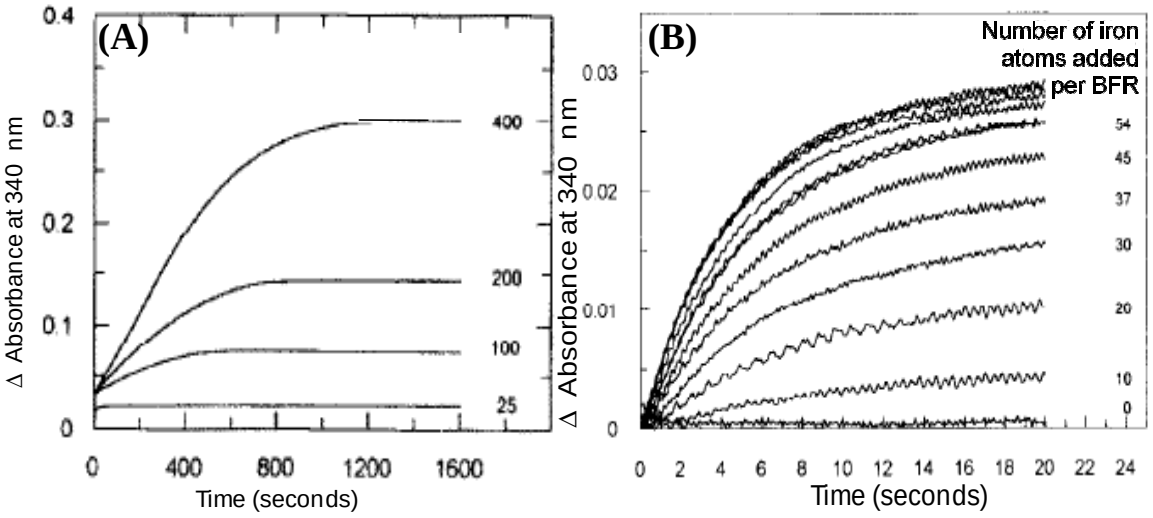

Figure 2-22: (A) Progress curves obtained upon addition of 30, 50, 100, 200 and 300 Fe^{2+} ions per Bfr molecule from *E.coli*. (B) Plots showing the saturation of the absorbance at 340 nm after adding 50 Fe^{2+} ions per Ec-Bfr molecule. Figures adopted from Le Brun N.E. et al, FEBS lettters,**1993**,(333),197-202 [5]

Discussion

Crystallization of BfrB

BfrB crystals were grown under aerobic conditions using sitting drop vapor diffusion method (Figure 2-23). This method formed crystals which were pure and large enough to obtain diffraction data to solve the structure of BfrB. The process of formation of crystals can be explained using the solubility diagram (Figure 2-24).

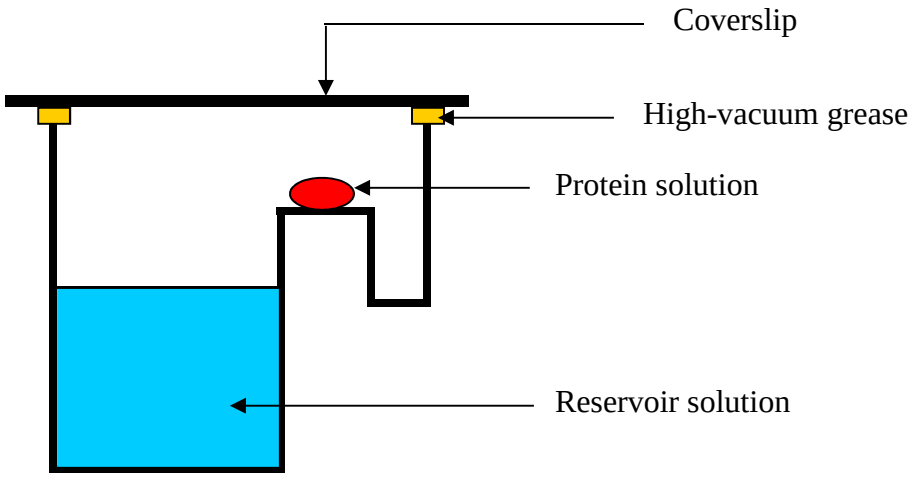

Figure 2-23: Schematics of a sitting drop vapor diffusion method used to grow BfrB crystals

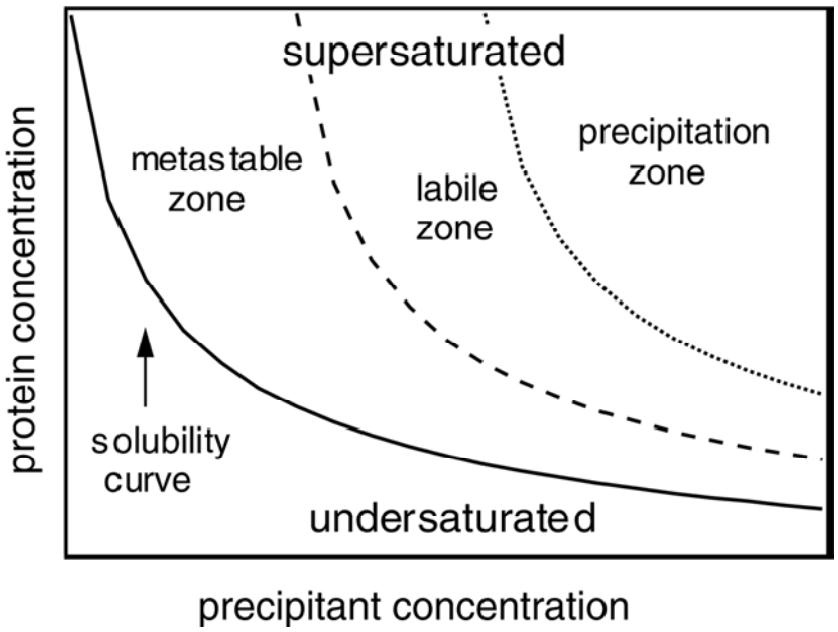

Figure 2-24: A Schematic phase diagram showing the variation of the solubility of aprotein as a function of the precipitant concentration [45].

As the diagram illustrates the solubility curve separates the protein into two main concentration zones called, undersaturated (below the solubility curve) and supersaturated

(above the solubility curve) phases of the protein. Supersaturated area is further divided into three areas where the crystals are expected to grow. However, the crystals will not be formed in the undersaturation phase. In the precipitation zone, the supersturation is very high that crystals will not be formed. However, protein can be seen to separate as large amorphous aggregates in this region. The metastable region forms crystals at a very slow rate unless seeding is introduced. In the nucleation zone, the saturation is optimal such that it forms crystals which may diffract well to obtain the structural data of the protein molecule [45].

The crystal structure of mineralized Pa BfrB, solved to 2.1 Å resolution was nearly identical to that of as isolated Pa BfrB. Both crystal structures did not show any metal] ions bound to the ferroxidase center. The observations made on the above crystal structures clearly indicate that the diiron center of Pa BfrB is unstable. However, the crystal structures of Bfrs from other organisms were shown to bind metal ions at the ferroxidase center [12-14,35-37].

Pa BfrB has a gated mechanism of iron uptake.

The mineralized Pa BfrB crystals, devoid of iron at the ferroxidase center, were soaked in a Fe^{2+} solution for 15 minutes. The resulted crystal structure (Fe soaked) contained a fully occupied ferroxidase center, confirming the fact that crystal form of Pa BfrB is functional. As mentioned in the results, two different conformations of His130 were observed in the mineralized and Fe soaked crystal structures, in which His130 is thought to be important in the process of iron internalization. Similarly, two different conformations (coordinative and non coordinative) of His130 have also been observed in the crystal structure of Av BfrB. These observations are in good agreement with the findings of Pa BfrB and may suggest that His 130 acts as a gate that allows the movement of iron from the ferroxidase center to the interior cavity

[12]. In addition, it has been shown that His130 side chain in Av Bfr changes its conformation from coordinative to non coordinative when the protein is reduced by dithionite [35]. This observation is in agreement with the hypothesis that the His130 side chain acts as a gate in the process of iron uptake by the ferroxidase center and iron internalization. Most of the structures of Bfr that have been studied contained metal ions such as iron, zinc, or manganese at the ferroxidase center. However, these metal ions showed a low occupancy at the Fe_2 position relative to Fe_1 [12-14, 35, 37]. In contrast to the previous observation, the as-isolated Dd Bfr structure showed a ferroxidase center fully occupied with iron. When Dd Bfr was reduced by dithionite and oxidized in air, the Fe_2 site of the ferroxidase center was observed to be empty [14]. Most of the Bfr structures that have been studied thus far showed a low occupancy at the Fe_2 site, suggesting the notion that translocation of Fe_2 from ferroxidase center to the interior cavity may be a part of the mechanism of iron uptake [12, 14, 35]. This interchangeable conformation of His130, observed in the process of iron internalization by Pa BfrB is clearly depicted in the figure 2-9. In addition to the changes observed in the conformation of His130, side chain of D50 was also observed to have important conformational changes in opening and closing the gate of the ferroxidase pore for iron internalization. In the investigations carried out with Ec and Dd Bfr, a similar pore has been observed on the external surface of the protein and it has been hypothesized to be a pathway of Fe^{2+} to enter the ferroxidase center [14, 36]. In Dd Bfr, when Fe^{2+} is oxidized to Fe^{3+} at the ferroxidase center, a relatively low occupancy of Fe_2 site is observed suggesting the moving of Fe^{3+} into the internal Bfr cavity [14, 38]. It has also been speculated that a concerted conformational change of the His59 and Glu131 side chains, which are assumed to act as a gate, is required to move Fe^{3+} ions from the Dd Bfr ferroxidase center to the interior cavity. It is important to note that the structures of Pa BfrB with the concerted

motion of His130 side chain and its gate open and gate closed conformations, are the first experimental observations that shows a pathway of a pore leading from the exterior surface of the protein to the ferroxidase center. Further, these structural studies also provide the first time direct experimental evidence of the concerted motion of D50 and His130 which forms a pathway to move iron from the ferroxidase center to the interior cavity of the protein. All these structural observations clearly indicate that the ferroxidase center of Pa BfrB is bifunctional, acting as a catalytic center and pore for iron internalization.

Pa BfrB has eight 3-fold pores and six 4-fold pores

The function of 3-fold channels in bacterioferritins, which are lined with both positively and negatively charged residues, is not yet established. However, the residual electron density data obtained from the structure of Fe soaked Pa BfrB crystals indicate the presence of sulfate ions in the 3-fold pores. This observation suggests that the 3-fold pores may function in anion trafficking through the pores. It is known that anions, especially the PO_4^{3-} ions are essential to form a mineral core in the interior cavity of Pa BfrB as these ions may be involved in nucleating and catalyzing the growth of the iron mineral [27, 31]. Therefore, it is important for Pa BfrB to have pathways to move both iron and phosphate ions in and out of the Pa BfrB molecule efficiently. Consequently, it can be hypothesized that the PO_4^{3-} ions required for the growth of a stable mineral core in Pa BfrB may enter the protein molecule via the 3 fold pores.

In eukaryotic ferritins, divalent cations have been observed in the 3-fold pores, which are lined with negatively charged amino acid residues [39]. Moreover, it has also been found that the replacement of these negatively charged residues in the 3-fold pores has a negative effect on the rate of iron uptake which may suggest that iron moves in and out of eukaryotic ferritins via the 3-

fold pores [39-41]. Studies carried out with eukaryotic ferritins have further revealed that localized unfolding at or near the 3-fold pores can accelerate the process of iron release from the eukaryotic ferritins. These findings are in good agreement with the fact that iron moves in and out of the ferritins via the 3-fold pores [31, 42,43].

Similar to 3-fold pores, the exact function of 4-fold pores of Pa BfrB is also not known. However, potassium ions were observed in the 4-fold pores of all the crystal structures obtained from Pa BfrB. Therefore, it is believed that cations (more likely iron ions) may move in and out of the protein via these 4-fold pores. No metal ion has been observed in the structures of Ec, Ms and Dd Bfr which may indicate that the structure and the function of the pores in all bacterioferritins are not the same [11, 13, 14, 36]. The molecular architecture of the 4-fold pores of Pa and Av Bfr are very similar. Each 4-fold pore is made of two layers; the outer layer is formed by Asn148 and the inner layer is formed by Gln151. In contrast to that, Ec., Ms, and Dd Bfr 4-fold pores are composed of three layers. In Ec Bfr 4-fold pores, the outer layer is made of Asn148 whereas Glu151 and Arg155 form the central and inner layers, respectively. The presence of metal ions in the 4-fold pores of Pa and Av BfrB structures, sharing the similar molecular architecture, is an indication of the function of 4-fold pores, which may be the trafficking of iron in and out of the protein molecule.

The ferroxidase pore is an iron entry port in Pa BfrB

The crystals grown from the mineralized protein did not contain iron. However, soaking those crystals in an iron solution showed iron at the ferroxidase center and on the external ($Fe_{(out)}$) and internal surface ($Fe_{(in)}$) of the protein. According to the above observations the ferroxidase pore leads to the ferroxidase center in which hydrophilic residues may move Fe^{2+}

from the outer surface to the ferroxidase center. At the ferroxidase center, iron ions are moved to the interior of the protein by the gated mechanism of His130. These findings suggest that the ferroxidase center is essential and plays a very important role in the process of iron internalization. In order to get more experimental evidence on the iron uptake via the ferroxidase center, the crystals of the mineralized protein were soaked in a Fe^{2+} solution for 15 minutes, followed by soaking in a non Fe^{2+} containing crystallization solution for 15 minutes. The resultant crystals did not have iron atoms in the structure and the ferroxidase center was also observed to be empty. The structural features of the ferroxidase center were very similar to that of non iron soaked mineralized protein, where His130 was at 100% occupancy in the gate-open conformation. These results show that the favored conformation of the empty ferroxidase center is the gate open conformation and confirms the hypothesis that iron ions are internalized through the ferroxidase center. This idea was further investigated using solution experiments.

According to the pervious findings, the iron uptake process by Ec-Bfr is described in three kinetically resolved phases: first, Fe^{2+} binds the ferroxidase center (phase 1), followed by the oxidation of Fe^{2+} forming a μ-oxo-bridged di-Fe^{3+} moiety (phase 2). Third phase is the formation of the Fe mineral inside the core. Phases 1 and 2 take place very fast ($t_{1/2}$ is ~5 ms and 15 s respectively) whereas the phase 3 occurs relatively slow ($t_{1/2}$ = ~15min) [5]. Experiments carried out with Ec Bfr show that upon addition of ~ 50 iron atoms to the protein, the absorbance at 340 nm saturates indicating that a stable di-iron center is formed at each subunit of Ec Bfr. When more Fe^{2+} ions are added, the absorbance at 340 nm increases relatively slowly indicating that phase 3 kinetics are being taken place [2, 5]. In contrast to the observations made on Pa BfrB, in Ec Bfr there is no structural evidence to indicate an existence of a clear pathway for the translocation of ferroxidase iron to the inner core. The observations of the kinetic experiments

on Ec Bfr and the absence of structural evidence of showing a pathway of ferroxidase iron to the core may imply that the ferroxidase center of Ec Bfr does not act as a pore for iron uptake. Therefore in Ec Bfr, once the ferroxidase center is formed, other Fe^{2+} ions are taken into the protein through the other pores of the protein and subsequently these iron ions are oxidized by transferring electrons to the ferroxidase iron, which in turn reduce molecular O_2[11]. On the other hand, the observations of the experiments carried out with Pa-BfrB are strikingly different from those of Ec-Bfr. Upon addition of 50 Fe^{2+} to Pa-BfrB, the absorbance ~ 300 nm does not saturate. Alternatively, a rapid increase of the absorbance near 300 nm is observed which rapidly reaches a plateau and remains constant until the next aliquot of iron is added. As seen in figure 2-20, the magnitude of the change in absorbance at 320 nm (ΔA_{320}) following the addition of each aliquot of Fe^{2+} remains nearly constant indicating that the ferroxidase center in Pa BfrB is indeed labile. Once all Fe^{2+} ions are oxidized and internalized, the ferroxidase center is vacated and this observation is consistent with the fact that the ferroxidase center in the as isolated, mineralized and double soak structures is empty. According to these results obtained from the solution phase suggest that, unlike in Ec Bfr, the ferroxidase center of Pa BfrB is labile and therefore corroborate the idea derived from the structural investigations that the ferroxidase center of Pa BfrB has a dual role of substrate oxidizing center and pore for iron internalization. Results from both structural and kinetic studies carried out with Pa-BfrB suggest that, eventhough all bacterioferritins possess similar molecular architecture, their mechanisms of iron trafficking in and out of the protein are not the same. The ferroxidase center of Ec-Bfr is stable and functions as a catalytic site but not as a pore for iron internalization. In comparison, the ferroxidase center of Pa BfrB functions as the center of oxidation and internalization of iron enabling the protein to capture, oxidize and store iron with a higher efficiency.

Appendices

Appendix I: Protein Crystallization Conditions-Wizard 11 random sparse matrix crystallization Conditions.

1 10% (w/v) PEG-3000 acetate pH 4.5 Zn(OAc)2

2 35% (v/v) 2-methyl-2,4-pentanediol MES pH 6.0 Li2SO4

3 20% (w/v) PEG-8000 Tris pH 8.5 MgCl2

4 2.0 M (NH4)2SO4 cacodylate pH 6.5 NaCl

5 20% (v/v) 1,4-butanediol HEPES pH 7.5 NaCl

6 10% (v/v) 2-propanol phosphate-citrate pH 4.2 Li2SO4

7 30% (w/v) PEG-3000 Tris pH 7.0 NaCl

8 10% (w/v) PEG-8000 Na/K phosphate pH 6.2 NaCl

9 2.0 M (NH4)2SO4 phosphate-citrate pH 4.2 none

10 1.0 M (NH4)2HPO4 Tris pH 8.5 none

11 10% (v/v) 2-propanol cacodylate pH 6.5 Zn(OAc)2

12 30% (v/v) PEG-400 cacodylate pH 6.5 Li2SO4

13 15% (v/v) ethanol citrate pH 5.5 Li2SO4

14 20% (w/v) PEG-1000 Na/K phosphate pH 6.2 NaCl

15 1.26 M (NH4)2SO4 HEPES pH 7.5 none

16 1.0 M sodium citrate CHES pH 9.5 none

17 2.5 M NaCl Tris pH 7.0 MgCl2

18 20% (w/v) PEG-3000 Tris pH 7.0 Ca(OAc)2

19 1.6 M NaH2PO4/0.4 M K2HPO4 phosphate-citrate pH 4.2 none

20 15% (v/v) ethanol MES pH 6.0 Zn(OAc)2

21 35% (v/v) 2-methyl-2,4-pentanediol acetate pH 4.5 none

22 10% (v/v) 2-propanol imidazole pH 8.0 none

23 15% (v/v) ethanol HEPES pH 7.5 MgCl2

24 30% (w/v) PEG-8000 imidazole pH 8.0 NaCl

25 35% (v/v) 2-methyl-2,4-pentanediol HEPES pH 7.5 NaCl

26 30% (v/v) PEG-400 CHES pH 9.5 none

27 10% (w/v) PEG-3000 cacodylate pH 6.5 MgCl2

28 20% (w/v) PEG-8000 MES pH 6.0 Ca(OAc)2

29 1.26 M (NH4)2SO4 CHES pH 9.5 NaCl

30 20% (v/v) 1,4-butanediol imidazole pH 8.0 Zn(OAc)2

31 1.0 M sodium citrate Tris pH 7.0 NaCl

32 20% (w/v) PEG-1000 Tris pH 8.5 none

33 1.0 M (NH4)2HPO4 citrate pH 5.5 NaCl

34 10% (w/v) PEG-8000 imidazole pH 8.0 none

35 0.8 M NaH2PO4/1.2 M K2HPO4 acetate pH 4.5 none

36 10% (w/v) PEG-3000 phosphate-citrate pH 4.2 NaCl

37 1.0 M K/Na tartrate Tris pH 7.0 Li2SO4

38 2.5 M NaCl acetate pH 4.5 Li2SO4

39 20% (w/v) PEG-8000 CAPS pH 10.5 NaCl

40 20% (w/v) PEG-3000 imidazole pH 8.0 Zn(OAc)2

41 2.0 M (NH4)2SO4 Tris pH 7.0 Li2SO4

42 30% (v/v) PEG-400 HEPES pH 7.5 NaCl

43 10% (w/v) PEG-8000 Tris pH 7.0 MgCl2

44 20% (w/v) PEG-1000 cacodylate pH 6.5 MgCl2

45 1.26 M (NH4)2SO4 MES pH 6.0 none

46 1.0 M (NH4)2HPO4 imidazole pH 8.0 NaCl

47 2.5 M NaCl imidazole pH 8.0 Zn(OAc)2

48 1.0 M K/Na tartrate MES pH 6.0 none

All formulations are made with ultrapure ASTM Type I water and sterile-filtered stock solutions. Store at 4-25 ºC.

Appendix II: Protein Crystallization Conditions-Cryo 1 sparse matrix crystallization conditions.

1 40% (v/v) 2-methyl-2,4-pentanediol phosphate-citrate pH 4.2 none

2 40% (v/v) ethylene glycol acetate pH 4.5 none

3 50% (v/v) PEG-200 citrate pH 5.5 none

4 40% (v/v) PEG-300 HEPES pH 7.5 0.2 M NaCl

5 40% (v/v) PEG-400 citrate pH 5.5 0.2 M MgCl2

6 40% (v/v) PEG-600 cacodylate pH 6.5 0.2 M Ca(OAc)2

7 40% (v/v) ethanol Tris pH 8.5 0.05 M MgCl2

8 35% (v/v) 2-ethoxyethanol cacodylate pH 6.5 none

9 35% (v/v) 2-propanol phosphate-citrate pH 4.2 none

10 45% (v/v) glycerol imidazole pH 8.0 none

11 35% (v/v) 2-methyl-2,4-pentanediol Tris pH 8.5 0.2 M (NH4)2SO4

12 50% (v/v) ethylene glycol acetate pH 4.5 5% (w/v) PEG-1000

13 30% (v/v) PEG-200 MES pH 6.0 5% (w/v) PEG-3000

14 20% (v/v) PEG-300 phosphate-citrate pH 4.2 0.2 M (NH4)2SO4, 10% (v/v) glycerol

15 50% (v/v) PEG-400 CHES pH 9.5 0.2 M NaCl

16 30% (v/v) PEG-600 MES pH 6.0 5% (w/v) PEG-1000, 10% (v/v) glycerol

17 40% (v/v) 1, 2-propanediol HEPES pH 7.5 none **18** 35% (v/v) 2-ethoxyethanol imidazole pH 8.0 0.05 M Ca(OAc)2

19 35% (v/v) 2-propanol Tris pH 8.5 none

20 30% (v/v) 1,2-propanediol citrate pH 5.5 20% (v/v) 2-methyl-2,4-pentanediol

21 40% (v/v) 1,2-propanediol acetate pH 4.5 0.05 M Ca(OAc)2

22 40% (v/v) ethylene glycol Na/K phosphate pH 6.2 none

23 40% (v/v) 2-methyl-2,4-pentanediol Tris pH 7.0 0.2 M (NH4)2SO4

24 40% (v/v) PEG-400 Na/K phosphate pH 6.2 0.2 M NaCl

25 30% (v/v) PEG-200 Tris pH 8.5 0.2 M (NH4)2HPO4

26 40% (v/v) PEG-300 CHES pH 9.5 0.2 M NaCl

27 30% (v/v) PEG-400 CAPS pH 10.5 0.5 M (NH4)2SO4, 10% (v/v) glycerol

28 30% (v/v) PEG-600 HEPES pH 7.5 0.05 M Li2SO4, 10% (v/v) glycerol

29 40% (v/v) PEG-300 CHES pH 9.5 0.2 M sodium citrate

30 35% (v/v) 2-ethoxyethanol citrate pH 5.5 none

31 35% (v/v) 2-propanol citrate pH 5.5 5% (w/v) PEG-1000

32 40% (v/v) 1,2-propanediol CHES pH 9.5 0.2 M sodium citrate

33 25% (v/v) 1, 2-propanediol imidazole pH 8.0 0.2 M Zn(OAc)2, 10% (v/v) glycerol

34 40% (v/v) 2-methyl-2,4-pentanediol imidazole pH 8.0 0.2 M MgCl2

35 40% (v/v) ethylene glycol HEPES pH 7.5 5% (w/v) PEG-3000

36 50% (v/v) PEG-200 Tris pH 7.0 0.05 M Li2SO4

37 40% (v/v) PEG-300 cacodylate pH 6.5 0.2 M Ca(OAc)2

38 40% (v/v) PEG-400 Tris pH 8.5 0.2 M Li2SO4

39 40% (v/v) PEG-600 phosphate-citrate pH 4.2 none

40 40% (v/v) ethanol phosphate-citrate pH 4.2 5% (w/v) PEG-1000

41 25% (v/v) 1, 2-propanediol phosphate-citrate pH 4.2 5% (w/v) PEG-3000, 10% (v/v) glycerol

41 25% (v/v) 1, 2-propanediol phosphate-citrate pH 4.2 5% (w/v) PEG-3000, 10% (v/v) glycerol

42 40% (v/v) ethylene glycol Tris pH 7.0 none

43 50% (v/v) ethylene glycol Tris pH 8.5 0.2 M MgCl2

44 50% (v/v) PEG-200 cacodylate pH 6.5 0.2 M Zn(OAc)2

45 20% (v/v) PEG-300 Tris pH 8.5 5% (w/v) PEG-8000, 10% (v/v) glycerol

46 40% (v/v) PEG-400 MES pH 6.0 5% (w/v) PEG-3000

47 50% (v/v) PEG-400 acetate pH 4.5 0.2 M Li2SO4

48 40% (v/v) PEG-600 imidazole pH 8.0 0.2 M Zn(OAc)2

All formulations are made with ultrapure ASTM Type I water and sterile-filtered stock solutions.

Store at 4-25 º

References

[1] Zhao, G.; Bou-Abdallah, F.; Arosio, P.; Levi, S.; Janus-Chandler, C.; Chasteen, N. D. (2003) MUlitiple Pathways for Mineral Core Fomation in Mammalian Apoferritin. The role of Hydrogen Peroxide. *Biochemistry 42*, 3142-3150.

[2] Yang, X.; Le Brun, N.E.; Thomson, A.J.; Moore G.R.; Chasteen, N.D. (2000) The Iron Oxidation and Hydrolysis Chemistry of Escherichia coli Bacterioferritin. *Biochemistry 39*, 4915-4923.

[3] Bunker, J.; Lowry, T.; Davis G.; Zhang, B.; Brosnahan, D.; Lindsay, S.; Costen, R.; Choi, S.; Arosio, P.; Watt, G.D. (2005) Kinetic Studies of Iron Deposition Catalyzed by Recombinant. Human Liver Heavy and Light Chain Ferritins and *Azotobactor vinelandii* bacterioferritin using O_2 and H_2O_2 as Oxidants. *Biophysical Chemistry 114*, 235-244.

[4] Levi, S.; Luzzago, A.; Cesareni, G.; Cozzi, A.; Franceschinelli, F.; Albertini, A.; Arosio, P. (1988) Mechanism of Ferritin Iron Uptake: Activity of the H-chain and Deletion Mapping of the Ferro-oxidase Site. *Journal of Biological Chemistry 263*, 18086-18092.

[5] Le Brun, N.E.; Wilson, M.T.; Andrews, S.C.; Guest, J.R.; Harrison, P.M.; Thomson, A.J.; Moore, G.R. (1993) Kinetic and Structural Characterization of an Intermediate in the Biomineralization of Bacterioferritin. *FEBS Letters 333*, 197-202.

[6] Baaghil, S.; Lwin, A.; Moore, G.R.; Le Brun, N.E.(2003) Core Formation in Escherichia coli Bacterioferritin Requires a Functional Ferroxidase Center. *Biochemistry 42*, 14047-14056.

[7] Lewin, A.; Moore. G.R.; Le Brun, N.E. (2005) Formation of Protein-Coated Iron Minerals. *Dalton Transactions 3*, 597-3610.

[8] Kurtz, D.M. (1997) Structural Similarity and Functional Diversity of Diiron-Oxo Proteins. *Jounal of Biological Inorganic Chemistry 2*, 159-167.

[9] Le Brun, N.E.; Andrews, S.C.; Guest, J.R.; Harrison, P.M.; Moore, G.R.; Thomson, A.J. (1995) Identification of the Ferroxidase Center of *Escherichia coli.* Bacteroferritin. *Journal of Biochemistry* 257, 7672-7677.

[10] Bou-Abdallah, F.; Woodhall, M.R.; Velázquez-Campoy, A.; Andrews, S.C.; Chasteen, N.D. (2005) Thermodyanamic Analysis of Ferous Ion Binding to *Escherichia coli* Ferritin EcFtnA. *Biochemistry 44*, 13837-13846.

[11] Crow, A; Lawson, T.L.; Lewin, A.; Moore, G.R.; Le Brun, N.E. (2009) Structural Basis for Iron mineralization by bacterioferritin. *Journal of American Chemical Society 131*, 6808-6813.

[12] Liu, H.L.; Zhou, H.N.; Xing, W.M.; Zhao, J.F.; Li, S. X.; Huang, J.F.; Bi, R.C. (2004) 2.6 Å Rroesolution of Crystal Structure of the Bacterioferritin from Azotobactor vinelandii FEBS Letters *573*, 93-98.

[13] Janowski, R.; Auerbach-Nevo, T.; Weiss, M.S. (2007) Bacterioferritin from Mycobacterium smegmatis Contains Zinc in its Dinuclear Site. Protein Science 17, 1138-1150.

[14] Macedo, S.; Romão, C.V.; Mitchell. E.; Matias, P.M.; Liu, M.Y.; Xavier, A.V.; LeGall, J.; Teixeira, M.; Lindley, P.(2003) The Nature of the Di-Iron Site in the Bcaterioferritin from Desulfovibrio desulfuricans. *Nature Structural Biology 10*, 285-290.

[15] Cobessi, D.; Huang, L.S.; Ban, M.; Pon, N.G.; Daldal, F.; Berry, E.A. (2002) The 2.6 Å Resolution Structure of Rhodobactor capsulatus Bacterioferritin with Metal-Free Dinuclear Site and Heme Iron in Crystallographic " Special Position" *Acta Crystallography D58*, 29-38.

[16] Ikemura, T. (1985) Codon Usage and and tRNA Content in Unicellular and Muliticellular Organisms. *Molecular Biology and Evolution 2*, 13-34.

[17] Berry, E.A.; Trumpower, B.L. (1987) Simultaneous Determination of Hemes a,b and c from Pyridine Hemochrome Spectra. *Analytical Biochemistry 161*, 1-15.

[18] Ringeling, P.L.; Davy, S.L.; Monkara, F.A.; Hunt, C.; Dickson, D.P.E.; Mcewan, A.G.; Moore, G.R. (1994) Characterization of Bacterioferritin and Formation of Non-Haem Iron Particles in Intact Cells. *Europian Journal of Biochemistry 223*, 847-855.

[19] Otwinowski, Z.; Minor, W. (1997) Processing of X-Ray Diffraction Data Collected in Oscillation Mode. *Methods Enzymology 276*, 307-326.

[20] Vagin, A.; Teplyakov, A. (1997) MOLREP: An Automated Program for Molecular Replacement. *Journal of Applied Crystallography 30*, 1022-1025.

[21] Murshdov, G.N.; Vagin, A.A.; Dodson, E.J. (1997) Refinement of Macromolecular Structures by the Maximum Likelyhood Method. *Acta Crystallography D53*, 240-255.

[22] Emsley, P.; Cowtan, K. (2004) Coot: Model-building tools for Molecular Graphics. *Acta Crystallography D60*, 2126-2132.

[23] Carson, M. (1997) Ribbons. *Metods Enzymology 277*, 493-505.

[24] Potterton, L.; McNicholas, S.; Krissinel, E.; Grubber, J.; Cowtan, K.; Emsley, P.; MUrshudov, G.N.; Cohen, S.; Perrakis, A.; Nobel, M (2004) Developments in the CCP4 Molecular-Graphics Project *Acta Crystallography D60*, 2288-2294.

[25] Lovell, S.C.; Davis, I.W.; Arendall, W.B.Jr.; de Bakker, P.I.; Word, J.M.; Prisant, M.G.; Richardson, J.S. (2003) Structure Validation and by C-α Φ C-β Deviation. *Proteins 30*, 437-450.

[26] Cheesman, M. R., Le Brun, N. E., Kadir, F. H., Thomson, A. J., Moore, G. R., Andrews, S. C., Guest, J. R., Harrison, P. M., Smith, J. A., and Yewdall, S. J. (1993) Haem and Non-Haem Iron Sites in *Escherichia coli* Bacterioferritin: Spectroscopic and Model Building Studies, *Biochemistry 292*, 47-56.

[27] Watt, G. D., Frankel, R. B., Jacobs, D., and Huang, H. (1992) Fe^{2+} and Phosphate Interactions in Bacterial Ferritin from *Azotobacter vinelandii*. *Biochemistry 31*, 5672-5679.

[28] Watt, G. D., Frankel, R. B., Papaefthymiou, G. C., Spartalian, K., and Stiefel, E. I. (1986) Redox Properties and Mössbauer Spectroscopy of *Azotobacter vinelandii* Bacterioferritin. *Biochemistry 1986*, 4330-4336.

[29] Yariv, J., Kalb, A. J., Sperling, R., Bauminger, E. R., S.G., C., and Ofer, S. (1981) The Composition and Structure of Bacterioferritin of *Escherichia coli*. *Biochem J 197*, 171-175.

[30] Andrews, S. C. (1998) Iron Storage in Bacteria. *Advances in Microbial Physiology 40*, 281-351.

[31] Mann, S., Williams, J. M., Treffry, A., and Harrison, P. M. (1987) Reconstituted and Native Iron-Cores of Bacterioferritin and Ferritin. *Journal of Molecular Biology 198*, 405-416.

[32] Aitken-Rogers, H., Singleton, C., Lewin, a., Taylor-Gee, A., Moore, G. R., and Le Brun, N. E. (2004) Effect of Phosphate on Bacterioferritin-Catalysed Iron(II) Oxidation. *Journal of Biological Inorganic Chemistry 9*, 161-170.

[33] Jones, T., Spencer, R., and Walsh, C. (1978) Mechanism and Kinetics of Iron Release from Ferritin by Dihydroflavins and Dihydroflavin Analogues. *Biochemistry 17*, 4011-4017.

[34] Theil, E. C., Liu, X. S., and Tosha, T. (2008) Gated Pores in the Ferritin Protein Nanocage. *Inorgnaica Chimica Acta 361*, 868-870.

[35] Swartz, L., Kuchinskas, M., Li, H., Poulos, T. L., and Lanzilotta, W. N. (2006) Redox-Dependent Structural Changes in the *Azotobacter vinelandii* Bacterioferritin: New Insights into the Ferroxidase and Iron Transport Mechanism. *Biochemistry 45*, 4421-4428.

[36] Frolow, F., Kalb, A. J., and Yariv, J. (1994) Structure of a Unique Twofold Symmetric Haem-Binding Site. *Nature Structural Biology 7*, 453-460.

[37] Eerde, A., Wolterink-van Loo, S., Van der Oost, J., and Dijkstra, B. W. (2006) Fortuitous Structure Determination of 'As-Isolated' *Escherichia coli* Bacterioferritin in a Novel Crystal Form. *Acta. Crystallographica F62*, 1061-1066.

[38] Carrondo, M. A. (2003) Ferritins, Iron Uptake and Storage from the Bacterioferritin Viewpoint. *EMBO Journal 22*, 1959-1968.

[39] Hempstead, P. D., Yewdall, S. J., Fernie, A. R., Lawson, D. M., Artymiuk, P. J., Rice, D. W., Ford, G. C., and Harrison, P. M. (1997) Comparison of the Three-Dimensional Structures of Recombinant Human H and Horse L Ferritins at High Resolution. *Journal of Molecular Biology 268*, 424-448.

[40] Levi, S., Santambrogio, P., Corsi, B., Cozzi, A., and Arosio, P. (1996) Evidence that Residues Exposed on the Three-Fold Channels Have Active Roles in the Mechanism of Ferritin Iron Incorporation. *Biochemistry 317*, 467-473.

[41] Reffry, A., Bauminger, E. R., Hechel, D., Hodson, N. W., Nowik, I., Yewdall, S. J., and Harrison, P. M. (1993) Defining the Roles of the Threefold channels in Iron Uptake, Iron Oxidation and Iron-Core Formation in Ferritin: A Study Aided by Site-Directed Mutagenesis. *Biochemistry 296*, 721-728.

[42] Liu, X., and Theil, E. C. (2005) Ferritins: Dynamic Management of Biological Iron and Oxygen Chemistry. *Accounts of Chemical Reserach 38*, 167-175.

[43] Takagi, H., Shi, D., Ha, Y., Allewell, N. M., and Theil, E. C. (1998) Localized Unfolding at the Junction of Three Ferritin Subunits. *Journal of Biological Chemistry 273*, 18618-18688.

[44] Lawson, D. M., Artymiuk, P. J., Yewdall, S. J., Smith, J. A., Livingstone, J. C., Treffry, A., Luzzago, A., Levi, S., Arosio, P., Cesareni, G., Thomas, C. D., Shaw, W. V., and Harrison, P. M. (1991) Solving the Structure of Human H Ferritin by Genetically Engineering Intermolecular Crystal Contacts. *Nature 349*, 541-544.

[45] McPherson, A. (1999) Crystallization of Biological Macromolecules, CSHL Press, Cold Spring Harbor.

[46] Asherie, N. (2004) Protein Crystallization and Phase Diagrams. *Methods* 34, 266-272.

CHAPTER III

Heme Mediated Mobilization of Core Mineral Iron from BacteriferritinB

Introduction

Bacterioferritin B (BfrB) is considered as the main iron storage protein in *Pseudomonas aeruginosa*. Pa BfrB functions by capturing excess cellular iron and storing them as a ferric iron mineral. When the cellular iron concentration becomes low, it is thought that the stored iron is mobilized from the mineral core of Pa BfrB with the aid of another small protein called Bacterioferritin associated ferrodoxin (Bfd). However, very little is known about the mechanism of iron mobilization from the Pa BfrB cavity when the cellular iron becomes limited

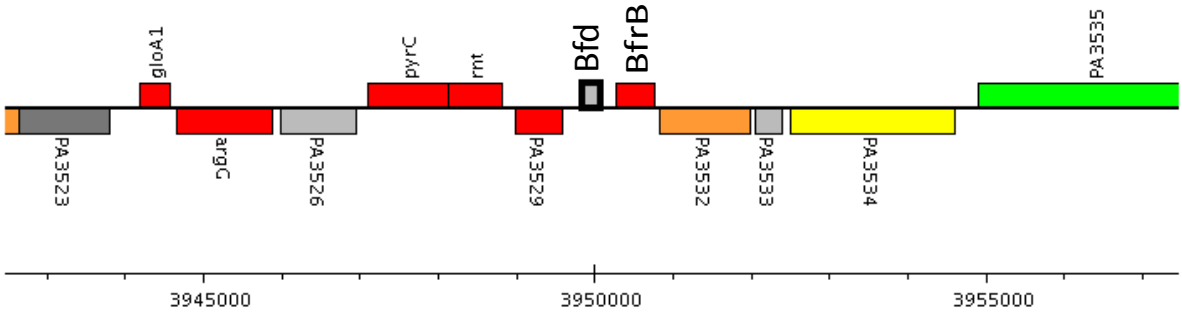

Figure 3-1: Organization of the *bfrB* and *bfd* genes in the *Pseudomonas aeruginosa* genome.

In the genome of *P.aeruginosa*, the *bfrB* gene (PA3530) is located adjacent to *bfd* gene (PA3531) which codes for Bfd and may suggest that these two proteins are functionally related (Figure 3-1). Bfd from *Escherichia coli* and *P.aeruginosa* have been identified as small ferredoxins that can bind [2Fe-2S] clusters [1,2,3] and led to the suggestion that these proteins

may act as scaffolds for [2Fe-2S] assembly or involve in the mechanisms of uptake or release of iron from Pa BfrB. In *E coli* it has been shown that Bfr form a complex with Bfd when these two proteins are in contact with each other [2]. As mentioned in Chapter 1 in detail, *P.aeruginosa* has two bacterioferritins called BfrB and BfrA (or FtnA). A study carried out on the global transcriptional response of iron starved cultures of *P.aeruginosa* revealed that the mRNA levels of *bfrB* increased by 24-fold when iron was made available. However, it has also been observed that the mRNA levels of *bfrA* remained unchanged [4]. Further, M.L.Vasil and coworkers found that in contrast to BfrB which is expressed under high iron conditions, BfrA from *P.aeruginosa* expressed constitutively [5, 6]. When the expression level of Bfd from *P.aeruginosa* is considered, it has been found that *bfd* gene is upregulated ~200 fold under iron starvation conditions [7]. According to the above findings, it is apparent that *bfrB* and *bfd* genes are differentially regulated in response to cellular iron levels. These findings suggest that Pa Bfd synthesized under iron limited conditions, may function to aid in the mobilization of iron stored in Pa BfrB molecules. In *P. aeruginosa*, BfrB is the main iron storage protein and functions by capturing excess cellular iron and storing it inside the inner core in the form of a ferric hydroxy phosphate mineral. When the cellular iron concentrations become low, the stored iron is mobilized from the inner core of Pa BfrB to meet the cellular metabolic demands.

Several investigations have been carried out to understand the mechanism of iron mineralization by bacterioferritins. As explained in chapter one, mineralization starts by binding of two Fe^{2+} ions to the ferroxidase center. Subsequently these Fe^{2+} ions are oxidized by O_2 and resultant Fe^{3+} ions are moved to the inner core and mineralization is initiated [8-11]. Nevertheless, the exact mechanism of iron mobilization from the bacterioferritin cavity is not yet known. In the case of eukaryotic ferritins, it has been suggested that the stored Fe^{3+} ions in the

cavity is reduced by the electrons from NADPH shuttled via a flavin molecule [12]. Further, recent investigations carried out on eukaryotic ferritins reveal that millimolar concentrations of urea cause a reversible unfolding of the pores of ferritin and consequently the rate of iron release from the ferritin core is significantly increased [13-15]. Observations of these studies suggest that a specific flavoprotein may bind near the pores of ferritin causing a change in the dynamics of pore opening and closing. As a result, the rate of the reduction of Fe^{3+} and mobilization of Fe^{2+} from the ferritin inner core is increased [16]. However, the exact mechanism of iron mobilization from Bfr is not yet known. Eventhough, it is thought that heme groups in Bfr may play a role in reducing core Fe^{3+} and aid in mobilization of Fe^{2+} from the inner cavity, it has not been experimentally demonstrated [17]. The research we carried out in our laboratory clearly indicates the fact that the mobilization of iron stored in Pa BfrB inner cavity requires the presence of the small ferredoxin, Pa Bfd. However, eventhough Pa Bfd is a [2Fe-2S] cluster containing ferredoxin which is thought to behave as a redox protein, in the mobilization of iron from Pa BfrB, Pa Bfd does not function as a redox protein. According to our observations, Pa Bfd devoid of the [2Fe-2S] cluster (apo-Bfd) promotes the rapid release of iron stored in the mineral core by binding to Pa BfrB. In addition, our investigations reveal that formation of a complex between Pa BfrB and Pa Bfd affects the heme group in Pa BfrB and have also demonstrated that the heme cofactor in Pa BfrB mediate electrons to the mineral core only if the Pa Bfd is bound to Pa BfrB [17].

Experimental Procedures

Expression and purification of P. aeruginosa wild type and Cys43Ser Bfd.

Wild type and Cys43Ser Bfd proteins were expressed using *E. coli* Arctic express RIL cells (Stratagene, La Jolla,CA) harboring the recombinant plasmids, pET11-a/*bfd* and pET11-a/C43S *bfd* respectively. A single colony of freshly transformed cells was cultured overnight at 37 °C in 50 mL of LB medium containing 100 μg/mL ampicilin and 20 μg/mL gentamicin. The cells were subsequently subcultured in 1 L of fresh LB containing no antibiotics and grown for 3 h at 37 °C. Cells were then transferred to a shaker incubator pre-equilibrated at 10 °C and incubated for 30 min before protein expression was induced by addition of isopropyl 1-thiol-D-galactopyranose (IPTG) to a final concentration of 1 mM. Cells were cultured for additional 48 h at 10 °C before they were harvested by centrifugation (4500 rpm for 10 min) and stored at -20 °C. The cell paste was resuspended in 50 mM potassium phosphate, (pH 7.0) (2 mL/g cell paste) and PMSF (0.5 mM), DTT (5 mM), protease inhibitor cocktail (Sigma-Aldrich, St. Louis, MO) and DNAse (Sigma-Aldrich, St. Louis, MO) were added before the cells were lysed by using constant cell disrupter (Constant Systems Ltd, LowMarch, Northants). Cell debris were pelleted by centrifugation at 4 °C and 19,500 rpm and the resultant supernatant was loaded onto a Q-Sepharose Fast Flow column (12 cm x 2.5 cm i.d.) equilibrated with 50 mM potassium phosphate, (pH 7.0). The column was washed with two column volumes of 50 mM potassium phosphate, (pH 7.0) before the protein was eluted using the same buffer and a linear gradient (0 mM - 600 mM) of NaCl. Fractions containing Bfd were pooled and concentrated to a volume of ~ 2 ml using centriprep filtration units with a molecular weight cut off 3000 kDa. The concentrated Bfd sample was passed down a G-50 column (1.5 cm x 100 cm) equilibrated with

50 mM potassium phosphate (pH 7.0), 100 mM NaCl and 1 mM DTT. Fractions containing Bfd were pooled and determined to be pure by 18 % SDS-PAGE.

Expression and purification of P. aeruginosa Fpr.

Pa-Fpr was expressed using *E. coli* Arctic express RIL cells (Stratagene, La Jolla, CA) harboring the recombinant plasmid, pET11-a/*fpr*. A single colony of freshly transformed cells was cultured overnight at 37 °C in 50 mL of LB medium containing 100 μg/mL ampicilin and 20 μg/mL gentamicin. The cells were subsequently subcultured in 1 L of fresh LB containing no antibiotics and grown for 3 h at 37 °C. Cells were then transferred to a shaker incubator pre-equilibrated at 10 °C and incubated for 30 min before protein expression was induced by addition of isopropyl 1-thiol-D-galactopyranose (IPTG) to a final concentration of 1 mM. Cells were incubated for additional 48 h at 10 °C before they were harvested by centrifugation (4500 rpm for 10 min) and stored at -20 °C. Cells were resuspended in lysis buffer (3 ml/g of cell paste). Deoxycholic acid (4 mg/g), Lysozyme (2 mg/g of cell paste), PMSF (32 μl/g of cell paste), $MgSO_4$ (4.2 mM final concentration), a pinch of Dnase were added to the cell suspension and stirred for 20 min at 4 °C. Cell suspension was then incubated at 37 °C for 20 min and stirred at ambient temperature for one hour. Finally it was sonicated at 4 °C and the cell debris was separated from the protein containing supernatant by centrifuging at 19,500 rpm for 1 hour. The supernatant was dialyzed against 4 L of 50 mM Tris-HCl (pH 7.5) at 4°C with at least three buffer changes over a period of approximately 16 hrs. The resultant solution was applied to a Q-Sepharose Fast Flow column (10 cm × 2.5 cm i.d.) previously equilibrated with 50 mM Tris-HCl (pH 7.5). The column was washed with 3 volumes of 50 mM Tris-HCl (pH 7.5) and the protein was eluted using the same buffer with a linear gradient (0 mM to 600 mM) of NaCl. Fractions containing Fpr (yellow) were pooled, concentrated and then loaded onto a Sephadex-G75 column (3.0 cm x 100 cm) equilibrated

with 100 mM sodium phosphate buffer containing 150 mM NaCl (pH 7.0) and protein was eluted using the same buffer. Fractions with absorbance ratio A_{280}/A_{450} less than 6 were pooled and *pa*-Fpr was determined to be pure by 12% SDS PAGE.

Expression and purification of P. aeruginosa BfrB

Expression and purification of Pa BfrB was carried out using the methods described in the experimental section of Chapter 2.

Mobilization of core iron from Pa BfrB.

Experiments to investigate the mobilization of core iron from Pa BrfB were carried out in an anaerobic chamber. Mineralized Pa BfrB was prepared as described in chapter 2. Iron mobilization reactions were conducted in a 1.0 cm path-length cuvette equipped with a magnetic stirring bar and monitored by electronic absorption spectroscopy using an Ocean Optics (Dunedin, FL) 2000 spectrophotometer. A few μL from stock protein solutions were added to a cuvette containing 3 mM 2,2, bipyrydil (bipy) in 1.5 mL of 20 mM potassium phosphate buffer (pH 7.6), to make a solution 15 μM in Pa Bfd, 15 μM in Fpr and 0.375 μM in Pa BfrB. The reaction was initiated by addition of NADPH to a final concentration of 1.5 mM and the progress of the reaction was monitored by following the time-dependent changes in intensity of the band at 523 nm that is formed when bipy binds Fe^{2+} to form the $[Fe(bipy)_3]^{2+}$ complex. Experiments with apo-Pa Bfd were conducted with a simple modification of the above procedure: Apo-Pa Bfd was prepared *in situ* from holo-Pa Bfd. To this end, holo-Pa Bfd (15 μM final concentration) was added to a stirred cuvette containing 3 mM bipy in 20 mM potassium phosphate buffer (pH 7.6). Sodium dithionite (5 mM) was added stoichiometrically to reduce the Fe^{3+} in holo Bfd to Fe^{2+}. Capturing of the ferrous ion by bipy was monitored by the time-dependent increase in the

523 nm absorbance, which was followed until it reached a plateau with intensity corresponding to the theoretical value calculated from the amount of holo Pa Bfd placed in the cuvette. At this point, the solution containing apo-Pa Bfd was reconstituted with Pa Fpr and Pa BfrB (final concentrations of 15 µM and 0.375 µM, respectively) and the iron mobilization reaction initiated by the addition of NADPH to a final concentration of 1.5 mM.

Results

Expression and purification of wild type Bfd and Cys43Ser Bfd.

Pa Bfd was first expressed in *E.coli* BL21 (DE3) cells at 30ºC. However, the protein produced using this procedure was not soluble and formed inclusion bodies. Consequently, purification of Pa Bfd required first denaturation of the protein with 6M urea to solublize the protein and then reconstitution of the [2Fe-2S] *in vitro* [3]. Subsequently, the solubilized and reconstituted protein was purified using column chromatographic techniques. Later it was found that expression of Pa Bfd in *E.coli* Arctic express RIL cells (Stratagene) produces soluble Pa Bfd with an intact iron sulfur cluster. Nevertheless, the yield of the pure soluble Pa Bfd was very low (1-2 mg/L). Poor yields have also been reported for the expression of recombinant Bfd from *E.coli* [2]. In addition, it was observed that the wild type Bfd from *P. aeruginosa* is fragile and has a tendency to gradually get damaged during the purification procedure and sometimes during storage. As shown in figure 3-2, Bfd from *P aeruginosa* has seven Cys residues, four of which are conserved in other organisms. The other three Cys residues (Cys22, 23 and 43) which are not conserved were mutated to Ser with the aim of increasing the yield of the expression and

stabilizing the iron-sulfur cluster of the protein. Mutations at Cys 22 and Cys 23 did not produce detectable amounts of protein, as observed by 18% SDS-PAGE.

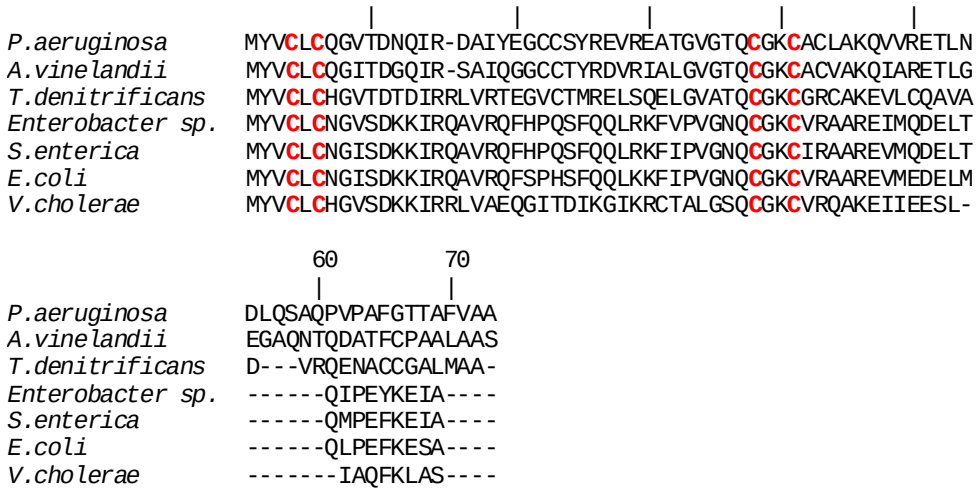

Figure 3-2: Bacterioferritin-associated ferredoxin sequences from different organisms aligned against that from *P. aeruginosa*. Conserved Cysteines forming the unique **C**-X-**C**-X_{31-32}-**C**-X_2-**C** arrangement (highlighted) are thought to bind iron in the [2Fe-2S] cluster of the holo-protein. The sequences were aligned with the aid of ClustalW [25].

It is apparent that the above two Cys residues (Cys 22 and Cys 23) may have affected the proper folding of the protein. With the aim of obtaining higher yields of recombinant Pa Bfd and avoiding the problems of fragility and low stability of the wild type Pa Bfd, the nonconserved Cys43 was also mutated to Ser. In contrast to other two mutations, the C43S mutant could be isolated and purified to homogeneity (Figure 3-3A) with a reasonably higher yield (4mg/ml) which is approximately 2-fold higher than the wild type Pa Bfd. The [2Fe-2S] cluster in wild type Pa Bfd is less stable than the C43S mutant as it tends to degrade during protein purification. The degradation of the [2Fe-2S] cluster leads to oligomerization, likely via formation of disulfide bonds. The iron sulfur cluster in the C43S mutant was observed to be much more stable than that of wild type during purification, manipulation and storage of the

protein. As shown in figure 3-3B, the UV visible spectra of wild type and C43S Bfd are identical, implying that the mutation has not impaired the folding of the protein or its ability to bind a [2Fe-2S] cluster.

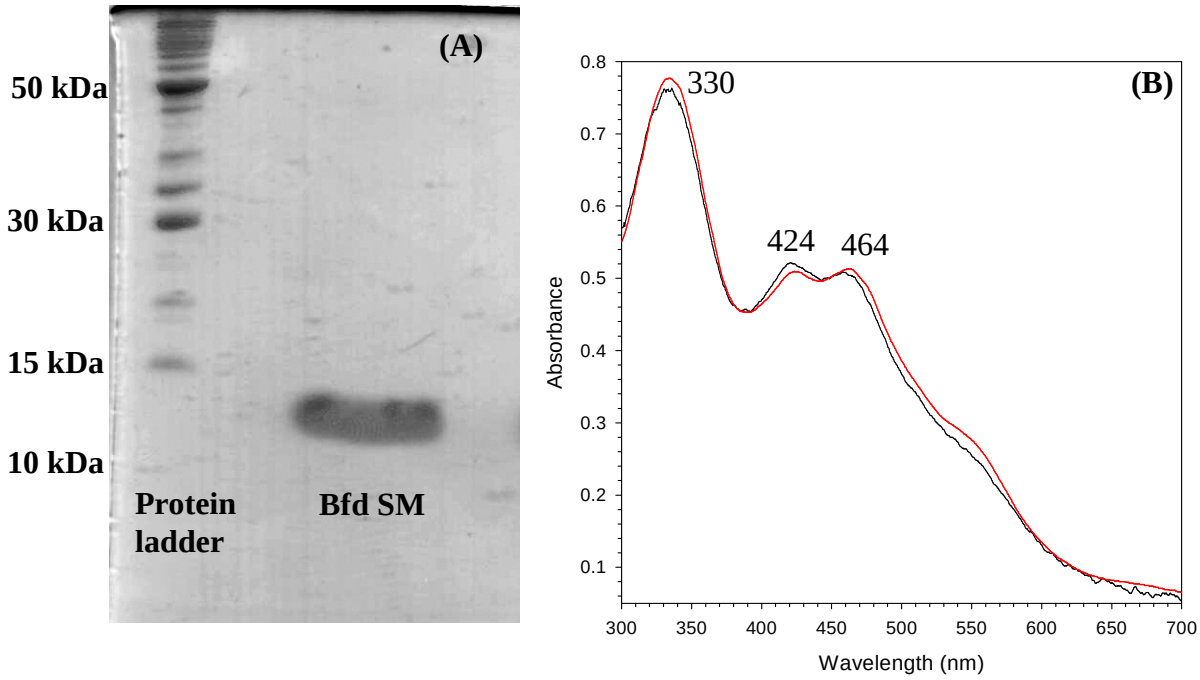

Figure 3-3: (A) 18% SDS-PAGE analysis of C43S Bfd (Bfd SM) purified to homogeneity. (B) Electronic absorption spectra of oxidized wild type Pa Bfd (black trace) and oxidized C43S Pa Bfd (red trace) in 50 mM potassium phosphate buffer, pH 7.0.

Interactions with apo Pa Bfd unlock the iron Stored in Pa BfrB.

All the experiments designed to study the mobilization of core iron from Pa BfrB mineral core were carried out under strict anaerobic conditions. As mentioned in the experimental, NADPH (final concentration of 1.5 mM) was added to a mixture of Pa BfrB, Pa Fpr, Pa Bfd and 2,2-bipyridyl (bipy) to initiate the iron mobilization. Fe^{3+} ions in the mineral core are reduced by Fpr which was first reduced by NADPH and released out as Fe^{2+}. Then these Fe^{2+} ions complex with bipy and make a ferrous bipy complex $[Fe\ (bipy)_3]^{2+}$ which

exhibits an absorption maxima at 523 nm (Figure 3-4A). The release of iron from Pa BfrB was monitored by following the formation of ferrous – bipy complex at 523 nm.

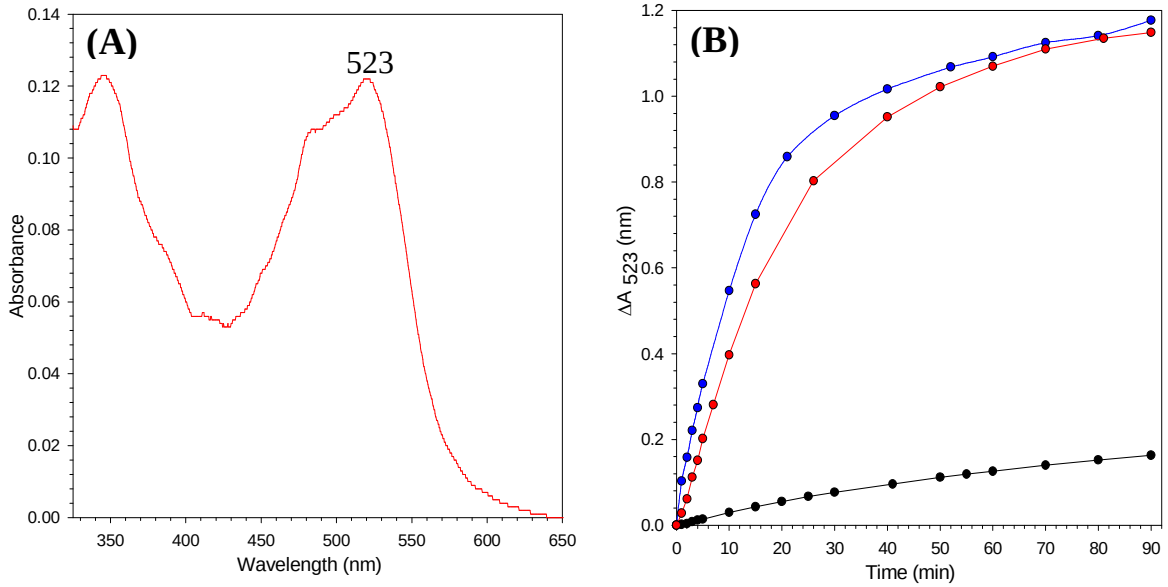

Figure 3-4: (A) The electronic absorption spectra of ferrous – bipy complex {$[Fe(bipy)_3]^{2+}$} and (B) Time dependent increase in the intensity of the 523 nm absorbance due to the formation of $Fe[(bipy)_3]^{2+}$ upon addition of NADPH (1.5 mM final concentration) to a solution containing Pa BfrB (0.375 µM), Pa FPR (15 µM), bipy (3 mM) and no Pa Bfd (black), 15 µM wild type holo-Bfd (red), and wild type apo-Bfd (blue).

The red and blue traces in figure 3-4B, correspond to the time dependent growth of the 523 nm band upon addition of NADPH to a solution containing Pa BfrB (.375 µM), Pa FPR (15 µm), holo and apo wild type Pa Bfd respectively. In this experiment it is apparent that the presence of Pa Bfd (15 µM) causes a significant acceleration in the rate of iron release. Further it was observed that in the presence of holo Pa Bfd the Soret band shifted from 417 nm to 425 nm whereas it remained unshifted at 417 nm in the absence of holo Pa Bfd (Figure 3-5).

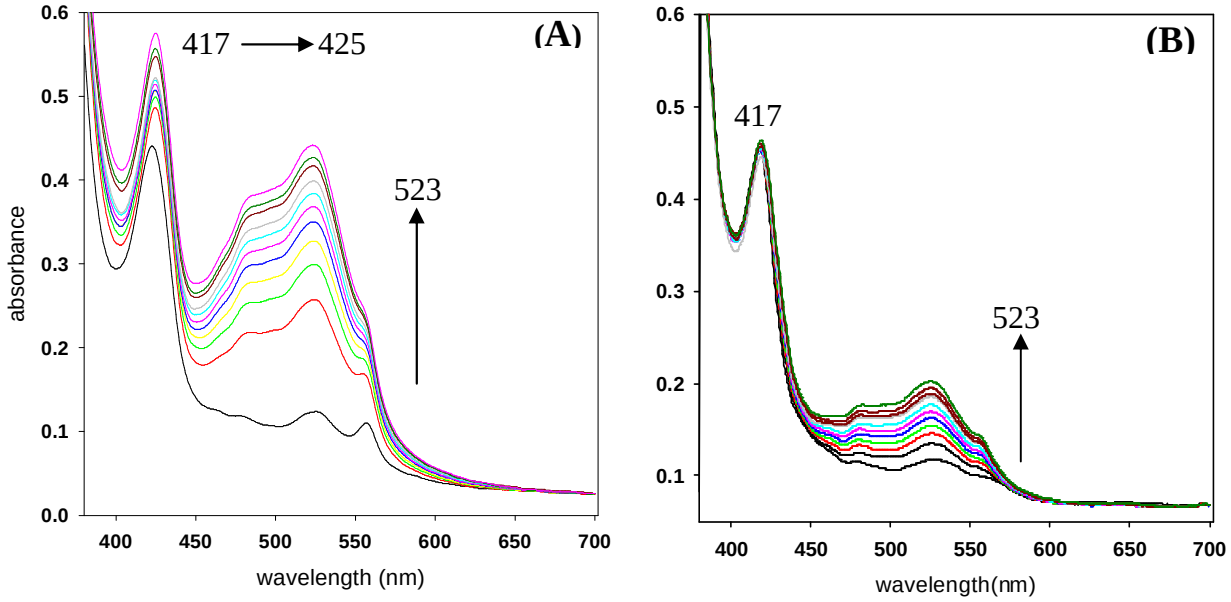

Figure 3-5: Family of electronic absorption spectra of $[Fe(bipy)_3]^{2+}$ complex illustrating the intensity changes at 523 nm in the iron mobilization reaction of Pa BfrB (A) in the presence and (B) absence of WT Pa Bfd.

These experimental results suggest that Pa Bfd plays an important role in the process of iron release from Pa BfrB mineral core either by changing the conformation of the Pa BfrB molecule or changing the redox potential of the heme group. In addition, the above results suggest that the [2Fe-2S] cluster of holo Pa Bfd may be catalyzing the iron mobilization by shuttling the electrons to Pa Fpr from Pa BfrB using the iron sulfur cluster. However, an experiment carried out with apo Pa Bfd, (Bfd without the iron sulfur cluster) instead of holo Pa Bfd showed that Pa Bfd does not participate in the reaction by mediating electrons from Pa Fpr to Pa BfrB. Consequently, all the later iron mobilization assays were carried out using apo Pa Bfd prepared *in situ* by incubating holo Pa Bfd with dithionite and excess bipy. In this reaction, two Fe^{3+} ions in the iron sulfur cluster are reduced by dithionite and the reduced Fe^{2+} ions are

captured by bipy forming the pink $[Fe(bipy)_3]^{2+}$ complex which absorbs at 523 nm. The formation of apo Pa Bfd by this method is relatively slow (~170 min) and the growth of characteristic 523 nm band was spectrophotometrically monitored.

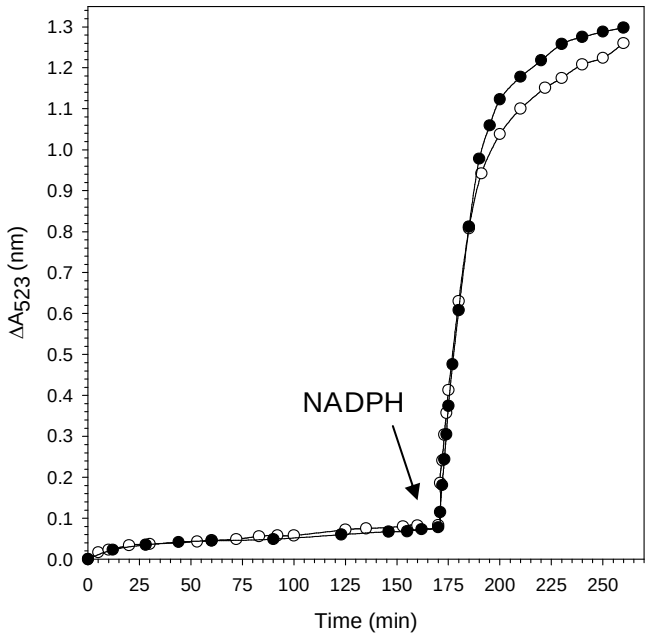

Figure 3-6: Before the arrow : time dependent absorption changes in the intensity of the 523 nm caused by sequestration of the iron in the [2Fe-2S] cluster of (●) 15 µM wild type holo-Bfd and (○) 15 µM holo-C43S Bfd by bipy (3 mM); the solution contained 15 µM sodium dithionite to reduce the two iron ions in holo-Bfd. After the arrow: the rapid time dependent increase in the 523 nm absorption of the resultant solution containing 15 µM apo-WT Bfd (●) or apo-C43S-Bfd (○), 0.375 µM in BfrB and 15 µM in FPR after the addition of NADPH (1.5 mM).

The quantitative formation of apo-Pa Bfd was obtained by calculating the amount of $[Fe(bipy)_3]^{2+}$ complex predicted to form if all the iron in the [2Fe-2S] is captured by bipy. Once all the holo Pa Bfd is converted to apo Bfd, Pa BfrB and Pa Fpr were added and the iron release reaction was initiated by adding NADPH (marked by an arrow in figure 3-6). Upon addition of

NADPH, a fast growth of the absorbance at 523 nm and a rapid reduction of heme were observed simultaneously. Figure 3-4B compares the time dependent changes in the intensity of 523 nm, in the presence of wild type holo and apo Pa Bfd. It can be clearly seen that the rate of iron release is slightly faster in the presence of apo Pa Bfd than that of holo Pa Bfd. These findings suggest that the [2Fe-2S] cluster of holo Pa Bfd is not necessary for the rapid mobilization of iron from the inner core and may not be functioning as a mediator to shuttle electrons to Pa BfrB. Consequently, it is thought that apo Pa Bfd may exert an effect on core iron mobilization from Pa Pa BfrB by binding to Pa BfrB molecule and inducing a conformational change that enables the iron release. Apo C43S Pa Bfd was prepared in the same way as apo wild type Pa Bfd. When all the iron from the [2Fe-2S] cluster of C43S Pa Bfd was quantitatively captured, Pa BfrB, Pa Fpr and NADPH were added to the cuvette and the growth of 523 nm was monitored. The time dependent release of iron with apo C43S Pa Bfd is nearly identical to that of with wild type apo Pa Bfd (Figure 3-6). Therefore, all the experiments involving Pa Bfd were carried out with C43S Pa Bfd because of its higher expression yields and enhanced stability. For simplicity, hereafter the C43S Pa Bfd will be referred to as Pa Bfd in this text.

Experiments were carried out to probe the effect of apo Pa Bfd on the rate of iron release from Pa BfrB iron core and results are summarized in Figure 3-7A. In these experiments, the concentrations of apo Bfd were varied while maintaining Pa BfrB (0.375 µM), Pa Fpr (15µM), NADPH (1.5 mM), and Bipy (3 mM) concentrations constant. As shown in figure 3-7A, the growth of the 523 nm band was monitored in each of the experiments carried out with different apo Bfd/BfrB ratios ; 40:1 (green), 30:1 (red), 20:1 (purple), 15:1 (cyan), 10:1 (blue), 5:1 (orange) and 0:1 (black).

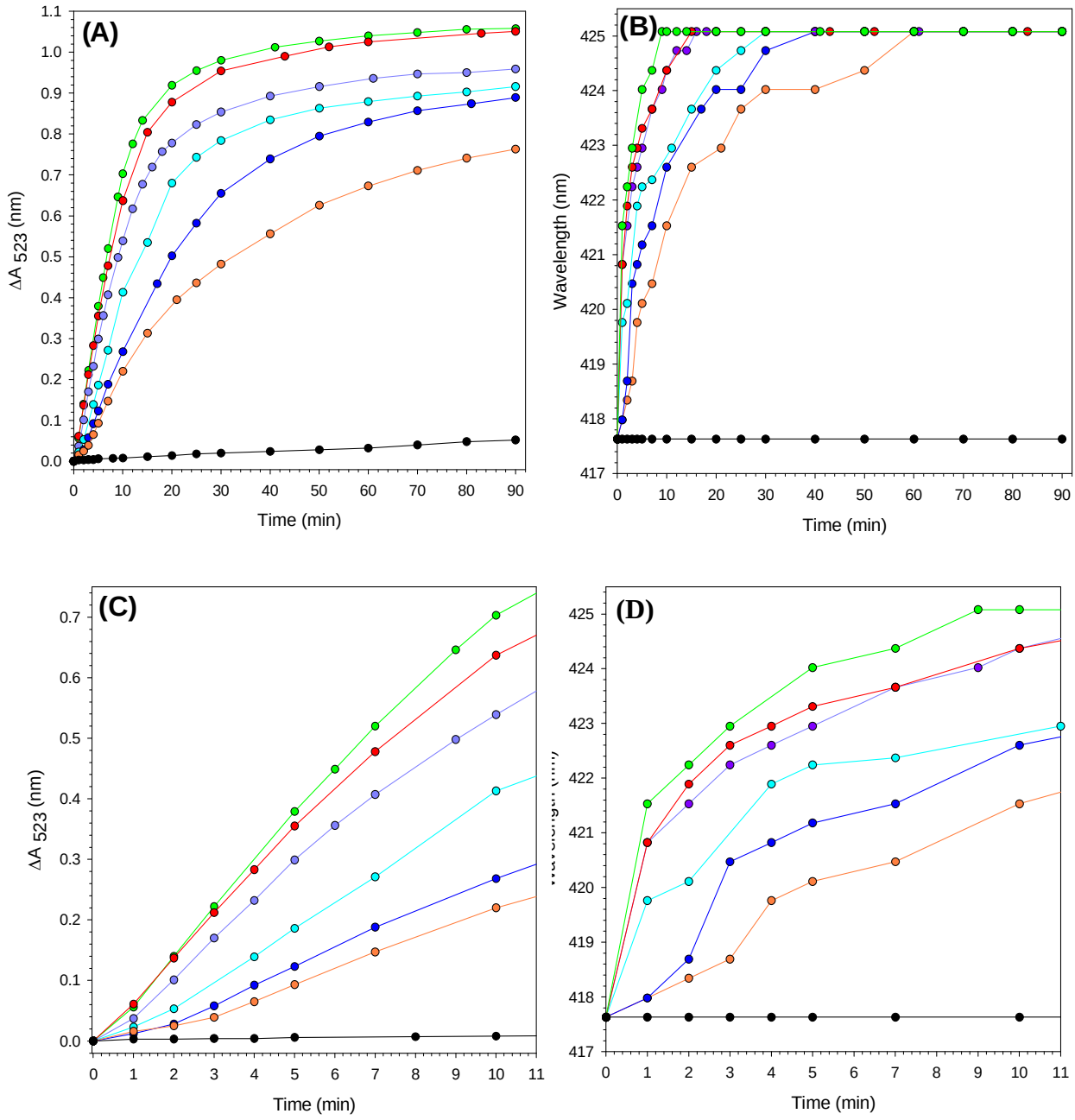

Figure 3-7: (A) Time dependent plot of absorption intensity change measured at 523 nm upon addition of NADPH (1.5 mM) to solutions containing 3.0 mM bipy, 15 µM FPR, 0.375 µM BfrB and apo-Bfd with Bfd/Bfrb molar ratio of 40 (green), 30 (red), 20 (purple), 15 (cyan), 12 (orange), 10 (blue), and 5 (black). (B) Time dependent changes in the position of the Soret band brought about by the addition of NADPH (1.5 mM) to the solutions in figure A; 417.5 nm and

425 nm correspond to fully oxidized and fully reduced heme, respectively. (C) Zoomed view (initial 11 min) of the time dependent absorption changes corresponding to the plots in A. (D) Zoomed view of the time dependent changes in the position of the Soret band corresponding to the plots in B.

It is clearly observed that when the Bfd/BfrB ratio is lowered the amount of iron released gradually decreases. In addition, a significant change in the rate of iron release can be observed when the Bfd/BfrB ratio is lowered from 5 to 0. The time dependent change of the Soret band at 417 nm of each of the above experiments has been plotted in Figure 3-7B and it is evident that when the ratio of Bfd/BfrB is larger than 5, the heme group is reduced in an initial "fast phase" followed by a "slower" phase which continues until the heme group is completely reduced (Soret band at 425 nm). It is important to note that in the absence of Bfd, Soret band remains unshifted at 417 nm (oxidized heme) throughout the experiment. However, in other experiments where ratios of Bfd/BfrB are 40 to 5, a progressive slowing of the reduction of heme can be observed. Figure 3-7C and 3-7D indicate a lag phase lasting approximately 1-3 minutes in iron mobilization and heme reduction when the Bfd/BfrB ratio is 20 or lower. The fact that the lag phases of both iron release and the heme reduction reactions occur during approximately the same time, implies that the electrons sent by Fpr (the reductase) are channeled into the inner core via the heme group. Additional experiments to confirm this idea have been carried out and will be discussed later in this chapter In order to have a more quantitative comparison of the effect of apo Pa Bfd on iron mobilization from the Pa BfrB core, pseudo rates of iron release were estimated by fitting each curve in figure 3-7A to an exponential function. However, the data points corresponding to the initial lag phase in each curve were excluded in calculating the

pseudo rate of iron release. The results are summarized in table 1 and figure 3-8 indicating a clear Bfd–dependent iron release from the Pa BfrB inner core.

Table 3-1: Pseudorates for the Pa Bfd-dependent release of core iron from Pa BfrB.

Bfd/BfrB molar ratio	Pseudorate of iron release (min^{-1})[a]
0	0.0087 ± 0.0002
5	0.029 ± 0.001
10	0.036 ± 0.002
15	0.058 ± 0.008
20	0.074 ± 0.008
30	0.089 ± 0.007
40	0.095 ± 0.004

[a]The standard deviations were obtained from triplicate measurements using proteins obtained from two independent preparations and all the measurements were carried out at 25° C.

Pa Bfd binds to** Pa **BfrB

The observations made on the previous experiments strongly suggest that Pa Bfd binds to Pa BfrB. To further corroborate this idea an experiment was carried out with the aid of size exclusion chromatography. A sample of Pa BfrB and a mixture of Pa BfrB and Pa Bfd were passed through a size exclusion column and the elution volumes were obtained. The average

elution volume (V_e) obtained upon loading a superdex 200 column with 1 mL of Pa BfrB containing 0.036 µmol is 58.9 ± 0.05 mL (open circle in figure 3-9A).

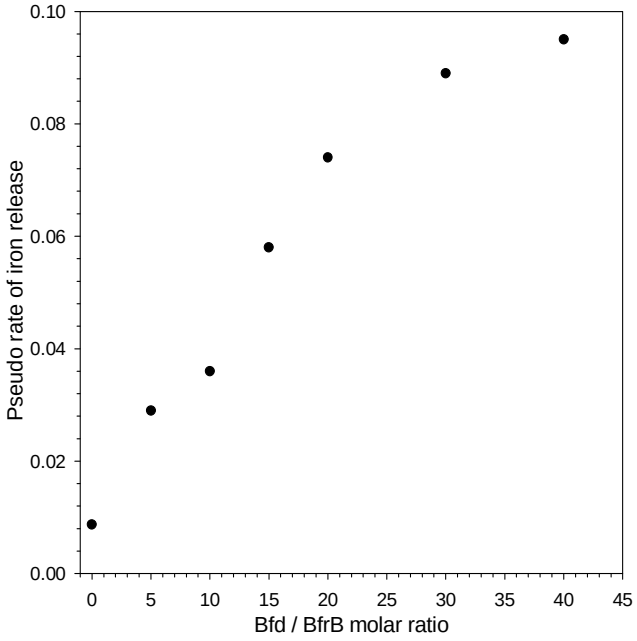

Figure 3-8: Pa Bfd-dependent release of core iron from Pa BfrB.

This value was nearly identical to the elution volume obtained upon loading the column with a sample of horse spleen ferritin standard (MW 447 ± 1 Da). Subsequently, 1 mL sample containing a mixture of 0.0036 µmol of Pa BfrB and 0.084 µmol of Pa Bfd was loaded on to the same column and obtained an elution volume (57.0 ± 0.6 mL) which corresponds to a molecular weight of 538 ± 30 kDa (open triangle in figure 3-9A). Excess Pa Bfd was observed to elute later with an elution volume of 96.3 ± 0.3 mL. The difference between the elution volumes of pure Pa BfrB and the mixture of Pa BfrB and Pa Bfd was 91 kDa which corresponds to approximately 12 Bfd molecules, each with a molecular mass of 7.82 kDa. This observation clearly indicates that 12 molecules of Pa Bfd can bind to a molecule of Pa BfrB and more likely one Pa Bfd molecule may bind to one subunit of Pa BfrB. Additional evidence for this

observation was obtained by analyzing the fractions corresponding to BfrB –Bfd mixture and excess Bfd eluted later by SDS-PAGE. Figure 3-9B shows that the peak with an elution volume 57.0 ± 0.6 mL (lane 2) indeed a mixture of Pa BfrB and Pa Bfd, whereas the peak with an elution volme 96.3 ± 0.3 mL (lane1) contains only Pa Bfd.

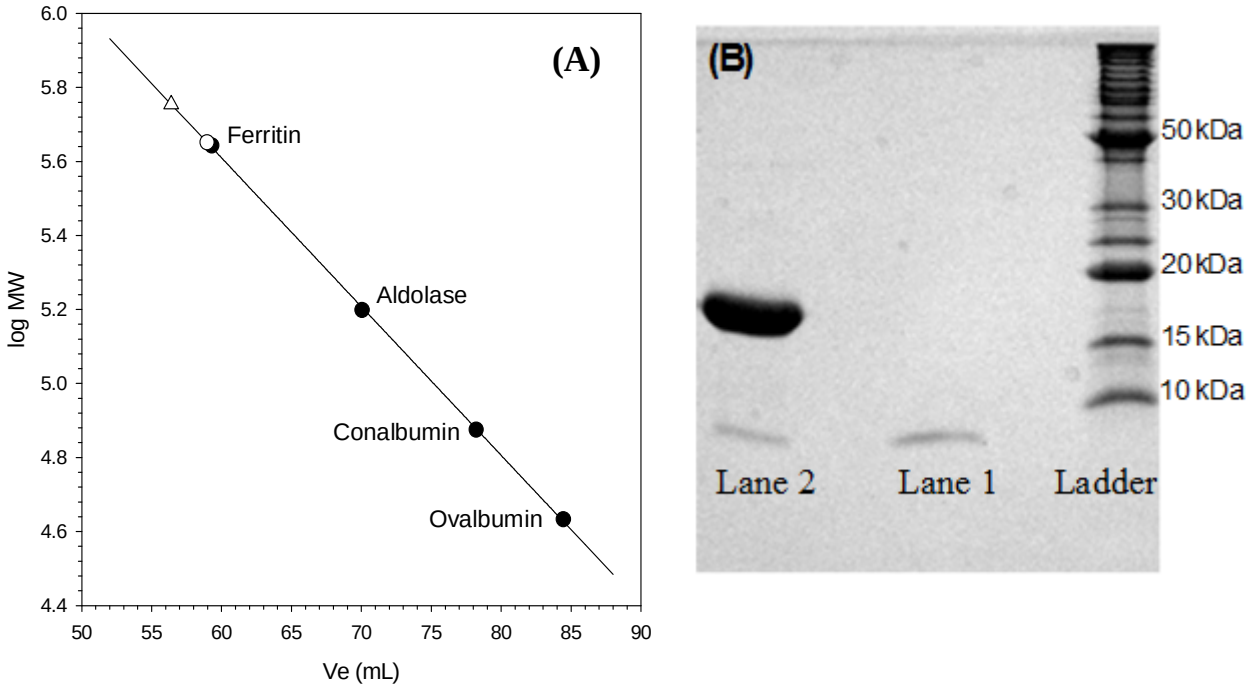

Figure 3-9. (A) The calibration curve obtained to estimate the molecular weight of BfrB (○) and that of the BfrB-Bfd complex (Δ) was constructed from the elution volume (V_e) obtained for each of the following standard molecular weight markers (●), ferritin (440 kDa), aldolase (158 kDa), conalbumin (75 kDa), and ovalbumin (44 kDa), loaded onto a Superdex 200 column. (B) SDS-PAGE (15%) analysis of the solution corresponding to a peak eluting with V_e 57.0 ± 0.6 mL (lane 2) and V_e 96.3 ± 0.3 mL (lane 1) upon loading the Superdex 200 column with a mixture of BfrB and Bfd in a Bfd/BfrB mole ratio of 24.

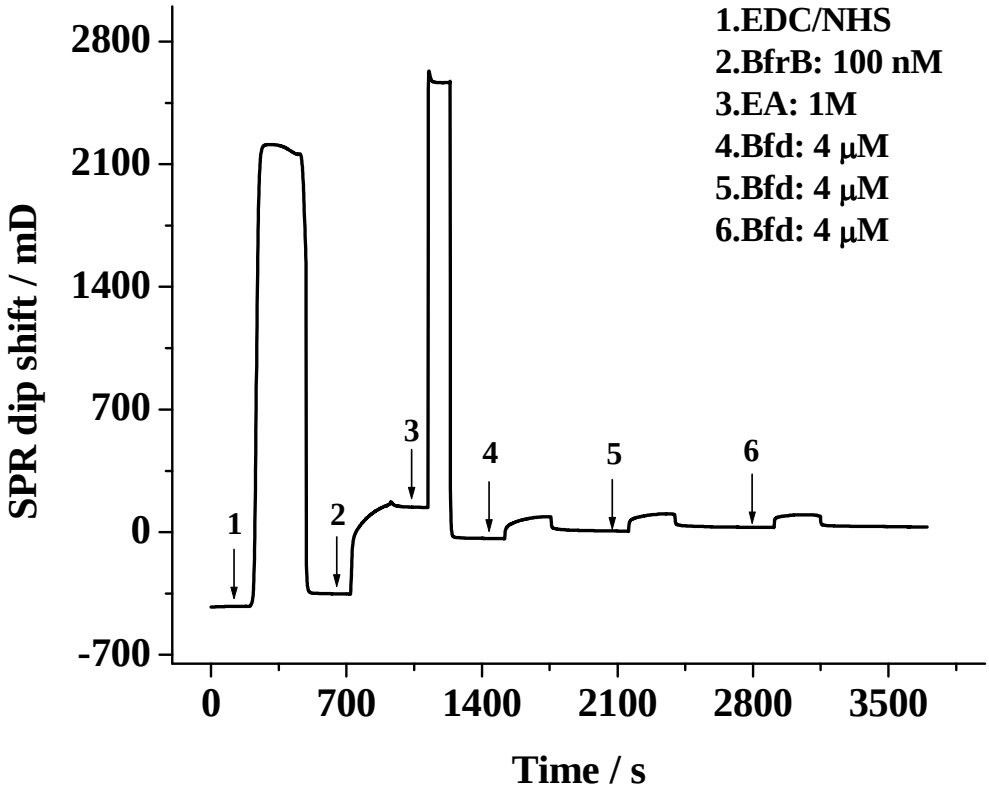

Figure 3-10: Chromatogram of Surface Plasmon Resonance experiment showing that molar ratio of the complex between Bfd and BfrB is 12.

In order to further exemplify the above notion of forming a complex between Pa BfrB and Bfd, one of our collaborators, Dr. Feimeng Zhou at California State University carried out a Surface Plasmon Resonance (SPR) experiment using Pa BfrB and Pa Bfd. Interestingly, SPR experiments confirmed the preliminary results we obtained using size exclusion chromatography. Dr Zhou was able to find out that the molar ratio of the complex formed between Pa Bfd and Pa BfrB is 12. The chromatogram of the SPR experiment is shown in figure 3-10.

Binding of* *Pa* *Bfd to* *Pa* *BfrB enables heme mediation of electron transfer to the core.

The previous observation made on the fact that the electron transfer from the reductase to the core mineral in BfrB is mediated by heme was further confirmed by carrying out an experiment where a limiting amount of NADPH (15% of the total reducing equivalents needed to reduce all the iron in the core) was added to a solution containing apo-Bfd, Fpr and BfrB in molar proportion of 40:40:1. The above ratio of Bfd:BfrB (40:40) was chosen as there was no lag phase observed in the iron mobilization or heme reduction (Figure 3-7A).

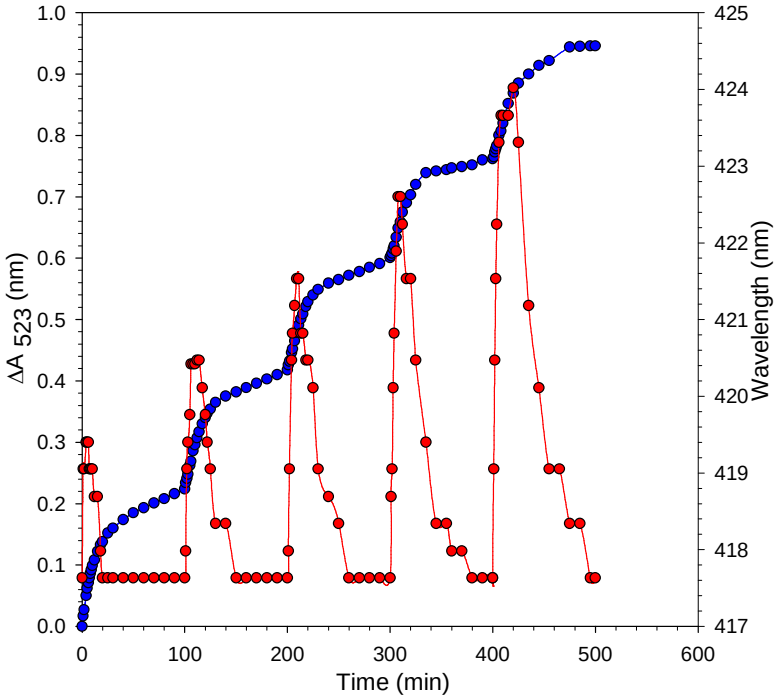

Figure 3-11: Time dependent changes in the intensity of absorption measured at 523 nm upon addition of aliquots of NADPH containing 15% of the total electron equivalents needed to reduce all the ferric ions in the core of BfrB (600 Fe^{3+} ions/BfB) to a solution containing BfrB (0.375 µM), Fpr (15 µM), apo-Bfd (15 µM) bipy (3 mM) (blue trace, left axis) and time dependent changes in the position of the heme Soret band following addition of each NADPH aliquot (red trace, right axis).

The results obtained from this experiment are summarized in Figure 3-11 and upon addition of each aliquots of NADPH a fast release of iron is observed. Further, it is important to note that the amount of Fe^{2+} released (0.043 ± 0.002 µmol) with each aliquot of NADPH is in good agreement with the number of electron equivalents (0.044 µmol) delivered, signifying quantitative utilization of NADPH. The plot of figure 3-10 also shows the shifting of the Soret band (red trace, right axis) following each addition of NADPH where it rapidly shifts from 417 nm to 425 nm and then shifts back to its original position. This observation suggests a transient build up of heme which indicates the balance between reduction and subsequent oxidation of heme. Further, it strongly implies that heme groups are reduced by the electrons from the reductase faster than it is reoxidized by sending those electrons to the iron core. In addition, the transient concentration of reduced heme is gradually increases with time upon each addition of NADPH because of the less demand for the electrons from the heme by the core mineral which becomes progressively smaller. Therefore, eventhough the electron flux from the reductase to the heme is similar after each addition of NADPH, the electron flux from the heme to the iron core decreases as the size of the iron mineral become smaller and can be clearly seen in the experimental observations summarized in Figure 3-10.

Discussion

Iron mobilization studies of ferritins in hepatic cells have been carried out using NADH or NADPH as the electron source and the electrons were shuttled to ferritin via flavin or xanthine containing oxidoreductases [19]. Therefore, in these experiments $FADH_2$ was utilized as the electron donor and in early work $FADH_2$ was generated by NADH-flavin oxidoreductase

[20]. However, in more recent studies, $FADH_2$ is generated by the beam of a spectrophotometer in the presence of NADH [21]. In comparison, early studies done on the core iron mobilization from Bfr have used small molecule reductants such as dithionite or methyl viologen [22].

Prior to the investigations carried out on iron mobilization from Pa BfrB in our laboratory, there was no any information regarding either the mechanism or the physiological partners involved in the iron mobilization process in bacterioferritins. The studies that we have carried out on iron mobilization from Pa BfrB core are based on the strong assumptions made on the information obtained by probing the global genetic response of *P. aeruginosa* to iron levels [7]. Among the genes reported which are positively regulated under low iron conditions, the genes coding for Pa Bfd and Pa Fpr were considered to be important because of their probable function in electron transfer [3]. From the previous studies on biochemical and structural characterization of Fpr, it was found that Fpr supports the catalytic activity of heme oxygenase by transferring the required seven electrons from NADPH to degrade heme and release its iron [3]. Pa Fpr with $FADH_2$ as its cofactor was used as the reductase in iron mobilization reactions, because it is a product of one of the genes that are upregulated under iron starvation conditions. Pa Bfd (Bacterioferitin associated ferredoxin) is the other putative electron transfer protein of the gene which is positively upregulated under iron starvation conditions. Bfd proteins from *P aeruginosa* and *E coli* have been found to bind a [2Fe-2S] cluster [1-3], which allowed us to hypothesize that Pa Bfd may function as an electron transfer protein by mediating electron from the reductase to the iron core of Pa BfrB [1, 2] or may function in iron mineralization by transferring electrons from the Pa BfrB core to an external oxidant [2]. It is important to note that under iron starvation conditions, Pa BfrB gene is downregulated [4] and Pa Bfd gene is strongly upregulated [7], implying that Bfd is synthesized to aid in the mobilization of iron from the Pa BfrB core to

sustain the metabolic activity inside the cell. According to the above hypothesis, holo-Bfd is thought to mediate electron transfer from NADPH to iron core of Pa BfrB and results obtained from the experiments carried out to test the above hypothesis seemed to suggest that Bfd is involved in shuttling electrons from NADPH to the iron core of Pa BfrB. However, additional experiments carried out to further test this idea, conclusively showed that apo- Pa Bfd is more effective than holo-Bfd, in transferring electrons from NADPH to the iron core to facilitate the release of Fe^{2+} from the Pa BfrB core. Consequently, the [2Fe-2S] cluster in holo Pa Bfd is not essential for Pa Bfd to enable the iron release from BfrB, indicating that the protein-protein interactions between apo- Pa Bfd and Pa BfrB promote the effective mobilization of iron stored in the iron core of Pa BfrB.

These findings are in good agreement with the fact that under iron starvation conditions, the cell would not synthesize an iron containing co-factor to mobilize stored iron in BfrB which is a favorable strategy for the cell under low cellular iron conditions. Therefore according to these observations, a cellular model for the efficient utilization of iron can be established: Downregulation of the *bfrB* gene indicates that synthesis of additional Pa BfrB proteins is not necessary during iron starvation. However, additional mechanisms may utilize to maintain the sustainability of the cell. At the same time, Pa BfrB makes a complex with Pa Bfd (stoichometry of 1:12) to efficiently mobilize the stored iron from the Pa BfrB core which in turn confirms the observation of strong upregulation of *bfd* gene under low iron conditions. In addition, utilizing apo- Pa Bfd to mobilize iron from Pa BfrB is a good economical strategy employed by the cell under these low iron conditions as it does not need to synthesize [2Fe-2S] cluster for holo Bfd which requires already scarce iron.

Binding of Pa Bfd to Pa BfrB enables heme mediation of electron transfer.

As shown in figure 3-5, the heme group in Pa BfrB is reduced only in the presence of Pa Bfd, suggesting that formation of BfrB-Bfd complex facilitating the heme mediated electron transfer from the reductase protein to the Pa BfrB core. The above observation is clearly illustrated in figure 3-11 where a transient build up of reduced heme is observed when limiting amount of NADPH (reducing power) is used. Eventhough the function of heme as an electron mediator in mobilization of iron in bacterioferritins has been speculated [22]; it has not been experimentally demonstrated prior to our investigations. Therefore, these findings from our investigations would be the first experimental evidence to establish the function of heme in bacterioferritins. In addition, it is important to note that the exact function of heme can only be examined upon formation of the BfrB-Bfd complex because binding of the physiological partner proteins is essential to make the heme conductive. The exact mechanism of making heme "conductive" by forming a BfrB-Bfd complex is not yet clear. However, three probable mechanisms can be proposed, (a) formation of a complex with Pa Bfd positively shifts the reduction potential of the heme in Pa BfrB which enables it to accept electrons from Pa Fpr, (b) binding of Pa Bfd causes a conformational change which facilitate a clear electron transfer pathway from the surface to the heme, (c) conformational change resulted by the formation of BfrB-Bfd complex may both alter the redox potential of heme and enable a pathway for electron conduction, (d) formation of BfrB-Bfd complex may induce the productive binding of Pa Fpr which may accelerate electron transfer to Pa BfrB which is channeled to the core via the heme group. Additional work has to be carried out to determine the specific mechanism of iron release via the heme group of BfrB. However, it is clear that the investigations, to probe the specific mechanism of iron mobilization of bacterioferritins have to be carried out in the presence of its

physiological partners in order to obtain more accurate results. For example, it has been recently demonstrated that Bfd is necessary to mobilize iron from Bfr in *Erwinia chrysanthemi* cells [22]. The recombinant Bfd protein from *E.coli* has been shown to bind a [2Fe-2S] cluster analogous to bacterial and plant ferredoxins [1, 2]. In addition, it has four cysteins which are conserved in the sequences of several Bfd genes, and led to its classification as a ferredoxin. This ferredoxin gene is located upstream of the *bfr* gene and hence named as bacterioferritin-associated ferredoxin. According to the observations made on the iron mobilization studies of Pa BfrB, it was clear that apo-Bfd can efficiently mobilize iron from Pa BfrB core, indicating that assembly of [2Fe-2S] cluster is not necessary. These findings strongly suggest that Pa Bfd does not function in transferring electrons between proteins. Consequently, Pa Bfd cannot be classified as a classic ferredoxin at least in these iron mobilization reactions in Pa BfrB. Figure 3-2 shows the amino acid sequence of Bfd containing four cystein residues which act as ligands to the [2Fe-2S] cluster has a unique arrangement of C-X-C-X_{31-32}-C-X_2-C. In addition the peptide of Pa Bfd is relatively shorter than (50 residues shorter) typical ferredoxins in Bacteria, plants, fungi and vertebrates, which also corroborate the idea that Pa Bfd does not function as a classic ferredoxin. The resonance raman spectrum of oxidized Pa Bfd is observed to be nearly identical to the [2Fe-2S] cluster of the second domain of Nifu [1, 3], a mulitimeric protein essential for the metallocluster in nitrognase [23]. This observation can be used to hypothesize that Bfds may function as a scaffold for the assembly of [2Fe-2S] clusters in other proteins and enzymes which require iron-sulfur clusters [1-3]. Having a transient [2Fe-2S] cluster in Pa Bfd may be important in the iron mobilization process in Pa BfrB, where iron released from the Pa BfrB core can be captured by the four cystein residues of apo-Bfd to form a mononuclear iron center. These mononuclear iron centers can deliver iron to where it is needed or these iron can be used

to form iron-sulfur clusters with the aid of iron sulfur cluster assemble machinery such as Isc and can be transferred to another new ferredoxin. The assembly of a [2Fe-2S] cluster from a tetra coordinated mononuclear iron center is thought to be taking place at the amino-terminal in the C-X-C motif (Figure 3-2) as it has the conformational freedom for Cys ligands to form a mono or di nuclear center.

References

[1] Quail, M.; Jordan, P.; Grogan, J.M.; Butt, J.N.; Lutz, M.; Thomas, A.J.; Andrews, S.C.; Guest, J.R. (1996) Spectroscopic and Voltammetric Characterization of Bacterioferritin-Associated Ferredoxin of *Escherichia coli*. *Biochemical Biophysical Research Communications* 229, 635-642.

[2] Garg, R.P.; Vargo, C.J.; Cui, X.; Kurtz, D.M.J. (1996) A [2Fe-2S] Protein Encoded by an Open Reading Frame Upstream of the *Escherichia coli* Bacterioferritin Gene. *Biochemistry* 35, 6297-6301.

[3] Wang, A., Zeng, Y., Han, H., Weeratunga, S., Morgan, B. N., Moënne-Loccoz, P., Schönbrunn, E., and Rivera, M. (2007) Biochemical and Structural Characterization of *Pseudomonas aeruginosa* Bfd and FPR: Ferredoxin $NADP^+$ Reductase and Not Ferredoxin is the Redox Partner of Heme Oxygenase under Iron-Starvation Conditions. *Biochemistry 46*, 12198-12211.

[4] Palma, M., Worgall, S., and Quadri, L. E. N. (2003) Transcriptome Analysis of the *Pseudomonas aeruginosa* Response to Iron. *Archives of Microbiology 180*, 374-379.

[5] Vasil, M. L., and Ochsner, U. A. (1999) The Response of *Pseudomonas aeruginosa* to Iron: Genetics, Biochemistry and Virulence. *Molecular Microbiology 34*, 399-413.

[6] Wilderman, P. J., Sowa, N. A., FitzGerald, D. J., FitGerald, P. C., Gottesman, S., Ochsner, U. A., and Vasil, M. L. (2004) Identification of Tandem Duplicate Regulatory Small RNAs in *Pseudomonas aeruginosa* Involved in Iron Homeostasis. *Proceedings of National Academy of Sciences U.S.A. 101*, 9792-9797.

[7] Stintzi, A.; Cornelis, P.; Hohnadel, D.; Meyer, J.M.; Dean, C.; Poole, K.; Kourambas, S.; Krishnapillai, V. (1996) Novel Pyoverdine Bio-Synthesis Genes of Pseudomonas aeruginosa PAO. *Molecular Microbiology 45*, 1277-1287.

[8] Pereira, A. S., Small, W., Krebs, C., Tavares, P., Edmondson, D. E., Theil, E. C., and Huynh, B. H. (1998) Direct Spectroscopic and Kinetic Evidence for the Involvement of Peroxodiferric Intermediate during the Ferroxidase Reaction in Fast Ferritin Mineralization. *Biochemistry 37*, 9871-9876.

[9] Le Brun, N. E., Wilson, M. T., Andrews, S. C., Guest, J. R., Harrison, P. M., Thomson, A. J., and Moore, G. R. (1993) Kinetic and Structural Characterization of an Intermediate in the Biomineralization of Bacterioferritin. *FEBS Letters 333*, 197-202.

[10] Carrondo, M. A. (2003) Ferritins, Iron Uptake and Storage from the Bacterioferritin Viewpoint. *EMBO Journal 22*, 1959-1968.

[11] Andrews, S. C. (1998) Iron Storage in Bacteria. *Advances in Microbial Physiology 40*, 281-351.

[12] Topham, R., Goger, M., Pearce, K., and Schultz, P. (1989) The Mobilization of Ferritin Iron by Liver Cytosol. *Biochemistry 261*, 137-143.

[13] Takagi, H., Shi, D., Ha, Y., Allewell, N. M., and Theil, E. C. (1998) Localized Unfolding at the Junction of Three Ferritin Subunits. *Journal of Biological Chemistry 273*, 18685-18618-18688.

[14] Liu, X., Jin, W., and Theil, E. C. (2003) Opening Protein Pores with Chaotropes Enhances Fe Reduction and Chelation of Fe from the Ferritin Biomineral. *Proceedings of National Academy of Sciences U.S.A. 100*, 3653-3658.

[15] Jin, W., Takagi, H., Pancorbo, B., and Theil, E. C. (2001) "Opening" the Ferritin Pore for Iron Release by Mutation of Conserved Amino Acids at Interhelix and Loop Sites. *Biochemistry 40*, 7525-7532.

[16] Liu, X., and Theil, E. C. (2005) Ferritins: Dynamic Management of Biological Iron and Oxygen Chemistry. *Accounts of Chemical Research 38*, 167-175.

[17] Weeratunga, S.K.; Gee, C.E.; Lovell, S.; Zeng, Y.;Woodin,Y.; Rivera,M. (2009) Binding of Pseudomonas aeruginosa Apobacterioferritin-Associated Ferredoxin to bacterioferritin B Promotes the Heme Mediation of Electron Delivery and Mobilization of core Mineral Iron. *Biochemistry 48*, 7420-7431.

[18] Andrews, S. C., Le Brun, N. E., Barynin, V., Thomson, A. J., Moore, G. R., Guest, J. R., and Harrison, P. M. (1995) Site-Directed Replacement of the Coaxial Heme Ligands of Bacterioferritin Generates Heme-free Variants. *Journal of Biological Chemistry 270*, 23268-23274.

[19] Topham, R., Goger, M., Pearce, K., and Schultz, P. (1989) The Mobilization of Ferritin Iron by Liver Cytosol. *Biochemistry 261*, 137-143.

[20] Jones, T., Spencer, R., and Walsh, C. (1978) Mechanism and Kinetics of Iron Release from Ferritin by Dihydroflavins and Dihydroflavin Analogues. *Biochemistry 17*, 4011-4017.

[21] Theil, E. C., Liu, X. S., and Tosha, T. (2008) Gated Pores in the Ferritin Protein Nanocage. *Inorganica Chimica Acta 361*, 868-874.

[22] Richards, T. D., Pitts, K. R., and Watt, G. D. (1996) A Kinetic Study of Iron Release from *Azotobacter Vinelandii* Bacterial Ferritin. *Journal of Inorganic Biochemistry 61*, 1-13.

[23] Dos Santos, P. C., Smith, A. D., Frazzon, J., Cash, V. L., Johnson, M. K., and Dean, D. R. (2004) Iron-Sulfur Cluster Assembly: NifU-Directed Activation of the Nitrogenase Fe Protein. *Journal of Biological Chemistry 279*, 19705-19711.

[24] Larkin, M. A., Blackshields, G., Brown, N. P., McGettigan, P. R., McWilliam, H., Valentin, F., Wallace, I. M., Wilm, A., Lopez, R., Thompson, J. D., Gibson, T. J., and Higgins, D. G. (2007) Clustal W and Clustal X Version 2.0. *Bioinformatics 23*, 2947-2948.

CHAPTER IV

Probing a Possible Pathway of Iron Release from the Mineral Core of Bacterioferritin B.

Introduction

Ferritins are ubiquitous iron storage proteins and have an important role in intracellular iron homeostasis [1, 2]. These proteins are capable of storing large amounts of iron and release it to the cytoplasm in times of iron deficit [3]. Iron is captured by ferritins in its Fe^{2+} oxidation state, oxidized at the ferroxidase center and subsequently internalized and mineralized inside the ferritin core. Under iron starvation conditions these Fe^{3+} ions in the mineral core are reduced to Fe^{2+} ions and released to the cytoplasm to be used by the bacteria for its various metabolic processes. Therefore, iron uptake and release from ferritin-like molecules are vital processes to a cell, because they maintain iron homeostasis in the cell. The mechanisms of iron oxidation and internalization of most of the ferritin members have been extensively studied and relatively well understood [4-7]. In comparison, very little is known about the mechanism of iron release from ferritins, particularly from bacterioferritins (Bfr). Three models of iron release from ferritins have been speculated and investigated [8]. The first model proposes that iron is released from the ferritin core by subunit displacement [9]. This method of iron release by subunit displacement is unlikely as the ferritin subunits show a high stability even at high temperatures, extreme pH, and denaturing agents such as urea [8]. The second model addresses iron release from eukaryotic ferritins and is based on the diffusion of molecules through the 3-fold channels. The 3-fold channels of eukaryotic ferritins, which are lined by negatively charged

amino acid residues, are believed to be involved in moving iron in and out of the ferritin [10]. It was initially thought that reducing and chelating agents diffuse through these pores to reduce the ferric ion core and chelate iron ions. The third model describes the gated mechanism of iron release where it is assumed that ferritin channels regulate the moving of iron ions by opening and closing of these channels [8]. It has been experimentally shown that physiological concentrations (2-7 mM) of denaturing agents such as urea can unfold the pores of ferritin while the rest of the ferritin molecule shows a high stability at that urea concentration [12]. Consequently iron is thought to be released through these unfolded ferritin pores suggesting that biological regulators can recognize these pores to regulate the opening and closing of these channels and subsequently release iron through these pores [13]. The oxidation and mineralization of iron by the bacterioferritins has been somewhat studied [14, 15]. However, the mechanism or the pathway of iron release from the inner core of bacterioferritins is not yet understood. Bacterioferritins are the heme containing counterparts of ferritins and found only in bacteria. In our laboratory, experiments were carried out to investigate the mechanism and the pathway of iron release from the mineral core of bacterioferritin B from *P.aeruginosa* (Pa-BfrB) and we were able to experimentally demonstrate that binding of a small ferredoxin called Bfd (bacterioferritin associated ferredoxin) facilitates the efficient release of iron from the inner core of BfrB (Chapter 3 and [14]). It was also found that electrons from the electron donor are transferred to the mineral core via the heme groups in Bfr, establishing the role of heme in bacterioferritins for the first time. These interesting findings of the mechanism of iron release from Pa BfrB tempted us to discover the pathway of iron release from Pa-BfrB.

The crystallographic studies of BfrB presented in Chapter 2, 3-fold pores of BfrB are lined with both positively and negatively charged residues. In addition, the Fe soaked crystal

structure of BfrB indicated residual electron density in the 3-fold pores and that revealed the presence of sulfate ions in these pores. This observation may suggest that 3-fold pores are involved in traffick of anions in and out of the molecule, thus further experimentation is required to clearly elucidate the function of these 3-fold pores. The B-pores of Pa BfrB, on the other hand, are lined with negatively charged amino acid residues such as aspartates, suggesting a possible pathway for the translocation of Fe^{2+} ions out of the molecule. However, no experimental evidence has been found yet to confirm the idea of cation trafficking through these B-pores. Some important observations from the crystallographic studies of Pa BfrB suggest that 4-fold pores, which are lined with both negatively and positively charged amino acid residues, can be one of the possible pathways of iron release from the mineral core. Crystal structures of mineralized and iron soaked ('as isolated' BfrB crystals, soaked in a Fe^{2+} solution) BfrB showed potassium ions in the 4-fold pores, coordinated by the side chains of Asn148 and Gln151 (see figure 2-15 in Chapter 2) [17]. In addition, Bfr from *Azatobacter vinelandii* has also been observed to contain cations such as iron and barium in the four fold pores, which have relatively similar architecture as the pores in Pa BfrB [25, 26]. The presence of cations in the 4-fold pores of Pa-BfrB and Av-Bfr would suggest the possibility of carrying out similar functions like, mobilization of iron.

Based on the assumption that 4-fold pores may be the dominant pathway of iron trafficking, experiments were carried out to elucidate the precise pathway of iron release from the core of Pa BfrB by mutating some of the residues in the four fold pore which are believed to be crucial for the process of iron release. In addition to the above observations, there is additional circumstantial evidence supporting the hypothesis that iron is released through the 4-fold pores of Pa BfrB: As mentioned in Chapter 3, we have experimentally demonstrated that

binding of Pa Bfd (a small ferredoxin called bacterioferritin-associated ferredoxin) facilitates the efficient release of iron from the inner core of Pa BfrB [14], suggesting that these two proteins function in concert to release iron from Pa BfrB. In the absence of Pa Bfd, no significant amount of iron is released from the core, indicating that Pa Bfd is essential for efficient release of iron from Pa BfrB.

In addition to the iron storing protein Pa BfrB, *P aeruginosa* has another iron storage protein called Pa FtnA. Our laboratory has shown that Pa FtnA, is a bacterial ferritin, which does not contain heme. In the *P aeruginosa* genome, *bfrB* gene is located downstream to the *bfd* gene where as *ftnA* gene is located downstream to *katA* gene, which codes for enzyme catalase A. Preliminary results of our studies on iron release from Pa FtnA revealed that Pa Bfd is not required for efficient release of iron from the inner core of Pa FtnA. Since our hypothesis is based on the Pa Bfd facilitated iron release through the 4-fold pores, it is important to investigate to find out if there is any structural and hence functional difference between the 4-fold pores of Pa BfrB and Pa FtnA.

The 4-fold channel of Pa-BfrB is made of several amino acid layers. The outer opening of the pore is made of an outer layer of Asn148 and inner layer of Gln151 followed by His153 and155 towards interior of the molecule [16] (Figure 4-1A). The inner most end of the pore is believed to be made from side chains of Asp157 and 158 (Figure 4-1B). However, these two residues are not visible in the crystal structure of Pa BfrB as these residues are disordered.

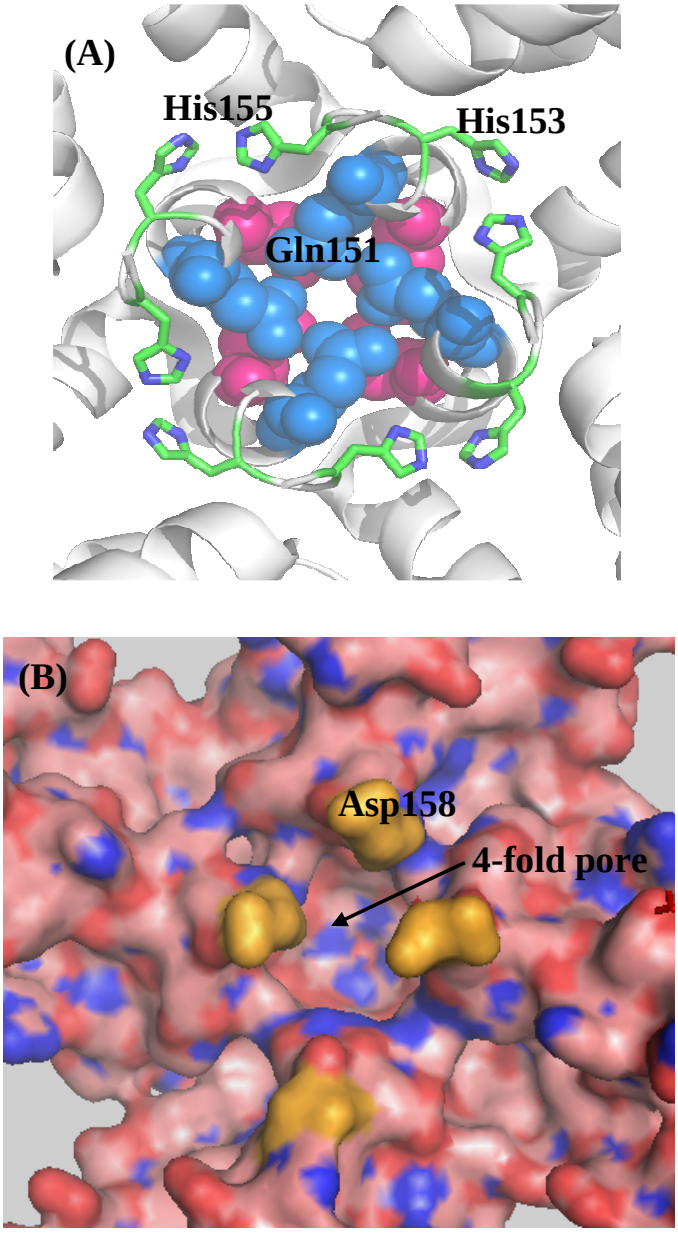

Figure 4-1: The structure of the 4-fold pore of Pa BfrB viewed from the interior of the protein. (A) The inner layer of Gln151 are shown in blue spheres and the Asp157 and Asp158 (last two residues at the C-terminus) which forms the inner end of the pore, however, are not visible in the crystal structure of BfrB. (B) Surface representation of the 4-fold pore of Pa BfrB (shown by the black arrow) showing the Asp157 and 158 residues (colored in bright orange) at the C terminal modeled by the Elastic Network Model calculations.

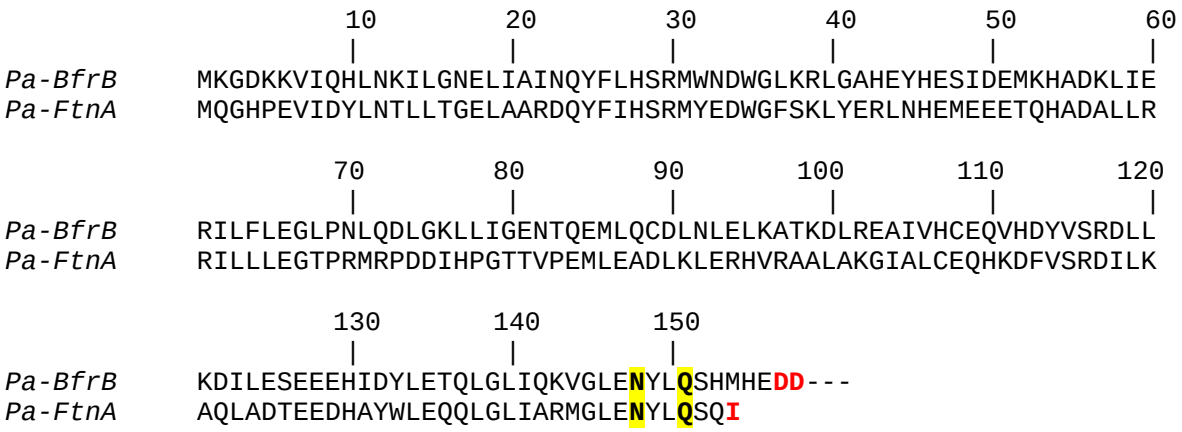

Figure 4-2: Sequence of *P. aeruginosa* BfrB aligned against the sequence of FtnA. The amino acid residues forming the outer part of the 4-fold pore (Asn148 and Gln151) are conserved in both proteins(highlighted in yellow). The C-terminus of Pa BfrB ends with two negatively charged Asp residues whereas that of Pa FtnA ends with a hydrophobic Ile residue (highlighted in red). The sequences were aligned with the aid of ClustalW [17]

According to the amino acid sequences of Pa BfrB and Pa FtnA (Figure 4-2), the two Asp residues (157 and 158) at the C-terminus of Pa BfrB, which is thought to be forming the inner opening of the 4-fold pore, are absent in the sequence of FtnA, and instead of that Pa FtnA has a hydrophobic Ile residue at its C-terminus. This observation suggests that the structure of 4-fold pore of Pa BfrB and hence the iron release mechanism may be different from that of Pa FtnA. It is possible that, the structural difference observed at the inner end of the 4-fold pore in Pa FtnA protein, likely the reason for the observed higher rates of iron release even in the absence of Pa Bfd. That result circumstantially suggests that Bfd may have an effect of opening of the 4-fold pores of Pa BfrB. Further, upon aligning the sequences of *bfr* genes which are located downstream to the *bfd* gene in the bacterial genome, it was observed that almost all those *bfr* genes end with negatively charged acidic residues (aspartates or glutamates) which are thought to be forming the inner end of the 4-fold pore (Appendix 1). This alignment data

suggest that, similar to Pa BfrB, all the other Bfrs which are located adjacent to Bfd, may require Bfd to open the 4-fold pores and release iron from the inner core.

In order to test this idea of Pa Bfd facilitated iron release through 4-fold pores, the structure of the four fold pore of Pa BfrB was altered by removing Asp157 and 158 residues at the C-terminus of the protein (truncated Pa BfrB) by site directed mutagenesis. Subsequently, the rate of iron release from the mineral core and the effect of Pa Bfd on the rate of iron release from truncated Pa BfrB were compared with those of the wild type Pa BfrB with the aim of establishing a precise pathway of iron release from Pa BfrB.

Experimental Procedures

Site directed mutagenesis of truncated (D157TAA) BfrB

Codone coding for residue Asp157 (GAT) was converted to a stop codon (TAA) and as a result protein will be expressed only upto the amino acid Glu156 (truncated Pa BfrB). Truncated *bfrB* gene was constructed using the recombinant pET11a plasmid harboring the gene coding for wild type Pa BfrB (Figure 4-3). The sequences of the primers designed for truncated BfrB are 5`-CAG AGC CAT ATG CAT GAA TAA GAT TAA GGA TCC GGC TGC-3` and 5`-GCA GCC GGA TCC TTA ATC TTA TTC ATG CAT ATG GCT CTG-3`. The GC content and the melting temperature (Tm) were calculated to be 46 %. and 75 ºC respectively. The primers were synthesized by Integrated DNA Technologies, Inc (Coralvile, IA). Mutagenesis was carried out using the QuickChange™ mutagenesis kit (Stratagene, La Jolla, CA). The recombinant constructs were then transformed into *E.coli* XL1 Blue supercompetent cells for DNA

amplification. Once the mutation was verified by sequencing, recombinant DNA plasmids were transformed into *E. coli* Arctic express RIL cells (Stratagene, La Jolla, CA).

5'*Nde*1

CATATG AAA GGC GAT AAA AAA GTG ATC CAG CAT CTG AAT AAA ATT

M K G D K K V I Q H L N K I

CTG GGT AAT GAA CTG ATT GCG ATT AAT CAG TAT TTT CTG CAT AGC CGC ATG

L G N E L I A I N Q Y F L H S R M

TGG AAT GAT TGG GGC CTG AAA CGT CTG GGC GCG CAT GAA TAT CAT GAA AGC

W N D W G L K R L G A H E Y H E S

ATT GAT GAA ATG AAA CAT GCG GAT AAA CTG ATC GAA CGT ATT CTG TTT CTG

I D E M K H A D K L I E R I L F L

GAA GGT CTG CCG AAT CTG CAG GAT CTG GGC AAA CTG CTG ATT GGT GAA AAC

E G L P N L Q D L G K L L I G E N

ACC CAG GAA ATG CTG CAG TGC GAT CTG AAT CTG GAA CTG AAA GCG ACC AAA

T Q E M L Q C D L N L E L K A T K

GAT CTG CGT GAA GCG ATC GTG CAT TGC GAA CAG GTG CAT GAT TAT GTT AGC

D L R E A I V H C E Q V H D Y V S

CGT GAT CTG CTG AAA GAT ATC CTG GAA AGC GAA GAA GAA CAT ATT GAT TAT

R D L L K D I L E S E E E H I D Y

CTG GAA ACC CAG CTG GGT CTG ATT CAG AAA GTG GGC CTG GAA AAC TAT CTG

L E T Q L G L I Q K V G L E N Y L

CAG AGC CAT ATG CAT GAA **TAA** GAT TAAGGATCC

Q S H M H E D ***Bam*H1 3'**

Figure 4-3: DNA and corresponding amino acid sequence of *truncated (D157TAA) bfrB* from *P. aeruginosa*. D157TAA mutation is highlighted. *Nde* I and *Bam*H I restriction endonuclease sites were constructed at the 5' and 3' ends for subcloning.

Expression and purification of truncated Pa BfrB.

The truncated Pa BfrB was expressed, lysed and purified following the same procedures as those of wild type, which are described in detail in the experimental procedures in Chapter 2. The purity of the protein was determined by SDS-PAGE and the pure protein was then passed through a calibrated high resolution size exclusion column (Superdex 200 10/300, GE Healthcare) equilibrated with 100 mM potassium phosphate (pH 7.6) and 1 mM tris (2-carboxyethyl)-phosphine hydrochloride (TCEP) to determine the size and confirm the oligomerization. Once the oligomerization is confirmed as 24mers, the pure protein was concentrated, flash frozen and stored at -80 ºC.

Mineralizaton of iron in the truncated Pa BfrB cavity.

Similar to wild type Pa BfrB, truncated Pa BfrB also contains a few iron ions in their cores (10-15 iron atoms per molecule). Therefore, the protein to be used in experiments was incorporated with ~ 600 iron atoms per molecule. The same mineralization procedure used for wild type BfrB, described in the experimental procedures in chapter 2 was followed for the mutant. Anaerobic solution of ferrous ammonium sulfate was added in aliquots delivering 50 Fe^{2+}/Pa BfrB to a stirred solution of 3 µM truncated BfrB in 100 mM potassium phosphate buffer, pH 7.6, to obtain a core of ~ 600 Fe^{2+}/Pa BfrB. Any precipitation formed during the mineralization was removed by centrifuging the sample for 10 minutes at 4000 rpm. The mineralization process was monitored spectrophotometrically following the absorbance near 320 nm with the aid of a USB 2000 spectrophotometer (Ocean Optics, Dunedin, FL).

Analysis of non-heme iron in the truncated Pa BfrB core.

Non-heme iron analysis of truncated Pa BfrB was carried out using Fe-ferrozine assay in the same way as described for wild type Pa BfrB in Chapter 2. The concentration of iron was determined from the electronic absorption spectrum using the absorbance at 562 nm (ε_{562} = 27.9 mM^{-1} cm^{-1}) [19].

Crystallization of truncated BfrB

Crystallization studies were carried out in the Protein Structure Laboratory at the Delbert M. Shankel Structural Biology Center (University of Kansas, Lawrence, KS). Mineralized truncated Pa BfrB was concentrated to 20 mg/mL in 100 mM potassium phosphate pH 7.6, 5 mM TCEP for crystallization. Crystals were grown under aerobic conditions in Clover Jr. (Emerald biosystems) sitting drop vapor diffusion plates using 1μL of crystallization solution and 1 μL of protein equilibrated against 100 μL of crystallization solution at 20 ^{o}C. Red prisms were obtained within 24 hours from the crystallization condition, 35% (v/v) 2-methyl-2,4-pentanediol, 100 mM MES pH 6.0, 200 mM Li_2SO_4 (Wizard 2 #2, Emerald biosystems).

Iron uptake by truncated Pa BfrB in solution

Truncated Pa BfrB to be used in the experiments was prepared by extensively dialyzing the pure, as-isolated protein against 100 mM potassium phosphate, pH 7.6. Aliquots of 50 mM ferrous ammonium sulfate containing 50 Fe^{2+}/BfrB molecule were added using a Hamilton microsyringe to a solution of truncated BfrB (0.8 μM) at 30 °C in a 1.0 cm path length cuvette equipped with a stirring bar. Changes in the intensity of the absorbance at 320 nm were recorded for 10 minutes for each addition of iron with the aid of a diode-array UV-vis spectrophotometer (Ocean Optics, Dunedin, FL).

Mobilization of core iron from truncated Pa BfrB

Experiments to investigate the iron release from truncated Pa BfrB were carried out in an anaerobic chamber. These reactions were conducted in a 1.0 cm path-length cuvette equipped with a magnetic stirring bar and monitored by electronic absorption spectroscopy using an Ocean Optics (Dunedin, FL) 2000 spectrophotometer. A few μL from stock protein solutions were added to a cuvette containing 3 mM 2,2, bipyridyl (bipy) in 1.0 mL of 20 mM potassium phosphate buffer (pH 7.6), to make a solution 15 μM in Pa Bfd, 15 μM in Pa Fpr and 0.375 μM in truncated Pa BfrB. The reaction was initiated by addition of NADPH to a final concentration of 1.5 mM and the progress of the reaction was monitored by following the time-dependent changes in intensity of the band at 523 nm that is formed when bipy binds Fe^{2+} to form the $[Fe(bipy)_3]^{2+}$ complex. All the experiments were conducted with apo Bfd and it was prepared *in situ* from holo-Bfd as described in Chapter 3. Experiments were carried out by varying the concentration of apo Bfd while maintaining Pa BfrB (0.375 μM), Pa Fpr (15μM), NADPH (1.5 mM), and Bipy (3 mM) concentrations constant. Iron mobilization experiments were also carried out using sodium dithionite as the reducing agent. Excess of sodium dithionite (twice the required stoichiometric amount) was added into a solution of 0.05 μM truncated Pa BfrB, 2 μM Pa Bfd and 0.4 mM ferrozine (Fe^{2+} chelating agent) and the iron release from Pa BfrB was monitored by following the time-dependent changes in intensity of the band at 562 nm which is formed due to the absorbance of the Fe-ferrozine complex. In order to compare the results with that of wild type BfrB, same experiment was carried out with wild type Pa BfrB under the same experimental conditions. The initial pseudo rates of iron release of each experiment were estimated by fitting each curve of iron release to an exponential function.

Iron mobilization from truncated Pa BfrB in the absence of Bfd.

Experiments to probe the effect of Pa Bfd on opening of the pore of Pa BfrB were carried out in an anaerobic chamber. Excess of 3 mM sodium dithionite solution (twice the stoichiometric amount) was added to a solution of 0.05 µM mineralized truncated Pa BfrB in 20 mM potassium phosphate buffer, pH 7.6 to reduce the iron core of Pa BfrB. The experiment was conducted in a 1.0 cm path-length cuvette equipped with a magnetic stirring bar and monitored by electronic absorption spectroscopy using an Ocean Optics (Dunedin, FL) 2000 spectrophotometer. Excess of 20 mM ferrozine solution was added to the protein to a final concentration of 0.4 mM in order to chelate Fe^{2+} ions releasing from the iron core of the protein. The release of iron was monitored by following the absorbance of Fe-ferrozine complex at 562 nm using an Ocean Optics (Dunedin, FL) 2000 spectrophotometer. As a control, the same experiment was carried out with wild type Pa BfrB under similar experimental conditions.

Reduction of the iron core of truncated Pa BfrB by dithionite.

Excess of sodium dithionite was added to a solution of 0.05 µM mineralized, truncated Pa BfrB in 20 mM potassium phosphate buffer (pH 7.6). The experiment was carried out in a 1.0 cm path-length cuvette equipped with a magnetic stirring bar in an anaerobic chamber. The decay of the absorbance of dithionite solution at 314 nm was monitored using an Ocean Optics (Dunedin, FL) 2000 spectrophotometer. As a control experiment, same amount of dithionite was added to a solution of non mineralized truncated BfrB of same concentration as mineralized, truncated Pa BfrB and monitored the decay of the absorbance of dithionite at 314 nm. As a control, another set of similar experiments were carried out with mineralized and non mineralized wild type Pa BfrB.

Results

Protein expression and purification

The truncated Pa BfrB expressed in *E.coli* arctic express RIL cells is soluble and can be purified to homogeneity as judged by SDS-PAGE (Figure 4-4A). The molecular weight of one subunit was ~18 kDa which is in agreement with the molecular mass calculated from the amino acid sequence of a truncated Pa BfrB subunit (18321 Da). The electronic absorption spectrum of pure truncated Pa BfrB was similar to that of wild type with a Soret band maximum at 418 nm and α and β bands at 567 nm and 527 nm, respectively (Figure .4-4B). The folding of the protein was confirmed as a 24 mer by using a previously calibrated Superdex 200 column. (10/300, GE Healthcare).

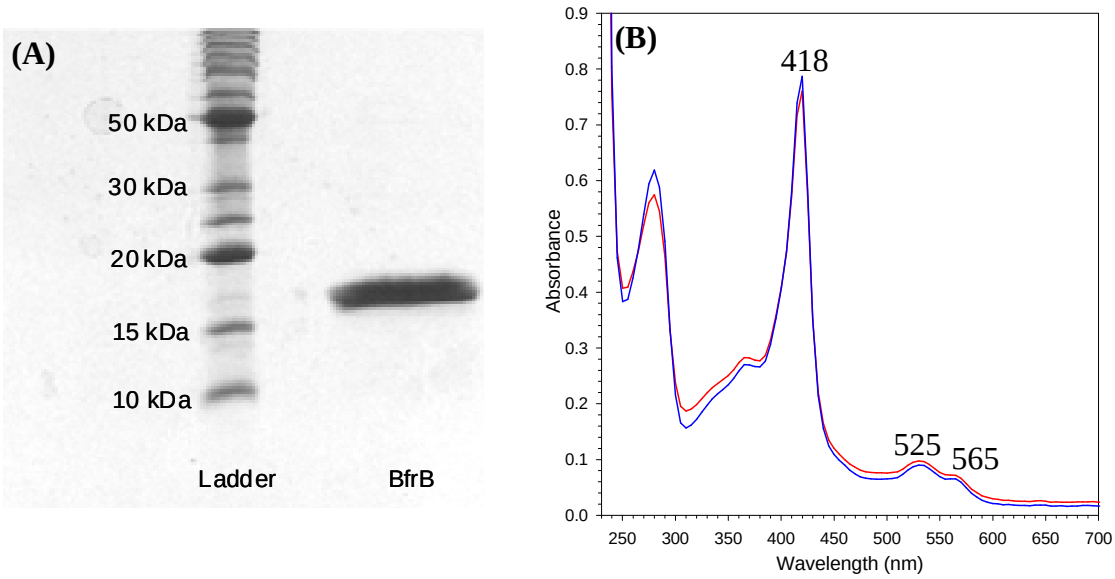

Figure 4-4: (A) 15 % SDS-PAGE analysis of truncated Pa BfrB purified to homogeneity and (B) the electronic absorption spectra of truncated Pa BfrB (blue trace) and wild type Pa BfrB (red trace) showing the Soret, α and β bands at 418 nm, 567 nm and 527 nm, respectively.

Mineralizaton of truncated Pa BfrB

An iron core of ~600 iron atoms could be formed by adding an anaerobic solution of Fe^{2+} into a solution of truncated Pa BfrB in air. Each time an aliquot of Fe^{2+} containing 50 Fe^{2+} ions were added to the protein solution. However, after adding ~400 iron atoms a slight precipitation was observed and it was removed by centrifuging the protein at 4000 rpm for 10 minutes. The family of spectra in figure 4-5 shows a small decrease in the intensity of Soret band which was due to the loss of a small amount of protein precipitated with the ferric iron colloid formed by the oxidation of Fe^{2+} in air.

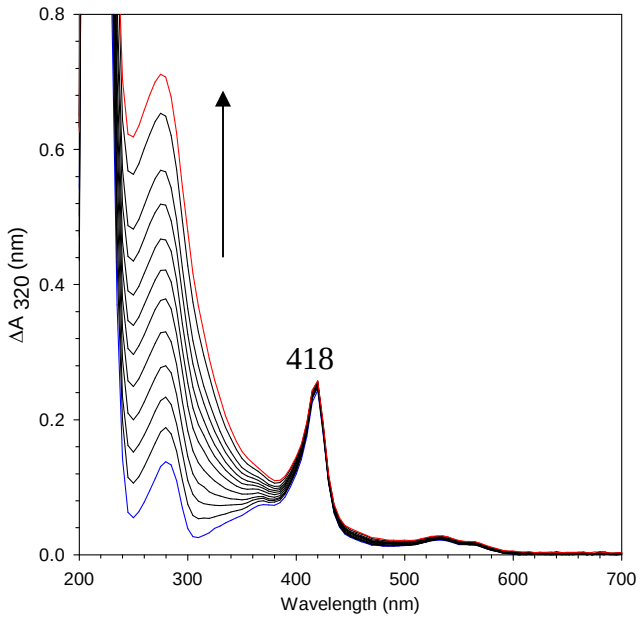

Figure 4-5: The family of electronic absorbance spectra showing the incorporation of iron into the core of truncated Pa BfrB. The initial spectrum of truncated Pa BfrB is shown in blue and the final spectrum is shown in red.

The addition of iron was continued with the supernatant obtained after centrifugation until a core of about 600 iron ions is formed. Subsequently, the protein solution was cleaned using a G-25 column (Amersham biosciences) to remove Fe^{2+} ions not incorporated into the protein. An iron core of 600 ± 20 iron ions was obtained when analyzed by the Fe-ferrozine assay described in Chapter 2.

Crystallization of truncated BfrB

The recombinant mineralized truncated Pa BfrB was concentrated to 20 mg/mL and formed red prismatic crystals within 24 hours from the crystallization condition, 35% (v/v) 2-methyl-2,4-pentanediol, 100 mM MES pH 6.0, 200 mM Li_2SO_4 (Wizard 2 #2, Emerald biosystems) (Figure 4-6).

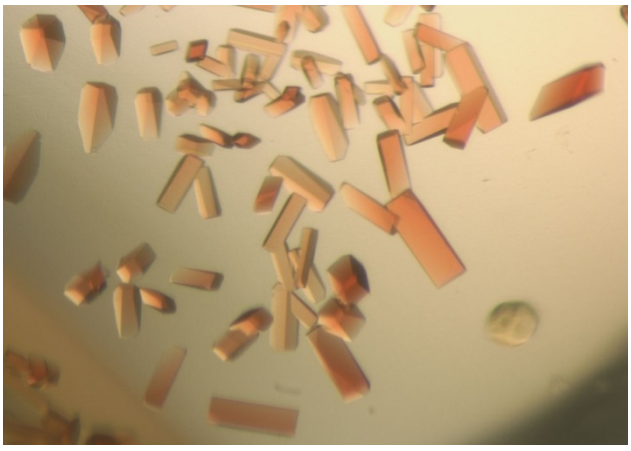

Figure 4-6: Crystals of recombinant truncated BfrB formed from the condition 35% (v/v) 2-methyl-2,4-pentanediol, 100 mM MES pH 6.0, 200 mM Li_2SO_4 (Wizard 2 #2, Emerald biosystems)

Red prismatic crystals were also formed from the conditions of pHAT buffer screen. Those crystals however, did not diffract well. Therefore, studies on the crystal structure of truncated Pa BfrB are expected to be carried out using the crystals formed from the Wizard 2 #2 condition.

Iron uptake in solution by Pa BfrB

The uptake of iron by as isolated (non-mineralized) truncated Pa BfrB was studied by adding aliquots of Fe^{2+} solution delivering 50 Fe^{2+} ions per Pa BfrB molecule. A rapid increase of the intensity of the absorbance near 320 nm was observed and recorded using a diode array UV-vis spectrophotometer. The observed results were similar to that of wild type BfrB [24], which showed a rapid increase of the intensity near 320 nm upon addition of Fe^{2+} ions and reached a plateau that remained constant until the next aliquot of iron is added (Figure 4-7).

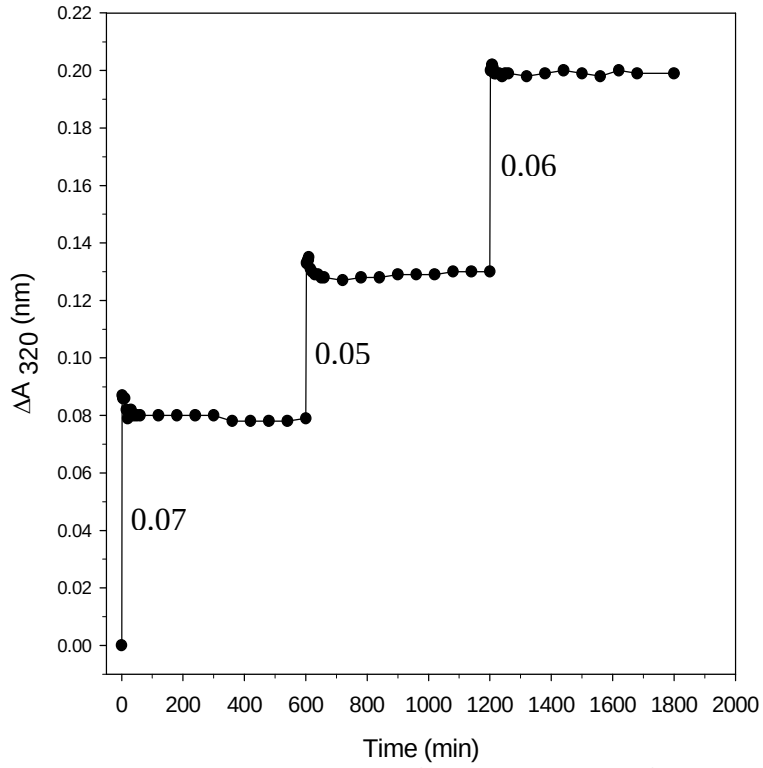

Figure 4-7: Changes in ΔA_{320} upon addition of Fe^{2+} aliquots (50 Fe^{2+}ions/BfrB molecule) to a solution of truncated Pa BfrB.

Aliquots of Fe^{2+} were added three times and the magnitude of the change of the absorbance at 320 nm at each addition of iron was nearly constant. These results show that the iron uptake mechanism of truncated Pa BfrB is similar to that of wild type Pa BfrB [16] and indicate that the mutation at the four fold pore region of truncated BfrB did not affect the function of the ferroxidase center. As these results suggest, the ferroxidase center of truncated Pa BfrB functions as a labile ferroxidase center similar to that of wild type BfrB (see Chapter 2 and [16].

Mobilization of core iron from truncated Pa BfrB

All iron mobilization experiments of truncated Pa BfrB were carried out under anaerobic conditions and the experiments were carried out similar to those with wild type Pa BfrB as described in Chapter 3. Iron release from truncated Pa BfrB was initiated by adding 1.5 mM NADPH to a solution containing 3 mM 2, 2, bipyridyl (bipy), 15 μM apo Pa Bfd, 15 μM Pa Fpr and 0.375 μM truncated Pa BfrB and it was monitored by following the time–dependent formation of the ferrous bipyridine complex [$Fe(bipy)_3$)], which absorbs at 523 nm (Figure 4-8A). Several iron mobilization experiments were carried out by varying the concentration of apo Pa Bfd while maintaining the concentrations of truncated Pa BfrB (0.375 μM) and Pa Fpr (15 μM) consant. The amount of iron released upon addition of 1.5 mM NADPH to the protein solutions with Bfd/BfrB molar ratio of 50 (pink), 40 (green), 20 (red), 15 (cyan), 10 (blue), 5 (dark yellow) and 0 (black) is shown in figure 4-8A. Results from a similar set of experiments carried out with wild type BfrB are shown in figure 4-8B and color coded as in figure 4-8A. A significant enhancement of the rate of iron release is observed in the presence of Pa Bfd in both sets of reactions carried out with wild type and truncated Pa BfrB.

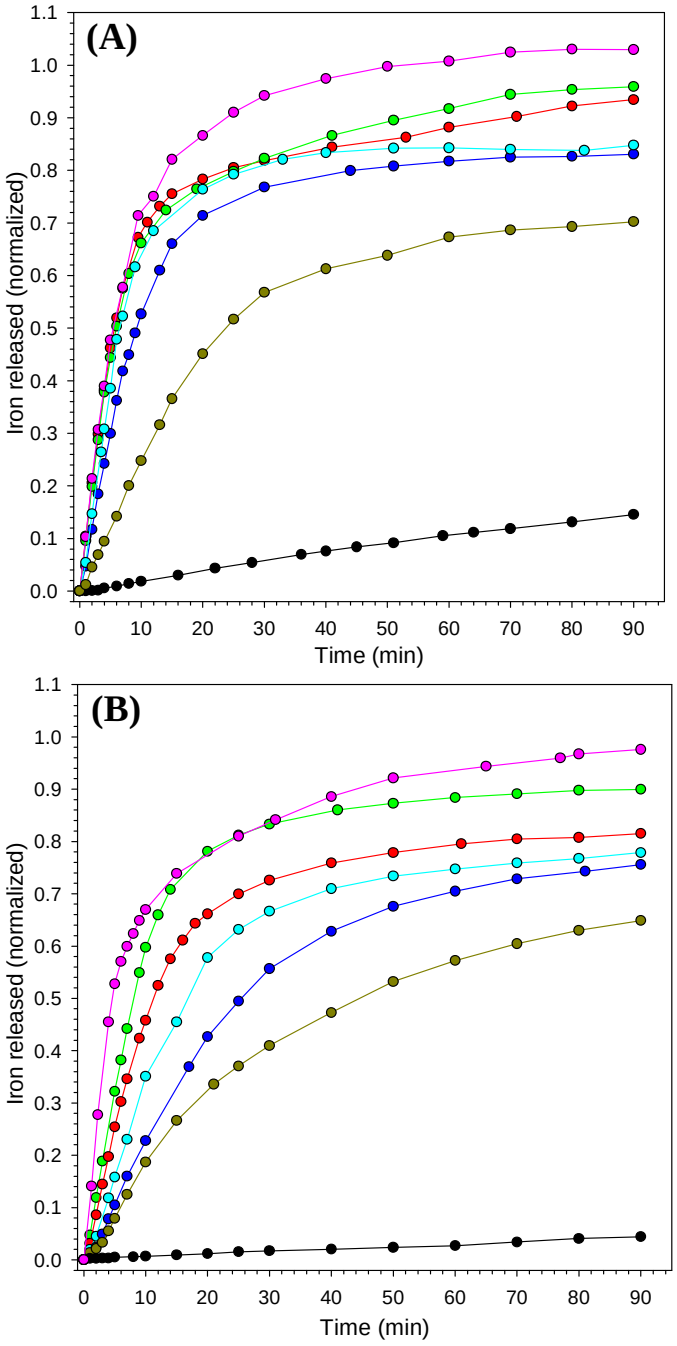

Figure 4-8: Effect of Pa Bfd concentration on the time dependent process of iron mobilization from the iron core of (A) truncated Pa BfrB and (B) wild type Pa BfrB, measured upon addition of NADPH (1.5 mM) to solutions containing 3.0 mM bipy, 15 µM Pa FPR, 0.375 µM truncated Pa BfrB and apo Pa Bfd with Bfd/BfrB molar ratio of 50 (pink), 40 (green), 20 (red), 15 (cyan), 10 (blue), 5 (dark yellow) and 0 (black).

However, with truncated Pa BfrB, the rates of iron release of all the experiments with different Pa Bfd concentrations seem to be significantly higher than that of with wild type Pa BfrB.

In order to compare the rates of iron release in a more quantitative manner, the initial pseudorates of iron release were estimated for each experiment with wild type and truncated BfrB by fitting the curves of iron release to an exponential function. The results are summarized in table 4-1 and in figure 4-9.

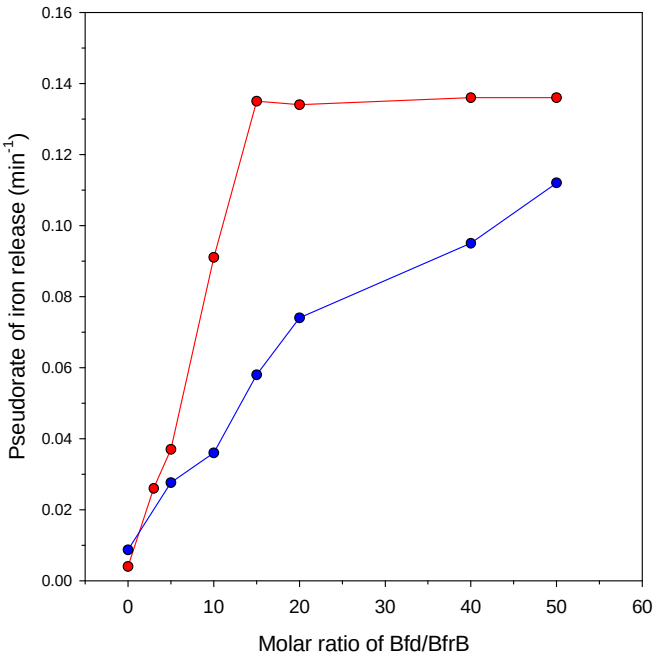

Figure 4-9: Bfd dependent iron release from truncated (red) and wild type (blue) BfrB.

In truncated Pa BfrB the rate of iron release increases rapidly as the Bfd/BfrB ratio increases and plateaus when the Bfd/BfrB is above 10. This suggests that once Bfd/BfrB ratio is 12, i.e. once it reaches the stoichiometric ratio of 12 (Bfd:BfrB), [15] the reaction achieves the maximum rate of iron release. These results imply that once Pa Bfd and Pa BfrB are reacting at a ratio below their stoichiometric ratio, the rate of iron release becomes sluggish, but when the two proteins reacts at or above the stoichiometric ratio the rate of iron release becomes

independent of the concentration of Pa Bfd. In the wild type Pa BfrB, on the other hand, the rate of iron release gradually increases with increasing Pa Bfd concentration, indicating that effect of Pa Bfd on the rate of iron release is different for wild type and truncated proteins, which are structurally different only at the 4-fold pore.

Table 4-1: A comparison of the pseudorates of the Pa Bfd dependent release of core iron from wild type and truncated Pa BfrB

Bfd/BfrB molar ratio	Pseudo rate of iron release (min^{-1}) at 25 ºC	
	WT Pa BfrB	Truncated Pa BfrB
0	0.0087 ± 0.0002	0.004 ± 0.0005
5	0.029 ± 0.001	0.037 ± 0.009
10	0.036 ± 0.002	0.091 ± 0.007
15	0.058 ± 0.008	0.135 ± 0.010
20	0.074 ± 0.008	0.134 ± 0.010
40	0.095 ± 0.007	0.136 ± 0.010
50	0.112 ± 0.004	0.136 ± 0.006

Further, upon addition of NADPH to initiate the reaction of iron release, the Soret band of wild t

However, the rate of the shift of the Soret band from 418 nm to 425 nm was also varied with varying concentration of Bfd. The fastest shift was observed with Bfd/BfrB ratio of 40 and the slowest shift was observed with the ratio of 5 and in the absence of Bfd, however, no shift of the soret band was observed (Figure 4-10). The same trend of the shifting of the Soret band was observed with truncated BfrB, implying that the rate of electron transfer from the reductase to the inner core via the heme group is relatively similar in both proteins.

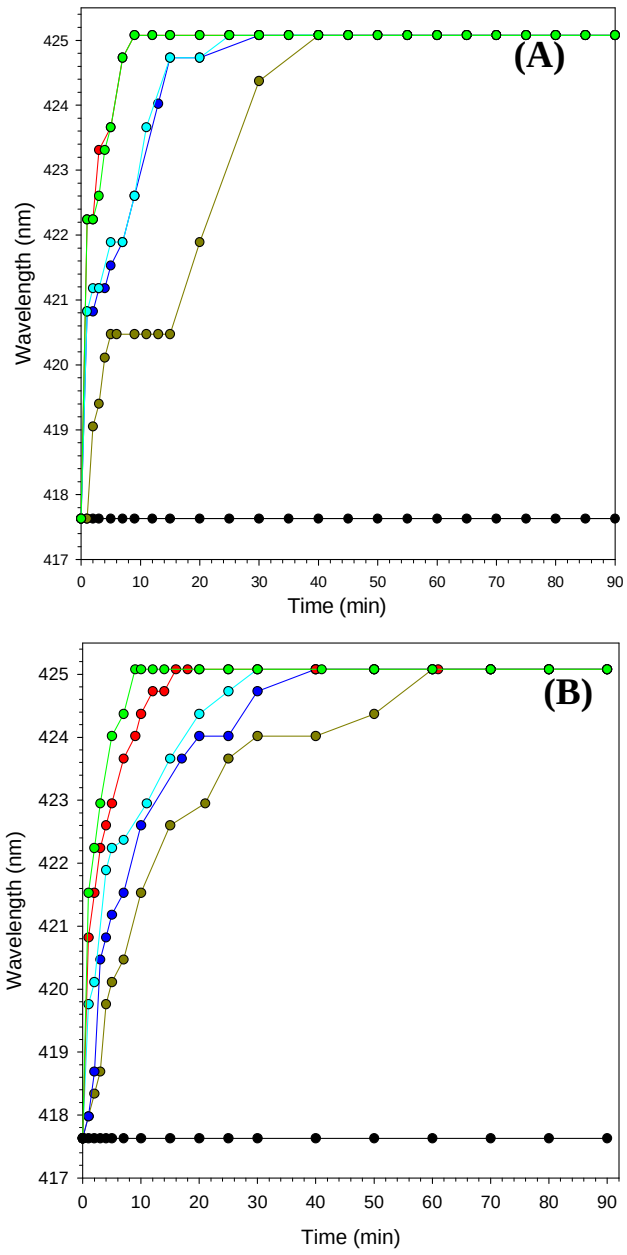

Figure 4-10: The shift of the Soret band in the (experiments shown in figure 4-8) reactions of iron mobilization from the iron core of (A) truncated Pa BfrB and (B) wild type Pa BfrB, observed upon addition of NADPH (1.5 mM) to solutions containing 3.0 mM bipy, 15 µM Pa FPR, 0.375 µM truncated Pa BfrB and apo Pa Bfd with Bfd/BfrB molar ratio of 50 (pink), 40 (green), 20 (red), 15 (cyan), 10 (blue), 5 (dark yellow) and 0 (black).

In the absence of Bfd, Fe^{2+} ions are trapped inside the Pa BrB core

Excess sodium dithionite was added to non mineralized, wild type Pa BfrB under strict anaerobic conditions and the decay of the intensity of the absorbance by sodium dithionite at 314 nm was monitored. The shift of the Soret band of Pa BfrB was monitored simulataneously (Figure 4-11A). The absorbance of dithionite at 314 nm slowly decayed for ~60 minutes and eventually became relatively constant. Non mineralized, wild type Pa BfrB usually contains few iron atoms in its inner core [14] and the electrons from the dithionite may have been used to reduce those few Fe^{3+} ions in the core which was indicated by the slow decay of the dithionite absorbance at 314 nm. The Soret band of wild type Pa BfrB gradually shifted from oxidized (418 nm) position to the fully reduced state (425 nm), showing the consumption of electrons by the heme group of Pa BfrB. These observations indicate that electrons provided by the dithionite is transferred though the heme group of Pa BfrB and since there are no significant amount of iron in the BfrB core, a higher accumulation of reduced heme are observed.

A similar experiment was carried out using mineralized, wild type Pa BfrB under the same experimental conditions. To this end, the non mineralized (as isolated) Pa BfrB was reconstituted with iron (Figure 2-5 in Chapter 2 and [14]) in order to form a mineral core of ~ 600 iron atoms. The decay of the dithionite absorbance at 314 nm and the shift of the Soret band of mineralized wild type BfrB were monitored. Contrary to the observations of non mineralized, wild type Pa BfrB, the dithionite absorbance at 314 nm decayed relatively fast and the Soret band shifted towards the reduced state very slowly (Figure 4-11B). Unlike in non mineralized BfrB, the Soret band of the mineralized protein did not shift to the fully reduced state; is stayed at ~419 nm.

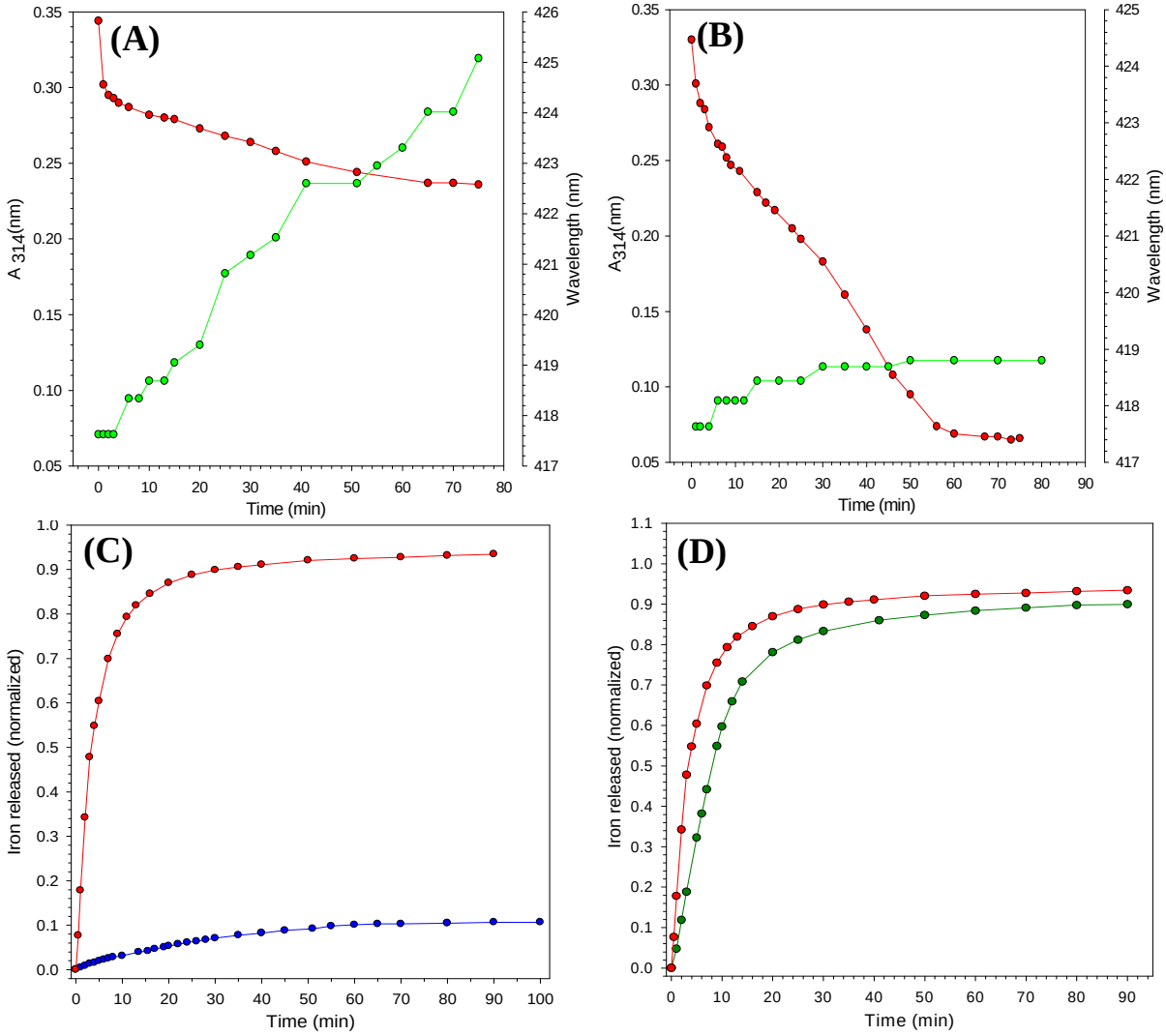

Figure 4-11: The reduction of the core of (A) non mineralized and (B) mineralized wild type Pa BfrB by dithionite. Decay of the absorbance of dithionite at 314 nm is shown by the red trace and the shift of the Soret band is shown by the green trace. (C) The amount of iron released from mineralized, wild type Pa BfrB, in the presence (red) and in the absence of Pa Bfd. (blue). (D) The amount of iron released from mineralized, wild type Pa BfrB, in the presence of Pa Bfd with sodium dithionite (red) and NADPH/Pa Fpr (green) as the reducing agent (molar ratio of Bfd/BfrB is 40).

These observations clearly indicate that the electrons provided by the dithionite are transferred to the large ferric ion mineral core of mineralized wild type Pa BfrB; consequently, only a slight accumulation of the reduced heme is observed. The observations obtained from both experiments suggest that the mineral core of Pa BfrB can be reduced by the electrons provided by dithionite, transferred into the core via the heme groups.

Another set of experiments were carried out to investigate the effect of Pa Bfd on the opening of the pores of Pa BfB. Excess sodium dithionite was added to wild type, mineralized BfrB in the presence of the Fe^{2+} chelating agent ferrozine, and the release of iron from the Pa BfrB core was monitored by following the absorbance of the Fe-ferrozine complex at 562 nm. In the absence of Pa Bfd, wild type Pa BfrB released less than 10% of iron (Figure 4-11C (blue)), suggesting that although the mineral core is reduced by dithionite, the reduced Fe^{2+} ions are trapped inside the core (red). However, in the presence of Pa Bfd, a significantly large amount of iron (~95%) is released from the core, indicating that Pa Bfd plays an important role in opening the pores of Pa BfrB. Another experiment was carried out with mineralized, wild type Pa BfrB, using NADPH and Pa Fpr as the reducing agent instead of dithionite. Interestingly, the rate of the iron released was faster with dithionite as the reducing agent than that of with NADPH/Pa Fpr as the reducing agent (Figure 4-11D). The faster rates of iron released observed with dithionite may be due to the fact that the smaller reducing agents such as sodium dithionite can access the core iron by moving directly into the core through the pores of BfrB, may be using a similar trajectory taken by the reduced iron ions.

Experiments similar to those depicted in Figure 4-11A and B were carried out with truncated Pa BfrB and the same results were obtained indicating that the mutation performed in the 4-fold pore of the truncated Pa BfrB did not affect the processes of electron transfer into the core or the reduction of the mineral core by the external reducing agents (Figure 4-12 A and B). Similar to the experiment carried out with wild type Pa BfrB shown in figure 4-11C, sodium dithionite was added to mineralized truncated Pa BfrB in the presence of chelating agent, ferrozine. As a result, ~ 30% of core iron was released from the truncated Pa BfrB, showing that the pores of truncated Pa BfrB, which are thought to be involved in the release of iron form the mineral core, has less control over the release of iron than that of wild type Pa BfrB (Figure 4-12C). Relatively higher amounts of iron released, observed in the truncated Pa BfrB with structurally altered 4-fold pores (without the inner most two Asp residues), may be an important evidence to show that the reduced iron is released through the 4-fold pores of Pa BfrB. In the presence of Pa Bfd, however, the rate of iron release was significantly high such that ~ 80% of core iron was released within ~5 minutes (Figure 4-12C). These observations indeed show that Pa Bfd facilitates the opening of the pores of Pa BfrB to release core iron. In addition, the higher rates of iron release observed in truncated Pa BfrB than that of with wild type Pa BfrB (in the presence of Pa Bfd) indicate the less resistance shown by the mutated 4-fold pores of truncated BfrB towards the process of iron release from the mineral core which can be considered as indirect evidence to support the idea of iron release through the 4-fold pores of Pa BfrB. Similar to wild type Pa BfrB, truncated Pa BfrB also showed higher rates of iron release with dithionite as the reducing agent than that of with NADPH/ Pa Fpr. However, the rates of iron release of truncated BfrB were observed to be faster than those with wild type Pa BfrB, suggesting that the altered 4-fold pores can release more iron than those of wild type BfrB.

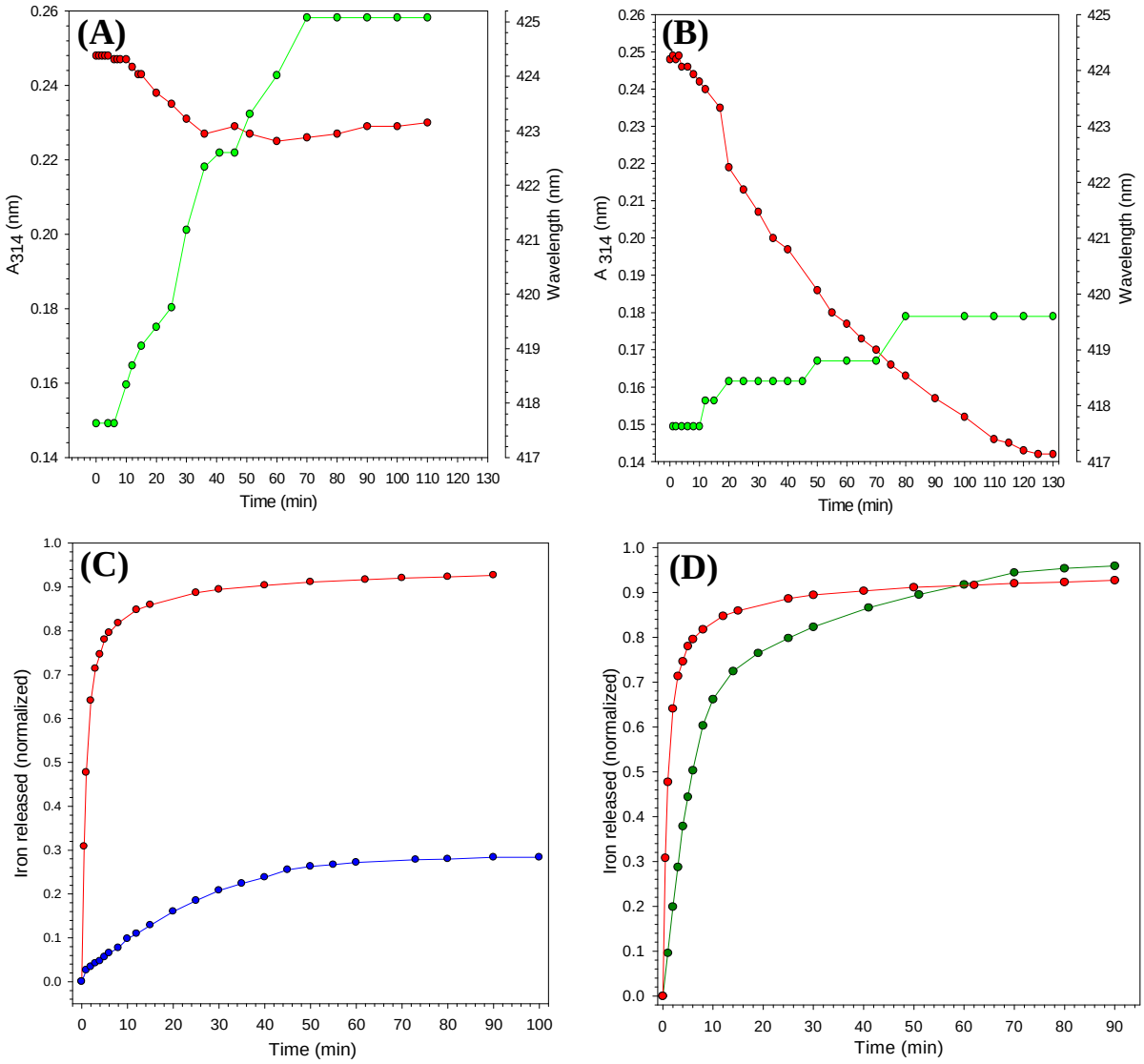

Figure 4-12: The reduction of the core of (A) non mineralized and (B) mineralized truncated Pa BfrB by dithionite. Decay of the absorbance of dithionite at 314 nm is shown by the red trace and the shift of the Soret band is shown by the green trace. (C) The amount of iron released from mineralized, truncated BfrB in the presence (red) and in the absence of Pa Bfd. (blue). (D) The amount of iron released from mineralized, truncated BfrB in the presence of Pa Bfd with sodium dithionite (red) and NADPH/Pa Fpr (green) as the reducing agent.(molar ratio of Bfd/BfrB is 40).

Discussion

According to the crystal structure of wild type Pa BfrB, six 4-fold pores are symmetrically distributed on the Pa BfrB molecule, each located along 4-fold symmetry axis of the molecule [16]. Four individual subunits interact to form one 4-fold pore. As shown in figure 4-1A, the outer part of these pores are composed of an outer layer of Asn148 residues and an inner layer of Gln151 residues. The interior of the pore is made of the C-terminus of each sub unit, (Asp157 and Asp158 from each subunit) which are also thought to be the inner most end of the pore (Figure 4-1B). However, these Asp residues are not visible in the crystal structure of BfrB, as their spatial arrangement is disordered [16]. In addition, there are two His residues (His153 and His 155) from each subunit located adjacent to the aspartates, which are believed to be functioning as gates in releasing iron through these pores.

Truncated BfrB with an altered 4-fold pore.

In the mutation we performed, Asp 157 and Asp 158 have been removed and in the resultant truncated protein the C-terminus ends at Glu156. Therefore, the 4-fold pores of the truncated protein are considered to be shorter in length than those of the wild type protein. When the structures of wild type and truncated Pa BfrB are considered, the only structural difference observed so far is the absence of two Asp residues (Asp 157 and 158) at the C-terminus of the truncated Pa BfrB. However, detailed structural studies of this protein are expected to be carried out in the future by X-ray crystallography. Similar to wild type Pa BfrB, it has been experimentally proved that truncated Pa BfrB is properly folded as a 24 mer with a full complement of 12 hemes per protein, indicating that the mutation performed did not affect the folding of the protein. In addition, with the aim of investigating the fact that whether the

ferroxidase center of truncated Pa BfrB was functioning similar to that of wild type Pa BfrB, an iron uptake experiment was carried out under the same experimental conditions as wild type Pa BfrB. Our previous findings of wild type BfrB showed a gated mechanism of iron uptake via the ferroxidase center (Chapter 2 and [16]). The experiment carried out with truncated Pa BfrB showed the same results (Figure 4-7) as wild type, where, upon addition of Fe^{2+} ions to a solution of truncated Pa BfrB a rapid increase ($\Delta A=0.07$) of the absorbance at ~320 nm was observed and then remained constant until the next aliquot of iron was added. Upon addition of the second and third aliquots of iron, relatively similar amounts of rapid increase ($\Delta A=0.05$ and 0.06) at 320 nm were observed indicating that the ferroxidase center of truncated Pa BfrB also has the gated mechanism of iorn uptake similar to wild type Pa BfrB. These observations show that the mutation performed at the 4-fold pore of the truncated Pa BfrB has not affected the iron uptake process. Since the truncated Pa BfrB shows the same mechanism of iron uptake as wild type Pa BfrB, it is believed that the changes observed in the process of iron release in truncated Pa BfrB may be due to its structurally altered 4-fold pores.

Truncated BfrB releases iron at a faster rate than wild type BfrB.

According to the results summarized in figures 4-8 and 4-9, significantly higher rates of iron release were observed in the truncated Pa BfrB than that of wild type Pa BfrB, suggesting that by removing the Asp residues from the C-terminus of the protein, which make the inner entrance of the 4-fold pore, the process of iron release has been significantly affected. Although, higher rates of iron release were observed with truncated Pa BfrB with a mutated 4-fold pore, it is somewhat difficult to conclude that the iron ions are released only through the 4-fold pores as there is a possibility that this mutation may have caused structural changes to the other pores of

the protein which have not been identified yet. Therefore, in order to support the idea that iron ions are released through the 4-fold pores of Pa BfrB, a careful and detailed analysis of its structural and kinetic observations were carried out.

According to the figure 4-9 and table 4-1, when the ratio of Bfd/BfrB is lower than 5, the rates of iron release from both wild type and truncated Pa BfrB are relatively similar. This observation may suggest that the rate of electron transfer from the reductase to the inner core via heme and/or the rate of iron release from the protein are relatively similar in both wild type and truncated Pa BfrB. However, the higher rates of iron release of truncated Pa BfrB, observed at higher ratios of Bfd/BfrB (>12), indicates that either the rate of electron transfer into the mineral core of truncated Pa BfrB or the rate of iron release from the core of truncated Pa BfrB has been increased by the mutation at the 4-fold pore. However, if the electron transfer in truncated Pa BfrB has been increased by the mutation, the rate of iron release would have been increased in all the experiments including the lower concentrations of Pa Bfd. Consequently, it can be strongly suggest that only the rate of iron release from the truncated Pa BfrB has been increased by the mutation and it also signifies the importance of 4-fold pore in the process of iron release from Pa BfrB.

Pa Bfd opens the 4-fold pore of Pa BfrB.

According to the results of the experiment shown in figure 4-11 B and 4-12B, it is known that the mineral core of Pa BfrB can be reduced by reducing agents. However, as figures 4-11C and 4-12C show, although the iron core is reduced, in the absence of Pa Bfd Fe^{2+} ions are not released from the core. Our previous studies have shown that the electrons from the reducing agent are first sent to the heme group [14] and subsequently these electrons are passed to the

mineral core to reduce the ferric ions. It is also known that when iron ions are released from the core, the heme groups of BfrB are also reduced, showing that electrons are passed into the core through the heme groups (Figure 4-10).

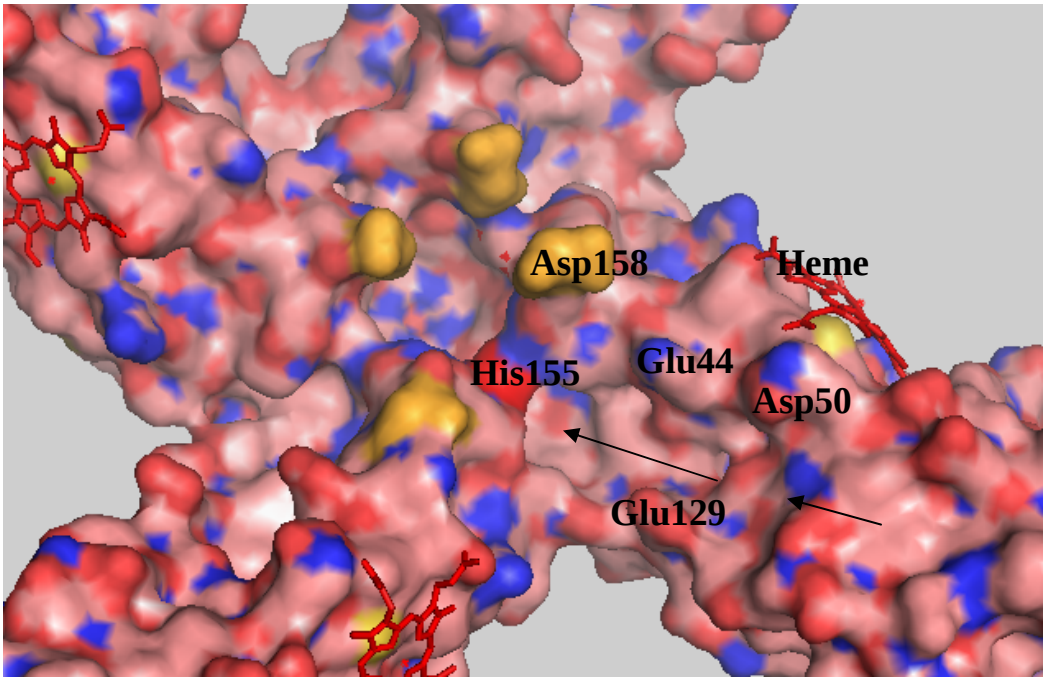

Figure 4-13: Surface representation of the 4-fold pore showing the Asp 158 residues (colored in bright orange) of the 4-fold pore of wild type Pa BfrB. His 155 which is thought to be functioning as the gates of the 4-fold pores is shown in red. The probable pathway of reduced iron ions moving towards the gate of the 4-fold pore is shown in black arrows.

As figure 4-13 depicts, it is believed that the ferric ions in the mineral, which are closer to the protein surface, are immediately reduced by the reduced heme groups of the protein and those reduced iron ions may be immediately captured by the negatively charged amino acid side chains such as Glu 18, Glu47, Asp50 and Glu 129 located closer to the heme group. A nicely arranged network of negatively charged residues can be seen in the protein molecule

making a pathway from heme towards the four fold pore. As a result of this network of negatively charged residues, reduced iron ions are thought to be moving towards the 4-fold pore, possibly along the trajectory shown by the black arrows in figure 4-13. Once these reduced iron ions reach the 4- fold pore, these iron ions are assumed to be captured by the side chain of His155 and His153 (Figure 4-1A and 4-13), which are beleived to be functioning as gates to release iron ions through the 4-fold pores. There are experimental evidence to show that these coordinating His155 and 153 residues are mobile and function as 'gates' to open the four fold pores: (1) the Fe soaked crystal structure of wild type Pa BfrB revealed that each of the 4- fold pores of Pa BfrB is surrounded by four iron atoms coordinated by His153 and 155 [16](2). When the Fe soaked crystals are reduced by dithionite, some of the reduced iron ions have been observed to be captured by the His 155 and 153 (3). Elastic Network Model (ENM) studies have also shown that His 155 and 153 around the four fold pores are highly mobile, particularly the His 155, suggesting that His 155 may be the residue that functions as a gate to open the 4-fold pores for the iron release. As shown in figure 4-13, the inner most end of the four fold pore of wild type Pa BfrB, made of Asp157 and 158, is considered 'closed' as these Asp residues are projected toward the interior of the molecule making the inner entrance of the pore narrower and less accessible to reduced iron ions from the core. Therefore, it is believed that the Fe^{2+} ions cannot directly go through this entrance of the pore. In order to enter the 4-fold pores, these ions may have to move via the network of negatively charged residues and subsequently through the gate of the His155. Our previous findings show that binding of Pa Bfd to Pa BfrB [14] facilitate the release of iron from the mineral core of BfrB. In addition, experiments shown in figures 4-8, 4-11C and 4-12C indicate that the rates of iron release are significantly accelerated in the

presence of Pa Bfd. However, the mechanism by which the Pa Bfd facilitates the higher rates of iron release from BfrB had been a mystery.

The results of our kinetic and ENM studies presented in this text provide the first evidence for the most probable mechanism of Pa Bfd facilitated iron release from Pa BfrB core. As mentioned before, the 4-fold pore of wild type Pa BfrB is considered as 'closed' with the Asp residues at the C-terminus of the protein. According to our preliminary studies, it is known that Bfd binds to the outer surface of Pa BfrB closer to the 4-fold pore. Therefore, it is believed that due to the protein-protein interaction between Pa Bfd and BfrB, the amplitudes of the motions of Asp (157, 158) and His (155, 153) residues are significantly enhanced. As a result of these increased motions, it is thought that the histidine gates are opened and the coordinated iron by these His residues are released to the 4-fold pores. However, in the absence of Pa Bfd, the motions of the Asp and His residues are slower, such that the 4-fold pores remains 'closed' by the His gates and as a result iron ions are not released out of the protein. These results are in good agreement with the results of our solution experiments showing that binding of Pa Bfd to Pa BfrB is essential to open the 4-fold pores of BfrB to release iron from the mineral core.

However, in the truncated Pa BfrB (without Asp157 and 158 residues at the end of the 4-fold pore) the 4-fold pores are considered 'open' and have less control over the motions of His 155 and 153. As a result, reduced iron ions can enter the 4-fold pore directly through the opening made due to the absence of Asp residues as well as by the freely fluctuating His gates. In addition it has been shown by the ENM studies His 155 and153 of the truncated BfrB has more motions than those of wild type BfrB, suggesting that more iron ions can be efficiently

moved by the Histidines towards the 4-fold pores. Therefore, faster rates of iron release can be observed from the truncated Pa BfrB than that of from the wild type Pa BfrB.

Elastic Network Model calculations further support the idea of iron release through the 4-fold pores.

To support the experimental evidence favoring the idea that iron is released from 4-fold pores of BfrB, Elastic Network Model (ENM) calculations on truncated and wild type BfrB were carried out by Dr. A. Ruvinsky (Department of Bioinformatics, University of Kansas).

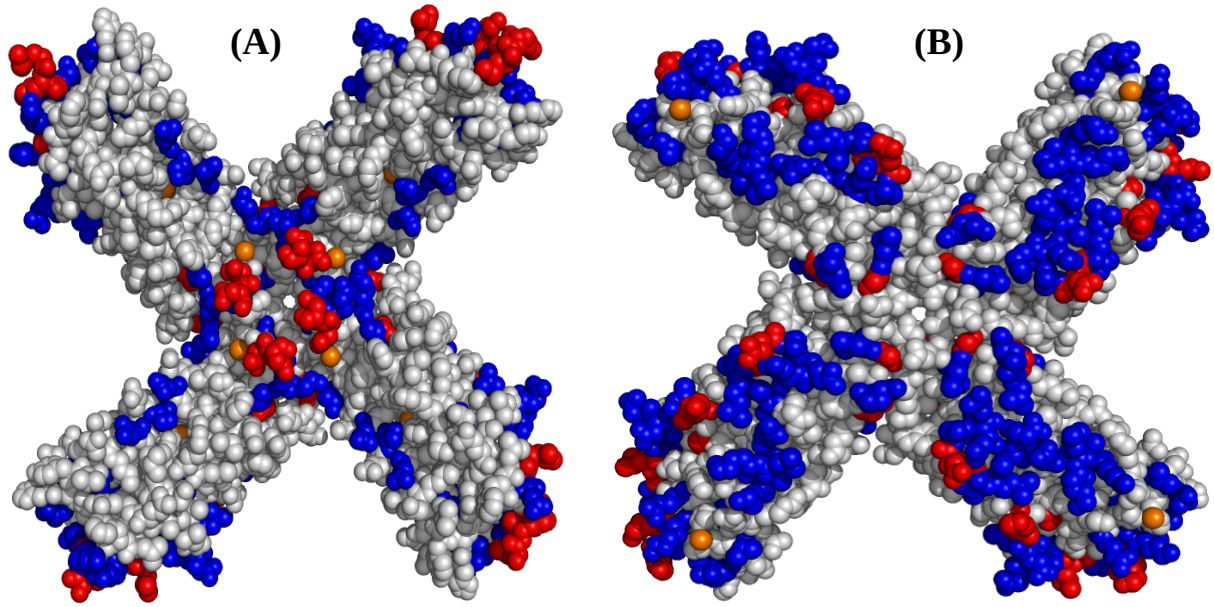

Figure 4-14: Distribution of the amino acid residue fluctuations in the 4-fold pore calculated by Elastic Network Model are shown in different colors. Highly fluctuating residues are shown in red and less fluctuating residues are shown in blue. (A) Enhanced fluctuations of the residues can be seen in the inner side of the four-fold pore including Asp157 and 158 residues (iron atoms are shown as gold spheres). (B) Relatively low or no fluctuations are seen in the outer side of the 4-fold pore.

The structure of the 4-fold pore of BfrB with Asp residues at the C-terminus was modeled by the ENM calculations and used to gain a clear insight for the elucidation of the mechanism of iron release through these 4-fold pores of Pa BfrB. In addition, ENM calculations carried out on wild type Pa BfrB have revealed that equilibrium fluctuations higher than the average fluctuations in Pa BfrB are mainly associated around the 4-fold pores, particularly with the terminal residues including Asp157 and 158 (Figure 4-14). Moreover, the ENM studies have shown that His 155 has more motions in the energy minimized structures of Pa BfrB, suggesting that His 155 may play an important role in the release of iron from Pa BfrB. To corroborate the observation of higher rates of iron release from truncated Pa BfrB than the wild type Pa BfrB, ENM studies have shown that the motions of histidiens are increased in the truncated Pa BfrB. Further, these observations suggest that the motions of His residues may be controlled by the Asp residues.

The results from our solution experiments and ENM studies show that the reactive and potentially toxic Fe^{2+} ions are released from the mineral core of BfrB, only when BfrB interact with its physiological partner Pa Bfd. i.e. the nature has evolved a well controlled mechanism of iron release in order to protect the cells from harmful effects of reactive Fe^{2+} ions. However, further studies are expected to be carried out to gain a further understanding of the mechanism of iron release from Pa BfrB.

Appendices

Appendix I: **The alignment of the sequences of Bacerioferritin genes which are located downstream to Bfd gene in the bacterial genome. Acidic residues at the C-terminus of Bfr are highlighted in red. The sequences were aligned with the aid of ClustalW.**

```
                                        10        20        30        40        50        60
                                         |         |         |         |         |         |
P.a BfrB                          MKGDKKVIQHLNKILGNELIAINQYFLHSRMWNDWGLKRLGAHEYHESIDEMKHADKLIE
Vibrio.furnissiiCIP102972         MKGDPIIIQHLNKILGNELIAINQYFLHARMYKDWGLKHLADKEYHESIDEMKHADHLIE
Aeromonas.salmonicidaA449         MKGDPKIIAHLNKVLANELIAINQYFLHARIYDDWGLKALGHKEYHESIDEMKHADELVK
P.fluorescens SBW25               MKGDISVIQQLNKILANELVAINQYFLHARMYDDWGLEKLGKREYKESIKAMKDADALIK
Sal.ente.sero.Ty. CT18            MKGDVKIINYLNKLLGNELVAINQYFLHARMFKNWGLTRLNDVEYHESIDEMKHADKYIE
Sal.ente.sero.Para. AKU12601      MKGDVKIINYLNKLLGNELVAINQYFLHARMFKNWGLTRLNDVEYHESIDEMKHADKYIE
Vib.parahaemoy.RIMD2210633        MKGDPIIIQHLNKVLGNELIAINQYFLHARMYKDWGLKHLADKEYHESIDEMKHADHLIR
Vib.chole.O1biovarElTorN16961     MKGDPVIIQHLNKVLANELIAINQYFLHARMYKDWGLKHLADKEYHESIDEMKHADHIVE
Vibrio cholerae MAK 757           MKGDPVIIQHLNKVLANELIAINQYFLHARMYKDWGLKHLADKEYHESIDEMKHADHIVE
Vibrio cholerae MJ-1236           MKGDPVIIQHLNKVLANELIAINQYFLHARMYKDWGLKHLADKEYHESIDEMKHADHIVE
Vibrio cholerae MO10              MKGDPVIIQHLNKVLANELIAINQYFLHARMYKDWGLKHLADKEYHESIDEMKHADHIVE
Enterobacter.Cloac.ATCC 13047     MKGDVKIISYLNKLLGNELVAINQYFLHARMFKNWGLMRLNDVEYHESIDEMKHADKYIE
Citrobacter koseriATCC BAA895     MKGDVKIINYLNKLLGNELVAINQYFLHARMFKNWGLTRLNDVEYHESIDEMKHADKYIE
Citrobacter rodentium ICC168      MKGDVKIINYLNKLLGNELVAINQYFLHARMFKNWGLKRLNDVEYHESIDEMKHADKYIE
Yer.pestis biovar Micro.91001     MKGDKKIIAHLNKLLGNELVAINQYFLHARMFKNWGLMRLNDKEYHESIDEMKHADKYIE
Yer.pseudotuberculosisIP32953     MKGDKKIIAHLNKLLGNELVAINQYFLHARMFKNWGLMRLNDKEYHESIDEMKHADKYIE
Pecto.carot.brasil. PBR1692       MKGDKKVITHLNKLLGNELVAINQYFLHARMFKNWGLTRLNDHEYHESIDEMKHADRYIE
Yersinia ruckeri ATCC 29473       MKGDKKIISHLNKLLGNELVAINQYFLHARMFKNWGLMRLNDKEYHESIDEMKHADRYIE
Pecto. atrosepticum SCRI1043      MKGDKKVITHLNKLLGNELVAINQYFLHARMFKNWGLTRLNDHEYHESIDEMKHADRYIE
Photorha.lumin.laumondii TTO1     MKGDKKMIAHLNKLLGNELVAINQYFLHARMFKNWGLTRLNDKEYHESIDEMKHADRYIE
Photorhabdus asymbiotica          MKGDKKIIAYLNKLLGNELVAINQYFLHARMFKNWGLTRLNEKEYHESIDEMKHADRYIE
Serratia odorifera 4Rx13          MKGDKKIIAHLNKLLGNELVAINQYFLHARMFKNWGLMRLNDKEYHESIDEMKHADRYIE
Proteus mirabilis HI4320          MKGDKKMIAHLNKLLGGELVAINQYFLHARMFKNWGFTRLNAMEYHESIDEMKHADKYIE
P.alteromonas haloplan.TAC125     MKGDKDVIAALNKVLANELVGINQYFLHARMFKDFGFSKLDKADYKVSIQKMKNADRLIE
Photobacterium profundum SS9      MKADPKIIQHLNKILGNELVAINQYFLHARMYKDWGLKHLADKEYHESIDEMKHADHLIE

                                        70        80        90       100       110       120
                                         |         |         |         |         |         |
P.a BfrB                          RILFLEGLPNLQDLGKLLIGENTQEMLQCDLNLELKATKDLREAIVHCEQVHDYVSRDLL
Vibrio.furnissiiCIP102972         RILFLEGLPNLQDLGKLMIGEDTKEMLECDLKLELAAIPDLRDAIAYAEDIRDYVSRDLF
Aeromonas.salmonicidaA449         RVLFLEGLPNLQDLGKLRIGETVEEMLRCDLSLEMDAIPDLKVAIAYAESVQDYISRDLF
P.fluorescens SBW25               RILFLEGLPNVQDLGKLNIGEHTQEMISSDLGFERKSHSDLKAAIAHCETKGDFGSRELL
Sal.ente.sero.Ty. CT18            RILFLEGIPNLQDLGKLGIGEDVEEMLRSDLRLELEGAKDLREAIAYADNVHDYVSRDMM
Sal.ente.sero.Para. AKU12601      RILFLEGIPNLQDLGKLGIGEDVEEMLRSDLRLELEGAKDLREAIAYADSVHDYVSRDMM
Vib.parahaemoy.RIMD2210633        -ILFLEGLPNLQDLGKLMIGEDTKEMLECDLKLEMAAIPDLKDAIAYAEDIRDYVSRDLF
Vib.chole.O1biovarElTorN16961     RILFLEGIPNLQDLGKLMIGEDVQEMLECDLKLELIAIPDLKEAIAYAEKVRDYVSRDLF
Vibrio cholerae MAK 757           RILFLEGIPNLQDLGKLMIGEDVQEMLECDLKLELIAIPDLKEAIAYAEKVRDYVSRDLF
Vibrio cholerae MJ-1236           RILFLEGIPNLQDLGKLMIGEDVQEMLECDLKLELIAIPDLKEAIAYAEKVRDYVSRDLF
Vibrio cholerae MO10              RILFLEGIPNLQDLGKLMIGEDVQEMLECDLKLELIAIPDLKEAIAYAEKVRDYVSRDLF
Enterobacter.Cloac.ATCC 13047     RILFLEGIPNLQDLGKLGIGEDVEEMLRSDLRLELEGAKDLREAIAYADSVHDYVSRDMM
Citrobacter koseriATCC BAA895     RILFLEGIPNLQDLGKLGIGEDVEEMLQSDLRLELEGAKDLREAIAYADSVHDYVSRDMM
Citrobacter rodentium ICC168      RILFLEGIPNLQDLGKLGIGEDVEEMLRSDLRLELEGAKDLREAIAYADSVHDYVSRDMM
Yer.pestis biovar Micro.91001     RILFLEGIPNLQELGKLNIGEDVEEMLKSDLALELSGATDLREGIAYADSIHDYVSRDLL
Yer.pseudotuberculosisIP32953     RILFLEGIPNLQELGKLNIGEDVEEMLKSDLALELSGAIDLREGIAYADSIHDYVSRDLL
Pecto.carot.brasil. PBR1692       RILFLEGIPNLQDLGKLNIGEDVEEILRSDLQLELDGAKNLREAIAYADSVHDYVSRDLM
Yersinia ruckeri ATCC 29473       RILFLEGIPNLQDLGKINIGEDVEEMLKSDLALELSGAKDLREGIAYADSIHDYVSRDLL
Pecto. atrosepticum SCRI1043      RILFLEGIPNLQDLGKLNIGEDVEEVLRSDLQLELDGAKNLREAIAYSDSVHDYVSRDLM
Photorha.lumin.laumondii TTO1     RILFLEGIPNLQDLGKLNIGEDIEEMLKSDLQLELQGAKDLKEAIAYADSIHDYVSRDLM
Photorhabdus asymbiotica          RILFLEGVPNLQDLGKLNIGEDIEEMLTSDLHLELQGAHDLREAIAYADSIHDYVSRDLM
Serratia odorifera 4Rx13          RILFLEGLPNLQDLGKLNIGEDIEEMLRSDLALELDGAKNLREAIAYADSIHDYVSRDLM
Proteus mirabilis HI4320          RILFLEGIPNLQDLGKLNIGEDVEEMLRSDLELELGGAKDLREAIAYADSIHDYVSRDLM
P.alteromonas haloplan.TAC125     RILFLEGLPNLQDLGRLRIGENSEEMIAANMSFELDTIDELRSAVKLAESKKDYITREAL
```

```
Photobacterium profundum SS9 RILFLEGLPNLQDLGKLNIGEDTQEMIESDLALEMAAIPDLRDAIAYSEEIRDYVSRDLF

                                                        130       140       150
                                                         |         |         |
```

```
P.a BfrB                                KDILESEEEHIDYLETQLGLIQKVGLENYLQSHMHEDD-
Vibrio.furnissiiCIP102972               QDILEDEEEHVDWLETQLGLIDMTGIENYLQAQFVDED-
Aeromonas.salmonicidaA449               QDILEDEEEHVDWLETQLDLIDRIGLENYQQSQLHHGSS
P.fluorescens SBW25                     EDILEDQEEHIDWLETQLGLIDKVSLENYLQSQMGE---
Sal.ente.sero.Ty. CT18                  IEILADEEGHIDWLETELDLIAKLGMQNYLQSQIKVTD-
Sal.ente.sero.Para. AKU12601            IEILADEEGHIDWLETELDLIAKLGMQNYLQSQIKVTD-
Vib.parahaemoy.RIMD2210633              QDILEDEEEHVDWLETQLGLIEMSGIENYLQAQYVDEE-
Vib.chole.O1biovarElTorN16961           QEILEDEEEHVDWLETQLGLIDMTGIQNYLQAQFVDDE-
Vibrio cholerae MAK 757                 QEILEDEEEHVDWLETQLGLIDMTGIQNYLQAQFVDDE-
Vibrio cholerae MJ-1236                 QEILEDEEEHVDWLETQLGLIDMTGIQNYLQAQFVDDE-
Vibrio cholerae MO10                    QEILEDEEEHVDWLETQLGLIDMTGIQNYLQAQFVDDE-
Enterobacter.Cloac.ATCC 13047           IQILADEEGHIDWLETELDLIGKIGLQNYLQSQIKVED-
Citrobacter koseriATCC BAA895           IEILTDEEGHIDWLETELDLIAKIGLQNYLQSQIKVDD-
Citrobacter rodentium ICC168            IEILADEEGHIDWLETELELINKMGIQNYLQAQIREEK-
Yer.pestis biovar Micro.91001           KEILVDEEEHIDWLETELSLIDRLGIQSYSQAQLAKD--
Yer.pseudotuberculosisIP32953           KKILVDEEEHIDWLETELSLIDRLGIQSYSQAQLAKD--
Pecto.carot.brasil. PBR1692             IEILADEEGHIDWLETELDLISRLGIQNYLQAQLKAE--
Yersinia ruckeri ATCC 29473             KSVLTEEEEHIDWLETELSLIERLGIQNYSQAQLAKE--
Pecto. atrosepticum SCRI1043            IEILADEEGHIDWLETELDLIARLGIQNYLQAQLKAE--
Photorha.lumin.laumondii TTO1           IDILDEEEKHIDWLETQFELIERMGIQNYTQSQILEGE-
Photorhabdus asymbiotica                IDILDAEEGHIDWLETQLELIERMGIQNYTQAQILEGE-
Serratia odorifera 4Rx13                IEILADEEGHIDWLETELDLIARLGIQNYAQAQVLERKD
Proteus mirabilis HI4320                LEILTDEEGHIDWIETQLELIERIGLQNYLQAQMIEE--
P.alteromonas haloplan.TAC125           DHILNEQEEQIDWLETQQLLIENTGLENYLQSQL-----
Photobacterium profundum SS9            QDILEEEEEHVDWLETQLGLIDKMGIANYNQAQIVDED-
```

References

[1] Andrews, S.C. (1998) Iron Storage in Bacteria, *Advances in Microbial Physiology 40*, 281-351.

[2] Harrison, P.M.; Arosio, P. (1996) The ferritins: molecular properties, iron storage function and cellular regulationtitle *Biochimica et Biophysica. Acta 1275*, 161-203.

[3] Abdul-Tehrani, H.; Hudson, J.A.; Chang, y.; Timms, A.R.; Hawkins, C.; Williams, J.M.; Harrison, P.M.; Guest, J.R.; Andrews, S.C. (1999) Ferritin Mutants of *Escherichia coli* are Iron Deficient and Growth Impaired, and *fur* Mutants are Iron Deficient. *Journal of Bacteriology* 181, 1415 -1428.

[4] Fu, X.P.; Deng, J.J.; Yang, H.X.; Masuda, T.; Goto, F.; Yoshihara, T.; Zhao, G.H. (2010) A novel EP-involved pathway for iron release from soya bean seed ferritin *Biochemistry 427*, 313-321.

[5] Lewin, A.; Moore. G.R.; Le Brun, N.E. (2005) Formation of Protein-Coated Iron Minerals. *Dalton Transactions* 3597-3610.

[6] Chasteen, N. D. (1998) Ferritin, Uptake, Storage and Release of Iron. *Metal Ions in Biological Sytems 35,* 479-514.

[7] Theil, E.C.; Matzapetakis, M.; Liu, X.F. (2006) Ferritins: iron/oxygen biominerals in protein nanocages. *Journal of Biological Inorganic Chemistry 11*, 803-810.

[8] Watt, R.K.; Hilton, R.J.; Graff, D.M. (2010) Oxido-Reduction is not the only Mechanism Allowing Ions to Traverse the ferritin Protein Shell. *Biochimica et Biophysica Acta 1800,* 745-759.

[9] Massover, W.H.(1993) Ultrastructure of Ferritin and Apoferritins: a Review. *Micron 24, 389-437.*

[10] Wardeska, J.G., Viglione, B.; Chasteen, N.D. (1986) Metal Iron Complexes of Apoferritin Evidence for Initial Binding in th Hydrophyllic Channels. *Journal of Biological Chemistry 261*, 6677-6683.

[11] Watt, G.D.; Jacobs, D.; Frankel, R.B.; (1988) Redox Reactivity of Bacterial and Mammalian Ferritin:Is Reductant Entry into the interior of Ferritin a Necessary step foe Iron Release? *Proceedings of National Academy of Sciences U.S.A. 85*, 7457-7461.

12] Liu, X.; Jin, W.; Theil, E.C. (2003) Opening Protein Pores with chaperons Enhances Fe Reduction and Chelation of Fe from the Ferritin Biomineral. *Proceedings of National Academy of Sciences U.S.A. 100, 3653-3658.*

[13] Theil. C.; Liu.X.S.; Tosha, T. (2008) Gated Pores in the Ferritin Protein Nanocage. *Inorganica Chimica Acta 361*, 868-874.

[14] Weeratunga, S. K.; Gee, C. E.; Lovell, S.; Zeng, Y. H.; Woodin, C. L.; Rivera, M. (2009) Binding of *Pseudomonas aeruginosa* Apobacterioferritin-Associated Ferredoxin to Bacterioferrtin B Promotes Heme Mediation of Electrons Delivery and Mobilization of Core Mineral Iron. *Biochemistry 48*, 7420-7431.

[15] Le Brun, N.E.; Andrews, S.C.; Guest, J.R.; Harrison, P.M.; Moore, G.R.; Thomson, A.J. (1995) Identification of the Ferroxidase Center of *Escherichia coli* Bacteroferritin. *Biochemistry* 257, 7672-7677.

[16] Weeratunga, S.K.; Lovell, S.; Yao,H.; Battaile, K.P.; Fischer, C.J.; Gee, C.E.; Rivera, M. (2010) Structural Studies of Bacterioferritin B from Pseudomonas aeruginosa Suggests a Gating Mechanism of Iron Uptake via the Ferreoxidase Center. *Biochemistry 49*, 1160-1175.

[17] Larkin, M. A., Blackshields, G., Brown, N. P., McGettigan, P. R., McWilliam, H., Valentin, F., Wallace, I. M., Wilm, A., Lopez, R., Thompson, J. D., Gibson, T. J., and

Higgins, D. G. (2007) Clustal W and Clustal X Version 2.0, *Bioinformatics 23*, 2947-2948.

[18] Ringeling, P.L.; Davy, S.L.; Monkara, F.A.; Hunt, C.; Dickson, D.P.E.; Mcewan, A.G.; Moore, G.R. (1994) Characterization of Bacterioferritin and Formation of Non-Haem Iron Particles in Intact Cells. *Europian Journal of Biochemistry* 223, 847-855.

Appendix II: Mutations of the four fold pores of Pa BfrB suggests a possible pathway of iron release via the four-fold pores

Introduction

The crystal structure of wild type Pa BfrB shows the presence of symmetrically distributed six 4-fold pores each located along the six 4-fold symmetry axis of the protein molecule. These pores are built mainly in two layers of acid residues. The inner layer is formed by four Gln residues whereas the outer layer is formed by four Asn residues. In the crystal structure of wild type Pa BfrB potassium ions were observed in these 4-fold pores coordinated by the side chains of four Asn and Gln residues. These potassium ions are thought to be incorporated into the protein from the protein storage buffer which is 100 mM potassium phosphate, pH 7.6. The presence of metal ions in the four fold pores has also been observed in the structures of Bfr from other organisms. For example, iron and Ba^{2+} ions have been observed in two independent crystal structures of Av Bfr [1, 2]. These observations together with the fact that 4-fold pore being hydrophilic in nature, lead us to hypothesize that iron ions may exit the protein through 4-fold pores. In order to test the above hypothesis, the structure of the four fold pore was altered by changing the amino acid composition of the pore using site directed mutagenesis. To this end, coordinating Asn148 residue found in the outer layer of the 4-fold

pore was mutated to non coordinating Leu residues. It is assumed that hydrophobic interactions between leucines may obstruct the pathway of iron and consequently the rate of iron release from N148L BfrB is expected to be lower than that of wild type Pa BfrB. In addition, Gly145 which constitutes a part of the outer wall of the four fold pore was mutated to Val and subsequently the rate of iron release of G145V Pa BfrB was compared with that of wild type.

Experimental Procedures

Site directed mutagenesis of N148L and G145V Pa BfrB

The N148L and G145V *bfrb* genes were constructed using the recombinant pET11a plasmid harboring the gene coding for wild type Pa BfrB. The primers designed for the mutation N148L BfrB had a melting temperature (Tm) of 78.4 ºC and GC content of 49%. The gene sequences of the primers used for N148L BfrB are, 5' CAG AAA GTG GGC CTG GAA CTG TAT CTG CAG AGC CAT ATG C 3', and 5' GCA TAT GGC TCT CAG ATA CAG TTC CAG GCC CAC TTT CTG 3'. The melting temperature (Tm) and the GC content of the primers designed for the G145V BfrB mutation were 81 ºC and 49%, respectively. The sequences corresponding to the forward and reverse primers of G145V BfrB are 5'-GGG TCT GAT TCA GAA AGT GGT GCT GGA AAA CTA TCT GCA GAG C-3 and '5-GCT CTG CAG ATA GTT TTC CAG CAC CAC TTT CTG AAT CAG ACC C-3'. All the primers were synthesized by Integrated DNA Technologies, Inc (Coravile, IA). Mutagenesis was carried out using the QuickChange™ mutagenesis kit (Stratagene, La Jolla, CA) and polymerase chain reaction (PCR). The recombinant constructs were then transformed into *E.coli* XL Blue supercompetent cells for DNA amplification. Once the mutation was verified by sequencing, recombinant DNA

plasmids were transformed into *E. coli* Arctic express RIL cells (Stratagene, La Jolla, CA). The sequences of the N148L and G145V BfrB genes with the restriction endonuclease sites are shown in figure 1 and 2, respectively.

5' Nde1

CATATG AAA GGC GAT AAA AAA GTG ATC CAG CAT CTG AAT AAA ATT
M K G D K K V I Q H L N K I
CTG GGT AAT GAA CTG ATT GCG ATT AAT CAG TAT TTT CTG CAT AGC CGC ATG
L G N E L I A I N Q Y F L H S R M
TGG AAT GAT TGG GGC CTG AAA CGT CTG GGC GCG CAT GAA TAT CAT GAA AGC
W N D W G L K R L G A H E Y H E S
ATT GAT GAA ATG AAA CAT GCG GAT AAA CTG ATC GAA CGT ATT CTG TTT CTG
I D E M K H A D K L I E R I L F L
GAA GGT CTG CCG AAT CTG CAG GAT CTG GGC AAA CTG CTG ATT GGT GAA AAC
E G L P N L Q D L G K L L I G E N
ACC CAG GAA ATG CTG CAG TGC GAT CTG AAT CTG GAA CTG AAA GCG ACC AAA
T Q E M L Q C D L N L E L K A T K
GAT CTG CGT GAA GCG ATC GTG CAT TGC GAA CAG GTG CAT GAT TAT GTT AGC
D L R E A I V H C E Q V H D Y V S
CGT GAT CTG CTG AAA GAT ATC CTG GAA AGC GAA GAA GAA CAT ATT GAT TAT
R D L L K D I L E S E E E H I D Y
CTG GAA ACC CAG CTG GGT CTG ATT CAG AAA GTG GGC CTG GAA **CTG** TAT CTG
L E T Q L G L I Q K V G L E **L** Y L
CAG AGC CAT ATG CAT GAA GAT GAT TAAGGATCC
Q S H M H E D D **BamH1 3'**

Figure 1: DNA and corresponding amino acid sequence of *N148L bfrB* from *P. aeruginosa*. N148L mutation is highlighted. *Nde* I and *Bam*H I restriction endonuclease sites were constructed at the 5' and 3' ends for subcloning.

Overexpression and purification of N148L and G145V BfrB.

The wild type BfrB was expressed, lysed and purified as described in detail in the experimental procedures in Chapter 2. Both N148L and Gi45V BfrB were also expressed and purified in the same way as wild type protein. The purity of the protein was determined by 15% SDS-PAGE.

5'*Nde*1

CATATG AAA GGC GAT AAA AAA GTG ATC CAG CAT CTG AAT AAA ATT
M K G D K K V I Q H L N K I
CTG GGT AAT GAA CTG ATT GCG ATT AAT CAG TAT TTT CTG CAT AGC CGC ATG
L G N E L I A I N Q Y F L H S R M
TGG AAT GAT TGG GGC CTG AAA CGT CTG GGC GCG CAT GAA TAT CAT GAA AGC
W N D W G L K R L G A H E Y H E S
ATT GAT GAA ATG AAA CAT GCG GAT AAA CTG ATC GAA CGT ATT CTG TTT CTG
I D E M K H A D K L I E R I L F L
GAA GGT CTG CCG AAT CTG CAG GAT CTG GGC AAA CTG CTG ATT GGT GAA AAC
E G L P N L Q D L G K L L I G E N
ACC CAG GAA ATG CTG CAG TGC GAT CTG AAT CTG GAA CTG AAA GCG ACC AAA
T Q E M L Q C D L N L E L K A T K
GAT CTG CGT GAA GCG ATC GTG CAT TGC GAA CAG GTG CAT GAT TAT GTT AGC
D L R E A I V H C E Q V H D Y V S
CGT GAT CTG CTG AAA GAT ATC CTG GAA AGC GAA GAA GAA CAT ATT GAT TAT
R D L L K D I L E S E E E H I D Y
CTG GAA ACC CAG CTG GGT CTG ATT CAG AAA GTG **GTG** CTG GAA AAC TAT CTG
L E T Q L G L I Q K V **V** L E N Y L
CAG AGC CAT ATG CAT GAA GAT GAT TAAGGATCC
Q S H M H E D D ***Bam*H1 3'**

Figure 2: DNA and corresponding amino acid sequence of *G145V bfrB* from *P. aeruginosa*. G145V mutation is highlighted. *Nde* I and *Bam*H I restriction endonuclease sites were constructed at the 5' and 3' ends for subcloning.

Pure protein was then passed through a previously calibrated high resolution size exclusion column (Superdex 200, 10/300, GE Healthcare) equilibrated with 100 mM potassium phosphate (pH 7.6) and 1 mM tris (2-carboxyethyl)-phosphine hydrochloride (TCEP) to determine the size and confirm the oligomerization. Once the oligomerization is confirmed as 24mers, the protein was concentrated, flash frozen and stored at -80 ºC.

Mineralizaton N148L BfrB

Similar to wild type BfrB, N148L BfrB as isolated contains a few iron ions in its inner core (10-15 iron atoms per molecule). Therefore, protein to be used in experiments was incorporated with ~ 600 iron atoms per molecule. Anaerobic solution of ferrous ammonium sulfate solution (details in Chapter 2 experimental) was added to a stirred solution of 0.0027 mM N148L BfrB in 100 mM potassium phosphate buffer, pH 7.6. The mineralization was carried out in a water bath, equilibrated at 42 ºC and the protein solution was also allowed to equilibrate at 42 ºC before starting the mineralization. Aliquots of Fe^{2+} solution delivering 48 iron atoms per protein molecule was added to a stirred solution of N148L BfrB. The resultant solution was then allowed to react for 15 minutes before the next aliquot of Fe^{2+} was added. Total of 600 Fe^{2+} ions were added and the mineralization process was monitored spectrophotomterically, with the aid of a USB 2000 spectrophotometer (Ocean Optics, Dunedin, FL). The iron loaded protein solution was incubated at 42ºC for three hours and cleaned to remove any excess iron ions using a G-25 column equilibrated using 100 mM potassium phosphate buffer, pH 7.6. The content of iron in the core was determined using the previously described methodology (experimental procedures in Chapter 2).

Mineralizaton of G145V BfrB

The same mineralization procedure used for wild type BfrB, described in the experimental procedures in Chapter 2 was followed for this mutant. Anaerobic solution of ferrous ammonium sulfate solution was added to a stirred solution of 3 μM G145V BfrB in 100 mM potassium phosphate buffer, pH 7.6 in aliquots delivering 50 Fe^{2+}/Pa BfrB, until a core of 600 Fe^{2+}/Pa BfrB is formed. Any precipitation formed during the mineralization was removed by centrifuging the sample for 10 minutes at 4000 rpm. The mineralization process was monitored spectrophotometrically following the absorbance near 320 nm with the aid of a USB 2000 spectrophotometer (Ocean Optics, Dunedin, FL).

Analysis of non-heme iron in the BfrB core.

Non-heme iron analysis of N148L and G145V BfrB were carried out using Fe-ferrozine assay in the same way as described for wild type BfrB in Chapter 2. The concentration of iron was determined from the electronic absorption spectrum using the absorbance at 562 nm (ε_{562} = 27.9 mM^{-1} cm^{-1}) [4].

Crystallization of N148L and G145V BfrB

Crystallization studies were carried out in the Protein Structure Laboratory at the Delbert M. Shankel Structural Biology Center (University of Kansas, Lawrence, KS). Mineralized N148L and G145V BfrB were concentrated to 16 mg/mL and 20 mg/ ml, respectively, in 100 mM potassium phosphate pH 7.6, 5 mM TCEP for crystallization. Crystals were grown under aerobic conditions in Compact Jr. (Emerald biosystems) sitting drop vapor diffusion plates using 1μL of crystallization solution and 1 μL of protein equilibrated against 100 μL of crystallization solution at 20^{o}C. Red prismatic crystals were obtained from both G145V

and N148L BfrB within 24 hours from the following condition 35% (v/v) 2-methyl-2,4-pentanediol, 100 mM MES pH 6.0, 200 mM Li_2SO_4 (Wizard 2 #2, Emerald biosystems).

Structure Solution and Refinement of N148L BfrB

Single crystals of N148L were transferred to a fresh drop of crystallization solution which also served as a cryoprotectant and frozen in liquid nitrogen for data collection. Data were collected at 100K at the Advanced Photon Source (APS) IMCA-CAT, sector 17ID using a Pilatus 6M pixel array detector. Data were collected at λ = 1.74013 Å which is near the Fe absorption edge.

Intensities were integrated and scaled using the XDS [5] and Scale [6] packages respectively. Structure solution was carried out by Fourier synthesis by refinement of the protein only model of apo BfrB (PDB: 3IS7 [7]) against the processed diffraction data. Structure refinement and manual model building were performed with REFMAC [8] and COOT [9] respectively. Structure validation was performed using MOLPROBITY [10].

Iron uptake in solution by G145V BfrB

G145V BfrB to be used in the experiments was prepared by extensively dialyzing the pure, as-isolated protein against 100 mM potassium phosphate, pH 7.6. Aliquots of 50 mM Ferrous ammonium sulfate containing 50 Fe^{2+}/ BfrB molecule were added using a Hamilton microsyringe to a solution of G145V BfrB (0.8 μM) at 30 °C in a 1.0 cm path length cuvette equipped with a stirring bar. Changes in the intensity of the absorbance at 320 nm were recorded for 10 minutes for each addition of iron with the aid of a conventional diode-array UV-vis spectrophotometer (Ocean Optics, Dunedin, FL).

Mobilization of core iron from G145 BfrB

Experiments to investigate the iron release from G145V BfrB were carried out in an anaerobic chamber. Several iron mobilization experiments were carried out varying the concentration of apo Bfd while maintaining the concentrations of Fpr (15 μM), Bipiridyl (3mM) and NADPH (1.5 mM) constant. Experimental conditions and the procedures were the same as those of truncated BfrB explained in experimental in Chapter 4.

Results and Discussion

Overexpression and purification of N148L and G145V BfrB

Both N148L and G145V BfrB expressed in *E.coli* Arctic express RIL cells were soluble and could be purified to homogeneity. The pure BfrB protein produced a single band in the 15% SDS-PAGE gel which corresponds to an approximate MW of 18000 Da. The oligomerization of the proteins was confirmed as a 24mer by using a calibrated size exclusion column (Superdex 200, 10/300 column, Amersham Biosciences). The electronic absorption spectra of pure N148L and G145V BfrB were similar to that of wild type BfrB and have a Soret band maximum at 418 nm and α and β bands at 567 nm and 527 nm respectively.

Mineralization of N148Land G415V BfrB

Mineralization of G145V BfrB was carried out under same experimental conditions as for wild type (experimental Chapter 2). However, a slight precipitation was observed in the solution after adding about ~ 400 iron atoms and was removed by centrifuging the protein solution for 10 minutes at 4000 rpm. Addition of iron was continued with the clear supernatant

obtained after centrifugation until an iorn core of ~600 iron ions was formed. Then the protein was cleaned to remove any excess iron atoms using the same procedure as in wild type BfrB (experimental Chapter 2).

Mineralization of N148L, on the other hand, was carried out following a slightly different procedure than that of wild type. First mineralization experiment of N148L BfrB was carried out at room temperature (25 ºC) under similar experimental conditions used in WT BfrB. Aliquots of anaerobic Fe^{2+} solution containing 48 iron atoms per molecule were added at a time with 15 minute intervals between two additions. However after adding ~ 200 iron atoms, a slight precipitation was observed in the protein solution. The solution was then centrifuged for 10 minutes at 4000 rpm to spin down the precipitation. A reddish-brown precipitate which may be colloidal iron (III) oxide formed from Fe^{2+} ions which did not oxidized and internalized by the ferroxidase center of the N148L BfrB, was observed at the bottom of the centrifuge tube. In addition, some of the protein molecules may also have precipitated together with the iron colloid as indicated by the lower intensity of the Soret band of the protein obtained after centrifugation than that of the initial spectrum. Mineralization was continued with the clear supernatant and a precipitation was formed again. After several additions of Fe^{2+} and centrifugation steps, about 600 iron ions were added to the protein and finally the protein sample was cleaned using a G-25 column equilibrated using 100 mM potassium phosphate buffer, pH 7.6 to remove excess iron ions. The content of iron was determined and only an iron core of ~ 300 Fe ions was observed. Most of the iron ions have been lost during the cleaning. Several experimental parameters were changed in order to prevent significant loss of protein while mineralization and to obtain a core of ~600 Fe ions. To this end, the pH of the solution was increased from 7.6 to 8.0 and mineralization was carried out at room temperature (25 ºC). However, similar to the previous

experiment, a significant amount of iron and the protein were precipitated and the resultant core was only about ~350 Fe atoms. In the next attempt, another sample of N148L BfrB in 100 mM potassium phosphate pH 7.6 was mineralized at a higher temperature, 37 ºC. Under these experimental conditions, protein seemed to uptake Fe^{2+} more efficiently than the sample at room temperature. A slight precipitation was observed after adding ~400 Fe^{2+} ions and more Fe^{2+} ions were added to the supernatant obtained after spinning down the precipitation to form a core of ~600 iron ions. Subsequently, the protein sample was incubated at 37ºC for two hours and cleaned in the same way as before using a pre-equilibrated G-25 column. Nevertheless, a considerable amount of protein has been lost while cleaning and only a core of ~250 iron atoms was formed. Eventhough a relatively small core was formed, uptake of iron at 37 ºC seemed faster and efficient. Therefore, another sample of N148L BfrB in 100 mM potassium phosphate pH 7.6 was mineralized at 42 ºC, by adding aliquots of Fe^{2+} solution containing a 48 Fe^{2+} ions at a time. The protein sample was incubated for ~ three hours and cleaned using a G-25 column (Pd-10, Amersham Biosciences). The content of iron in the core was determined to be ~450 Fe atoms. Since it was the best mineralized protein sample, those experimental conditions were considered as the optimized conditions for the mineralization of N148L BfrB. Subsequently several mineralization trials with different amounts of proteins were carried out under these conditions to verify the method and all the samples were mineralized well.

Crystallization of N148L BfrB and G145V BfrB

Both N148L and G145V BfrB formed red prismatic crystals from the condition, 35% (v/v) 2-methyl-2,4-pentanediol, 100 mM MES pH 6.0, 200 mM Li_2SO_4 (Wizard 2 #2, Emerald

biosystems). Crystallographic studies of only N148L BfrB are discussed in this text and the studies on G145V BfrB are expected to investigate in the future.

Few crystals of mineralized N148L BfrB were soaked in the crystallization solution containing 50 mM $FeSO_4$ (Fe soaked Pa-BfrB) for 15 minutes and both mineralized and Fe soaked crystals were used to acquire diffraction data. Crystallographic data for mineralized N148L BfrB are presented in table 1.

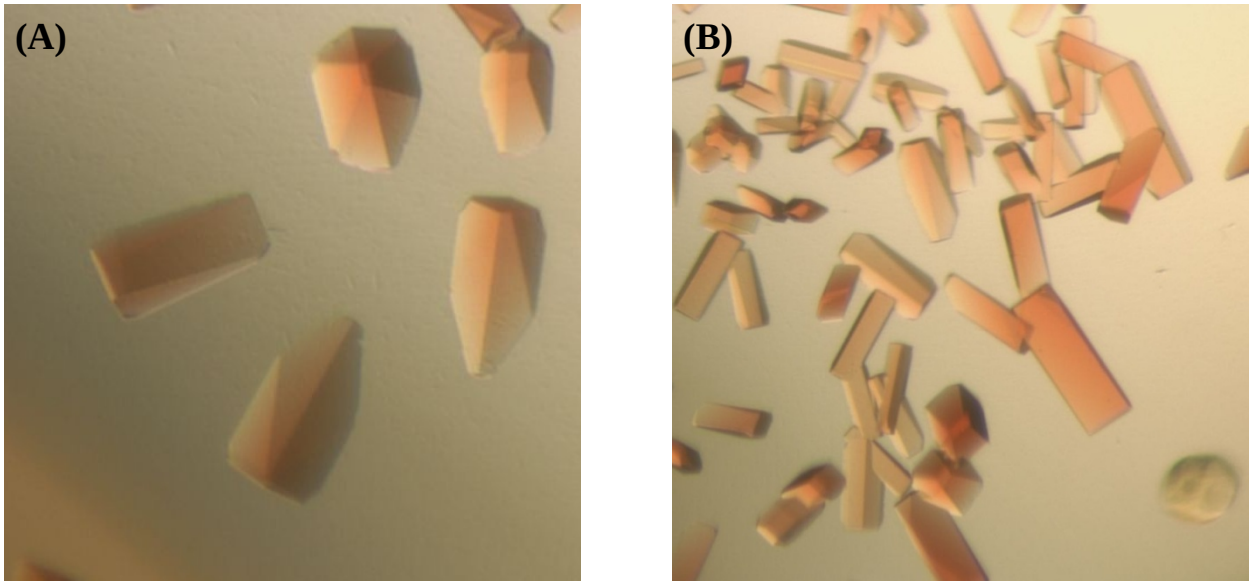

Figure 3: Red prismatic single crystals of recombinant (A) N148L and (B) G145V BfrB formed in compact Jr. sitting drop vapor diffusion plates.

Table 1. Crystallographic data for Apo BfrB N148L refined to 2.0Å resolution.

	Apo BfrB N148L
Data Collection	
Unit-cell parameters (Å, ^{o})	a=125.73, b=203.35, c=208.27
Space group	$P2_12_12_1$
Resolution (Å)	50-2.00 (2.11-2.00)
Wavelength (Å)	1.74013
Observed reflections	2,270,194
Unique reflections	356,578
$\langle I/\sigma(I)\rangle$[1]	10.7 (2.3)
Completeness (%)[1]	99.7 (98.0)
Multiplicity[1]	6.4 (5.5)
R_{merge} (%)[1, 2]	10.5 (62.6)
R_{meas} (%)[1, 4]	12.9 (78.0)
R_{pim} (%)[1, 4]	5.1 (32.5)
Refinement	
Resolution (Å)	50.00-2.00
Reflections (working/test)	338,156 / 17,941
R_{factor} / R_{free} (%)[3]	18.6 / 21.8
No. of atoms (protein / heme / sodium / water)	30,456 / 516 / 6 / 1,618
Model Quality	

R.m.s deviations	
Bond lengths (Å)	0.015
Bond angles (^{o})	1.272
Average *B* factor (Å^2)	
All Atoms	33.4
Protein	33.0
Heme	36.7
Sodium	32.5
Water	38.9
Coordinate error based on maximum likelihood (Å)	0.10
Ramachandran Plot	
Most favored (%)	99.9
Additionally allowed (%)	0.1

1) Values in parenthesis are for the highest resolution shell.
2) $R_{merge} = \Sigma_{hkl}\Sigma_i |I_i(hkl) - \langle I(hkl)\rangle| / \Sigma_{hkl}\Sigma_i I_i(hkl)$, where $I_i(hkl)$ is the intensity measured for the *i*th reflection and $\langle I(hkl)\rangle$ is the average intensity of all reflections with indices hkl.

3) $R_{factor} = \Sigma_{hkl} ||F_{obs}(hkl)| - |F_{calc}(hkl)|| / \Sigma_{hkl} |F_{obs}(hkl)|$; Rfree is calculated in an identical manner using 5% of randomly selected reflections that were not included in the refinement
4) R_{meas} = redundancy-independent (multiplicity-weighted) R_{merge}[2]. R_{pim} = precision-indicating (multiplicity-weighted) R_{merge}[8].

The ferroxidase center of N148L BfrB is different from WT BfrB

According to the crystallographic data of N148L BfrB, most of the structural features are similar to that of wild type BfrB except the structure of the feroxidase center. Eventhough the six amino acid residues that coordinate the two ferroxidase iron ions in the WT BfrB are present at the feroxidase center of N148L BfrB, their spatial arrangement is different. In WT BfrB, Glu18, His54 and Glu94, His130 act as capping ligands and Glu127 and Glu51 act as bridging ligands for two iron ions (Figure 5A). As explained in detail in chapter 2, one of the ferroxidase iron ligands, the side chain of His130, has two different conformations depending upon whether the ferroxidase center is vacant or occupied. When the ferroxidase center is empty, the side chain of His130 is rotated away from the ferroxidase center (Figure 5A) whereas when it is occupied, the side chain of His130 is properly oriented to bind the ferroxidase iron ion (Figure 5B). In order to obtain structural details of N148L BfrB, the crystals of N148L BfrB were soaked in a crystallization solution containing 50 mM ferrous sulfate and the crystals were flash frozen to obtain diffraction data. Interestingly, the conformations of the side chain of His130 in both iron soaked and non iron soaked crystal structures were the same. In addition, eventhough the conformations of the side chains of Glu18 and His54 are similar to that of WT BfrB, conformations of the side chains of all the other four residues are different from those of WT BfrB.

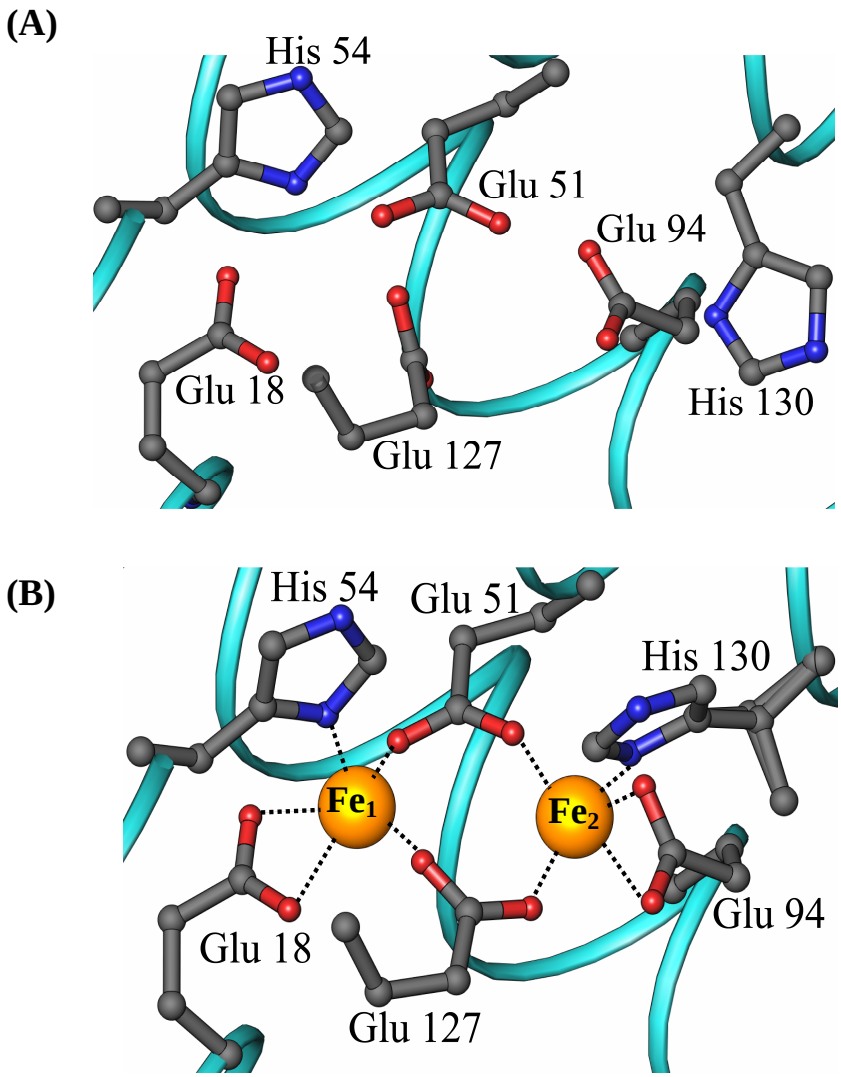

Figure 4: Structure of (A) empty ferroxidase center and (B) iron bound ferroxidase center of WT BfrB showing two different conformations of the side chains of His130.

It is apparent that the ferroxidase center of N148L BfrB is completely disorganized and the difficulties encountered in mineralizing this protein may be due to this defective ferroxidase center. In the WT BfrB, the side chain of His 130 acts as a gate to uptake iron efficiently into the ferroxidase center and as a result the protein can be mineralized easily to obtain an iron core of ~ 600 iron ions. However, in N148L BfrB, the side chain of His 130

seems locked at one conformation (gate open conformation) and consequently the side chain of His 130 either may not be operating as a gate as in wild type BfrB in uptaking iron or may be functioning as a gate but at an extremely slower rate at the room temperature. As previously explained, N148L BfrB, was difficult to mineralize at room temperature (25 ºC), but when the temperature of the protein solution was increased to 42 ºC, the protein could be mineralized without forming any precipitation. When Fe^{2+} ions are added to the protein solution, they are oxidized by two competitive reactions: one is the oxidation of Fe^{2+} ions by the ferroxidase center in the protein using oxygen as the electron acceptor and the other process is the oxidation of Fe^{2+} ions by oxygen in air which forms insoluble ferric hydroxide. The formation of insoluble ferric ion colloid can lead to a significant loss of protein as protein molecules can also electrostatically attached to the iron colloid and precipitate. In N148L BfrB, the first oxidation reaction by the protein may be extremely sluggish as side chain of His 130 is not functioning as a ligand to bind incoming Fe^{2+} ions. Consequently many Fe^{2+} ions are floating freely in the solution and eventually oxidized by air and form the insoluble ferric colloid. In contrast to that, when the temperature of the reaction medium is increased, as the thermal energy increases the motions of the residues, the side chain of His 130 may become more active and start functioning as a gate to incorporate iron into the ferroxidase center. Consequently, the oxidation of Fe^{2+} ions by the protein becomes the more dominant process than that of by oxygen in air. Therefore no precipitation is formed in the reaction medium and protein could be mineralized with ~ 600 iron ions. At the end of the mineralization, protein is passed through a G-25 column, to remove any excess iron that was not incorporated into the protein and analyzed for the iron content in the core. Eventhough ~600 iron ions were added to the protein, only a core of about ~400 iron atoms was observed. Some of the iron ions have not been mineralized inside the core and it may

be due to the abnormalities of other residues in this protein which have not been identified yet. Further refinement of the crystal structure of N148L BfrB may provide significant data to better elucidate this observation. Nevertheless, it is apparent that the mutation in the 4-fold pore (Asn148Leu) has caused significant structural changes of the amino acid residues in the other regions of the protein molecule which may have affected not only the hypothesized mechanism of iron release by the 4-fold pores but also the iron uptake mechanism by the ferroxidase pores. These observations suggest an existence of a strong communication network among the amino acid residues in this protein in which if one residue is affected, it could impair most of the other vital processes of the protein molecule. However, further detailed investigations are necessary to obtain experimental evidence to show that iron release is decelerated by changing the coordinating Asn residues to non coordinating Leu residues, suggesting that iron ions are released through 4 fold pores.

Iron uptake by G145V BfrB

As figure 6 shows, upon addition of 50 Fe^{2+} ions to G145V BfrB, a rapid increase of the absorbance near 300 nm (plotted at 320 nm) is observed and then reaches a plateau and remains constant thereafter. The magnitude of the increase of absorbance at 320 nm at every addition of an aliquot of iron was observed to be nearly constant, suggesting that the ferroxidase center of G145V BfrB is labile and functions similar to wild type BfrB. Once all the Fe^{2+} ions are oxidized at the ferroxidase center, it becomes empty.

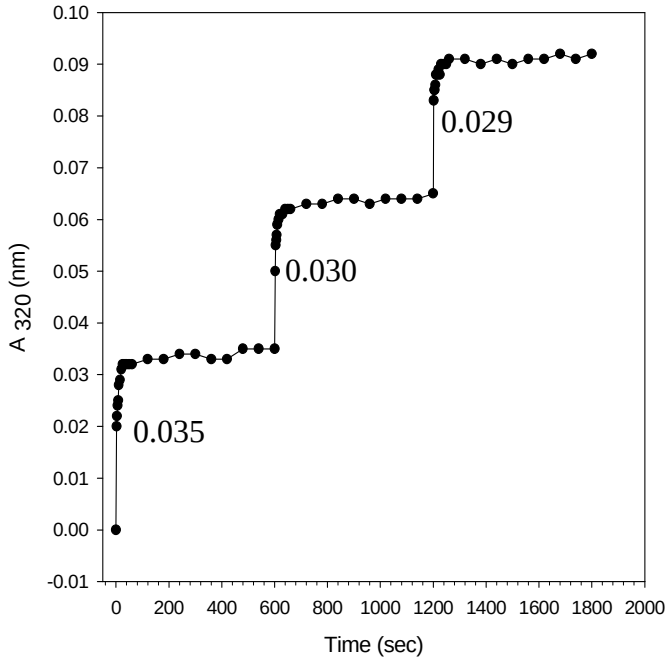

Figure 5: Change in ΔA_{320} upon subsequent additions of Fe^{2+} aliquots (50 Fe^{2+} ions per BfrB molecule) to a solution of G145V BfrB (0.8 μM) in 100 mM potassium phosphate buffer, pH 7.6.

These observations, similar to those observed in wild type BfrB (results in chapter 2) indicate that the ferroxidase center of G145V BfrB has not been affected by the mutation of G145V in the 4-fold pore region. Consequently, G145V BfrB is believed to function similar to wild type BfrB except a possible change in the rate of iron release as it is hypothesized that iron ions from the inner core is released through the 4-fold pores.

Mobilization of core iron from G145 BfrB

As shown in figure 7A the growth of the 523 nm band was monitored in each of the experiments carried out with different apo Bfd/BfrB ratios; 40:1 (red), 30:1 (yellow), 20:1 (pink), 10:1 (green), and 0:1 (black). It is clear that when the Bfd/BfrB ratio is incresed the amount of iron released gradually increases. In addition, more iron is released in G145V BfrB than that of with wild type in the absence of Bfd which may be suggesting that there is less resistance to release iron from the inner core of G145V BfrB than that of from wild type BfrB. Furthermore, similar to the observations made in the experiments with wild type BfrB, the Soret band of G145V BfrB shifts from 417 nm (oxidized) to 425 nm (reduced) only in the presence of Bfd. However, it is important to note that in the absence of Bfd, the heme groups of both G145V BfrB and wild type BfrB do not shift to the reduced state and remain at oxidized state throughout the experiment. The time dependent change of the Soret band at 417 nm of each of the above experiments has been plotted in figure 7B and it is evident that in all the experiments with different concentrations of Bfd, heme groups of G145V BfrB shift to the reduced state (425 nm) at similar rates. In comparison, in the experiments with wild type BfrB, heme groups of BfrB with different concentrations of apo Bfd, shifts to the reduced state at different rates. For example, the curve corresponding to the ratio of Bfd/BfrB is 10, the heme group of wild type BfrB takes about 40 minutes to shift to the completely reduced position whereas that of G145V BfrB takes only 20 minutes.

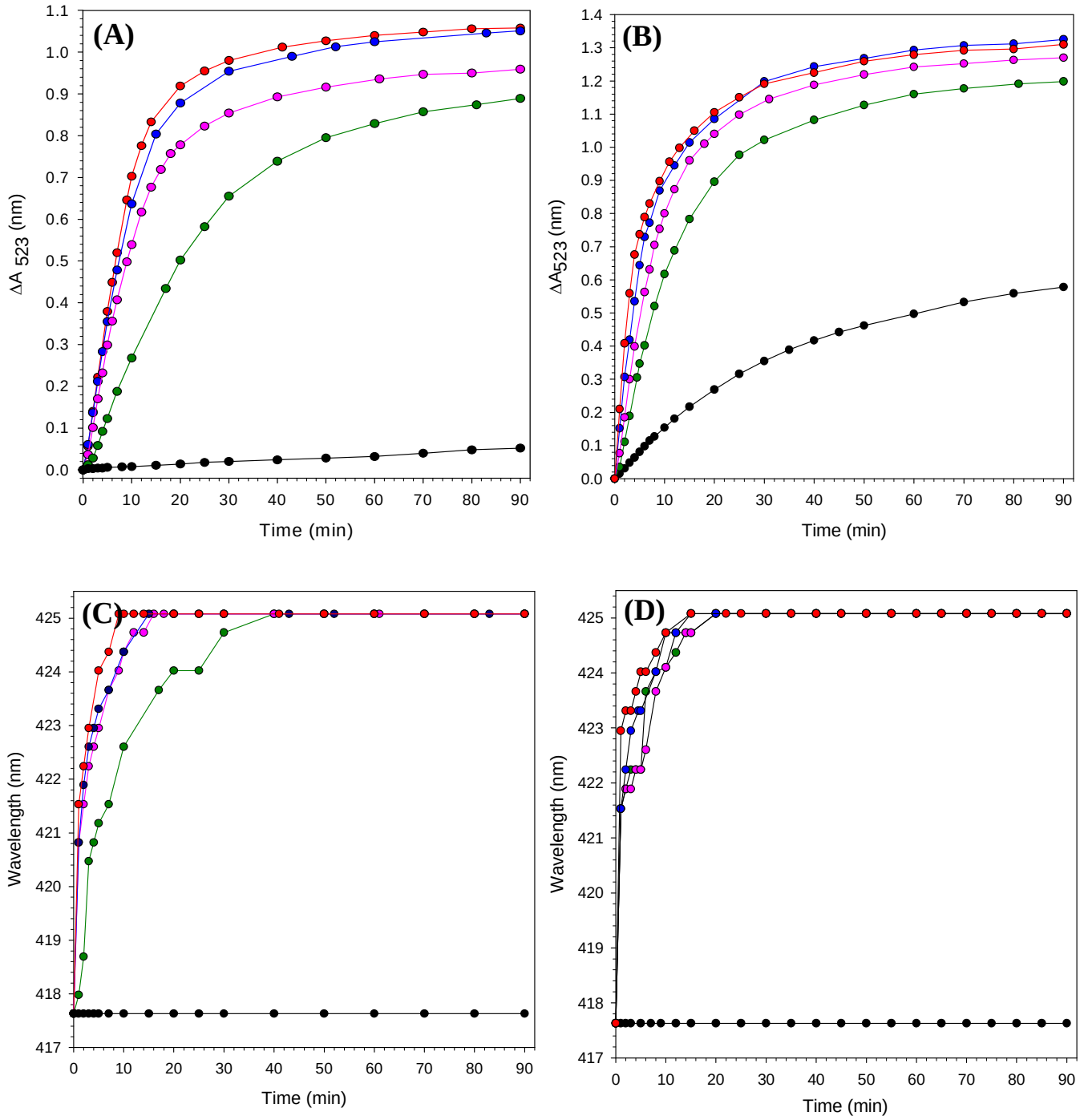

Figure 6: Time dependent plot of absorption intensity change measured at 523 nm upon addition of NADPH (1.5 mM) to solutions containing 3.0 mM bipy, 15 µM FPR, 0.375 µM (A) wild type BfrB and (B) G145VBfrB and apo-Bfd with Bfd/BfrB molar ratio of 40 (red), 30 (blue), 20 (pink), 10 (green), and 5 (black). Time dependent changes in the position of the Soret band

brought about by the addition of NADPH (1.5 mM) to the solutions in figure A; 417.5 nm and 425 nm correspond to fully oxidized and fully reduced heme, respectively.

These observations may suggest that in G145V BfrB the rate of electron transfer from the reductase to the heme group, does not depend on the concentration of Bfd as much as it does with wild type BfrB. According to the results of SPR and size exclusion chromatography experiments carried out with Bfd and BfrB (details in chapter 3), it is known that Bfd binds to BfrB in 12:1 molar ratio [11] and in addition, results of our preliminary experiments suggest that Bfd binds closer to the 4- fold pore of BfrB. The observation of the relatively similar rates of heme reduction in G145V BfrB with any concentration of Bfd may suggest that, binding of Bfd causes conformational changes in G145V BfrB in a different manner than that occurs in wild type BfrB. This conformational change may enable a fast transfer of electrons from the surface of the protein to the heme.

Table 2: Pseudorates for the Bfd-dependent release of core iron from G145VBfrB.

Bfd/BfrB molar ratio	Pseudo rate of iron release (min^{-1}) at 25 ºC	
	WT BfrB	G145V BfrB
0	0.0087 ± 0.0002	0.015 ± 0.001
10	0.029 ± 0.001	0.065 ± 0.005
20	0.036 ± 0.002	0.100 ± 0.0005
30	0.058 ± 0.008	0.124 ± 0.013
40	0.074 ± 0.008	0.134 ± 0.004

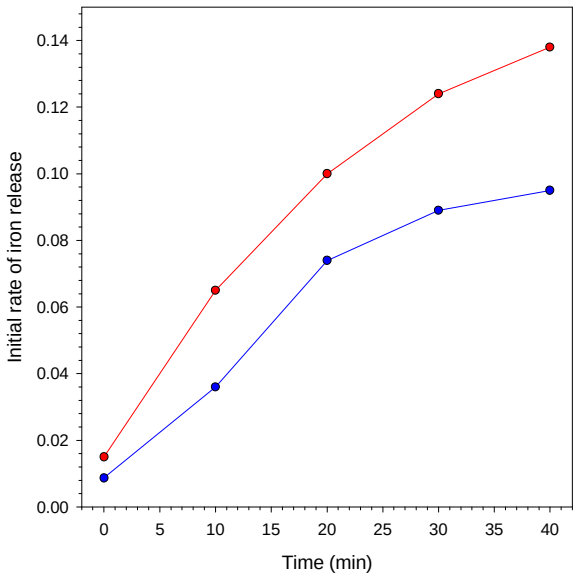

Figure 7: Bfd dependent iron release from G145V (red) and wild type (blue) BfrB.

Consequently, heme can transfer electrons to the iron core of G145V BfrB much faster than that of wild type and therefore, within a given period of time, the number of reduced iron ions in the core of G145V BfrB is higher than that of in the wild type. Hence more iron is observed o release from the G145V BfrB than that of from wild type. On the other hand, since a smaller amino acid residue Gly has been mutated to larger amino acid Val, the possible "breathing" motions of the 4-fold pore may have become slower and consequently the duration that the pore remains open is longer than that of a typical 4-fold pore of wild type BfrB. Therefore, the rate of iron release can be higher than that of wild type BfrB. Although additional kinetic and structural investigations are required to elucidate the mechanism and the pathway of iron release, it is clear that the G145V mutation has caused significant structural and hence functional changes in the 4-fold pore and its surroundings which resulted in much higher rates of iron release than that observed in wild type. Therefore, according to the results of our preliminary experiments, 4-fold pores can be one of the most possible routes of iron release from the inner core of BfrB.

References

[1] Swartz, L., Kuchinskas, M., Li, H., Poulos, T. L., and Lanzilotta, W. N. (2006) Redox-Dependent Structural Changes in the *Azotobacter vinelandii* Bacterioferritin: New Insights into the Ferroxidase and Iron Transport Mechanism. *Biochemistry 45*, 4421-4428.

[2] Liu, H.L.; Zhou, H.N.; Xing, W.M.; Zhao, J.F.; Li, S. X.; Huang, J.F.; Bi, R.C. (2004) 2.6 Å Rroesolution of Crystal Structure of the Bacterioferritin from Azotobactor vinelandii. FEBS Letters 573, 93-98.

[3] Cheesman, M. R., Le Brun, N. E., Kadir, F. H., Thomson, A. J., Moore, G. R., Andrews, S. C., Guest, J. R., Harrison, P. M., Smith, J. A., and Yewdall, S. J. (1993) Haem and Non-Haem Iron Sites in *Escherichia coli* Bacterioferritin: Spectroscopic and Model Building Studies. *Biochemistry 292*, 47-56.

[4] Ringeling, P.L.; Davy, S.L.; Monkara, F.A.; Hunt, C.; Dickson, D.P.E.; Mcewan, A.G.; Moore, G.R. (1994) Characterization of Bacterioferritin and Formation of Non-Haem Iron Particles in Intact Cells. *Europian Journal of Biochemistry 223*, 847-855.

[5] Kabsch, W. (1988) Automatic indexing of rotation diffraction patterns. *Journal of Applied Crystallography 2*, 67-72.

[6] Evans, P. (2006) Scaling and assessment of data quality. *Acta Crystallographica D Biological Crystallography 62*, 72-82

[7] Weeratunga, S.K.; Lovell, S.; Yao, H.; Battaile, K.P.; Fischer, C.J.; Gee, C.E.; Rivera, M.(2010) Structural studies of bacterioferritin B from Pseudomonas aeruginosa suggest agating mechanism for iron uptake via the ferroxidase center. *Biochemistry* 49, 1160-1175.

[8] Murshudov, G.N.; Vagin, A.A.; Dodson E.J. (1997) Refinement of macromolecular structures by the maximum-likelihood method. *Acta Crystallographica D Biological Crystallography* 53 240-55.

[9] Emsley, P.; Cowtan, K. (2004) Coot: model-building tools for molecular graphics. *Acta Crystallographica D Biological Crystallography* 60 2126-2132.

[10] Chen, V.B.et al. (2010) MolProbity: all-atom structure validation for macromolecular crystallography. *Acta Crystallographica D Biological Crystallography* 66 12-21.

[11] Weeratunga, S.K.; Gee, C.E.; Lovell, S.; Zeng, Y.;Woodin,Y.; Rivera,M. (2009) Binding of Pseudomonas aeruginosa Apobacterioferritin-Associated Ferredoxin to bacterioferritin B Promotes the Heme Mediation of Electron Delivery and Mobilization of core Mineral Iron. *Biochemistry 48*, 7420-7431.

CHAPTER V

Summary

Many pathogenic bacteria, including *Pseudomonas aeruginosa* require iron for successful colonization (infection) of mammalian hosts [1]. Therefore these bacteria have developed efficient strategies to acquire and store iron in a readily available form. Among other ferritin-like iron storage proteins, Bacterioferritins can be considered as the main iron storage proteins in bacteria. These proteins store iron as a solid ferric oxide mineral (~4500 iron ions) inside the protein shell and release to the bacterial cytoplasm when needed for various cellular metabolic processes.

BacterioferritinB (BfrB) plays an important role in the metabolism and pathogenicity in *Pseudomonas aeruginosa.* *P.aeruginosa* being an aerobic bacterium requires iron for its aerobic respiration as iron is a key component in most of the respiratory enzymes. Therefore, under iron depleted conditions, *P aeruginosa* cannot survive inside a host organism [2]. Consequently, it is believed that inhibiting pathways of iron acquisition would be an effective way of preventing *P.aeruginosa* infections. However, in order to implement that *in vivo*, a better understanding of the structure, function and the protein-protein interactions that facilitate iron uptake and release inside the bacterial cell, is essential. To achieve these goals, we carried out our investigations on Pa BfrB using many bio analytical techniques and had the opportunity to have many new discoveries about this protein. Based on our experimental results, our findings on Pa BfrB and the conclusions drawn can be summarized as follows.

1. Recombinant Pa-BfrB was overexpressed, purified and crystallized.

Recombinant Pa-BfrB was overexpressed, and purified to homogeneity and it is noteworthy that Pa BfrB purified in our laboratory was the first bacterioferritin to be purified with a fully assembly of heme (12 hemes/protein).

Pure Pa BfrB formed red prismatic crystals from various crystallization conditions. Basically four types of crystal structures of Pa-BfrB were solved: (a) BfrB as isolated, (b) mineralized, (c) iron soaked and (d) double soaked crystal structure. These structures were solved to a resolution of 2.07, 2.10, 2.25 and 2.80 Å respectively (Table 1 of Chapter 2) and these crystallographic data were used to obtain many important information regarding the structure of Pa BfrB.

Pa BfrB is a symmetric (432 octahedral) molecule composed of 24 subunits assembled as a hollow sphere with an external diameter of ~118 Å and an internal diameter of ~73 Å. One Pa BfrB molecule can bind 12 heme groups where each heme group is axially coordinated by two adjacent subunits via bis-methionine (Met52) ligation. Six 4-fold channels and eight 3-fold channels are symmetrically distributed in the molecule and these channels are located along the non-crystallographic 3- and 4-fold axis, respectively. In addition, another type of channels called B pores (12channels/molecule) are also found at the interfaces of two subunits. However, the physiological functions carried out by each of these pores are yet to be determined.

2. The ferroxidase center of Pa-BfrB is unstable.

Ferroxiadse center of Pa-BfrB is located in the middle of each subunit and made of six amino acid residues which are highly conserved among all bacterioferritins of known structure (Figure 2-1A of Chapter 2). The ferroxidase center of Pa-BfrB was found to be a labile ferroxidase center which functions as a gate to uptake iron ions into the protein. To investigate

the structure, function and the nature of the ferroxidase center of Pa BfrB, many structural and solution investigations were carried out. To this end, crystal structure of as isolated Pa BfrB was studied in detail and it revealed that the ferroxidase center of the 'as-isolated' BfrB was empty. However, when those crystals were soaked in a crystallization solution containing 50 mM Fe^{2+} ions (iron soaked) ferroxidase center with two iron atoms coordinated by the ferroxidase ligands was observed. On the other hand, double soaked crystal structure obtained by soaking the Fe-soaked crystals in the crystallization solution without iron ions, revealed a ferroxidse center devoid of iron, (Figure 2-9A of Chapter 2) implying that the ferroxidase center of BfrB is not stable. The kinetic experiments carried out using the stopped-flow spectrophotometer clearly shows that the ferroxidase center of Pa BfrB does not saturate upon addition of ~50 iron atoms to the protein, which is in clear contrast with the results obtained from the experiments of Ec-Bfr with a stable ferroxidase center (Figure 2-21A, B and 2-22A, B in Chapter 2). Therefore, the results obtained from both crystallographic and kinetic studies clearly indicate that the ferroxidase center of Pa-BfrB is unstable.

3. Crystal structure of Pa BfrB suggests a gated mechanism of iron uptake via the ferroxidase center.

According to the crystal structure of iron soaked Pa BfrB, it is thought that Fe^{2+} ions enter the Pa BfrB molecule via the ferroxidase pore (Figure 2-13 in Chapter 2) which is thought to be the main route for the uptake of iron from the outside. When these Fe^{2+} ions reach the ferroxidase center, the side chain of His130 moves toward the ferroxidase center and binds the incoming Fe^{2+} ions (gate-closed conformation). However, upon oxidation of Fe^{2+} ions to Fe^{3+} ions, His130 moves away from the ferroxidase center (gate-open conformation), and subsequently the oxidized Fe^{3+} ions are released and move towards the inner cavity (Figure 2-9

in Chapter 2). These observations from the crystallographic studies elegantly show that His 130 at the ferroxidase center of Pa BfrB acts as a gate to in uptake of iron ions. As mentioned above, the results obtained from the stopped flow experiments also suggest a gated mechanism of iron uptake and indicate that the rates/kinetics of the three phases of the Pa-BfrB iron uptake mechanism is clearly different from that of *E.coli* iron uptake mechanism. Therefore it can be concluded that the observed mechanism of iron uptake is unique to Pa-BfrB due its unique molecular architecture.

4. Binding of apo-Bfd to Pa BfrB facilitates the heme mediated mobilization of core iron.

The iron uptake mechanisms of ferritin-like molecules have been studied extensively in some ferritins and bacterioferritins. However, much less is known about the mechanisms of iron release of these molecules. Based on the observations of the global transcriptional response of iron-starved cultures of *P.aeruginosa* [3], it was hypothesized that Pa Bfd and Pa Fpr are the physiological partners of Pa BfrB in the mobilization of iron from the mineral core. Initially it was thought that Pa Bfd is functioning as a classical ferredoxin to transfer electrons from Fpr/NADPH to Pa BfrB core. However, our experimental results indicate that the apo form of Pa Bfd can efficiently facilitate the mobilization of iron from the core which negates the need of bacteria to produce 2Fe-2S cluster containing holo Bfd under iron depleted conditions. In addition, results of our additional experiments show that 12 Bfd molecules bind to one Pa BfrB molecule forming a protein complex to mobilize iron from the inner core (Figure 3-9 and 3-10 in Chapter 3). The presence of heme groups in BfrB is characteristic to all bacterioferritins. However, the exact function of these heme groups in Bfrs has been a mystery. Although, it has been speculated that the heme groups of Bfrs may have a

function in transferring electrons to the inner core, it has not been experimentally demonstrated. According to the results obtained from our experiments (Figure 3-11 in Chapter 3), we were able to show that the physiological function of heme in BfrB is the transfer of electrons from the reductase into the mineral core. In addition, it was also found out that heme group is reduced only in the presence of Pa Bfd, which further proves the idea that Pa BfrB and Pa Bfd are in fact the physiological partners in the mobilization of core iron from Pa BfrB.

5. Four fold pores are the dominant pathway of iron release from the mineral core of Pa BfrB.

To test our hypothesis on iron release through the four fold pores, site directed mutagenesis studies were carried out and some of the residues at the 4-fold pore, that were thought to be important in the process of iron release from the mineral core were mutated. Subsequently, the effect of those mutations on the process of iron release from Pa BfrB was assessed by comparing the rates of iron release of the mutants with that of wild type BfrB. First, two Asp residues (Asp 157 and 158) located at the very end of the C-terminus of the protein forming the inner end of the 4-fold pore, were removed by truncating the protein up to Glu156. These two Asp residues cannot be seen in the crystal structure of Pa BfrB as they are disordered. Therefore, Elastic Network Model studies were used to model these two residues in the structure of Pa BfrB (Figure 4-1B in Chapter4). Comparative iron mobilization experiments carried out with truncated and wild type BfrB clearly showed that reduced iron ions are released faster from truncated BfrB than that from wild type BfrB. In addition, additional experiments carried out with truncated BfrB indicated that although the core iron was reduced by reducing agents, iron ions were trapped inside the core and released only in the presence of Bfd, suggesting that Bfd is required to open the pores of BfrB. Further, ENM calculations revealed

that highly fluctuating residues are found in the 4-fold region of BfrB, including Asp 157,158 and His155, indicating that these residues are significantly important in the process of iron release from BfrB. As shown in figure 4-13 in Chapter 4, reduced iron ions are thought to be moving via a network of negatively charged residues towards the 4-fold pore and are subsequently coordinated by His155 and 153. However, upon binding of Bfd to BfrB, the amplitudes of the motions of Asp157 and 158 residues and particularly His155 are thought to be increased, and as a result iron ions are released from His residues. Subsequently, those iron ions released from His residues enter the 4-fold pores and may exit the protein through these four fold pores. ENM studies together with the results of our solution experiments strongly suggest that Bfd facilitates the opening of four fold pores and consequently reduced iron ions are released through the 4-fold pores of BfrB.

We were able to achieve many findings on bacterioferritin from *P.aeruginosa* by biochemically and structurally characterizing the protein. In addition, the experiments aiming at the protein-protein interactions of BfrB, eventually led us to find the physiological partners of BfrB in the process of iron release, which is an important molecular function of BfrB. All these discoveries we have made by studying Pa BfrB in the molecular level, will be a great contribution to the effort of constituting a new class of antibiotic to prevent *pseudomonas* infections.

REFERENCES

[1] Arrevalo-Ferro, C.; Hentzer, M.; Reli, G. (2003) Identification of Quorum Sensing Regulated Proteins in the Opportunistic Pathogen *Pseudomonas aeruginosa* by Proteomics. *Environmental Microbiology 5*, 1350-1369.

[2] Nouwens, A.; Beatson, S. A.; Whitchurch, C. B.; Nalsh, B. J.; Schweizer, H. P.; Mattick, J. S.; and Cordwell, S. J. (2003) Proteome Analysis of Extracellular Proteins Regulated by las and rhl Quorum Sensing System in Pseudomonas PAO1. *Microbiology 149*, 1311-1322.

[3] Palma, M.; Worgall, S.; and Quadri, L. E. N. (2004) Transcriptome Analysis of the Transcriptome Analysis of the *Pseudomonas aeruginosa* Response to Iron. *Archives of Microbiology 180*, 374-379.